

**THE SRICOS-EFA METHOD FOR COMPLEX PIER
AND CONTRACTION SCOUR**

A Dissertation

by

JUN WANG

Submitted to the Office of Graduate Studies of
Texas A&M University
in partial fulfillment of the requirements for degree of

DOCTOR OF PHILOSOPHY

May 2004

Major Subject: Civil Engineering

**THE SRICOS-EFA METHOD FOR COMPLEX PIER
AND CONTRACTION SCOUR**

A Dissertation

by

JUN WANG

Submitted to the Office of Graduate Studies of
Texas A&M University
in partial fulfillment of the requirements for degree of

DOCTOR OF PHILOSOPHY

Approved as to style and content by:

Jean-Louis Briaud
(Chair of Committee)

Hamn-Ching Chen
(Member)

Kuang-An Chang
(Member)

William Byant
(Member)

Paul Roschke
(Head of Department)

May 2004

Major Subject: Civil Engineering

ABSTRACT

The SRICOS-EFA Method for Complex Pier and Contraction Scour. (May 2004)

Jun Wang, B.S., Tongji University, Shanghai, China;

M.S.Eng., University of New South Wales, Sydney, Australia

Chair of Advisory Committee: Dr. Jean-Louis Briaud

A method called SRICOS-EFA is presented in this dissertation for scour prediction. The method is based on the calculation of two basic parameters: the maximum depth of scour and the initial rate of scour. The maximum depth of scour is based on an equation obtained from flume tests and the initial rate is based on an equation giving the initial shear stress obtained from numerical simulations. The initial scour rate is then read on the Erosion Function Apparatus (EFA) erosion function curve at the corresponding value of the calculated shear stress. A hyperbola is used to connect the initial scour rate to the maximum scour depth and describes the complete scour depth vs. time curve. The erodibility function curve can be measured in the EFA. As the results show, the SRICOS-EFA method can handle the multi-flood hydrograph and multilayer soil system. It can be used to solve the complex pier and contraction scour alone; it can also handle the superposition of complex pier scour and contraction scour.

A simplified SRICOS-EFA method was developed based on the case histories for contraction scour. EFA tests were performed to investigate the influence of different pH values and different levels of salinity on the soil erodibility. An attempt was made to find the correlation between the critical shear stress, and the initial slope of the erodibility function on the one hand and some geotechnical parameters on the other. A

solution for future hydrograph prediction was developed in this dissertation. The prediction consists of using a past hydrograph, preparing the frequency distribution plot for the daily stream flows, sampling the distribution randomly and preparing a future hydrograph, which has the same mean and standard deviation as the measured hydrograph. A frequency distribution plot of scour depths can be used to quote a scour depth with a corresponding probability of occurrence and risk level based on future hydrographs. In the verification process, 10 bridge case histories and 3 scour databases were used to check whether the method is good enough to provide sound results in real cases.

ACKNOWLEDGMENTS

First, I would like to express my sincere gratitude to my advisors Dr. Jean-Louis Briaud and Dr. Hamn-Ching Chen for their expert guidance, encouragement and assistance throughout my PhD study. Special heartfelt gratitude is expressed to Dr. Jean-Louis Briaud, the leader of our research project, for his academic counseling and financial support. I also would like to thank Dr. Kuang-An Chang for his help and valuable suggestions during my studies at Texas A&M University. I wish to thank Dr. William Bryant for his time and efforts in serving as an advisory committee member.

I want to especially thank Ya Li, Praharo Nurtjahyo, Wei Wang, Yanfeng Li for their friendship and help during different phases of this research. Appreciation is extended to Andrew Fawcett and Matt Potter for their help on the EFA maintenance.

TABLE OF CONTENTS

		Page
ABSTRACT.....		iii
ACKNOWLEDGMENTS.....		v
TABLE OF CONTENTS.....		vi
LIST OF FIGURES.....		x
LIST OF TABLES.....		xx
CHAPTER		
I	INTRODUCTION AND RESEARCH OBJECTIVES.....	1
	1.1 General.....	1
	1.2 Research Objectives.....	3
	1.3 Research Approaches and Methodologies.....	4
II	FUNDAMENTAL CONCEPTS AND PARAMETERS OF BRIDGE SCOUR.....	11
	2.1 Introduction.....	11
	2.2 Types of Bridge Scour.....	11
	2.3 Factors Influencing the Scour Process.....	17
III	EXISTING METHODS FOR BRIDGE SCOUR PREDICTION... 19	
	3.1 Introduction.....	19
	3.2 Literature Review for Simple Pier Scour in Cohesive Soil..	20
	3.3 Literature Review for Complex Pier Scour in Sand.....	27
	3.4 Literature Review for Contraction Scour in Sand.....	35
	3.5 Summary.....	40

CHAPTER	Page
IV	SRICOS-EFA METHOD OVERVIEW..... 42
	4.1 Introduction..... 42
	4.2 Erosion Function Apparatus (EFA) Overview..... 45
	4.3 Maximum Scour Depth of Complex Pier Scour..... 52
	4.4 Maximum Shear Stress in Complex Pier Scour..... 60
	4.5 Maximum Scour Depth of Contraction Scour..... 68
	4.6 Maximum Shear Stress in Contraction Scour..... 72
	4.7 Conclusions..... 77
V	SIMPLE SRICOS-EFA METHOD FOR CONTRACTION SCOUR..... 84
	5.1 Introduction..... 84
	5.2 Basic Assumptions..... 84
	5.3 Equivalent Time Equation Development for Contraction Scour in SRICOS-EFA Method..... 88
VI	SRICOS-EFA METHOD FOR COMPLEX PIER AND CONTRACTION SCOUR AND SRICOS-EFA COMPUTER PROGRAM..... 124
	6.1 Introduction..... 124
	6.2 Integrated SRICOS-EFA Method..... 125
	6.3 The SRICOS-EFA Method Program..... 141
	6.4 The Input of SRICOS-EFA Program..... 150
	6.5 The Output of SRICOS-EFA Program..... 153
VII	FUTURE HYDROGRAPHS & SCOUR RISK ANALYSIS..... 156
	7.1 Background..... 156
	7.2 Preparation of the Future Hydrographs..... 158
	7.3 Risk Approach to Scour Predictions..... 163
	7.4 Observations on Current Risk Levels..... 166

CHAPTER		Page
VIII	INFLUENCING FACTORS OF SCOUR RATE IN COHESIVE SOILS ON EFA TESTS.....	169
	8.1 Introduction.....	169
	8.2 pH Tests.....	170
	8.3 Salinity Tests.....	176
	8.4 Other Influencing Factors of Scour Rate in Cohesive Soils on EFA Test.....	182
	8.5 Conclusions.....	185
IX	VERIFICATION CASE STUDIES.....	187
	9.1 General.....	187
	9.2 Verification Case Study 1: The Woodrow Wilson Bridge over the Potomac River.....	189
	9.3 Verification Case Study 2: The New Sloop Channel Bridge on Sloop Channel on Wantagh Parkway.....	213
	9.4 Verification Case Study 3: The New Goose Bridge on Goose Creek on Wantagh Parkway.....	245
	9.5 Verification Case Study 4: Contraction Scour Study at the Indian River Bridge on Indian Bay, Delaware.....	262
	9.6 Verification Case Study 5: Reevaluation of Pier Scour for 6 selected Bridges in Texas.....	276
	9.7 Verification Case Study 6: Mueller (1996) Database, Froehlich (1988) Database and Gill (1981) Database.....	291
X	CONCLUSIONS AND RECOMMENDATIONS.....	301
	10.1 Conclusions.....	301
	10.2 Recommendations.....	307

	Page
REFERENCES.....	309
APPENDIX.....	317
VITA.....	336

LIST OF FIGURES

FIGURE	Page
1.1 Causes of Bridge Failure in England (after Smith, 1976).....	1
2.1 Different Types of Scour in a Typical Bridge Cross Section.....	12
2.2 Flow Pattern around a Bridge Pier (after Herbich, 1984).....	14
2.3 Parameters in Contraction Scour.....	16
3.1 Piers with Different Shapes but the Same Projection Width (after Mostafa, 1994).....	34
4.1 EFA Conceptual Diagram.....	46
4.2 Photography of EFA.....	47
4.3 Typical EFA Test Result.....	49
4.4 Moody Chart [Reprinted with Permission from Munson et al.] (1990).....	50
4.5 Diagram of the Flume System (Not to Scale, after Li, 2002).....	53
4.6 Diagram of ADV.....	55
4.7 Parameter Definitions in Shallow Water Effect.....	56
4.8 Parameter Definitions in Pier Spacing Effect.....	58
4.9 Parameter Definitions in Pier Shape Effect.....	59
4.10 Parameter Definitions in Flow Attack Angle Effect.....	59
4.11 Relationship between k_w ($= \tau_{\max} / \tau_{\max(\text{deep})}$) and H/B	65
4.12 Relationship between k_{sp} ($= \tau_{\max} / \tau_{\max(\text{single})}$) and S/B for deep water $H/B > 2$).....	66

FIGURE	Page
4.13 Relationship between k_{sh} ($= \tau_{max}/\tau_{max (circle)}$) and L/B for Deep Water ($H/B>2$).....	67
4.14 Relationship between k_a ($= \tau_{max}/\tau_{max (0 \text{ degree})}$) and α for Deep Water ($H/B>2$).....	68
4.15 Grid System for the Simulation in the Case of $B_2/B_1 = 0.25$ (after Nurtjahyo,2002).....	74
4.16 Relationship between k_{c-R} and $\frac{B_1}{B_2}$	75
4.17 Relationship between $k_{c-\theta}$ and $\frac{\theta}{90}$	76
4.18 Relationship between k_{c-L} and $\frac{L}{B_1 - B_2}$	76
4.19 General Process of SRICOS-EFA Method.....	82
5.1 Basic Assumption of Simple SRICOS-EFA Method.....	87
5.2 Locations of Case History Bridges.....	89
5.3 Definitions of Contraction Ratio and Transition Angle.....	90
5.4 Profiles of Navasota River Bridge at SH 7.....	92
5.5 Profiles of Brazos River Bridge at US 90A.....	93
5.6 Profiles of Trinity River Bridge at FM 787 in 1976.....	94
5.7 Profile of San Marcos River Bridge at SH 80 in 1939.....	95
5.8 Profile of Sims Bayou Bridge at SH 35 in 1993.....	96
5.9 Profile of Bedias Creek Bridge at US 75 in 1947.....	97
5.10 Discharge Hydrograph of Navasota River Bridge at SH 7.....	98
5.11 Hydrograph of Brazos River Bridge at US 90A.....	99

FIGURE	Page
5.12 Hydrograph of Trinity River Bridge at FM 787.....	99
5.13 Hydrograph of San Marcos River Bridge at SH 80.....	100
5.14 Hydrograph of Sims Bayou Bridge at SH 35.....	100
5.15 Hydrograph of Bedias Creek Bridge at US 75.....	101
5.16 Relationship between Discharge and Velocity – Navasota River.....	105
5.17 Relationship between Discharge and Water Depth - Navasota River.....	105
5.18 Relationship between Discharge and Velocity – Brazos River.....	106
5.19 Relationship between Discharge and Water Depth – Brazos River.....	106
5.20 Relationship between Discharge and Velocity – Trinity River.....	107
5.21 Relationship between Discharge and Water Depth – Trinity River.....	107
5.22 Relationship between Discharge and Velocity – San Marcos River.....	108
5.23 Relationship between Discharge and Water Depth – San Marcos River...	108
5.24 Relationship between Discharge and Velocity – Sims Bayou.....	109
5.25 Relationship between Discharge and Water Depth - Sims Bayou.....	109
5.26 Relationship between Discharge and Velocity – Bedias Creek.....	110
5.27 Relationship between Discharge and Water Depth – Bedias Creek.....	110
5.28 Scour Rate vs. Shear Stress –Navasota River Layer 1.....	113
5.29 Scour Rate vs. Shear Stress –Navasota River Layer 2.....	113
5.30 Scour Rate vs. Shear Stress –Brazos River Layer 1.....	114
5.31 Scour Rate vs. Shear Stress –Trinity River Layer 1.....	114
5.32 Scour Rate vs. Shear Stress –Trinity River Layer 2.....	115

FIGURE	Page
5.33 Scour Rate vs. Shear Stress –San Marcos River Layer 1.....	115
5.34 Scour Rate vs. Shear Stress –San Marcos River Layer 2.....	116
5.35 Scour Rate vs. Shear Stress –Sims Bayou Layer 1.....	116
5.36 Scour Rate vs. Shear Stress –Bedias Creek Layer 1.....	117
5.37 Scour Rate vs. Shear Stress –Bedias Creek Layer 2.....	117
5.38 Comparison of Equivalent Time t_{equiv}	120
5.39 Comparison of Results by Using SRICOS-EFA and Simple SRICOS-EFA.....	123
6.1 Three types of contraction scour profiles (after Li, 2002).....	125
6.2 Step I - Bridge Scour Input Data and Primary Calculation.....	128
6.3 Step II - Contraction Scour Calculation and Distribution.....	130
6.4 Steps III and IV – Calculations of Pier Scour and Superposition.....	132
6.5 Plan-view of Complex Pier Scour and Contraction Scour.....	133
6.6 Scour due to a Sequence of Two Flood Events.....	137
6.7 Scour of a Two-Layer Soil System.....	140
6.8 Flow Chart of SRICOS-EFA Method.....	143
6.9 The Main Window of SRICOS-EFA Program.....	145
6.10 The Geometry Data (Pier Scour) Input Screen.....	145
6.11 The Soil Data (Pier Scour) Input Screen.....	146
6.12 The Water Data (Pier Scour) Input Screen.....	147
6.13 The Output Table Screen.....	147

FIGURE	Page
6.14 The Output Plots Screen.....	148
6.15 Example of EFA Test Result.....	151
6.16 Example of Hydrograph Transforming for Pier 1E of the Woodrow Wilson Bridge on the Potomac River in Washington D.C.....	152
6.17 Example of SRICOS-EFA Program Output Table.....	154
6.18 Example of Plot from Output Plots in SRICOS-EFA Program.....	155
7.1 Woodrow Wilson Measured Hydrograph Spiked with a 500-year Flood...	157
7.2 Original Hydrograph & Scour Depth vs. Time near Woodrow Wilson Bridge Site.....	162
7.3 Predicted Hydrograph and Scour Depth vs. Time Curve near Woodrow Wilson Bridge Site Using Existing Hydrograph Approach (Projected Time = 75 Years).....	162
7.4 Predicted Hydrograph and Scour Depth vs. Time Curve near Woodrow Wilson Bridge Site Using Q_{100} and Q_{500} Approach (Projected Time = 75 Years).....	163
7.5 Probability Distribution of Scour Depth, d , for Different Lengths of the Projected Life, L_t	164
7.6 Risk Associated with Different Design Values of the Final Scour Depth, d , and Different Lengths of the Projected Life, L_t	165
7.7 Flood-frequency Curve for the Potomac River at the Woodrow Wilson Bridge.....	168
8.1 Relationship between Erosion Rate and Velocity for Different pH Values.....	173
8.2 Relationship between Erosion Rate and Shear Stress for Different pH Values	173
8.3 Relationship between Erosion Rate and Shear Stress for Different Concentrations of Eroding Fluid (after Arulanandan, 1975).....	177

FIGURE	Page
8.4 Relationship between Erosion Rate and Velocity for Different Concentrations of Salinity of Eroding Fluid.....	179
8.5 Relationship between Erosion Rate and Shear Stress for Different Concentrations of Salinity of Eroding Fluid.....	179
8.6 (a) Relationship between Critical Shear Stress vs. Water Content; (b) Relationship between Initial Slope S_i vs. Water Content.....	183
8.7 (a) Relationship between Critical Shear Stress vs. Undrained Shear Strength; (b) Relationship between Initial Slope S_i vs. Undrained Shear Strength.....	183
8.8 (a) Relationship between Critical Shear Stress vs. Plasticity Index; (b) Relationship between Initial Slope S_i vs. Plasticity Index n	184
8.9 (a) Relationship Between Critical Shear Stress vs. Percentage Passing #200 Sieve; (b) Relationship Between Initial Slope S_i vs. Percentage Passing #200 Sieve.....	184
9.1 Pier Locations and Soil Stratigraphy Profile for Woodrow Wilson Bridges (after Kwak, 2002).....	190
9.2 Woodrow Wilson Bridge Hydrograph from 1960 to 1998.....	191
9.3 Relationship between Discharge and Velocity at Pier 1E Location.....	193
9.4 Relationship between Discharge and Water Depth at Pier 1E Location.....	193
9.5 Erosion Function for a Soil Sample Taken near Pier 1E of the Existing Woodrow Wilson Bridge (4.0 – 4.6 m depth) (a) Scour Rate vs. Velocity, (b) Scour Rate vs. Shear Stress.....	197
9.6 Erosion Function for a Soil Sample Taken near Pier 1E of the Existing Woodrow Wilson Bridge (10.0 – 10.6 m depth) (a) Scour Rate vs. Velocity, (b) Scour Rate vs. Shear Stress.....	198

FIGURE	Page
9.7 Erosion Function for a Soil Sample Taken near Pier 27E of the Existing Woodrow Wilson Bridge (2.6 – 3.2 m depth) (a) Scour Rate vs. Shear Stress, (b) Scour Rate vs. Velocity.....	199
9.8 Erosion Function for a Soil Sample Taken near Pier 27E of the Existing Woodrow Wilson Bridge (11.2 – 11.7 m depth) (a) Scour Rate vs. Shear Stress, (b) Scour Rate vs. Velocity.....	200
9.9 Scour Depth Measurements in Pier 5E (after Kwak, 2000).....	202
9.10 Scour Depth vs. Time in Pier 1E of Existing Woodrow Wilson Bridge over the Potomac River.....	205
9.11 Scour Depth vs. Time in Pier 27E of the Woodrow Wilson Bridge over the Potomac River.....	210
9.12 Comparison of Measured and Predicted Pier Scour Depths	211
9.13 Comparisons between the Predictions for 100 and 500 Year Floods from SRICOS-EFA and HEC-18 in the Woodrow Wilson Bridge Case....	212
9.14 Location of the Existing Sloop Channel Bridge over Sloop Channel on Wantagh Parkway.....	213
9.15 Sloop Channel Bridge Historic Streambed Elevations in Different Years.....	214
9.16 Overview and Cross Section of the New Sloop Channel Bridge over Sloop Channel on Wantagh Parkway.....	217
9.17 Measured Velocities during a 12 Hour Period in Two Different Locations near the Sloop Channel Bridge.....	220
9.18 One Part of the 500 Year Flood Hydrograph for the Sloop Channel on Wantagh Parkway.....	221
9.19 Erosion Function for Soil Sample (DB-N-110, Tube 3) of the Sloop Channel (21.49 – 21.79 m depth) (a) Scour Rate vs. Velocity, (b) Scour Rate vs. Shear Stress.....	224

FIGURE	Page
9.20 Erosion Function for Soil Sample (DB-N-110, Tube 4) of the Sloop Channel (22.10 – 22.40 m depth) (a) Scour Rate vs. Velocity, (b) Scour Rate vs. Shear Stress.....	225
9.21 Erosion Function for Soil Sample (DB-N-110, Tube 5) of the Sloop Channel (22.71 – 23.01 m depth) (a) Scour Rate vs. Velocity, (b) Scour Rate vs. Shear Stress.....	226
9.22 Erosion Function for Soil Sample (DB-N-110, Tube 7) of the Sloop Channel (26.21 – 26.51 m depth) (a) Scour Rate vs. Velocity, (b) Scour Rate vs. Shear Stress.....	227
9.23 Erosion Function for Soil Sample (DB-N-111, Tube 2) of the Sloop Channel (21.60 – 22.10 m depth) (a) Scour Rate vs. Velocity, (b) Scour Rate vs. Shear Stress.....	228
9.24 Erosion Function for Soil Sample (DB-N-111, Tube 4) of the Sloop Channel (28.00 – 28.70 m depth) (a) Scour Rate vs. Velocity, (b) Scour Rate vs. Shear Stress.....	229
9.25 Geometry of the Bascule Pier at the New Sloop Channel Bridge.....	231
9.26 Geometry of the Franking Pier at the New Sloop Channel Bridge.....	231
9.27 Definition Sketch for Scour Components for a Complex Pier Case (Richardson and Davis, 2001).....	232
9.28 Comparison of Pier Scour Predictions between SRICOS-EFA and HEC-18 for the Sloop Channel Bridge Case.....	242
9.29 Comparison of Combined Scour Depths between the Superposition Method and the Integrated Method in the Sloop Channel Bridge Case.....	243
9.30 Scour Profiles for the New Sloop Channel Bridge on Wantagh Parkway.....	244
9.31 Location of the New Goose Creek Bridge on Wantagh Parkway.....	245
9.32 Cross Section View of the New Goose Creek Bridge and Historical Streambed Elevations.....	247

FIGURE	Page
9.33 One Part of the 500 Year Flood Hydrograph for the Goose Creek on Wantagh Parkway.....	249
9.34 Comparison of Pier Scour Predictions between SRICOS-EFA and HEC-18 in the Goose Creek Bridge Case.....	260
9.35 Comparison of Contraction Scour Predictions between SRICOS-EFA and HEC-18 in the Goose Creek Bridge Case.....	261
9.36 Aerial Photo of Indian Inlet.....	263
9.37 Overview of Indian River Inlet.....	263
9.38 River Bottom Profile from Indian River Bay, Looking from East.....	264
9.39 Location of USGS Gaging Station 01484525.....	265
9.40 Downloaded Hydrograph from Gaging Station 0148425.....	266
9.41 Flood-frequency Curve of USGS Gaging Station 01484525.....	269
9.42 Discharge Hydrograph at Indian River Inlet.....	270
9.43 Relationships between the Discharge vs. Upstream Velocity and Discharge vs. Upstream Water Depth of Indian River Inlet.....	272
9.44 Maximum Contraction Scour Depths for Different Critical Shear Stresses.....	275
9.45 Location of Case History Bridges.....	277
9.46 Relationship between Discharge and Velocity at Bent 3 at the Navasota River Bridge.....	282
9.47 Relationship between Discharge and Velocity at Bent 5 at the Navasota River Bridge.....	282
9.48 Relationship between Discharge and Velocity at Bent 3 at the Brazos River Bridge.....	283
9.49 Relationship between Discharge and Velocity at Bent 9 at the San Marcos River Bridge.....	283

FIGURE	Page
9.50 Relationship between Discharge and Velocity at Bent 3 at the Trinity River Bridge.....	284
9.51 Relationship between Discharge and Velocity at Bent 4 at the Trinity River Bridge.....	284
9.52 Relationship between Discharge and Velocity at Bent 3 at the Sims Bayou Bridge.....	285
9.53 Relationship between Discharge and Velocity at Bent 26 at the Bedias Creek Bridge.....	285
9.54 Profile of the Navasota River Bridge at SH-7.....	288
9.55 Profile of the Brazos River Bridge at US 90A.....	288
9.56 Predicted and Measured Pier Scour for the SRICOS-EFA Method.....	290
9.57 SRICOS-EFA Predictions against the Mueller (1996) Database.....	292
9.58 HEC-18 Method against the Mueller (1996) Database.....	293
9.59 SRICOS-EFA Predictions vs. the Mueller Database for Various Ranges of D_{50}	294
9.60 HEC-18 Predictions vs. the Mueller Database for Various Ranges of D_{50}	295
9.61 SRICOS-EFA Predictions against the Froehlich (1988) Database.....	296
9.62 HEC-18 Predictions against the Froehlich (1988) Database.....	297
9.63 SRICOS-EFA Predictions against the Gill (1981) Database.....	299
9.64 HEC-18 Predictions against the Gill (1981) Database.....	300

LIST OF TABLES

TABLE	Page
3.1 Effect of Aspect Ratio of Rectangular Pier on Sour Depth.....	32
3.2 Pier Shape Factors (after Hoffmans G.J.C.M. and Verheij H.J., 1997).....	33
3.3 Scour Depth for Different Pier Shapes with Same Projection Width.....	34
3.4 Equations for Uniform Contraction Scour in Live-bed Condition (after Li, 2002).....	38
3.5 Equations for Uniform Contraction Scour in Clear Water Conditions (after Li, 2002).....	39
4.1 Geotechnical Properties of the Porcelain Clay.....	55
4.2 Parameters in the Numerical Simulations (Nurtjahyo, 2002).....	73
5.1 Channel Information for Case Histories in Simple SRICOS-EFA Method Development for Contraction Scour.....	91
5.2 Typical Values of Manning's Coefficient (after Young et al., 1997).....	103
5.3 Average Slopes of Selected Channels (after Kwak, 2000).....	104
5.4 Soil Properties of 6 Selected Channels.....	112
5.5 Equivalent Time t_{eqiv} (Contraction Scour) and Selected Parameters.....	119
5.6 Comparison of Results by Simple SRICOS-EFA and SRICOS-EFA Method.....	122
6.1 Summary of Geometry Factors.....	153
7.1 Risk of Failure Associated with Different Design Values of Scour Depth and Projected Life.....	168
8.1 Chemical Properties of Eroding Water in pH Test.....	172
8.2 Chemical Properties of Eroding Water in Salinity Test.....	178

TABLE	Page
9.1 Geotechnical Soil Properties Testing Results (after Kwak, 2000).....	196
9.2 Measured Pier Scour Depths in the Existing Woodrow Wilson Bridge....	202
9.3 Summary of Data Input (Pier 1E).....	204
9.4 Predicted Pier Scour Depths at the Existing Woodrow Wilson Bridge by Using the SRICOS-EFA Method from 1960 to 1998 Period.....	206
9.5 100 Year and 500 Year Flood Discharges for the Potomac River at the Woodrow Wilson Bridge.....	207
9.6 Predicted Maximum Pier Scour Depths at the Existing Woodrow Wilson Bridge Using the SRICOS-EFA Method and HEC-18 for a 100 Year Flood Event.....	208
9.7 Predicted Maximum Pier Scour Depths at the Existing Woodrow Wilson Bridge Using the SRICOS-EFA Method and HEC-18 for a 500 Year Flood Event.....	208
9.8 Measured Velocities during One Day Period in Two Different Locations near the Sloop Channel Bridge.....	219
9.9 General Subsurface Information & Laboratory Test Data for the Sloop Channel.....	223
9.10 Pier Scour Predictions by SRICOS-EFA for Short Duration Flood Events in the Sloop Channel Bridge.....	235
9.11 Pier Scour Predictions by HEC-18 for Short Duration Flood Events in the Sloop Channel Bridge.....	235
9.12 Pier Scour Predictions by SRICOS-EFA for Different Hydrographs.....	236
9.13 Contraction Scour Predictions by SRICOS-EFA for Short Duration Flood Events.....	238
9.14 Contraction Scour Predictions by SRICOS-EFA for Different Hydrographs.....	238
9.15 Pier Scour + Contraction Scour Predictions (SRICOS-EFA Integrated Method) for Different Hydrographs.....	239

TABLE	Page
9.16 Summary Table of the Sloop Channel Bridge Scour Analysis.....	239
9.17 Information on Piers at the New Goose Creek Bridge.....	251
9.18 Pier Scour Predictions by SRICOS-EFA for Short Duration Flood Events at the Goose Creek Bridge.....	252
9.19 Pier Scour Predictions by HEC-18 for Short Duration Flood Events at the Goose Creek Bridge.....	252
9.20 Pier Scour Predictions by SRICOS-EFA for the Normal Hydrograph and the Normal Hydrograph with the 500Year Flood.....	253
9.21 Contraction Scour Predictions by SRICOS-EFA for Short Duration Flood Events.....	256
9.22 Contraction Scour Predictions by HEC-18 for Short Duration Flood Events.....	256
9.23 Contraction Scour Predictions by SRICOS-EFA for Different Hydrographs.....	257
9.24 Pier + Contraction Scour Predictions by SRICOS-EFA Integrated Method for Different Hydrographs.....	257
9.25 Summary Table for the Goose Creek Bridge Scour Analysis.....	258
9.26 Maximum and Uniform Contraction Scour Depths for 100 Year and 500 Year Floods in the Indian Inlet Case.....	274
9.27 The USGS Gaging Station Numbers of Bridge Cases.....	281
9.28 Full Scale Bridges as Case Histories.....	289

CHAPTER I

INTRODUCTION

1.1 GENERAL

Bridge scour is a common cause of bridge failure. One thousand bridges have collapsed over the last 30 years in the United States. 60% of the failures are due to scour (Shirole and Holt 1991) and only 2% are due to earthquakes based on the same study. Smith (1976) did a survey of bridge failure in England. The survey indicates that 49% of these failures were due to scour. Figure 1.1 shows the different causes of bridge failures in Smith's survey and their relative percentages. This information indicates that bridge scour is crucial to bridge failure.

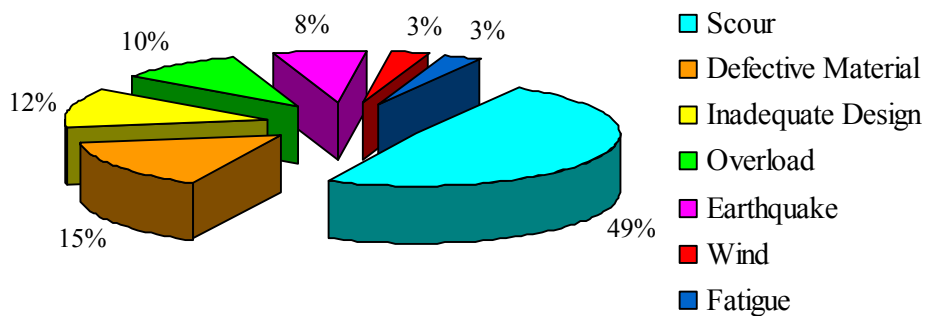


Figure 1.1: Causes of Bridge Failure in England (after Smith 1976)

Scour is a very important consideration relating to bridge design and maintenance. Many geotechnical engineers don't fully understand the scour problem.

This dissertation follows the style and format of *Journal of Geotechnical and Geoenvironmental Engineering*, ASCE.

Scour is the interaction between soil and flowing water. It is the result of the erosive action of flowing water, which excavates and carries away material from stream beds and banks. The flowing water induces shear stress on the soil in the river bottom. The stress is proportional to the velocity gradient and the fluid viscosity. In the past several decades, much research has succeeded in developing applicable methods for precisely predicting bridge scour. The most important contribution of scour prediction is HEC-18, which was published as the FHWA Hydraulic Engineering Circular No.18, so it was titled as HEC-18 (Richardson and Davis, 2001). Most methods of predicting bridge scour are based on non-cohesive materials in the flume laboratory. HEC-18 recommends that the scour equations be applicable in cohesive soils as well, but no profound research has been performed on cohesive soil in this scour prediction method. It is commonly known that the scour process in non-cohesive soil is very different from the same process in cohesive soil. Scouring in cohesive soil is much slower than in non-cohesive soil. Briaud et al. (2001) stated that scour and erosion rates in cohesive soils could be 1000 times slower than in non-cohesive soils. And a few days of this process may generate only a small fraction of the maximum scour depth. Gudavalli (1997) came to a similar conclusion. He conducted a series of flume tests in the hydraulic laboratory at Texas A&M University. His observations showed the same phenomena as described in Briaud et al. (2001). Hence the present challenge for research is applying the same equations for non-cohesive soil on cohesive soils without being concerned the time effect on the scour process will be too conservative. For example, if a bridge foundation in cohesive soil is designed to resist scour for the long term, the bridge foundation

design will be too deep due to using the conservative scour prediction method. Therefore, it is necessary to consider the erosion rate of stream materials in predicting scour for cohesive soil.

1.2 RESEARCH OBJECTIVES

The objectives of this research are as follows:

1. Develop the SRICOS-EFA scour prediction method including an appropriate superposition principle of pier and contraction scour based on flume testing and numerical simulation, which can handle the multiflood hydrograph and multilayer soil system. SRICOS stands for Scour Rate In Cohesive Soil, and EFA stands for Erosion Function Apparatus;
2. Develop a simplified version of the SRICOS-EFA method to determine the contraction scour depth z versus time t ;
3. Develop a simplified model to predict the future hydrograph based on the existing hydrograph, and find the risk level for differing scour depths;
4. Develop a computer program to generate the multi-flood hydrograph and multilayer soil system, which is associated with SRICOS-EFA method;
5. Try to find some potential relationships between the soil erodibility and soil properties;
6. Verify the SRICOS-EFA method by using the existing scour database and the full-scale bridge cases.

1.3 RESEARCH APPROACHES AND METHODOLOGIES

The research approaches and methodologies are designed to achieve the research objectives listed in the previous section. The best solution to these objectives can be reached by using a proper balance of the literature review, EFA erosion tests, applying proper theory models and principles and verification by using case histories. Literature review can give good results and suggestions from the research of others' work and can avoid the unnecessary duplication of research; erosion tests show the fundamental erosion behavior of the soil; case histories are a way to verify the proposed technique. The combination of these methods leads to a thorough approach with the goal of proposing a solution for the research objectives.

1.3.1 LITERATURE REVIEW

Through literature review, a large range of references about complex pier and contraction scour have been studied. For complex pier scour, the review has focused on existing complex pier scour prediction equations, and the correction factors relating to complex pier scour. For contraction scour, uniform scour depth for long term contraction in sand was the major concern. The factors influencing soil erodibility was another issue, and through the literature review many such factors were found, which provided good hints for my research. Through the literature review, some well documented cases of pier scour and contraction scour were found. The review provided some good scour databases for the verification task.

1.3.2 HYPERBOLA MODEL

As stated in the General section in this chapter, it is important to consider the time factor in developing the scour prediction equations. The hyperbola model has been verified to be the best model to fit the scour depth versus time development in pier scour cases. Briaud et al. (1999) concluded that the pier scour depth development could be extrapolated by the following equation:

$$z(t) = \frac{t}{\frac{1}{\dot{z}_i} + \frac{t}{Z_{\max}}} \quad (1.1)$$

Where $z(t)$ is the scour depth at time t , Z_{\max} is the maximum scour depth; and \dot{z}_i is the initial scour rate.

The hyperbola model was originally developed for pier scour. This study found that the hyperbola model could be used to predict contraction scour and the combined scour of complex pier and contraction scour. The hyperbola model is an essential element in the SRICOS-EFA method development.

1.3.3 ACCUMULATION ALGORITHM AND SUPERPOSITION PRINCIPLE

Algorithms are used to incorporate the effect of varying velocities and multilayered soil systems in the SRICOS-EFA method. The fundamental basis for accumulation algorithms is that the velocity histogram is a step function with a constant velocity value for each time step. The principle of accumulation algorithm is based on an equivalent time calculation, which is the time required for a flood in the hydrograph to create the same scour depth as created by all previous floods in the hydrograph. A

method called the Integrated SRICOS-EFA Method, based on the superposition principle, was developed to handle the combination of complex pier and contraction scour. The superposition principles will be used to deal with the accumulations of maximum scour depth in combined pier and contraction scour. Contraction scour is assumed to happen first, without considering pier scour. This doesn't imply that pier scour has no influence on contraction scour; indeed the piers are considered in the contraction scour calculation because their total projection width is added to calculate the total contraction ratio. Then the pier is calculated in the next step. There are two options for pier scour calculations: (1) if contraction scour calculations indicate that there is no contraction scour at the bridge site, then the pier scour is calculated by following the SRICOS-EFA complex pier scour calculation procedure; (2) If the calculations indicate that contraction scour occurs at the bridge site, then the pier scour calculations are made by using the critical velocity, which can be obtained from the EFA tests or the equations developed in the HEC-18, and the water depth will be the total depth of the original water depth and the calculated contraction scour in the contracted section. The maximum scour of combined contraction scour and pier scour can be calculated by adding the maximum scour depth of these two scours. The detailed principles and procedures of this method will be developed and will be presented in this dissertation.

1.3.4 EQUIVALENT TIME DEVELOPMENT IN A SIMPLIFIED SRICOS-EFA METHOD FOR CONTRACTION SCOUR

In most cases the SRICOS-EFA method needs to use the whole river hydrograph during the analysis period or bridge design life. But sometimes the river hydrographs miss some data because the gaging stations have not been installed or have malfunctioned data recording or because of other reasons. So the purposes of this research are: (1) to develop a simplified method associated with the SRICOS-EFA method that can be used when the whole hydrograph doesn't exist, (2) and to develop a simplified method of using only hand calculations in the scour analysis. Kwak (2000) has developed the Simple SRICOS-EFA for pier scour calculation. In this research a simplified version of the SRICOS-EFA method for contraction scour will be developed. A new concept, named equivalent time t_{equiv} , will be introduced, which is the time required for the maximum velocity in the hydrograph to create the same scour depth generated by all previous hydrographs. Six rivers were selected to find the regression equation of the equivalent time t_{equiv} for contraction scour. These six rivers are: Navasota River at SH 7, Brazos River at US 90A, Trinity River at FM 787, San Marcos River at SH 80, Sims Bayou at SH 35, and Bedia Creek at US 75. Finally, the equivalent time equation for contraction scour will be proposed and the procedures of the simple SRICOS-EFA method will be addressed in this dissertation.

1.3.5 FORTRAN AND VISUAL C++ FOR SRICOS-EFA COMPUTER PROGRAM DEVELOPMENT

The old version of the SRICOS-EFA computer program was written in FORTRAN by using FORTRAN 5.0, which is associated with the SRICOS-EFA method. The first version, developed by Kwak (2000), was to solve the problem of a cylindrical pier in deep water. The second version has been completed, which is to solve complex pier scour, contraction scour and the superposition of these two scours in the following conditions: the multiflood hydrograph and a multilayered soil system. The second version of the SRICOS-EFA program has been transferred from the DOS environment to the WINDOWS environment by using Visual C++. Prediction of future hydrographs and risk analysis for scour depths were added as new features of the program.

1.3.6 EFA TESTING FOR SOIL ERODIBILITY AND FINDINGS RELATING TO RELATIONSHIPS OF SOIL PROPERTIES

Briaud et al. (1999) summarized the factors influencing critical shear stress of soil based on the literature review. The factors include soil water content, soil unit weight, soil plasticity, soil shear stress, soil void ratio, soil swell, soil mean grain size, soil percentage passing the No. 200 sieve, soil clay mineral, soil dispersion ratio, soil cation exchange capacity, soil sodium absorption ratio, soil pH, soil temperature and the water chemical composition. In order to find out the correlation between these factors and the erosion of cohesive soils, two major factors referring to water chemical composition were selected and a series of tests were run in the EFA for this purpose. The

selected influencing factors were: pH value and salinity level in eroding water. The possible relationships between the factors and soil properties and conclusions on this issue will be addressed in the dissertation.

1.3.7 CASE HISTORIES FOR METHOD VERIFICATION

The verification process is very important for a method development because it can check whether a method is good enough to generate sound results in actual cases, and the process can provide more feedback for improving the methodology. Two kinds of case histories are used in this task. One is the databases found in existing literature: for complex pier scour, the Mueller (1996) database and the Froehlich (1988) database were used; for contraction scour, the Gill (1981) database was used. The other type of case history is full-scale bridges or channels. The case histories had to satisfy the following requirements: (1) channel contraction or bridges with piers in the water; (2) a gauge station which gives a hydrograph over the analysis period; (3) the site can be accessed with a drill rig for soil sampling; (4) the river cross-sections were documented at the beginning and at the end of the analysis period. After careful consideration, the following bridges were selected as having qualified case histories for verification purposes: the Woodrow Wilson Bridge over the Potomac River in Washington D.C, the Sloop Channel Bridge over Sloop Channel in Wantagh Parkway and 6 selected Texas bridges. Two other bridges were also adopted for the verification, although these two bridges did not satisfy all the selection criteria. However, performing the scour analysis for these kinds of cases can provide supplementary verification when the verification case histories are not enough. These two bridges are: The Indian Inlet over Indian River

in Delaware, and the Goose Creek Bridge over Goose Creek in Wantagh Parkway. The calculation results of using SRICOS-EFA method will be compared by the field measurements. Conclusions and comparisons will be presented in this dissertation.

CHAPTER II

FUNDAMENTAL CONCEPTS AND PARAMETERS OF BRIDGE SCOUR

2.1 INTRODUCTION

Scour is the interaction between flowing water and streambed materials. Flowing water provides the erosive force, which can be represented by shear stress applied on streambed materials. On the other hand, streambed materials can generate a resistant force to stop the scouring. The resistant force can be represented as critical shear stress of streambed materials. When the critical shear stress is less than the erosive shear stress, the scour process will occur. The scour process will be stopped when these two stresses reach a balance. The hydraulic flow properties can be changed due to the obstruction of bridge structures and geometric alteration such as flood plain changing. They can induce the flow acceleration near the bridge, which can increase the shear stress on the riverbed. Hence there is a tendency for scouring to expose the foundations of a bridge. Basically bridge scour includes the following three types: general scour, contraction scour and local scour. This chapter will introduce an overview of bridge scour concepts and the basic mechanisms for contraction scour and local scour.

2.2 TYPES OF BRIDGE SCOUR

The types of scour that can occur at the bridge crossing section typically include general scour, contraction scour, and local scour. At a particular bridge crossing section,

any or all of the different types of scour can occur simultaneously and interactively, as illustrated in the following Figure 2.1.

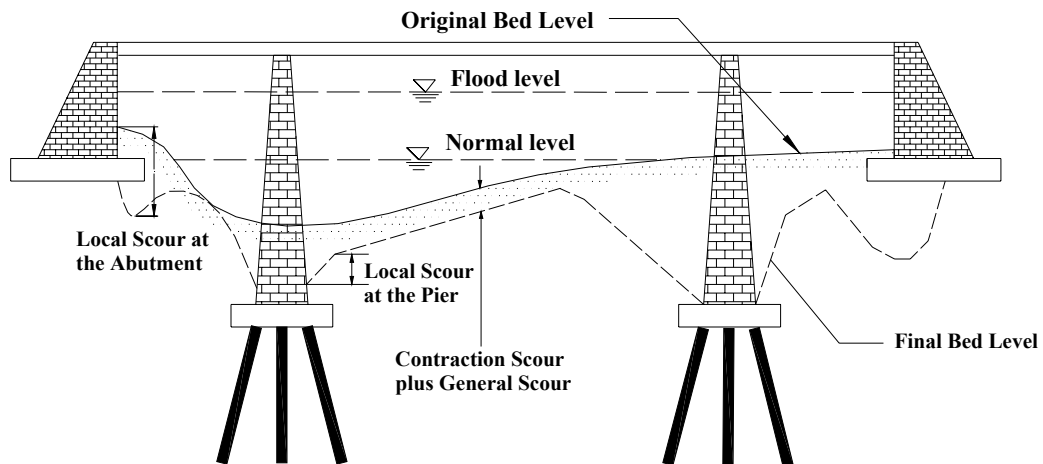


Figure 2.1: Different Types of Scour in a Typical Bridge Cross Section

2.2.1 GENERAL SCOUR

General scour consists of two types: aggradation and degradation. These are long-term streambed elevation changes due to natural or man-induced causes, which can affect the reach of the river on which the bridge is located (Richardson and Davis, 2001). Aggradation involves the deposition of the excavated materials from the channel upstream of the bridge, whereas degradation involves the scouring of the streambed due to the deficit of sediment from upstream. General scour can be due to channel alteration, dam/reservoir construction, stream-bed mining, land-use changes, climates, etc.

2.2.2 PIER SCOUR AND ITS MECHANISMS

Pier scour involves removal of streambed material from around piers. The acceleration of the flow due to the bridge piers will induce a horse vortex and a wake vortex around the bridge piers. The horse vortex at the base of bridge piers is basically the direct force which erodes streambed materials. Bridge piers in a flow cause a horizontal constriction of the flow (Hoffmans and Verheij, 1997). The shape and depth of local scour around bridge piers depends primarily on the geometry of the pier. The flow pattern and scour-hole at a pier is illustrated in Figure 2.2. The phenomenon of the bridge pier scour process is relatively complicated. This complex flow pattern in the scour hole has been described in detail by several authors, for example Breusers & Raudkivi (1991), Dargahi (1987), and Herbich (1984). The principal features of the flow in pier scour are the down flow ahead of the pier, the horseshoe vortices at the base of the pier, the surface roller ahead of the pier, and the wake vortices downstream of the pier. The down flow is the consequence of the obstruction of the pier, which decelerates the flow velocity ahead of the pier. The down flow impinging on the streambed acts like a vertical jet. A groove can be generated immediately to the front of the pier. Both the horseshoe and wake vortices remove the streambed materials from the pier base region. However, the intensity of wake vortices diminishes rapidly as the distance downstream of the pier increases (Richardson and Davis, 2001). Therefore, immediately downstream of a long pier there is often deposition of streambed materials.

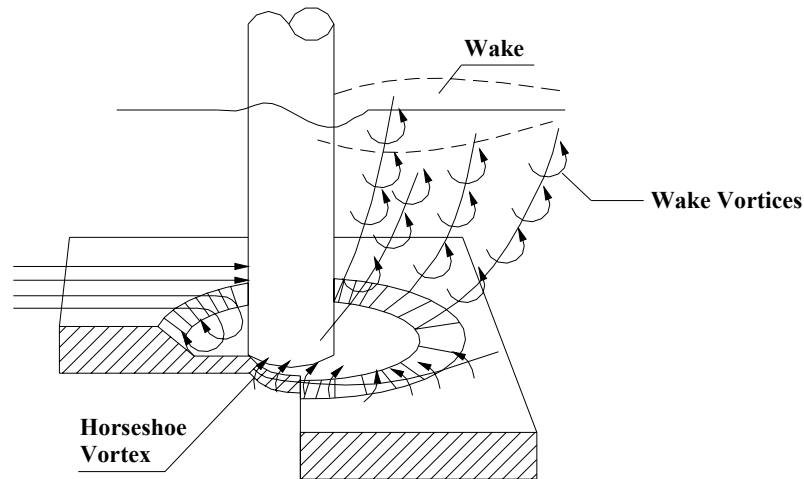


Figure 2.2: Flow Pattern around a Bridge Pier (after Herbich, 1984)

2.2.3 CONTRACTION SCOUR AND ITS MECHANISMS

Contraction scour, in a natural channel or at a bridge crossing section, involves the removal of materials from the bed and banks across all or most of the channel width. Flow properties can be changed due to the abutment of the bridge or its road approaches which cause some constriction of the flow. An example is bridge approaches encroaching on the floodplain of a river. A changing flow pattern simulates contraction scour, which induces increased velocity and shear stress. Contraction scour can be caused by the following factors (Richardson et al., 2001):

- Natural stream constrictions
- Long highway approaches to the bridge over the floodplain
- Ice formation or jams
- Natural beams along the banks due to sediment deposits

- Islands or bar formations upstream or downstream of the bridge
- Debris
- Vegetative growth in the channel or floodplain.

The most common cause of contraction scour is the approach embankment of the bridge encroaching into the channel or onto the floodplain and causing flow contraction. In this research only this situation will be considered as the cause of contraction scour. When bridge structures constrain the flow, the flow will be accelerated, according to the flow continuity theory, due to the decreasing flow area when the flow passes the bridge cross section or the contracted channel. Besides, more flow turbulence will be created by the contraction. Hence the average flow velocity and the shear stress applied on the streambed will be increased due to an increasing velocity and turbulence, which will cause more streambed materials to be removed. When the erosive shear stress is larger than the critical shear stress of streambed materials, the contraction scour occurs. As the channel bed is being scoured, the increasing flow area will decrease the average flow velocity. Meanwhile, the shear stress decreases as well, so when the erosive shear stress and the critical shear stress of soil reach an equilibrium, the contraction scour stops. Figure 2.3 shows a simplified contracted channel. The basic parameters for contraction are shown in this figure as well.

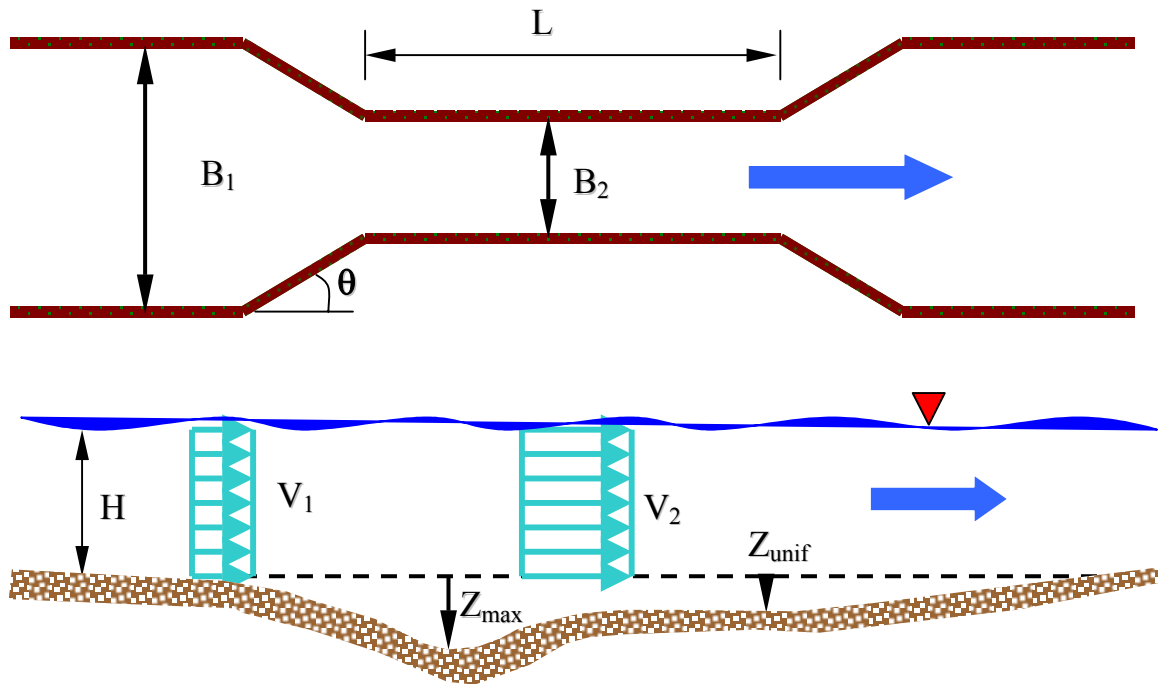


Figure 2.3: Parameters in Contraction Scour

B_1 and B_2 are the upstream and contracted widths of the channel; L is the length of contraction; θ is the angle of the contraction transition angle; V_1 is the mean depth velocity in the upstream channel; V_2 is the mean depth velocity in the contracted section of the channel; H is the upstream channel water depth.

In contraction scour, two scour types can happen in different locations: Z_{max} (Cont) is the maximum contraction scour, which is the maximum depth of scour along the centerline of the channel, and Z_{unif} (Cont) is the uniform contraction scour depth, which is the uniform depth of scour along the centerline of the channel.

2.3 FACTORS INFLUENCING THE SCOUR PROCESS

Several factors influence the scour process, i.e. the geometry of the channel or bridge, the flow conditions, and soil properties. From the macro-view, Neil (1973) summarized the influence factors for any given bridge.

- Slope, natural alignment and channel shift;
- Type and amount of bed-material in transport;
- History of former and recent floods;
- Accumulations of ice, logs or other debris;
- Constriction and/or realignment of flow due to the bridge and its approaches;
- Layout and geometry of modification works;
- Geometry and alignment of piers;
- Placement or loss of rip-rap and other protective materials;
- Natural or man-made changes in flow or sediment regime;
- Accidents, such as collapse of a nearby structure.

From the micro-view, the factors influencing scour will involve soil properties. The erosive power of flowing water in a channel boundary is determined primarily by local shear stress, but also by associated velocities and turbulent fluctuations of velocities near the boundary. The relationship of local velocities and cross-sectional average velocities is complex and depends on depth of flow, boundary roughness and channel geometry. Average velocity and depths therefore give the best indication of erosive power, because calculations based on more refined measures are impractical for engineers in many

cases. Neil (1973) found that the resistance to erosion of non-cohesive materials depends on primarily on grain size, size distribution, grain density, and to a lesser extent on grain shape, orientation, and packing arrangement. Practically speaking, sand and gravel are often based only on grain size in scour analysis.

The influence factors for cohesive materials are more complicated than for non-cohesive materials. The resistance erosion of fine-grained cohesive materials depends on a number of physiochemical and environmental factors, since the bonding force between particles must be broken down before erosion can occur.

CHAPTER III

EXISTING METHODS FOR BRIDGE SCOUR PREDICTION

3.1 INTRODUCTION

In the last several decades, local scour around the bridge piers has been extensively investigated by many researchers. Many contributions have been made toward predicting bridge pier scour depth on non-cohesive soils and contraction scour in long rectangular channels. Some prediction methods have been extensively used; for example, HEC-18 (Richardson and Davis, 2001). Commonly, it is more straightforward to develop the prediction method in non-cohesive soils because the scour process is mainly governed by gravitational and frictional laws. On the other hand, for cohesive soils, the scour process not only depends on the physical properties of soil particles but also on chemical and other properties. Only a few have done research on cohesive soils in contrast to non-cohesive soils.

Most developed pier scour prediction equations apply to simple bridge pier conditions; very few apply to complex pier conditions. Hence, pier scour studies on both non-cohesive and cohesive soils have been like two non-parallel developments. This indicates that more emphasis is needed on the study of cohesive soils. For contraction scour, scour depth in long rectangular contraction channels under live-bed conditions in sand has been the major concern in previous studies. Similarly, previous contraction scour studies deal only with limited conditions.

Although scour studies on cohesive soils are limited, previous research provides much valuable information for our project. There is a considerable amount of literature that gives very useful hints concerning research in cohesive soils. In this chapter, a summary of such literature will be presented, which includes the following sections: simple pier scour in cohesive soils, complex pier scour in non-cohesive soils and contraction scour in non-cohesive soils.

3.2 LITERATURE REVIEW FOR SIMPLE PIER SCOUR IN COHESIVE SOILS

Simple pier scour has been studied extensively in contrast to other scour types. In most cases, simple pier scour is defined in terms of the following conditions.

1. Deep water: Involving a ratio between water depth and a pier width larger than 2.5 (Johnson, 1994)
 2. Single pier no influence from adjacent piers
 3. Cylindrical pier
- **Annandale (1995)** The Erodibility Index Method was developed by Annandale (1995). This method can be used to estimate scour of rock or other resistant earth materials around bridge piers. The method is based on a relationship between the ability of rock and other earth materials to resist erosion (required erosive power) and the magnitude of the erosive power of water (available erosive power). The required erosive power is the erosive power necessary to erode the soil away, and the available erosive power is the erosive power provided by the flowing water. Pier scour occurs when the available erosive power is greater than the required erosive power. But pier scour stops if

the available erosive power is less than the required erosive power. The available erosive power around a bridge pier decreases at the base of a pier which has an increasing depth of scour. The ability of earth material to resist erosion usually increases with an increasing depth below the original riverbed. The maximum scour depth can be estimated by comparing the available erosive power to the required erosive power.

Annandale (1995) used Kirsten's classification system to develop the Erodibility Index Method. The Erodibility Index, which is identical to Kirsten's Excavatability Index K (Kirsten, 1982), can be expressed as the following equation:

$$K = M_s K_b K_d J_s \quad (3.1A)$$

Where K is the Erodibility Index, M_s is the intact material strength number, K_b is the particle/block size number, K_d is the shear strength number, and J_s is the relative ground structure number. Each parameter can be obtained from borehole logs and standard laboratory tests. The required stream power can be calculated from the erodibility index by the following equations:

$$P_{required} = \begin{cases} K^{0.75} & K > 0.1 \\ 0.96K^{0.44} & K < 0.1 \end{cases} \quad (3.1B)$$

The available stream power at the base of a pier can be calculated for different types of piers using the method developed by the Federal Highway Administration's (FHWA) hydraulic laboratory for granular materials.

Annandale constructed relationships between stream power amplification at the base of bridge piers P_c/P_a and dimensionless scour depth z/z_{max} by fitting experimental data for different types of piers as follows:

For round piers

$$\frac{P_c}{P_a} = 3.2997 \left(\frac{z}{z_{\max}} \right)^2 - 9.6589 \left(\frac{z}{z_{\max}} \right) + 7.661 \quad (3.1C)$$

For square piers

$$\frac{P_c}{P_a} = -4.0741 \ln \left(\frac{z}{z_{\max}} \right) + 1.3186 \quad (3.1D)$$

For rectangular piers (0 degree skew angle)

$$\frac{P_c}{P_a} = 11.643 \left(\frac{z}{z_{\max}} \right)^2 - 22.71 \left(\frac{z}{z_{\max}} \right) + 12.614 \quad (3.1E)$$

For rectangular piers (15 degrees skew angle)

$$\frac{P_c}{P_a} = 5.1806 \left(\frac{z}{z_{\max}} \right)^2 - 13.212 \left(\frac{z}{z_{\max}} \right) + 9.3696 \quad (3.1F)$$

For rectangular piers (30 degrees skew angle)

$$\frac{P_c}{P_a} = 6.1026 \left(\frac{z}{z_{\max}} \right)^2 - 16.998 \left(\frac{z}{z_{\max}} \right) + 12.267 \quad (3.1G)$$

Where z is the scour depth, Z_{\max} is the maximum scour depth calculated by using the HEC-18 equation, P_c is the stream power at the pier base (or the available stream power), and P_a is the approach stream power per unit area in the upstream reach and calculated by the FHWA equation.

- **Guadavalli (1997)** Guadavalli conducted extensive experimental research on cylindrical pier scour for different soil beds in the flume. The results indicated that the existence of cohesive soils has no noticeable influence on the maximum scour depth

comparing the values predicted by HEC-18. A relatively simple equation was proposed to predict simple pier scour as:

$$z_{\max} = 0.18 \left(\frac{BV}{\nu} \right)^{0.635} \quad (3.2)$$

Where B is the pier diameter, V is the mean approaching velocity, and ν is the kinematical viscosity of water.

In the study it was also found that the hyperbola model works well to simulate the time history of scour development, especially for scour in cohesive soils where scour depth strongly depends on the scouring time.

- **Hosny (1995)** Hosny conducted flume tests with circular piers, with diameters measuring from 0.1 to 0.15 meters in different soil layers; i.e., mixed beds (cohesive and non-cohesive soil), unsaturated cohesive soil and saturated cohesive soil. He found that the clay content, the soil compaction and the initial water content (IWC) could affect local pier scour depth. He also found that the existence of cohesive soil could reduce the final scour depth, and that the time required to reach maximum scour depth in saturated cohesive soils was longer than that in mixed soils. Hosny developed the following equations for local pier scour prediction. Relationships were established between scour depth, clay content, compaction, initial water content, and the Froude Number. The equations were developed on the basis of the data regression analysis and dimensional analysis:

For sandy-clay soil:

$$Z_{\max} = 18.9B \left(\frac{Fr}{1+C} \right)^2 \quad (3.3A)$$

For unsaturated and saturated cohesive soil:

$$Z_{\max} = 0.9B(IWC)^{-2/3} Fr^{3/2} Comp^{-2} \quad (3.3B)$$

Scour depth Z_{\max} relates to the volume of the scour hole V_s as:

$$Z_{\max} = kB \left(\frac{V_s}{B^3} \right)^{k'} \quad (3.3C)$$

Where Z_{\max} is the maximum scour depth, B is the pier diameter, C is the clay content, $Comp$ is the degree of compaction ($0.58 < Comp < 1$), IWC is the initial water content ($0.15 < IWC < 0.5$), k is a constant, k' is a constant ($0.4 < k' < 0.7$), V_s is the volume of scour, $Fr = V / \sqrt{gH}$ is the Froude number ($0.18 < F < 0.51$), V is the average approach velocity, H is water depth and g is the gravitational acceleration.

- **Iverson (1998)** The pier scour equation in Richardson and Davis (1996) proposed a K_4 correction factor, which considered the armoring effect of the scour hole due to the size of bed materials. This factor only considered the D_{50} equal to or larger than 0.06m ($D_{50} \geq 0.06m$) cases, so that this correction factor is not applicable for clay. Iverson (1998) developed a new bed material size factor K_4 for clay soils. He found that this K_4 factor related to unconfined compression strength. He recommended the following equation for the K_4 factor calculation:

$$K_4 = 0.677 \log \left(500 \frac{B}{S_u} \right) \quad (3.4)$$

Where B is the pier width (inches), S_u is the unconfined compressive strength of clay (lbs/ft^2). In order to apply this correction factor to HEC-18, the unconfined compressive strength (lbs/ft^2) has to be greater than 17 times that of the pier width (inches).

- **Kwak (2000)** Kwak extended Guadavalli's (1997) pier scour research to include multi-flood and multilayered soil conditions, and the SRICOS method was proposed. In this method, soil erosion functions measured by EFA (Erosion Function Apparatus) and flow conditions were combined together in a series of hyperbola models, which were joined together in a time sequence to simulate the whole time history of scour development.
- **Molinas et al. (1999)** Molinas et al. (1999) investigated bridge pier scour in unsaturated and saturated cohesive soils in three large flumes. The diameters of piers were 0.152 m and 0.102 m. From the flume tests, they found that the clay content, soil compaction, and initial water content (IWC) would influence the pier scour depth. Molinas et al. (1999) developed the following equations for pier scour prediction based on dimensional analysis and experimental data regression:

For unsaturated cohesive soil

$$\frac{z_{\max}}{B^{0.66} H^{1.13}} = \begin{cases} 0 & \begin{pmatrix} Fr \leq 0.2 \\ Comp \geq 0.85 \end{pmatrix} \\ 45.95(IWC)^{-0.36} Fr^{1.92} Comp^{1.62} & \begin{pmatrix} Comp < 0.85 \\ Fr > 0.2 \end{pmatrix} \end{cases} \quad (3.5A)$$

For saturated cohesive soil

$$\frac{z_{\max}}{H} = \begin{cases} 0 & Fr < Fr_i \\ 9.61 \left(\frac{B}{H} \right)^{0.66} (IWC)^{2.62} (Fr - Fr_i)^{0.32} & Fr > Fr_i \end{cases} \quad (3.5B)$$

Where Z_{\max} is maximum scour depth, H is depth of approach flow, B is pier width, $Comp$ is degree of compaction, IWC is initial water content, $Fr = V/\sqrt{gH}$ is the Froude number, V is the approach average velocity, H is water depth, g is the gravitational acceleration $Fr_i = V_i/\sqrt{gH}$ is the scour initiating Froude number, and $V_i = 0.065/(IWC)^{2.92}$ is the scour initiating velocity.

- **Richardson and Davis (2001)** The pier scour prediction equation is the most commonly used equation for bridge pier scour prediction, which is from the FHWA Hydraulic Engineering Circular called HEC-18. Richardson and Davis (2001) proposed the following equation to predict the depth of bridge pier scour:

$$Z_{\max} = 2H \cdot K_1 K_2 K_3 K_4 \left(\frac{B}{H} \right)^{0.65} F_r^{0.43} \quad (3.6)$$

Where H is the upstream water depth, m; K_1 is the correction factor for pier nose shape; K_2 is the correction factor for angle of attack of the flow; K_3 is the correction factor for the bed condition; K_4 is the correction factor for armoring by material size; B is the pier width, m; F_r is the Froude number defined as V/\sqrt{gH} where V is the upstream velocity, m/s; and g is the acceleration of gravity (9.81 m/s^2).

3.3 LITERATURE REVIEW FOR COMPLEX PIER SCOUR IN SAND

Compared with simple pier cases, complex pier cases involve the following factors that don't relate to simple pier cases: (1) shallow water effect, (2) pier spacing effect, (3) pier shape effect, and (4) attack angle effect. Studies on complex pier scour relating to non-cohesive soils are relatively more developed than those relating to cohesive soils. Most previous researchers have dealt with complex pier scour by applying correction factors to simple pier cases.

3.3.1 SHALLOW WATER EFFECT

The shallow water effect on pier scour is also called "wide pier effect." This occurs when the flow depth, H , is relatively small compared to the pier size, B . Observations show that the scour depth increases with the depth of flow until a deep water condition is reached, where the scour depth is almost independent of the flow depth. The shallow water effect is a common phenomenon in pier scour evaluations. It should be noticed that, although some pier scour prediction equations include water depth terms in formulas such as HEC-18, the shallow water effect was not fully reflected because the original equation was obtained in a relatively deep water situation. Research on the shallow water effect in non-cohesive soils can provide a firm basis for studying the shallow water effect in cohesive soils. The best known studies on the shallow water effect in non-cohesive soils were contributed by Ettema (1980), Johnson (1994) and Melville (1999).

- **Ettema (1980)** Ettema stated that the shallow water effect was influenced by the ratio of the pier size to the size of sediment, and suggested that $H/B=3$ could be a good

range in which to define shallow water in coarse sands. Ettema (1980) also concluded that three factors lead to the shallow water effect: (1) The degree to which the portion of approaching flow available to be diverted into the scour hole diminishes, (2) The development of the scour hole as influenced by the formation of a sediment bar behind the pier, (3) The formation of a surface roller as an opposite sense of rotation to the horseshoe vortex and down-flow into the scour hole.

- **Johnson (1994)** Johnson conducted a set of pier scour experiments to determine the shallow water effect on pier scour, using these experiment data as well as other laboratory data from Chiew (1984), Colorado State University (CSU) (1966), Chabert and Engeldinger (1956), Hancu (1971), Jain and Fischer (1979), Shen et al. (1969), and Yanmaz and Altinbilek (1991). Johnson and Torrico found that scour depth increases with increasing flow depth. There is a limited flow depth beyond which the pier scour depth is unaffected by flow depth. The correction factor for the shallow water effect as a supplementary to HEC-18 equation is:

$$K_w = 1.04 \left(\frac{H}{B} \right)^{0.15} Fr^{0.21} \quad (3.7A)$$

The equation is only valid for $H/B < 0.8$ and $Fr < 0.8$.

At the same time, water depth has been already considered, especially for deep-water cases, in HEC-18 as:

$$z_{\max} = 2.0K_1 K_2 K_3 K_4 H^{0.135} B^{0.65} \left(\frac{V}{\sqrt{g}} \right)^{0.43} \quad (3.7B)$$

So, the total term for water depth effect in Johnson's equation should be a combination of (3.7A) and (3.7B) as:

$$K_w = 1.04 \left(\frac{H}{B} \right)^{0.15} Fr^{0.21} H^{0.135} \quad (3.7C)$$

- **Melville (1999)** Melville and Sutherland (1988) found that the water depth effect on pier scour depth has been studied by the following researchers: Chabert and Engeldinger(1956), Lausen and Toch(1956), Hancu(1971), Bonasoundas(1973), Basak(1975), Jain and Fisher(1979), Chee(1982), Chiew (1984), and Ettema(1980). According to the ratio of water depth to pier width, Melville (1999) classified piers as either narrow pier (deep-water), intermediate pier (intermediate-water), or wide pier (shallow-water). The scour depth of the narrow pier type was controlled by pier width; wide pier was controlled by water depth; and intermediate pier was controlled by both. The corresponding correction factor is:

$$K_w = \begin{cases} \frac{8}{15} \frac{B}{H} & B/H < 0.7 \\ \frac{4}{9} \sqrt{\frac{B}{H}} & 0.7 < B/H < 5 \\ 1 & B/H > 5 \end{cases} \quad (3.8)$$

where H is water depth and B is the diameter of a single pier

3.3.2 PIER SPACING EFFECT

Spacing between the piers is one of the most important factors to affect pier scour depth around a group of piles. The pier scour depth decreases as the spacing between the piers increases because of less interference from adjacent piers. As the

spacing between the piers decreases, the scouring development will be affected by two processes. First, the vortices created around the piers will interact with each other; secondly, the flow will accelerate due to the contraction created by the adjacent piers (Elliott et. al., 1985).

- **Elliott et al. (1985)** Elliott conducted flume tests in a 0.61m wide flume on sand beds under clear-water conditions with S/B ranging from 1.6 to 13.2. The D_{50} of the sand was 0.5mm and the measured critical velocity was 0.3m/s. The pier models were rectangular blocks with front semi-circular noses (46mm wide and 150mm long). The flow depth was kept at 100mm. The pier spacing effect was represented in Equation 3.9.

$$K_{sp} = \begin{cases} 1 + \frac{1.79}{\left[\left(\frac{S}{B}\right) - 1\right]^{0.695}} & S/B < 4 \\ 4.34 - 0.62\left(\frac{S}{B}\right) & 4 < S/B < 7 \\ 1 & S/B > 7 \end{cases} \quad (3.9)$$

where S is the center-to-center spacing of piers and B is the diameter of a single pier

- **Gao (1993)** Gao summarized the development and verification of scour equations based on laboratory studies and a large amount of field data that is currently used in bridge design in China. Chinese methods for pier scour prediction provide for a pier spacing correction factor as follows:

$$K_{SP} = 1 + 5 \left(\frac{1}{1 + \left(\frac{S}{D}\right)} \right)^2 \quad (3.10)$$

where S is the center-to-center spacing of piers and D is the diameter of a single pier.

- **Mohammad and Jones (1998)** conducted flume experiments to measure pier scour around exposed pier groups for various conditions including different spacing, different flow attack angles, and so on. They studied the pier spacing effect in a 1.8m wide flume with water depth of 0.27m under clear-water conditions. The soil bed was composed of very uniform sand with D_{50} of 0.28mm. The test model was square piles arrayed in a 3x3 matrix in the middle of the flume. He developed the following equation for a pier spacing correction factor:

$$K_{sp} = A \left(1 - e^{\left(1 - \frac{S}{D}\right)} \right) + e^{0.5 \left(1 - \frac{S}{D}\right)} \quad (3.11)$$

where S is the center-to-center spacing of the piers; D is the diameter or width of a single pier; $A = 0.47$ for the best equation for the flume test result; and $A = 0.57$ for the high boundary of the flume test result.

- **Raudkivi (1991)** Raudkivi investigated the pier spacing effect in flume tests on sand bed conditions. The D_{50} of sand is 0.75mm and the standard deviation of the particle size is 1.32. During the tests, water depth was kept at 140mm and flow velocity at 0.285m/s, which was 92% of the critical velocity. Two cylindrical piers with 33mm diameter were installed in the middle of the flume. When the two piers were in one column (0° attack angle), the observations were:

- (1) When the two piers touch each other, the scour depth of the front pier is the same as a single pier in the flow.
- (2) When the two piers are separated, the scour depth of the rear pier begins to increase but eventually falls off.

- (3) When the two piers are separated, the scour depth of the front pier is not influenced by the rear pier.
- (4) The scour depth of the rear pier is always smaller than that of the front pier.
- (5) The scour depth between the piers diminishes rapidly and is negligible when the spacing is 10 times larger than the diameter.

3.3.3 PIER SHAPE EFFECT

The shape of bridge piers can strongly influence the flow pattern around it. Sharp or round nosed piers always produce weak horseshoe vortices which may cause less scour depth.

- **Dietz (1972)** investigated the influence of the aspect ratio of rectangular piers on the pier scour depth by comparing this with the scour depth of cylindrical piers, and the results are summarized in Table 3.1.

Table 3.1: Effect of Aspect Ratio of Rectangular Pier on Scour Depth

Shape	Rectangular Pier		
Aspect Ratio (L/B)	1:1	1:3	1:5
Depth Ratio to Cylindrical Pier	1.4	1.2	1.1

The influence of pier shape on pier scour, in both horizontal and vertical cross sections, has been extensively investigated by Laursen and Toch (1956) and Neill (1973). From the results of these authors, some typical values of the shape correction factor K_{sh} , cylindrical piers as the reference case, are summarized in Table 3.2.

Table 3.2: Pier Shape Factors (after Hoffmans G.J.C.M. and Verheij H.J. 1997)

Types of Cross Sections		K_{sp}
Horizontal	Lenticular	0.7 to 0.8
	Elliptic	0.6 to 0.8
	Circular	1.0
	Rectangular	1.0 to 1.2
	Rectangular with semi-circular nose	0.90
	Rectangular with chamfered corners	1.01
	Rectangular nose with wedge-shaped tail	0.86
	Rectangular with sharp nose 1:2 to 1:4	0.65 to 0.76
Vertical	Pyramid-like (narrowing upwards)	0.76
	Inverted pyramid (broadening upwards)	1.2

3.3.4 ATTACK ANGLE EFFECT

Attack angle is the angle between the longitudinal direction of a bridge pier and the flow direction. Attack angle is another important factor relating to pier scour depth. Attack angle is a composite effect including the changes in the shapes of a pier confronting the flow as well as the projection width of a pier. Projection width is the pier width perpendicular to the flow direction. Some literature recognized the pier projection width as the equivalent parameter for the attack angle effect.

- **Mostafa, E.A (1994)** He compared the influence of projection width on pier scour depth between piers with different shapes but the same projection width in sand. The pier shapes adapted in the experiments are plotted in Figure 3.1 and the pier scour depth comparison is summarized in Table 3.3, where the reference case was Case G.

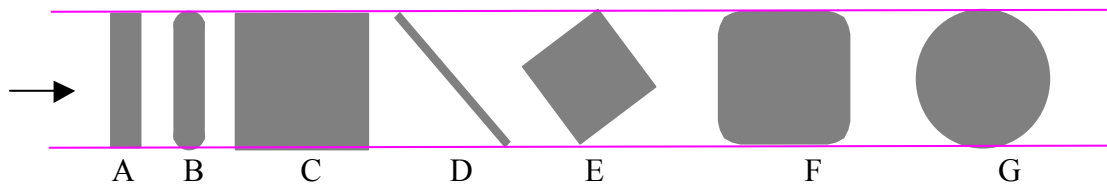


Figure 3.1: Piers with Different Shapes but the Same Projection Width
(after Mostafa, 1994)

Table 3.3: Scour Depth for Different Pier Shapes with the Same Projection Width

Shape	L/B	B (mm)	Z _{max} /Z _{max(G)}
A	4	140	1.5
B	4		1.33
C	1		1.29
D	200		1.28
E	1		1.28
F	1		1.07
G	1		1

- **Mueller (1996)** He used the concept of pier projection width to predict the 256 real pier scour cases and found it worked well by comparing it with the field measurements.
- **Raudkivi, A.J (1991)** He pointed out that the scour hole would be changed when the attack angle changed. As the flow attack angle increased, the location of maximum scour depth moved gradually along the exposed side of the pier towards the rear side. The value of the attack angle effect on the pier scour depth depended on the ratio of pier length to pier width. He indicated that the scour depth was a function of the projected width as well.

3.4 LITERATURE REVIEW FOR CONTRACTION SCOUR IN SAND

The most common cause of contraction scour is the encroachment of bridge approach embankments either into the main channel or into the flood plain, which will increase the flow velocity and the corresponding shear stress on the contracted channel streambed.

- **Laursen (1963)** He provided live and clear-water contraction scour equations on sand.

For contraction scour (live-bed case):

$$\frac{H_2}{H_1} = \left[\frac{Q_2}{Q_1} \right]^{6/7} \left[\frac{B_1}{B_2} \right]^{K_1} \begin{cases} V_* / W < 0.5, & K_1 = 0.59 \\ 0.5 < V_* / W < 2.0, & K_1 = 0.64 \\ V_* / W > 2.0, & K_1 = 0.59 \end{cases} \quad (3.12.A)$$

For contraction scour (clear water case):

$$H_2 = \left[\frac{0.025Q^2}{D_m^{2/3} B_2^2} \right]^{3/7} \quad (3.12.B)$$

$$Z_{\max} = H_2 - H_1 \quad (3.12.C)$$

Where H_1 is the average water depth in the main upstream channel, m; H_2 is the average water depth in the contracted section, m; Q_1 is the flow in the upstream channel transporting sediment, Q_2 is the flow in the contracted channel, Q is the discharge through the bridge or on the over bank at the bridge associated with the width, m^3/s ; B_1 is the width of the main upstream channel, m; B_2 is the width of the main channel in the contracted section, m; K_1 is a non-dimensional exponent; V_* is the shear velocity in

the upstream section defined as $(gH_1S_1)^{0.5}$ where g is the acceleration of gravity (9.81 m/s^2), S_1 is the slope of energy grade line of the main channel, m/m ; W is the fall velocity of bed material based on D_{50} , m/s ; D_m is the diameter of the smallest non-transportable particle in the bed material ($1.25 D_{50}$) in the contracted section, m.

To determine if the flow upstream of the bridge is transporting bed material, calculate the critical velocity for the beginning of motion V_c of the D50 size of the bed material being considered for movement and compare it with the mean velocity V of the flow in the main channel or over bank area upstream of the bridge opening. If the critical velocity of the bed material is larger than the mean velocity ($V_c > V$), then clear-water contraction scour will occur. If the critical velocity is less than the mean velocity ($V_c < V$), then live-bed contraction scour will occur. To calculate the critical velocity use Equation 3.13:

$$V_c = K_u y^{\frac{1}{6}} D_{50}^{\frac{1}{3}} \quad (3.13)$$

where V_c is the critical velocity above which bed material of size D and smaller will be transported, m/s ; y is the average depth of flow upstream of the bridge, m ; D is the particle size for V_c , m ; D_{50} is the particle size in a mixture of which 50 percent are smaller, m ; $K_u = 6.19$ SI units.

Straub (1934), Komura (1966), Gill (1981), and Lim (1998) studied the uniform contraction scour in a long contraction channel with a rectangular cross-section in sand, which is the simplest contraction case. In this case a uniform flow can be reasonably assumed at the section far from the contraction opening and the associated unidirectional flow parameters can be easily calculated by open channel theories. In the live-bed case, the continuity equations of water and sediments are satisfied. The difference between contraction scour equations depends only on the selection of sediment transport models. In the clear-water case, it is based on clear-water scour starts when the boundary shear stress is equal to the critical shear stress of streambed material, so clear water equations could be derived from this theory and the continuity equation of water.

- **Li (2002)** He summarized prediction equations for uniform contraction scour through the literature review. His works are shown in Table 3.4 and Table 3.5.

Table 3.4: Equations for Uniform Contraction Scour in Live-bed Condition (after Li, 2002)

Name and Date	Contraction Scour Prediction Equation	Flow Continuity Equation	Sediment Continuity Equation	Sediment Transportation Equation	Other Equations
Straub (1934)	$\frac{H_2}{H_1} = \left(\frac{B_2}{B_1}\right)^{6/7} \left[\left(\frac{B_2}{B_1}\right)^{1/m} \left(1 - \frac{\tau_c}{\tau}\right) + \frac{\tau_c}{\tau} \right]^{-3/7}$ (m=1.5~3.0)	$H_1 V_1 B_1 = H_2 V_2 B_2$	$B_1 q_{s1} = B_2 q_{s2}$	$q_s = [g(S_s - 1)D^3]^{1/2} \left[\frac{\tau}{\tau_c} - 1 \right]^m$	$v = \frac{1}{n} H^{2/3} S e^{1/2}$ $\tau = \frac{\rho g n^2 v^2}{H^{1/3}}$
Laursen (1960)	$\frac{H_2}{H_1} = \left(\frac{Q_t}{Q_c}\right)^{6/7} \left(\frac{B_1}{B_2}\right)^{\frac{6.2+a}{7.3+a}} \left(\frac{n_2}{n_1}\right)^{\frac{6}{7.3+a}}$	$Q = \frac{1.49}{n} B H^{5/3} S^{1/2}$	$C_1 Q_c = C_2 Q_t$	$C = \left(\frac{D}{H}\right)^{7/6} \left(\frac{\tau'_0}{\tau_c} - 1\right)^b \left(\frac{\sqrt{\tau_0/\rho}}{w}\right)^a$	$\frac{\tau'_0}{\tau_c} = \frac{V^2}{120 H^{1/3} D^{2/3}}$ $\sqrt{\tau_0/\rho} = \sqrt{gHS}$
Komura (1966)	$\frac{H_2}{H_1} = \left(\frac{\tau_{b1}}{\tau_{b2}}\right)^{\frac{2}{7}} \left(\frac{B_1}{B_2}\right)^{6/7}$	$H_1 V_1 B_1 = H_2 V_2 B_2$	$B_1 q_{s1} = B_2 q_{s2}$	$\frac{qS}{U_* D} = as \left\{ \frac{U_*^2}{\left[\left(\frac{\rho}{\rho} - 1\right)gD\right]} \right\}^p$	$\frac{U}{U_*} = E \left(\frac{R}{ks}\right)^q$ $\frac{ks}{D} = K \left\{ \frac{U_*}{\left[\left(\frac{\rho}{\rho} - 1\right)gD\right]} \right\}^m$
Gill (1981)	$\frac{H_2}{H_1} = C \left(\frac{B_2}{B_1}\right)^{6/7} \left[\left(\frac{B_2}{B_1}\right)^{1/m} \left(1 - \frac{\tau_c}{\tau}\right) + \frac{\tau_c}{\tau} \right]^{-3/7}$ (m=1.5~3.0)	$H_1 V_1 B_1 = H_2 V_2 B_2$	$B_1 q_{s1} = B_2 q_{s2}$	$q_s = [g(S_s - 1)D^3]^{1/2} \left[\frac{\tau}{\tau_c} - 1 \right]^m$	$v = \frac{1}{n} d^{2/3} S e^{1/2}$ $\tau = \frac{\rho g n^2 v^2}{d^{1/3}}$
Lim (1998)	$\frac{H_2}{H_1} = \left(\frac{B_2}{B_1}\right)^{0.75}$	$H_1 V_1 B_1 = H_2 V_2 B_2$	$B_1 q_{s1} = B_2 q_{s2}$	$q_b = c(v - v_c)^4$	$\frac{v}{v^*} = m \left(\frac{d}{2d_{50}}\right)^p$ (P=1/3, m=3.9)
Graf (1998)	$\frac{H_2}{H_1} = \left(\frac{B_1}{B_2}\right)^{6/7} \left(\frac{t_1}{t_2}\right)^{3/7} \left(\frac{r_1}{r_2}\right)^{1/7}$	$H_1 V_1 B_1 = H_2 V_2 B_2$	$B_1 q_{s1} = B_2 q_{s2}$		

Table 3.4: Continued

Name and Date	Contraction Scour Prediction Equation	Flow Continuity Equation	Sediment Continuity Equation	Sediment Transportation Equation	Other Equations
Chang & Davis (1998)	$H_s = K \left(\frac{B_1}{B_2} \right)^\alpha (H_1 V_1)^\alpha - H_1$	$H_1 V_1 B_1 = H_2 V_2 B_2$	$B_1 q_{s1} = B_2 q_{s2}$		

Table 3.5: Equations for Uniform Contraction Scour under Clear Water Conditions (after Li, 2002)

Name and Date	Contraction Scour Prediction Equation	Flow Continuity Equation	Critical Equation	Other Equation
Lausen. (1963)	$\frac{H_2}{H_1} = 0.13 \left(\frac{Q}{D^{1/3} d_1^{7/6} B_2} \right)^{6/7}$	$H_1 V_1 B_1 = H_2 V_2 B_2$	$\tau_c = 4D$	$\tau_0 = \frac{V_1^2}{120 D^{2/3} d_1^{1/3}}$
Komura (1966)	$\frac{H_2}{H_1} = \left(\frac{\tau_{c1}}{\tau_{c2}} \right)^{2/7} \left(\frac{B_1}{B_2} \right)^{6/7}$	$H_1 V_1 B_1 = H_2 V_2 B_2$	$\frac{\tau_c}{\rho} = ac \left[\left(\frac{\rho}{\rho} \right) - 1 \right] gD$	$\frac{U}{U_*} = E \left(\frac{R}{ks} \right)^q, \quad \frac{ks}{D} = K \left\{ \frac{U_*}{\left[\left(\frac{\rho}{\rho} - 1 \right) gD \right]} \right\}^m$
Iverson (1998)	$\frac{H_2}{H_1} = \left(\frac{2.32 q_2^3 n^2 Q}{d_1^{10/3} (\log S_u - 2.367)} \right)^{3/10}$	$H_1 V_1 B_1 = H_2 V_2 B_2$	$\tau_c = \frac{12.11 \log Su - 28.67}{V^2}$	$\tau = \frac{\mathcal{W}^2 n^2}{1.49 d^{1/3}}$

3.5 SUMMARY

Pier Scour: The influence of the existence of clay content on pier scour depth has been somewhat examined in the previous research. The reduction of pier scour depth due to clay content was clearly addressed and modeled in much literature. The critical velocity initiating the scour was introduced by Annandale (1995) and Molinas (1999). The equation calculating the critical velocity was developed by Molinas (1999), but it doesn't cover the most general cases. Richardson and Davis (2001) and Guadavalli (1997) arrived at a similar conclusion: that the maximum pier scour depths were almost the same in cohesive soil and in non-cohesive soil. However, the case for arguing this issue still exists for other researchers.

Contraction Scour: Much achievement has been made in contraction scour research, but improvements are still needed. The major concerns for potential improvement could be stated as follows:

- Soil Type: Most of the current contraction scour research was based on non-cohesive soils. Only Iverson (1998) introduced the empirical relationship between contraction scour depth and undrained shear strength of cohesive soil. However, it had not been verified by real cases.
- Research Direction: All equations in the table can only predict the uniform contraction scour depth. As it was described in Section 2.2.3, uniform contraction scour (Z_{unif}) is not the only scour happening in contraction scour. For bridge foundation design, determining the maximum contraction scour (Z_{max}) depth and its location is more important than paying attention to uniform contraction scour (Z_{unif}).

- **Contraction Geometry:** Bridges typically imposing short, abrupt contractions with complex cross-sections are generally confronted in reality with other than long rectangular channels in the flume test. The applicability of long rectangular contraction solutions to the prediction of contraction scour at bridges is uncertain (Melville and Coleman, 1999).
- **Flow Turbulence:** From the literature, all the contraction scour equations were simply based on uniform flow using open channel theories. The turbulence within the contracted channel, which is caused by merging and conflicting flows from upstream, is neglected as one of the assumptions. This leads to an underestimation of shear stress and contraction scour depth.

CHAPTER IV

SRICOS-EFA METHOD OVERVIEW

4.1 INTRODUCTION

The most widely used pier scour prediction equation is Richardson and Davis (2001), which is based on scaled model experiments in sand and has been evaluated against the observations of 56 full-scale bridges founded primarily on sand. In HEC-18 equation, nothing was found that the soil properties relate to the maximum pier scour depth. The equations in HEC-18 to predict the contraction scour depth, for live-bed and clear water cases, involve one soil parameter: the main grain size.

During the scour process, the non-cohesive soil can be eroded particle by particle. There are only gravitational and frictional laws to govern the erosion process in non-cohesive soils. Electromagnetic and electrostatic forces between particles will be neglected in non-cohesive soils. Cohesive soil may also be eroded particle by particle, but the electromagnetic and electrostatic forces between the particles will increase the scour resistance in cohesive soils (Briaud et al., 1999). Hence the scour process in cohesive soils and non-cohesive soils is different. Solely gravitational and frictional laws control the scour process in non-cohesive soils, whereas physicochemical law governs the scour process in cohesive soils. Therefore, it is not applicable for HEC-18 equations to be used in the bridge design when it is founded on the cohesive soils. Also, if doing

so, it appears to be overly conservative in the cohesive soils and therefore expansive in the bridge foundation design without considering time effect on the scour development process.

Briaud et al. (1999) developed a method called SRICOS method that stands for Scour Rate In Cohesive Soils. It is a method to predict the scour depth versus time curve around a cylindrical bridge pier. This method also can handle the multiflood hydrograph and multilayer soil system. The method fundamentally is based on the calculation of two parameters: the maximum depth of pier scour and the initial rate of scour. The maximum depth of scour can be calculated by using an equation obtained from flume tests, and the initial rate is based on an equation giving the initial shear stress obtained from numerical simulations. Then the initial scour rate will be read on the EFA erosion function curve at the corresponding value of the calculated shear stress. A hyperbola is used to connect the initial scour rate to the maximum or asymptotic scour depth and describes the complete scour depth vs. time curve. Accumulation algorithms are used to incorporate the effect of varying velocities and multilayer soil systems. There are three major components which are essential in SRICOS method. They are: soil, which represents the soil erosion properties; water, which represents the flow hydraulic conditions; and geometry of bridges or channel.

SRICOS method consists of the following steps:

1. Obtain standard 76.2 mm diameter Shelby tube samples as close to the pier as possible,
2. Perform EFA tests on the samples from the site to obtain the curve linking the erosion rate \dot{z} and hydraulic shear stress imposed τ ,
3. Determine the maximum shear stress τ_{\max} , which will exist on the river bottom around the pier at the beginning of the scour process,
4. Obtain the initial scour rate \dot{z} corresponding to τ_{\max} ,
5. Calculate the maximum depth of scour z_{\max} ,
6. Develop the complete scour depth z versus time t ,
7. Predict the depth of scour by reading the z versus t curve at the time corresponding to the duration of the flood.

The SRICOS method can only solve the single cylindrical pier in the deep water case. It is not useful for predicting the complex pier scour and contraction scour. The SRICOS-EFA method is an extension scour prediction method based upon SRICOS method. It significantly extends the applicable range. This new method can be used to handle the complex pier alone, or contraction scour alone and it can also handle the combined case of complex pier scour and contraction scour (Integrated SRICOS-EFA Method, which will be presented in Chapter VI). For complex pier case, SRICOS-EFA method will consider the effect of shallow water, the effect of pier shape, the effect of flow attack

angle on rectangular pier, and the effect of spacing between piers arrayed in a row perpendicular to the flow. For contraction scour, SRICOS-EFA method proposed the maximum contraction scour equation and initial maximum shear stress equation that include the effects of the ratio of the contracted channel width over the approach channel width, the contracted channel length, and the transition angle of channel contraction. The essential parameters of SRICOS-EFA method will be the erosion function apparatus, maximum scour depth of complex pier scour or contraction scour, maximum shear stress on complex pier scour and contraction scour, and initial scour rate for complex pier scour or contraction scour.

4.2 EROSION FUNCTION APPARATUS (EFA) OVERVIEW

EFA was developed by Dr. Jean-Louis Briaud at Texas A&M University in 1991. Now EFA has been improved to the third generation, which has been manufactured and licensed by Humboldt Manufacturing Company in Chicago.

4.2.1 BASIC FACTORS OF EFA

EFA is used to measure the erosion rate of different types of soils, ranging from clay to gravel, and from soft soils to soft rocks. EFA can measure the soil erosion behavior directly from the soil sample. The conceptual diagram and photograph of EFA will be shown in Figure 4.1 and Figure 4.2.

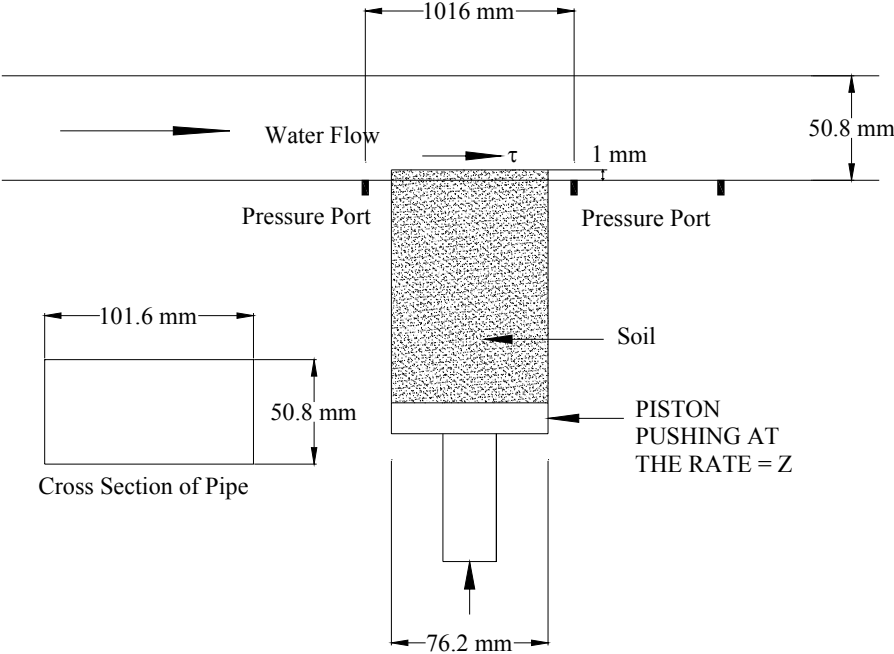


Figure 4.1: EFA Conceptual Diagram



Figure 4.2: Photography of EFA

The soil sample prepared for an EFA test is taken from the bridge site by pushing an ASTM standard Shelby tube with 76.2 mm outside diameter (ASTM 1999a). If the tested material is soft rock, a soft rock core sample can be obtained and placed in the Shelby tube. The Shelby tube will be put into the rectangular cross section pipe through a circular opening in the bottom of the pipe. The dimension of the rectangular cross section of the pipe is 101.6×50.8 mm. The end of the Shelby tube is kept flush with the bottom of the rectangular pipe. A piston pushes the soil sample until it protrudes 1mm of

soil sample into the rectangular pipe. This 1mm protrusion soil sample will be eroded by the flowed water with time. The length of the horizontal pipe in EFA is approximately 1.5 m. The water is driven through the pipe by a pump. A valve is used to adjust and regulates the flow velocities and a flow meter is installed to measure the flow rate.

4.2.2 GENERAL PROCEDURE OF EFA TEST

The general procedure of the EFA test is as follows: (After Briaud et al. 2001)

1. Place the sample in the EFA, fill the pipe with water, and wait one hour.
2. Set the initial low water velocity
3. Push 1mm soil sample into test section
4. Continue pushing the soil sample to maintain a soil or soft rock protrusion between 0 mm and 1 mm into the flow until 50 mm height of soil is eroded or 1 hour has passed, whichever comes first. The scour rate corresponding to that velocity is calculated as the total soil push divided by the time it takes to be eroded.
5. Stop the pump, take out the Shelby tube, trim the surface to be flush with the bottom of the rectangular pipe and then repeat Step 2 to 4 with another water velocity.
6. Once 6 to 8 velocities have been tested, the scour rate vs. velocity curve is obtained, and it is further converted into the scour rate vs. shear stress curve.

4.2.3 EFA TEST RESULTS DATA REDUCTION

The test result consists of the erosion rate \dot{z} versus shear stress τ curve (Figure 4.3). For each flow velocity, the erosion rate (mm/hr) is simply obtained by dividing the length of sample eroded by the time required to do so. After several attempts at measuring the shear stress τ in the apparatus it was found that the best way to obtain τ was by using the Moody Chart (Moody, 1944) for pipe flows.

$$\tau = \frac{1}{8} f \rho V^2 \quad (4.1)$$

Where τ is the shear stress on the wall of the pipe, f is the friction factor obtained from Moody Chart (Figure 4.4), ρ is the mass density of water (1000 kg/m³) and V is the mean flow velocity in the pipe.

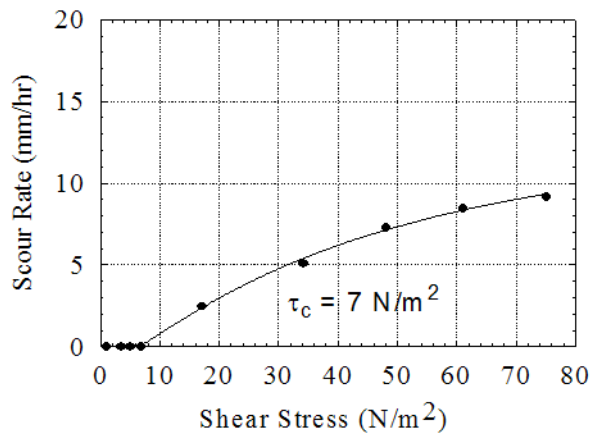


Figure 4.3: Typical EFA Test Result

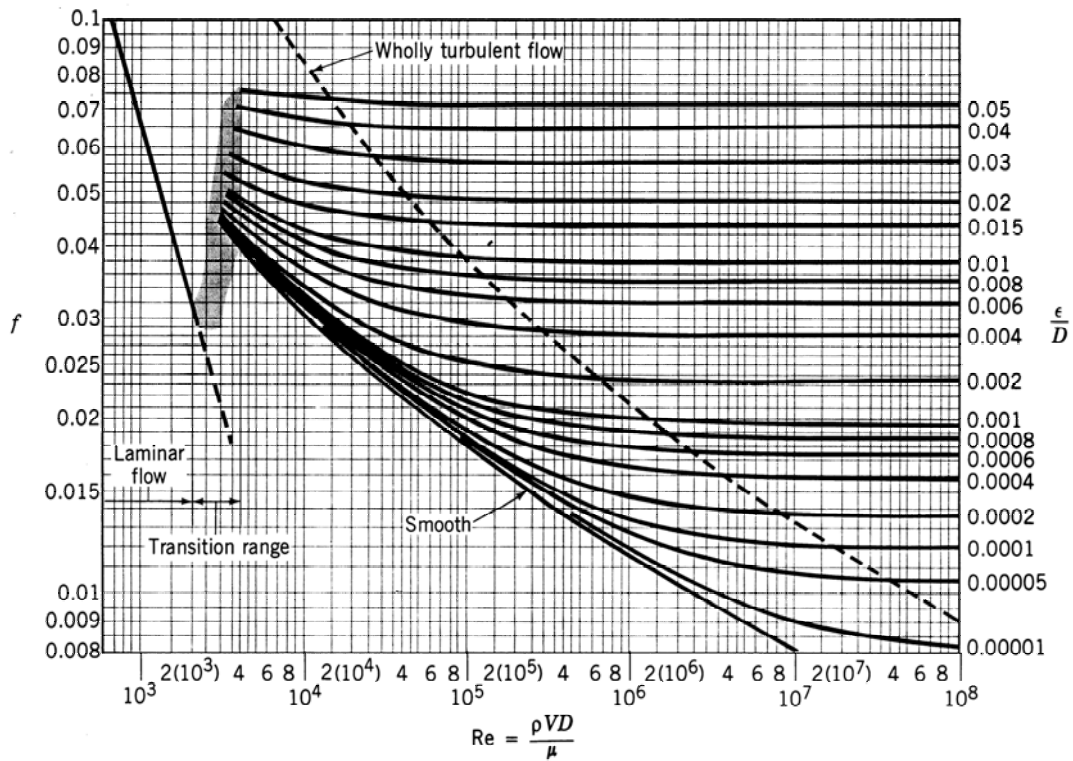


Figure 4.4: Moody Chart [Reprinted with Permission from Munson et al.] (1990)

4.2.4 ADVANTAGES OF EFA

1. Minimum sample disturbance
2. Measurement of erosion rate vs. shear stress curve
3. Measurement of the critical shear stress for the soil or soft rock directly
4. Shear stress applied on the top of sample
5. Positive pressure applied on the sample
6. Test results incorporated in a scour prediction method (SRICOS-EFA)

4.2.5 DISADVANTAGES OF EFA

After conducting more than 100 EFA tests, some disadvantages of EFA were detected, which need to improve in the future version of EFA. Additionally Humboldt Manufacturing Company (the manufacturer), has delivered the EFA to the State Department of Transportation in Maryland, Minnesota, Illinois, North Carolina, and Texas. They have performed some EFA tests and provided some valuable comments and feedback to us. Following is the summary of the disadvantages of EFA we have so far:

1. The measurement of erosion on the top of sample is based on the operator's subjective judgment. A laser device to measure the scour automatically and a warning system to remind the examiner to push one more 1 mm during test are needed.
2. Water velocities limited to a range of 0.1 m/s ~6 m/s
3. Water pressure on the sample is set at 1000 N/m²
4. Lowest detectable erosion rate 0.04 mm/hr

Humboldt and our team will continue to cooperate in order to improve the EFA and let the general EFA operation procedure be simpler, more convenient, and let the measurements be more precise. Also our team will continually trace the feedback of the Department of Transportation in different states and consider their beneficial comments in our improvement efforts.

4.3 MAXIMUM SCOUR DEPTH OF COMPLEX PIER SCOUR

4.3.1 INTRODUCTION

The equation for maximum pier scour depth Z_{\max} for cohesive soil in simple pier case was developed by a number of flume tests (Gudavalli, 1997). The flume tests were performed in different conditions by changing the pier size, water depth, water velocity, and soil type. Z_{\max} is defined as the ultimate scour depth at scouring time $t = \infty$. The equation for maximum pier scour depth was proposed as following:

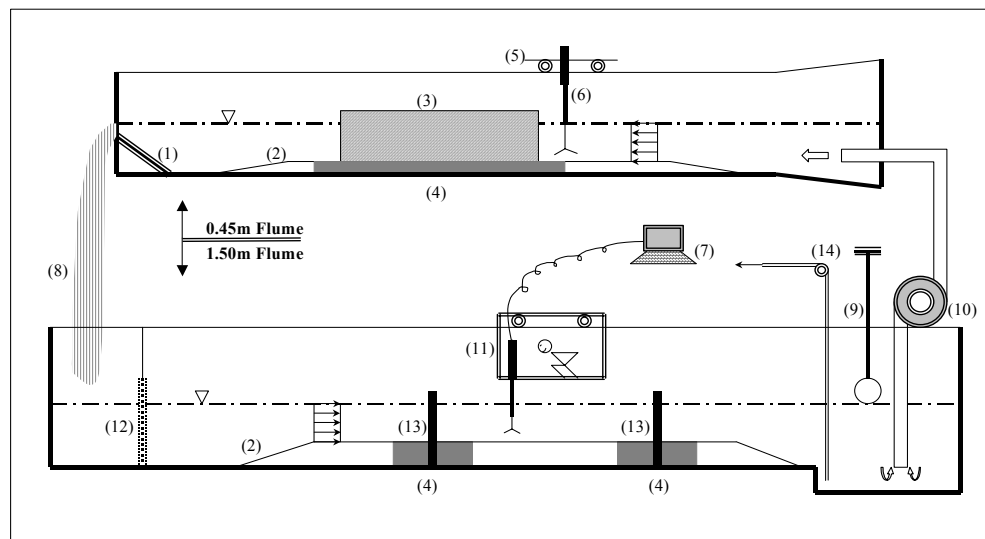
$$Z_{\max} = 0.18 \left(\frac{VB}{\nu} \right)^{0.635} \quad (4.2)$$

This equation was derived from the experiments that tested cylindrical piers in deep water cases. The complex pier case deals with the different pier shape, such as rectangular and square piers; it deals with piers attacked by the flow at a non zero angle between the flow direction and the main axis of the pier; it deals with piers in the shallow water condition; it deals with piers arranged in group piers condition, a new method need to be developed. The SRICOS-EFA method was developed for this purpose. The approach of SRICOS-EFA method consists of using the solution for the case of the cylindrical pier in deep water (Equation 4.2) and developing the correction factors including the effects of the various situations of complex pier case. Since the case of the cylindrical pier in deep water was developed on the basis of two fundamental equations (maximum scour depth and initial maximum shear stress), two sets of

correction factors had to be developed. The correction factors for the maximum scour depth were developed on the basis of flume tests, while the correction factors for the initial maximum shear stress were developed on the basis of numerical simulations. These two sets of correction factors will be presented in the following sections respectively.

4.3.2 GENERAL INFORMATION FOR THE FLUME TESTS

Li (2002) performed a series flume tests to determine the maximum pier scour depth and correction factors for the complex pier case. Two flumes are in the hydraulic laboratory at Texas A&M University. Figure 4.5 is the diagram of the flume system.



- | | | | |
|---------------|------------------------|---------------------------|------------------|
| (1) Tail Gate | (2) False Bottom | (3) Contraction Abutments | (4) Soil Tank |
| (5) Carriage | (6) ADV and Point Gage | (7) Computer | (8) Water Fall |
| (9) Switch | (10) Pumps | (11) Measuring Cage | (12) Screen Wire |
| (13) Piers | (14) Mini Pump | | |

Figure 4.5: Diagram of the Flume System (Not to Scale, after Li, 2002)

One is an in-floor concrete flume, which is 1.5 m wide, 30.48 m long and 3.8 m deep. This flume is connected as a closed system by a wooden flume, which is 0.45 m wide, 36 m long and 1.22 m deep. The in-floor concrete flume was used to conduct the complex pier scour tests, while the wooden flume was used for the contraction scour tests.

The ADV (Acoustic Doppler Velocimeter) was adopted to measure the flow velocity in the flume and is shown in Figure 4.6. The ADV uses acoustic techniques to measure the velocity of the flow. The upstream depth velocity was the basic parameter recorded for pier tests. For contraction tests, the ADV was used to measure the velocity distribution along the centerline of the contraction channel at certain water depths before the scour started and after the scour stopped. Water depth and velocity were measured in the middle of the channel 1.5 m upstream of the pier to make sure that there was no influence on these two parameters due to the existence of pier. The velocities were kept constant during the experiment. A point gage was designed for the scour depth measurement.

The soil adopted in the tests was porcelain clay, which has the predominant component of Kaolinite. The geotechnical properties of porcelain clay are summarized in the following Table 4.1.

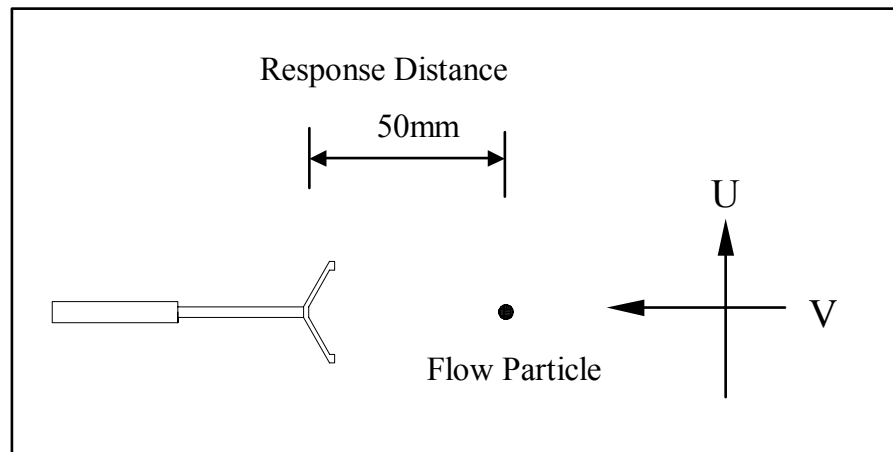


Figure 4.6: Diagram of ADV

Table 4.1: Geotechnical Properties of the Porcelain Clay

	Property	Sample 1	Sample 2
1	Liquid Limit, %	40.23	37.7
2	Plastic Limit, %	19.17	14.4
3	Plastic Index (PI), %	21.06	23.3
4	Bulk Unit Weight (KN/m^3)	19.65	24.99
5	Water Content, %	27.35	30.5
6	Shear Strength, Kpa	10.7	18.1

4.3.3 INFLUENCING EFFECTS ON MAXIMUM PIER SCOUR DEPTH IN COMPLEX PIER CASE

From literature review, the complex pier scour can be affected by following factors: 1: the effect of shallow water depth; 2: the effect of pier shapes; 3: the effect of

flow attack angle; and 4: the effect of spacing between piers, which are located in a row perpendicular to the flow direction. The effect factors were defined as K_w , K_{sh} , K_α , K_{sp} respectively. After conducting flume tests, Li (2002) summarized the testing results and proposed the correction factor equations for pier scour prediction in SRICOS-EFA method, which will be presented as following.

4.3.3.1 SHALLOW WATER EFFECT

The correction factor for shallow water effect is calculated as the ratio of the scour depth under shallow flow to the scour depth under the reference condition, where the water depth has no noticeable influence on the scour depth. The shallow water effect on pier scour depth is generally represented as a correction factor, K_w . Figure 4.7 illustrates the definitions of parameters relating to the shallow water effect.

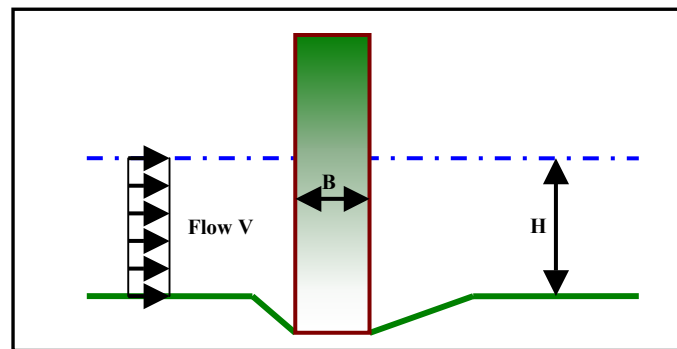


Figure 4.7: Parameter Definitions in Shallow Water Effect

Based on the flume testing results and data regression, the expression for K_w is:

$$K_w = \begin{cases} 0.85 \left(\frac{H}{B} \right)^{0.34} & H/B < 1.62 \\ 1 & H/B \geq 1.62 \end{cases} \quad (4.3)$$

where V is the upstream mean depth velocity; H is the water depth of the flow; B is the diameter of pier.

4.3.3.2 PIER SPACING EFFECT

Pier spacing effect will contribute to the pier scour due to the interaction of the adjacent piers, when the center to center spacing is too close. Pier spacing effect can be two types based on two types of piers installation: (1) in a matrix (2) in a line. In the current study, the piers are arrayed in a row with the longitude direction perpendicular to the flow direction. The pier spacing effect on pier scour depth is generally represented as a correction factor, K_{sp} , which is calculated as the ratio of the maximum scour depth of group pier (Figure 4.8) to the scour depth under reference condition. The correction factor K_{sp} proposed by Li (2002) can be written as Equation 4.4.

$$K_{sp} = \frac{B_1}{(B_1 - nB)} \quad (4.4)$$

where B is the diameter of pier; S is center to center spacing of piers; B_1 is the width of upstream channel; n is the number of piers.

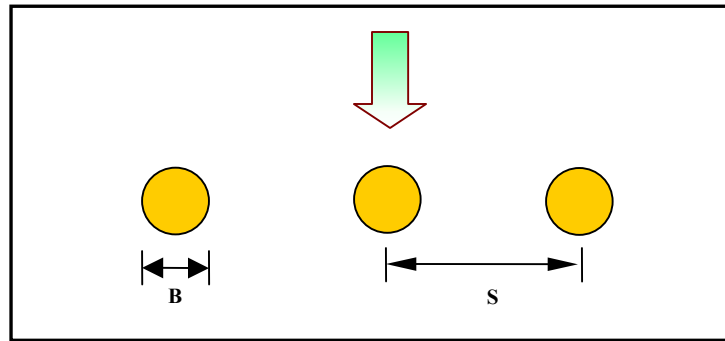


Figure 4.8: Parameter Definitions in Pier Spacing Effect

4.3.3.3 PIER SHAPE EFFECT

In order to derive the pier shape correction effect, the cylindrical pier test was the reference case. The correction factor, K_{sh} , is the ratio of the maximum pier scour depth to the reference case. It was concluded by Li (2002) that a pier shape correction factor 1.1 is approximately value for the maximum scour depth around the rectangular piers in both sand and clay when the ratio of length to width of pier (L/B) is larger than 1. The result is consistent with the correction factor is recommended by Richardson and Davis (2001). Figure 4.9 presents the basic parameters of pier shape effect.

4.3.3.4 ATTACK ANGLE EFFECT

Attack angle α is the angle between the longitudinal direction of pier and the flow direction. Correction factor, K_{α} , is represented as the flow attack angle on pier scour, which is calculated as the ratio of a given case scour depth to the reference case

scour depth. The reference cases of attack angle effect are zero attack angles for different L/B ratios of rectangular piers (Figure 4.9).

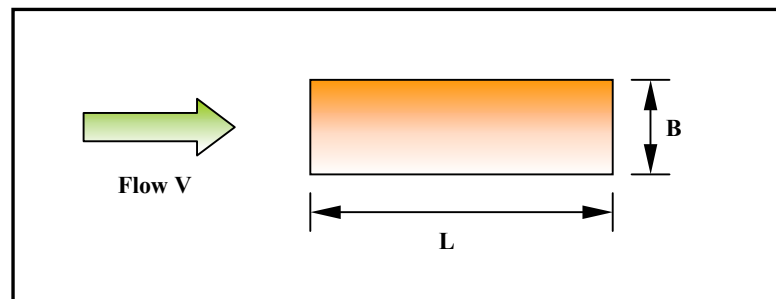


Figure 4.9: Parameter Definitions in Pier Shape Effect

where L is the length of pier; B is the width of pier.

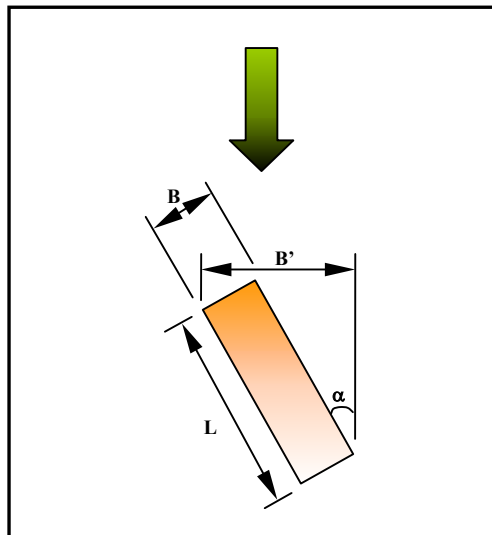


Figure 4.10: Parameter Definitions in Flow Attack Angle Effect

From the literature review Mueller (1996), Raudkivi (1991) and Mostafa (1994), Li (2002) summarized that the pier projection width, B' , is a widely accepted concept to evaluate the attack angle effect for rectangular pier (Figure 4.10). The projection width, B' , can be calculated as the following equation:

$$B' = L \sin \alpha + B \cos \alpha = B \left(\frac{L}{B} \sin \alpha + \cos \alpha \right) \quad (4.5)$$

The commonly used pier scour equations for 0° attack angle are in the form:

$$Z_{\max} = f(V, H, \text{etc}) B^n \quad (4.6)$$

Li (2002) also suggested that if the projection width, B' , is equal to pier width in Equation 4.2, the correction factor K_α can be calculated as:

$$K_\alpha = \frac{Z_{\max}(B')}{Z_{\max}(B)} = \left(\frac{L}{B} \sin \alpha + \cos \alpha \right)^n \quad (4.7)$$

In the SRICOS-EFA method, n is equal to 0.635.

4.4 MAXIMUM SHEAR STRESS IN COMPLEX PIER SCOUR

4.4.1 INTRODUCTION

The initial scour rate is an essential part of SRICOS-EFA method. The initial scour rate and the maximum scour depth are two fundamental parameters used to describe the scour development as a function of time. In complex piers scour case, the initial scour rate is obtained by calculating the maximum shear stress τ_{\max} existing around the pier before the scour hole occurs. Then the initial scour rate is read on the

erosion function curve from EFA test. Wei et al. (1997) performed a numerical simulation of the scour process in cohesive soils around cylindrical bridge piers. A method called Chimera RANS was used to simulate the scour process. The scour rate was interpolated into the streambed shear stress by a linear function. The simulation considered the flow features such as the horseshoe vortex ahead of the pier and the flow recirculation behind the pier. Based on a number of parametric runs, an empirical formula for the maximum streambed shear stress for a cylindrical pier in deep water case is presented as follows:

$$\tau_{\max}(Pier) = 0.094 \rho V^2 \left[\frac{1}{\log R_e} - \frac{1}{10} \right] \quad (4.8)$$

The approach to obtain the maximum shear stress equation in complex pier case is the same as the approach for the maximum pier scour equation in simple pier case. The formula of maximum shear stress for the case of the cylindrical pier in deep water (Equation 4.8) will be the basic equation. The correction factors including the effects of shallow water, pier shape, pier spacing and flow attack angle for complex pier case will be developed then applied to the simple pier case.

4.4.2 GENERAL INFORMATION OF THE NUMERICAL SIMULATIONS FOR MAXIMUM SHEAR STRESS IN COMPLEX PIER CASE

In the present study, the three dimensional flow Chimera RANS (Reynolds Averaged Navier Stokes) method of Chen et al (1993, 1995a, b, 1997) is used. The

computational domain is first divided into a number of smaller grid blocks, which allow complex configurations and flow conditions to be modeled efficiently through the judicious selection of different block topology, flow solvers and boundary conditions. The Chimera domain decomposition technique was used to connect the overlapped grids together by interpolating information across the block boundaries. The Reynolds stresses were evaluated using the two-layer turbulence model of Chen and Patel (1988). The mean flow and turbulence quantities were calculated using the finite-analytical method of Chen, Patel, and Ju (1990). The SIMPLER/PISO pressure-velocity coupling approach of Chen and Patel (1989) and Chen and Korpus (1993) were used to solve for the pressure field. A detailed description of the multiblock and chimera RANS methods is given in Chen and Korpus (1993) and Chen, Chen and Davis (1997). A useful summary of that method can be found in Nurtjahyo (2002). This summary discusses the governing equations including turbulence modeling (Reynolds-Averaged Navier-Stokes or RANS equations), the boundary conditions on the pier surface, the river bottom, the outer boundaries, and the free water surface.

The computer code has the ability to simulate the development of the scour hole around the pier as a function of time. This is done by including an erosion function and linking the vertical erosion rate to the shear stress at the interface between the water and the soil. The program then steps into time by adjusting the mesh in the vertical direction

after each time step as the scour hole develops. This option is not necessary to obtain the maximum shear stress before scour starts, since in this case the bottom of the river is kept flat.

A typical run consists of the following steps:

1. Obtain the information for the problem: water depth, mean depth velocity at the inlet, pier size and pier shape.
2. Calculate the Reynolds Number and Froude Number because they influence the size and distribution of the grid elements.
3. Generate the grid using a program called GRIDGEN (about 4 days work).
4. The input consists of the Reynolds Number, the Froude Number, and the boundary conditions on all surfaces. The initial condition consists of the velocity profile at the inlet and is automatically generated by the program on the basis of the inlet mean depth velocity and the geometry.
5. Typical runs last 5 hours of CPU time on the Texas A&M University SGI supercomputer when only the bed shear stress is required. The CPU time increases to 20 hours when the scour development needs to be simulated.
6. The output consists of the following parameters in the three dimensions: velocity vectors, pressure, bed shear stress, and turbulent kinetic energy.

4.4.3 INFLUENCING EFFECTS ON MAXIMUM SHEAR STRESS IN COMPLEX PIER CASE

Four effects were considered in the maximum shear stress in complex pier case. These effects include: the effect of shallow water depth; the effect of pier shapes; the effect of flow attack angle; and the effect of spacing between piers, which are located in a row perpendicular to the flow direction. The effect factors were defined as $k_w, k_{sh}, k_\alpha, k_{sp}$ respectively. Nurtjahyo (2002) proposed the calculation equations for the four effect factors by using the numerical simulations.

4.4.3.1 SHALLOW WATER EFFECT ON MAXIMUM SHEAR STRESS

The τ_{\max} is the maximum shear stress that exists on the river bed just before the scour starts to develop. The parameter $\tau_{\max(\text{deep})}$ is the value of τ_{\max} for the deep water case and is given by Equation 4.8. The shallow water correction factor, k_w , is the ratio of $\tau_{\max}/\tau_{\max(\text{deep})}$. The data points on Figure 4.11 correspond to the results of the four numerical simulations. By regression, Equation 4.9 proposed for the correction factor k_w giving the influence of the water depth on the maximum shear stress is:

$$k_w = \frac{\tau_{\max}}{\tau_{\max}(\text{deep})} = 1 + 16e^{-\frac{4H}{B}} \quad (4.9)$$

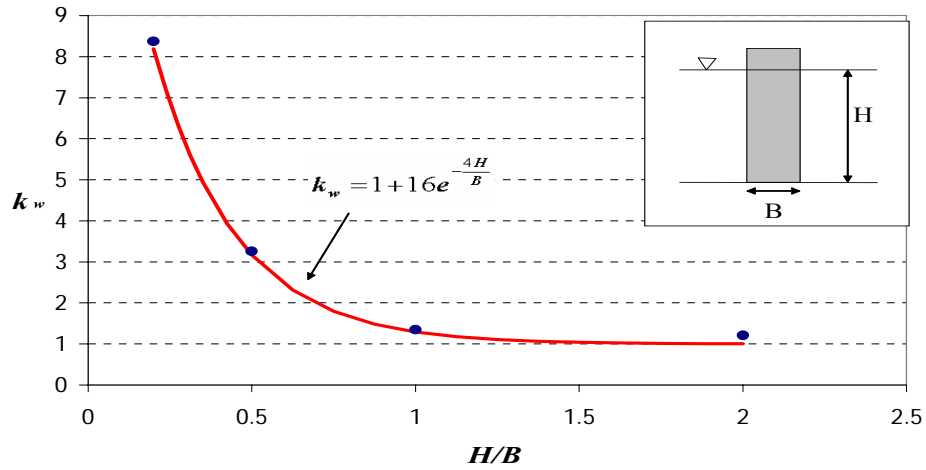


Figure 4.11: Relationship between $k_w (= \tau_{\max}/\tau_{\max(\text{deep})})$ and H/B

4.4.3.2 PIER SPACING EFFECT ON MAXIMUM SHEAR STRESS IN COMPLEX PIER CASE

The parameter $\tau_{\max(\text{single})}$ is the value of τ_{\max} for the case of a single pier in deep water and is given by Equation 4.8. The pier spacing correction factor, k_{sp} , is the ratio $\tau_{\max}/\tau_{\max(\text{single})}$. The data points on Figure 4.12 correspond to the results of the four numerical simulations. By regression, the Equation 4.10 proposed for the correction factor k_{sp} giving the influence of the pier spacing on the maximum shear stress is:

$$k_{sp} = \frac{\tau_{\max}}{\tau_{\max(\text{single})}} = 1 + 5e^{-1.1\frac{S}{B}}. \quad (4.10)$$

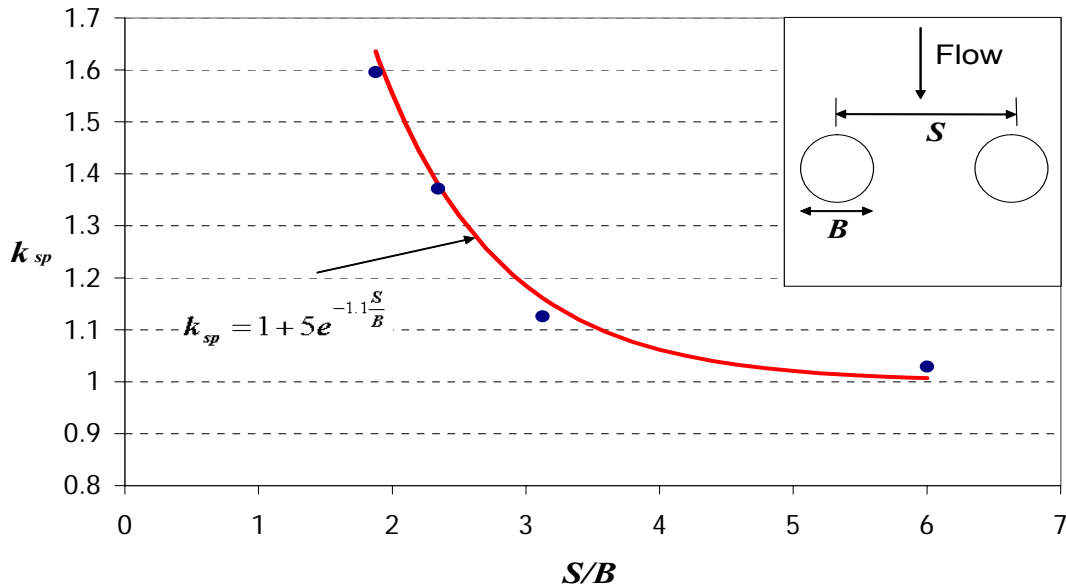


Figure 4.12: Relationship between k_{sp} ($= \tau_{\max}/\tau_{\max(\text{single})}$) and S/B for deep water $H/B > 2$)

4.4.3.3 PIER SHAPE EFFECT ON MAXIMUM SHEAR STRESS IN COMPLEX PIER CASE

The parameter $\tau_{\max(\text{circle})}$ is the value of τ_{\max} for the case of a circular pier in deep water and is shown by Equation 4.8. The pier shape correction factor, k_{sh} , is the ratio $\tau_{\max}/\tau_{\max(\text{circle})}$. The data points on Figure 4.13 correspond to the results of the seven numerical simulations. The correction factor for shape effect, k_{sh} is given by the following Equation 4.11 which was obtained by regression of the data points on Figure 4.13.

$$k_{sh} = 1.15 + 7e^{-4\frac{L}{B}} \quad (4.11)$$

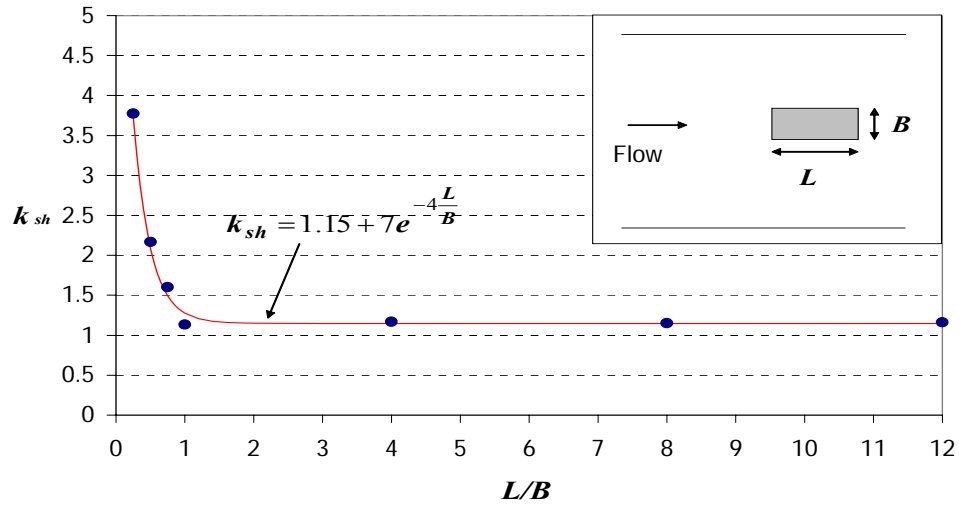


Figure 4.13: Relationship between k_{sh} ($= \tau_{\max}/\tau_{\max(\text{circle})}$) and L/B for Deep Water ($H/B > 2$)

4.4.3.4 ATTACK ANGLE EFFECT ON MAXIMUM SHEAR STRESS IN COMPLEX PIER CASE

The parameter $\tau_{\max(0 \text{ degree})}$ is the value of τ_{\max} for the case of a pier in line with the flow in deep water and is shown by Equation 4.8. The attack angle correction factor, k_{α} , is the ratio $\tau_{\max}/\tau_{\max(0 \text{ degree})}$. The data points on Figure 4.14 correspond to the results of the five numerical simulations. By regression, the Equation 4.12 proposed for the correction factor k_{α} giving the influence of the attack angle on the maximum bed shear stress is:

$$k_a = \frac{\tau_{\max}}{\tau_{\max(0 \text{ deg})}} = 1 + 1.5 \left(\frac{\alpha}{90} \right)^{0.57} \quad (4.12)$$

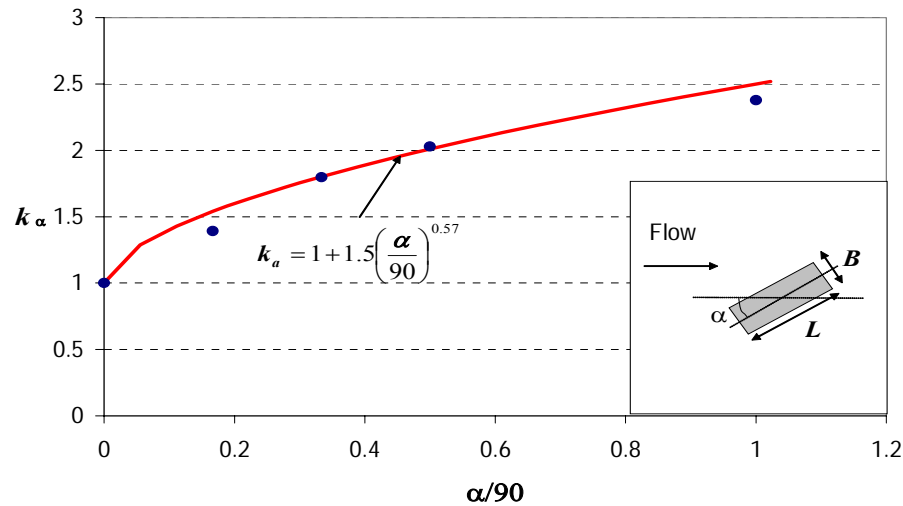


Figure 4.14: Relationship between k_α ($= \tau_{\max}/\tau_{\max}(0 \text{ degree})$) and α for Deep Water ($H/B > 2$)

4.5 MAXIMUM SCOUR DEPTH OF CONTRACTION SCOUR

4.5.1 INTRODUCTION

When flow is constrained by the bridge structures and if the bed shear stress provided by flowing water exceeds the critical shear stress of the streambed materials, contraction scour develops. The profiles of contraction scour look like the one shown in Figure 2.4. Two separate scour depths were identified in Figure 2.4: the maximum contraction scour depth $Z_{\max}(\text{Cont})$, which occurs in the location X_{\max} and the uniform scour depth $Z_{\text{unif}}(\text{Cont})$, which occurs relatively far away from the start of the contracted channel.

A series of flume tests were performed by Li (2002) to develop equations for predicting the values of $Z_{\max}(\text{Cont})$, X_{\max} , and $Z_{\text{unif}}(\text{Cont})$ in cohesive soils. One of the

important parameters for contraction scour is the mean depth velocity of the flow. The values of mean depth velocity in different locations can be critical for contraction scour depth calculation. Indeed the velocity which controls the contraction scour is the velocity V_2 , which is the velocity in the contracted section of the channel. This velocity can be estimated by using the velocity in the un-contracted channel V_1 and the contraction ratio B_2/B_1 or by using a program such as HEC-RAS to obtain V_2 directly. Two sets of equations were developed on the basis of the different velocities, V_1 and V_2 .

4.5.2 GENERAL INFORMATION FOR THE FLUME TESTS

Li (2002) performed the flume tests for contraction scour in the 0.45 m wide flume in the hydraulic laboratory at Texas A&M University. The ADV system and point gage were used to measure the velocities and scour depths respectively. The soil was used in contraction scour, which is the same to the soil used for complex pier tests. The detailed soil properties were described in Table 4.1.

4.5.3 MAXIMUM AND UNIFORM CONTRACTION SCOUR DEPTHS IN CONTRACTION SCOUR

After the analysis of the flume testing results, Li (2002) used the regression techniques to develop the following equations to determine the maximum contraction scour depth Z_{\max} (Cont), and uniform contraction scour depth Z_{unif} (Cont).

$$Z_{\max}(Cont) = K_{\theta}K_L \times 1.90 \left(\frac{1.38 \left(V_1 \frac{B_1}{B_2} \right)}{\sqrt{gH_1}} - \frac{\left(\frac{\tau_c}{\rho} \right)^{0.5}}{gnH_1^{1/3}} \right) H_1 \geq 0 \quad (4.13)$$

$$Z_{\max}(Cont) = K_{\theta}K_L \times 1.90 \left(\frac{1.49V_2}{\sqrt{gH_1}} - \frac{\left(\frac{\tau_c}{\rho} \right)^{0.5}}{gnH_1^{1/3}} \right) H_1 \geq 0 \quad (4.14)$$

$$Z_{unif}(Cont) = K_{\theta}K_L \times 1.41 \left(\frac{1.31 \left(V_1 \frac{B_1}{B_2} \right)}{\sqrt{gH_1}} - \frac{\left(\frac{\tau_c}{\rho} \right)^{0.5}}{gnH_1^{1/3}} \right) H_1 \geq 0 \quad (4.15)$$

$$Z_{unif}(Cont) = K_{\theta}K_L \times 1.41 \left(\frac{1.57V_2}{\sqrt{gH_1}} - \frac{\left(\frac{\tau_c}{\rho} \right)^{0.5}}{gnH_1^{1/3}} \right) H_1 \geq 0 \quad (4.16)$$

It is very important to know the location of the maximum contraction scour for the bridge design. Based on the flume test observations, the maximum contraction scour generally occurs close to and behind the opening of the contraction. The flume tests results and observations indicated that X_{\max} is mostly controlled by the contracted channel width B_2 and the contraction ratio B_2/B_1 . By regression, the best fit equation for X_{\max} proposed by Li (2002) is:

$$\frac{X_{\max}}{B_2} = K_{\theta}K_L \times \left(2.25 \frac{B_2}{B_1} + 0.15 \right) \quad (4.17)$$

where $Z_{\max}(\text{Cont})$ is the maximum depth of scour along the centerline of the contracted channel m , $Z_{\text{unif}}(\text{Cont})$ is the uniform depth of scour along the centerline of the contracted channel m , X_{\max} is the distance from the beginning of the fully contracted section to the location of Z_{\max} (m), V_1 is the mean velocity in the approach channel (m/s), V_2 is the velocity in the contracted channel (m/s), B_1 is the width of the approach channel (m), B_2 the width of the contracted channel (m), τ_c the critical shear stress measured by the EFA (KN/m^2), ρ the mass density of water (kg/m^3), n Manning's coefficient ($\text{m}/\text{s}^{1/3}$), H_1 the water depth in the approach channel (m).

Common sense tells us that a smooth transition angle leads to less turbulence in the contraction section; therefore the transition angle effect was considered as an effect to influence the contraction scour. In the flume tests, the test with the 90° transition angle was selected as the reference case for the transition angle effect, and the correction factors were calculated as the ratios between 0° and 90° for transition angle values. The transition angle effect factors for contraction scour K_θ , in the three aspects of $Z_{\max}(\text{Cont})$, $Z_{\text{unif}}(\text{Cont})$ and X_{\max} , are:

$$\begin{cases} K_{\theta/Z_{\max}} = 1.0 \\ K_{\theta/Z_{\text{unif}}} = 1.0 \\ K_{\theta/X_{\max}} = 0.48 / \tan \theta + 0.95 \end{cases} \quad (4.18)$$

Bridge contractions are often short because it is not necessary to build the abutments too long in the real design. In the short contraction condition, the uniform

contraction scour depth cannot fully be developed, which was verified by the flume tests. The long contraction channel with the ratio of $L/B_1 = 3.38$ was chosen as the reference case. The correction factors K_L for contraction length effect on contraction scour, in the three aspects of $Z_{\max}(\text{Cont})$, $Z_{\text{unif}}(\text{Cont})$ and X_{\max} , are:

$$\begin{cases} K_{L/Z_{\max}} = 1.0 \\ K_{L/Z_{\text{unif}}} = \text{void} \\ K_{L/X_{\max}} = 1.0 \end{cases} \quad (4.19)$$

4.6 MAXIMUM SHEAR STRESS IN CONTRACTION SCOUR

4.6.1 INTRODUCTION

The initial rate of scour for a given contraction scour problem is obtained by first calculating the maximum shear stress τ_{\max} existing in the contracted channel before the scour starts (flat river bottom) and then reading the initial scour rate on the erosion function obtained in the EFA test. Therefore the problem of obtaining the initial rate of contraction scour is brought back to the problem of obtaining the maximum shear stress in the contracted channel before scour starts. This problem was solved by numerical simulations using the Chimera RANS method. This section will describe the simulations that were performed and the associated results.

The equation for the maximum shear stress τ_{\max} at the bottom of an open channel without contraction is given by Munson et al. (1990):

$$\tau_{\max} = \gamma n^2 V^2 R_h^{-\frac{1}{3}} \quad (4.20)$$

where γ is the unit weight of water (KN/m^3), n is Manning's roughness coefficient ($\text{s/m}^{1/3}$), V is the mean depth velocity (m/s), and R_h is the hydraulic radius defined as the cross section area of the flow divided by the wetted perimeter (m).

The objective of the numerical simulations was to obtain correction factors for the maximum shear stress in the contracted channel, which would introduce the effect of the contraction ratio, the transition angle, and the length of the contracted zone.

4.6.2 GENERAL INFORMATION OF NUMERICAL SIMULATIONS FOR MAXIMUM SHEAR STRESS IN CONTRACTION SCOUR

One of the flume tests was chosen to perform the numerical simulation to find the correction factors and will be used as the comparison purpose to the flume test. The parameters of the numerical simulations are listed in Table 4.2.

Table 4.2: Parameters in the Numerical Simulations (Nurtjahyo, 2002)

Contraction Ratio Effect	B ₁ /B ₂				V ₁ (m/s)	B ₁	H (m)	θ	L/(B ₁ -
	0.25	0.5	0.75		0.45	0.45	0.12	90°	6.76
Transition Angle Effect	θ				V ₁ (m/s)	B ₁	H (m)	B ₁ /B ₂	L/(B ₁ -
	15	30	45	90	0.45	0.45	0.12	0.5	6.76
Contraction Length Effect	L/(B ₁ -B ₂)				V ₁ (m/s)	B ₁	H (m)	θ	B ₁ /B ₂
	0.25	0.5	1	6.76	0.45	0.45	0.12	90	0.5

Where V_1 is upstream mean depth velocity, H is the upstream water depth, B_1 is the width of channel, B_2 is the width of contracted section, L is the length of abutment, θ is the transition angle of contraction.

In order to reduce the calculation time for the computer, a half domain is used based on the symmetry of the problem. The grid was made of four blocks in the contraction scour case as shown in figure 4.15.

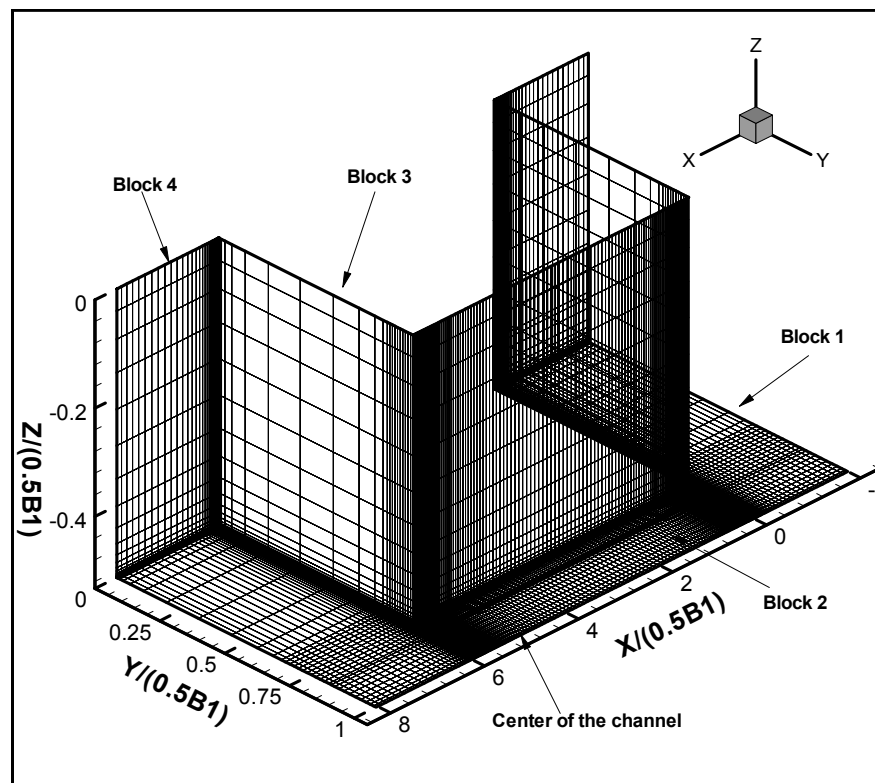


Figure 4.15: Grid System for the Simulation in the Case of $B_2/B_1 = 0.25$
(after Nurtjahyo, 2002)

4.6.3 INFLUENCING EFFECTS ON MAXIMUM SHEAR STRESS IN CONTRACTION SCOUR CASE

The influence of four parameters on the maximum shear stress and its location near a channel contraction was investigated by numerical simulation. These factors are: the contraction ratio (B_2/B_1), the transition angle (θ), the length of contraction (L), and the water depth (H). The correction factor for a given influencing parameter is defined as the ratio of the τ_{\max} value including that parameter to the τ_{\max} value for the case of the open channel without any contraction. The results of the numerical simulations were used to plot the shear stress as a function of each influencing parameter. Regressions were then used to obtain the best-fit equation to describe the influence of each parameter.

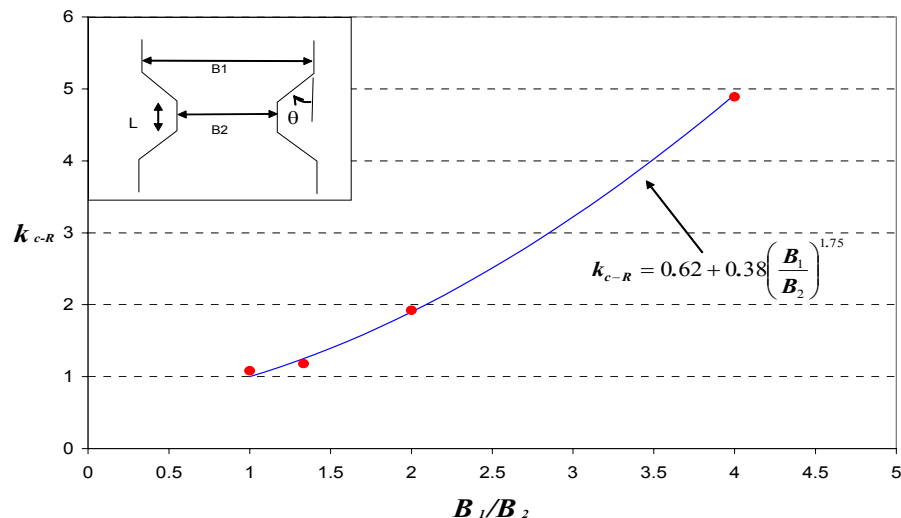


Figure 4.16: Relationship between k_{c-R} and $\frac{B_1}{B_2}$

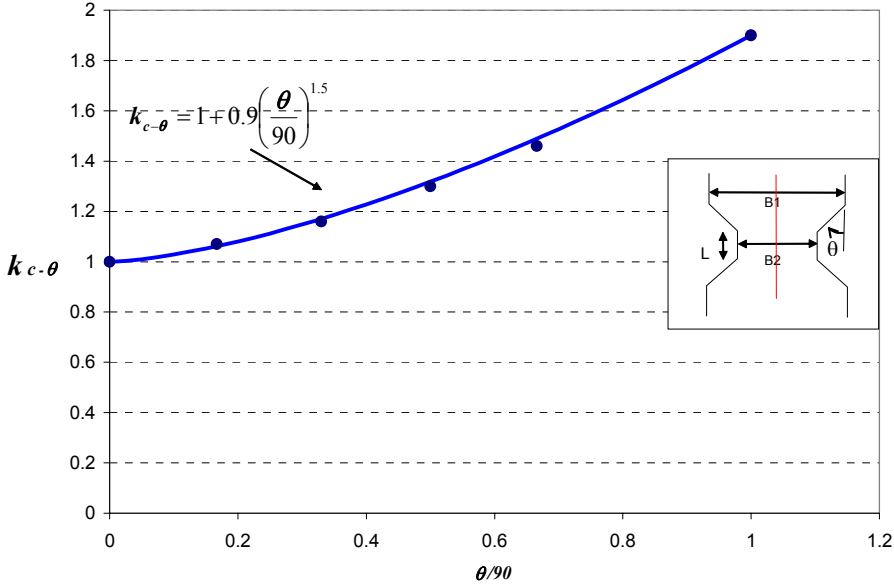


Figure 4.17: Relationship between $k_{c-\theta}$ and $\frac{\theta}{90}$

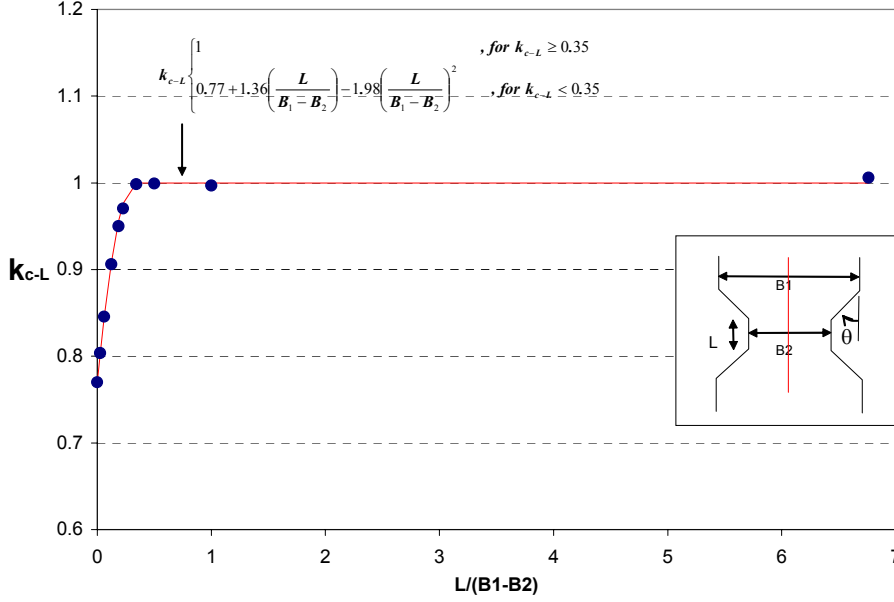


Figure 4.18: Relationship between k_{c-L} and $\frac{L}{B_1 - B_2}$

k_{c-R} is the correction factor for the contraction ratio, given by

$$k_{c-R} = 0.62 + 0.38 \left(\frac{B_1}{B_2} \right)^{1.75} \quad (\text{Figure 4.16}) \quad (4.21)$$

$k_{c-\theta}$ is the correction factor for the contraction transition angle, given by

$$k_{c-\theta} = 1 + 0.9 \left(\frac{\theta}{90} \right)^{1.5} \quad (\text{Figure 4.17}) \quad (4.22)$$

k_{c-L} is the correction factor for the contraction length, given by

$$k_{c-L} = \begin{cases} 1 & , \text{for } k_{c-L} \geq 0.35 \\ 0.77 + 1.36 \left(\frac{L}{B_1 - B_2} \right) - 1.98 \left(\frac{L}{B_1 - B_2} \right)^2 & , \text{for } k_{c-L} < 0.35 \end{cases} \quad (\text{Figure 4.18}) \quad (4.23)$$

k_{c-H} is the correction factor for the water depth effect on contraction scour. Since the water depth has a negligible influence, then $k_{c-H} \approx 1$.

Where B_1 is the upstream channel width (m), B_2 is the contracted channel width (m), θ is the contraction transition angle (in degrees), L is the contracted length of the channel (m).

4.7 CONCLUSIONS

4.7.1 SRICOS-EFA METHOD FOR MAXIMUM SCOUR DEPTH AT COMPLEX PIER CASES

In the previous sections, individual effects on the maximum pier scour depth were studied by flume testing. A series of figures and equations were given to quantify the corresponding correction factors. However, bridge piers are likely to exhibit a

combination of these effects and recommendations are needed to combine these effects in the calculations. It is recommended that the correction factors be multiplied in order to represent the combined effect. This is a common approach which implies that the effects are independent, and has been used in many instances, for example, (HEC-18, Melville (1997)).

$$Z_{\max} (mm) = 0.18 \cdot K_w \cdot K_{sp} \cdot K_{sh} \cdot \left(\frac{B'V}{\nu} \right)^{0.635} \quad (4.24)$$

where: Z_{\max} is the maximum depth of scour (mm), V is depth average velocity at the location of the pier if the pier or bridge was not there (m/s), B' is the projection width of the pier (m), ν is the kinematic viscosity of water (10E-6 (m²/s) at 20°C), K_w is correction factor for shallow water effect (equation 4.3), K_{sp} for pier spacing effect (equation 4.4), and K_{sh} for pier shape effect (1.1 for rectangular piers), B' is the pier projection width (equation 4.5 for rectangular pier).

4.7.2 SRICOS-EFA METHOD FOR MAXIMUM SHEAR STRESS AT COMPLEX PIER CASES

The proposed equation for calculating the maximum shear stress for a complex pier before the scour process starts is:

$$\tau_{\max} = k_w k_{sp} k_{sh} k_a \times 0.094 \rho V^2 \left[\frac{1}{\log \text{Re}} - \frac{1}{10} \right] \quad (4.25)$$

where V is the upstream velocity (m/s), ρ is the density of water (kg/m^3), Re is the Reynolds number, defined as $\text{Re} = \frac{VB}{\nu}$, ν is the kinematic viscosity (m^2/s), B is the pier width (m), k_w is the correction factor for the effect of water depth, k_{sp} is the correction factor for the effect of pier spacing, k_{sh} is the correction factor for the effect of pier shape, $k_{sh} = 1$ for circular shape, k_a is the correction factor for the effect of attack angle.

4.7.3 SRICOS-EFA METHOD FOR CONTRACTION SCOUR DEPTHS

The following equations summarize the results from this chapter.

$$Z_{\max}(\text{Cont}) = K_{\theta} K_L \times 1.90 \left(\frac{1.38 \left(V_1 \frac{B_1}{B_2} \right)}{\sqrt{gH_1}} - \frac{\left(\frac{\tau_c}{\rho} \right)^{0.5}}{gnH_1^{1/3}} \right) H_1 \geq 0 \quad (4.26)$$

$$Z_{\max}(\text{Cont}) = K_{\theta} K_L \times 1.90 \left(\frac{1.49V_2}{\sqrt{gH_1}} - \frac{\left(\frac{\tau_c}{\rho} \right)^{0.5}}{gnH_1^{1/3}} \right) H_1 \geq 0 \quad (4.27)$$

$$Z_{\text{unif}}(\text{Cont}) = K_{\theta} K_L \times 1.41 \left(\frac{1.31 \left(V_1 \frac{B_1}{B_2} \right)}{\sqrt{gH_1}} - \frac{\left(\frac{\tau_c}{\rho} \right)^{0.5}}{gnH_1^{1/3}} \right) H_1 \geq 0 \quad (4.28)$$

$$Z_{\text{unif}}(\text{Cont}) = K_{\theta} K_L \times 1.41 \left(\frac{1.57V_2}{\sqrt{gH_1}} - \frac{\left(\frac{\tau_c}{\rho} \right)^{0.5}}{gnH_1^{1/3}} \right) H_1 \geq 0 \quad (4.29)$$

$$\frac{X_{\max}}{B_2} = K_{\theta} K_L \times \left(2.25 \frac{B_2}{B_1} + 0.15 \right) \quad (4.30)$$

where $Z_{\max}(\text{Cont})$ is the maximum depth of scour along the centerline of the contracted channel, $Z_{\text{unif}}(\text{Cont})$ is the uniform depth of scour along the centerline of the contracted channel, V_1 is the mean velocity in the approach channel, V_{Hec} is the velocity in the contracted channel given by HEC-RAS, B_1 is the width of the upstream channel, B_2 the width of the contracted channel, τ_c is the critical shear stress, ρ the mass density of water, n Manning's coefficient, H_1 the water depth in the approach channel, K_θ the correction factor for the influence of the transition angle as given by equation 4.31 below, and K_L the correction factor for the influence of the contraction length as given by equation 4.32 below.

$$\begin{cases} K_{\theta/Z_{\max}} = 1.0 \\ K_{\theta/Z_{\text{unif}}} = 1.0 \\ K_{\theta/X_{\max}} = 0.48 / \tan \theta + 0.95 \end{cases} \quad (4.31)$$

$$\begin{cases} K_{L/Z_{\max}} = 1.0 \\ K_{L/Z_{\text{unif}}} = \text{void} \\ K_{L/X_{\max}} = 1.0 \end{cases} \quad (4.32)$$

4.7.4 SRICOS-EFA METHOD FOR MAXIMUM SHEAR STRESS AT CONTRACTION SCOUR

The proposed equation for calculating the maximum shear stress within the contracted length of a channel along its centerline is:

$$\tau_{\max} = k_{c-R} k_{c-\theta} k_{c-H} k_{c-L} \gamma n^2 V^2 R_h^{-\frac{1}{3}} \quad (4.33)$$

where γ is the unit weight of water (kN/m^3), n is Manning's roughness coefficient ($\text{s/m}^{1/3}$), V is the upstream mean depth velocity (m/s), θ is the contraction transition angle (in degrees), R_h is the hydraulic radius defined as the cross section area of the flow divided by the wetted perimeter (m), k_{c-R} is the correction factor for the contraction ratio, $k_{c-\theta}$ is the correction factor for the contraction transition angle, k_{c-L} is the correction factor for the contraction length, k_{c-H} is the correction factor for the water depth effect on contraction scour. Since the water depth has a negligible influence, then $k_{c-H} \approx 1$.

4.7.5 GENERAL PROCEDURES OF SRICOS-EFA METHOD FOR COMPLEX PIERS SCOUR AND CONTRACTION SCOUR IN COHESIVE SOILS

The general process of SRICOS-EFA method is illustrated in Figure 4.19. Three basic components constitute this method: geometry, water and soil. The maximum scour depth and maximum shear stress are calculated by geometry and water conditions. The soil samples tested on the EFA provide the erosions functions. The initial scour rate is obtained by reading the EFA curves corresponding to the maximum shear stress. Then the hyperbola model can be built on the basis of the maximum scour depth, the initial scour rate and time.

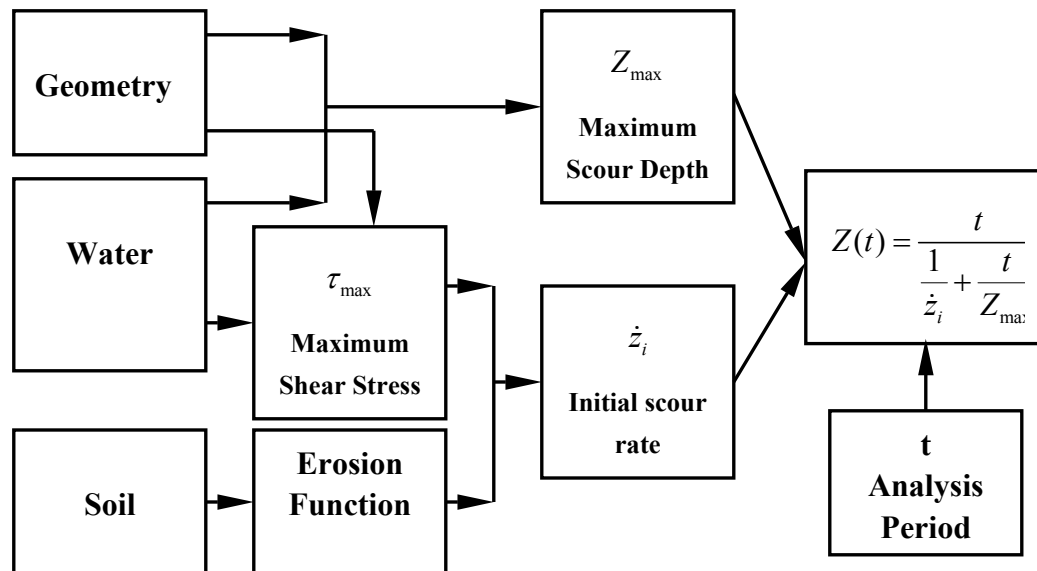


Figure 4.19: General Process of SRICOS-EFA Method

The SRICOS-EFA method was assembled based on the equations, which were presented in this chapter. The rules of accumulation due to the hydrograph, and due to the multilayer system developed for the simple pier scour method were adapted for the complex pier and contraction scour conditions, which leads to the following steps for the SRICOS-EFA method for predicting the scour depths for a complex pier or contraction scour. This step by step procedure has been automated in a windows environment computer program.

1. Collect the input data: velocity and water depth hydrograph, geometry of the pier or of the contracted channel, erosion functions of the soil layers.

2. Calculate the maximum pier scour depth or contraction scour depth for the i^{th} velocity in the hydrograph.
3. Calculate the initial maximum shear stress for pier scour or contraction scour using the i^{th} velocity in the hydrograph.
4. Read the initial scour rate corresponding to the initial maximum shear stress of step 3 on the erosion function of the soil layer corresponding to the current scour depth.
5. Use the results of steps 2 and 4 to construct the hyperbola describing the scour depth vs time for the pier scour or contraction scour.
6. Calculate the equivalent time for the given curve of step 5. The equivalent time is the time required for the i^{th} velocity on the hydrograph to scour the soil to a depth equal to the depth scoured by all the velocities occurring prior to the i^{th} velocity.
7. Read the additional scour generated by the i^{th} velocity starting at the equivalent time and ending at the equivalent time plus the time increment.
8. Repeat steps 2 to 9 for the $(i+1)^{\text{th}}$ velocity and so on until the entire hydrograph is consumed.

CHAPTER V

SIMPLE SRICOS-EFA METHOD FOR CONTRACTION SCOUR

5.1 INTRODUCTION

In Chapter IV, the SRICOS-EFA method was discussed in detail. Hydrograph is one of three essential components for SRICOS-EFA method. The hydrograph for the channel during the analysis period or bridge design life is very important for SRICOS-EFA method, because it provides the hydraulic conditions in the bridge site. But in many cases the hydrograph data will be missed because the gaging stations have not been installed when the bridge was built or the gaging stations were malfunctioned during data recording. Hence, it is necessary to find a way to make the SRICOS-EFA method be applicable even when the whole hydrograph is not available. Therefore the purposes of this research are:

1. To obtain a simple method associated with SRICOS-EFA method that can be used in the situation where the whole hydrograph doesn't exist.
2. To simplify the method so that only hand calculation will be needed.

This simplified method will be named as Simple SRICOS-EFA method. Kwak (2000) has developed the Simple SRICOS-EFA method for pier scour calculation. In this chapter, the simple SRICOS-EFA Method for contraction scour will be developed.

5.2 BASIC ASSUMPTIONS

Kwak (2000) conducted a parametric study on the influence of different parameters on pier scour. His results indicated that the flow velocity had a similar impact on the pier scour with pier width and more significant impact compared to the critical

shear stress and scour rate. Velocity in HEC-18 pier scour prediction equation was presented by the Froude number with the biggest exponent value as 0.45. So it can be reasonable to conclude that velocity is one of the most influential parameters on the pier scour. A similar condition is found in the contraction scour as well. The maximum contraction scour depths equation from SRICOS-EFA method is following:

$$Z_{\max}(Cont) = K_{\theta}K_L \times 1.90 \left(\frac{1.49V_{hec}}{\sqrt{gH_1}} - \frac{\left(\frac{\tau_c}{\rho}\right)^{0.5}}{gnH_1^{1/3}} \right) H_1 \geq 0 \quad (5.1)$$

$$\tau_c = \left(\frac{\rho gn^2 V_c^2}{H_1^{1/3}} \right) \quad (5.2)$$

Substituting Equation 5.2 into Equation 5.1, the following Equation 5.3 will be found.

$$Z_{\max}(Cont) = K_{\theta}K_L \times 1.90 \sqrt{\frac{H_1}{g}} (1.49V_{hec} - V_c) \geq 0 \quad (5.3)$$

The simplified Equation 5.3 indicates the velocity is one of the most influential parameters in the contraction scour depth calculation. Hence the first basic assumption for simple SRICOS-EFA method is that the maximum velocity V_{\max} during the contraction scour analysis is considered the most influential parameter on contraction scour depth. The second assumption, and most important assumption, is that the whole hydrograph during the analysis period can be regarded as a constant flow with the maximum velocity in the hydrograph lasting a certain time. In order to transform the whole period hydrograph into a constant flow with the value as the maximum velocity, one important concept should be introduced, which is equivalent time t_{equiv} . The conceptual diagram of t_{equiv} is shown in Figure 5.1. Equivalent time t_{equiv} is the time required for the maximum velocity in the hydrograph to create the same scour depth generated by the whole hydrograph. The equation for t_{equiv} will be the target of this chapter and it will be developed based on the case histories and regression techniques. The proposed equation for t_{equiv} will reflect not only the properties of soils but also the characteristics of flow.

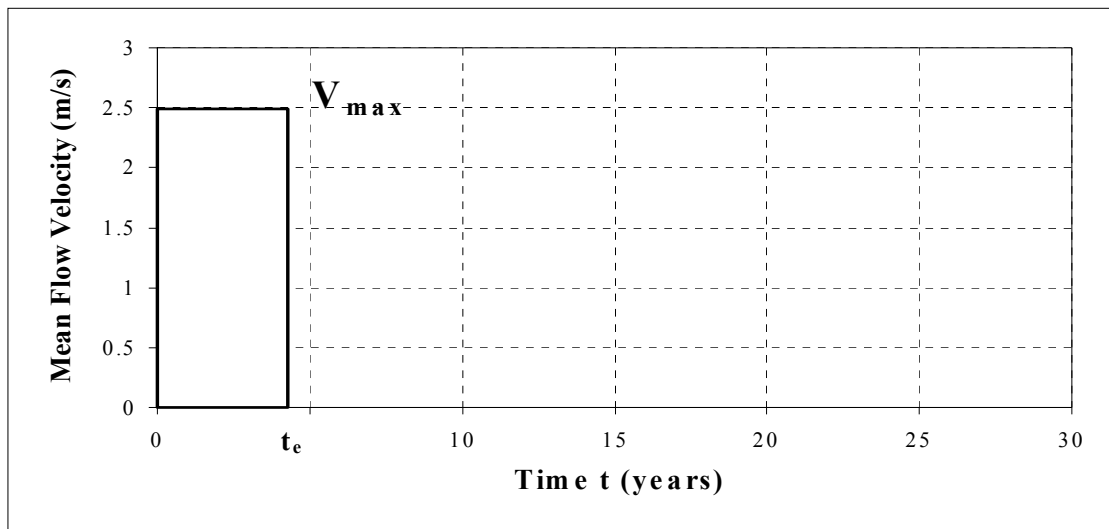
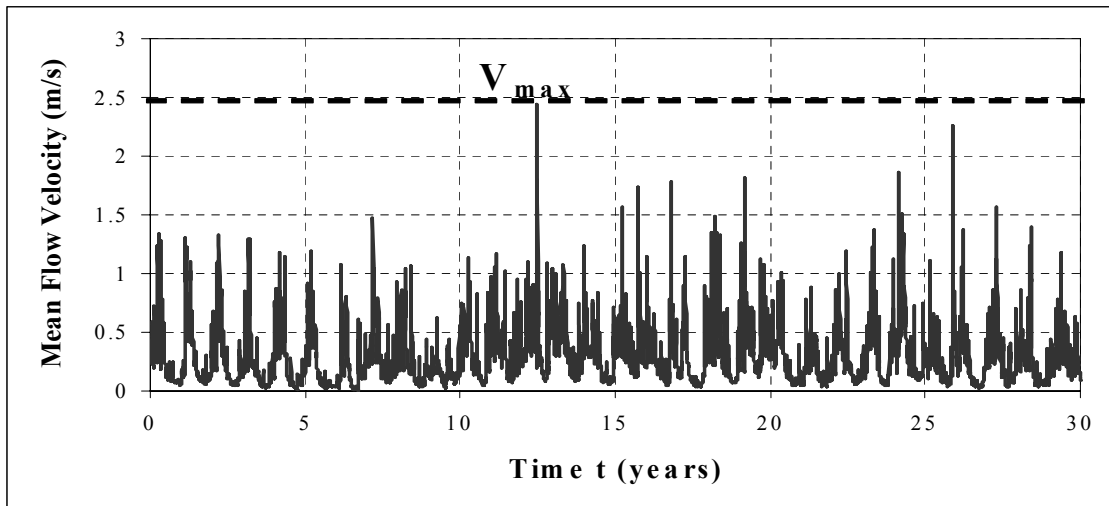


Figure 5.1: Basic Assumption of Simple SRICOS-EFA Method

5.3 EQUIVALENT TIME EQUATION DEVELOPMENT FOR CONTRACTION SCOUR IN SRICOR-EFA METHOD

5.3.1 GENERAL

Several case histories were selected for obtaining the t_{equiv} equation for contraction scour. These histories were collected by Kwak (2000). The following criteria and characteristics were set up for selecting the bridges:

- The soil type was clay,
- River banks and, if possible the river bed, must be accessible with a drilling rig to collect Shelby tube soil samples,
- The river bed profiles have been well documented, and
- The gaging station should be found at the bridge or near the bridges.

Kwak selected 6 bridges for developing the t_{equiv} equation of pier scour after site investigation and careful consideration based on the criteria and characteristics discussed above. General information about the bridges was collected from the district offices of the Texas Department of Transportation. The locations of the bridges are shown in Figure 5.2.

Some efforts were made to find the case histories for the contraction scour, but it is difficult to find good and suitable bridge cases for the contraction scour. In most cases, the deficient documentation of scour development is a big barrier to obtain accurate and useful history cases. However the t_{equiv} calculation is not a verification process, it just uses some cases for equation development purpose. Hence the cases histories for pier scour

can be used for contraction scour cases except that some necessary contraction parameters need to be assumed, for example, the channel contraction ratio, channel contraction length, channel transition angle etc.

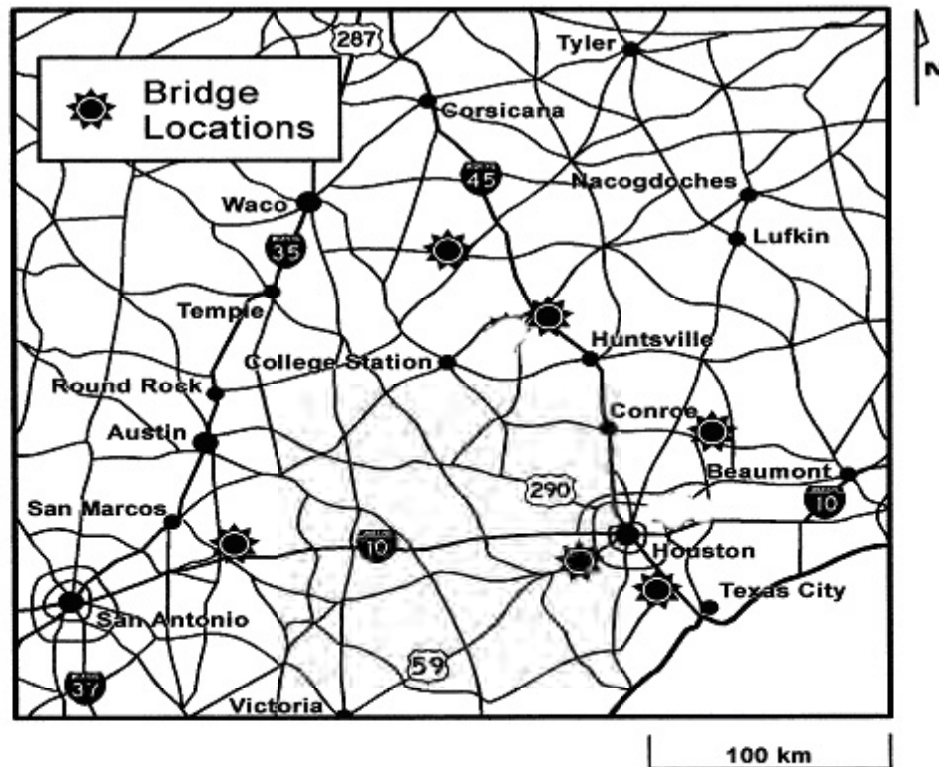


Figure 5.2: Locations of Case History Bridges

There are three important parameters in contraction scour calculation: contraction ratio, contraction length and transition angle. The contraction ratio is calculated as the width of the channel in contracted section divided by the width of upstream, B_2/B_1 . The contraction length usually is the length of the bridge contraction length. The transition

angle is the angle between the contraction channel and riverbank, θ . Figure 5.3 shows the definitions of these three parameters.

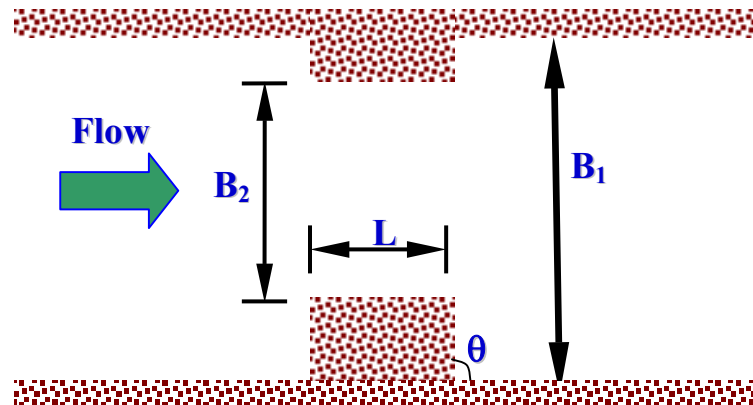


Figure 5.3: Definitions of Contraction Ratio and Transition Angle

These three parameters can vary from place to place. Before the values of these three parameters were found, endeavors were made to find the reasonable values of contraction ratio, contraction length and transition angle. A survey had been done for this purpose. Some information was collected, and the collected information indicated that most of the bridges have the range of contraction ratio from 0.3 to 0.5 and no obvious tendency of transition angle of the channel. Hence, in this research, an averaged contraction ratio of 0.4 was adopted associated with transition angle as 90° . General bridges have 2 traffic lanes in each direction, according to the design guideline of highway and street. The width of each traffic lane is 3.66 m (12 ft), so the width of four lanes road will be approximately 15 m. Therefore it is reasonable to assume the

contraction lengths for these case histories are 15 m. The information of the bridge is listed in Table 5.1.

Table 5.1: Channel Information for Case Histories in Simple SRICOS-EFA Method Development for Contraction Scour

Bridge	Year Built	Average Upstream Width (m)	Contraction Length (m)	Contraction ratio*	Transition angle*
Navasota River at	1956	26.5	15	0.4	90
Brazos River at US	1965	41.5	15	0.4	90
Trinity River at FM	1976	43.3	15	0.4	90
San Marcos River at	1939	14.6	15	0.4	90
Sims Bayou at SH	1993	22.3	15	0.4	90
Bedias Creek at US	1947	17.5	15	0.4	90

5.3.2 CHANNEL INFORMATION FOR CASE HISTORIES

- **The Navasota River Bridge at SH 7**

The Navasota River Bridge at SH 7 is located approximately 13 km downstream and south of the Lake Limestone reservoir dam in Robertson County, Texas. The main bridge has an overall length of 82.8 m and consists of 3 continuous steel girder main spans with 4 concrete pan girder approach spans on steel pile bents. The piling at bent 5 and 6 also has concrete web walls and concrete caps at mid-height. The piling at bent 5 is embedded 5.5 m below the channel bed, which consists of silty clay and sandy clay extending down to the bottom of the piling. The channel profile is shown in Figure 5.4.

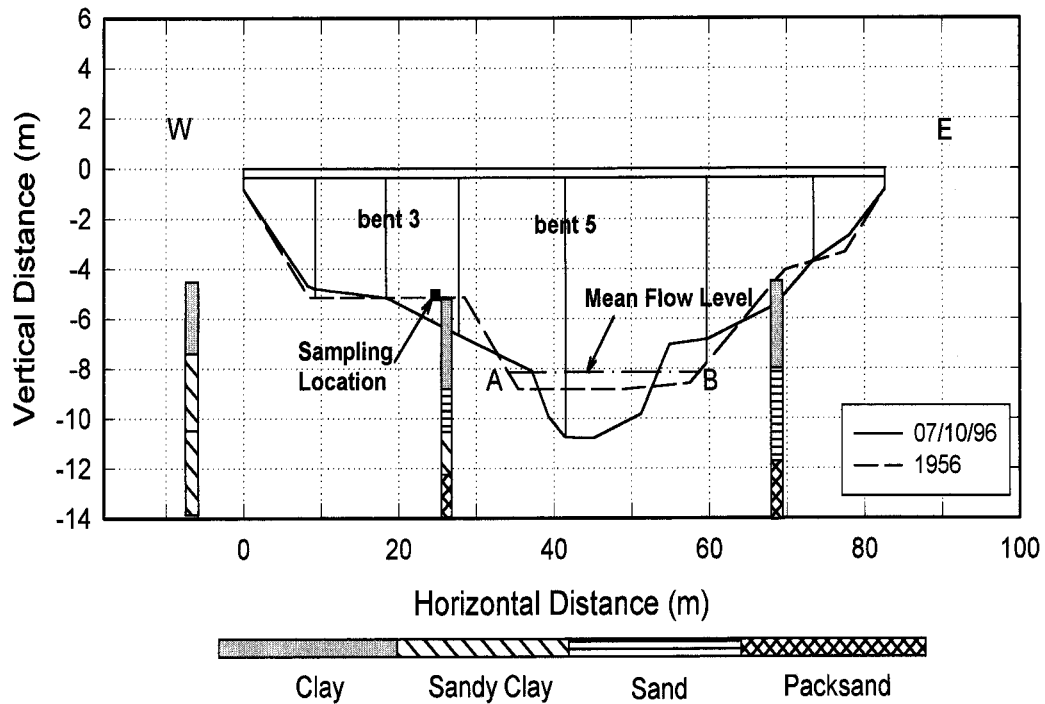


Figure 5.4: Profiles of Navasota River Bridge at SH 7

- **The Brazos River Bridge at US 90A**

The Brazos River Bridge at US 90A is located in the city of Richmond, Texas. The bridge has a 3-span, continuous steel plate girder unit with 8 pre-stressed concrete approach spans and the overall length is 287 m. Supports are concrete piers founded on concrete piles. The channel profile is shown in Figure 5.5.

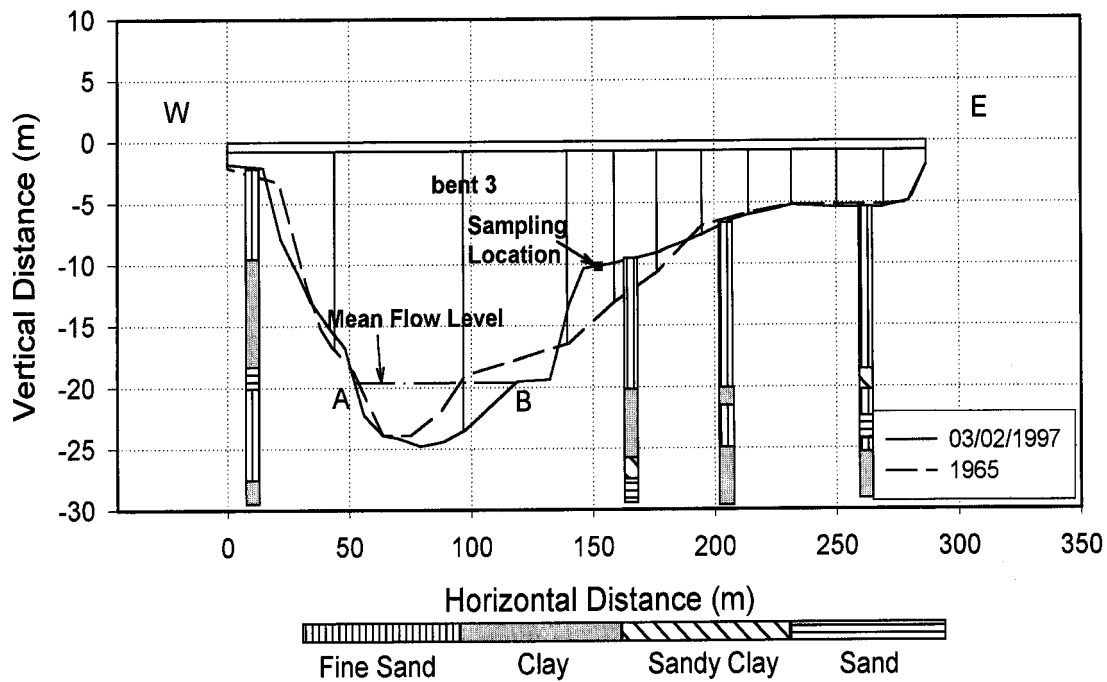


Figure 5.5: Profiles of Brazos River Bridge at US 90A

- **The Trinity River Bridge at FM 287**

The Trinity River Bridge at FM 287 is located approximately 2.4 km south of the city of Romayor, Texas. This bridge has 3 main spans and 3 approach spans with an overall length of 165.2m. The two intermediate piers are two column piers with a web wall founded on a pile cap on timber piling. The west bank of the waterway has undergone severe erosion in the past due to its location in a bend of the waterway. The bank has been repaired with rock rubbles rip-rap and appears stable. The channel profile is shown in Figure 5.6.

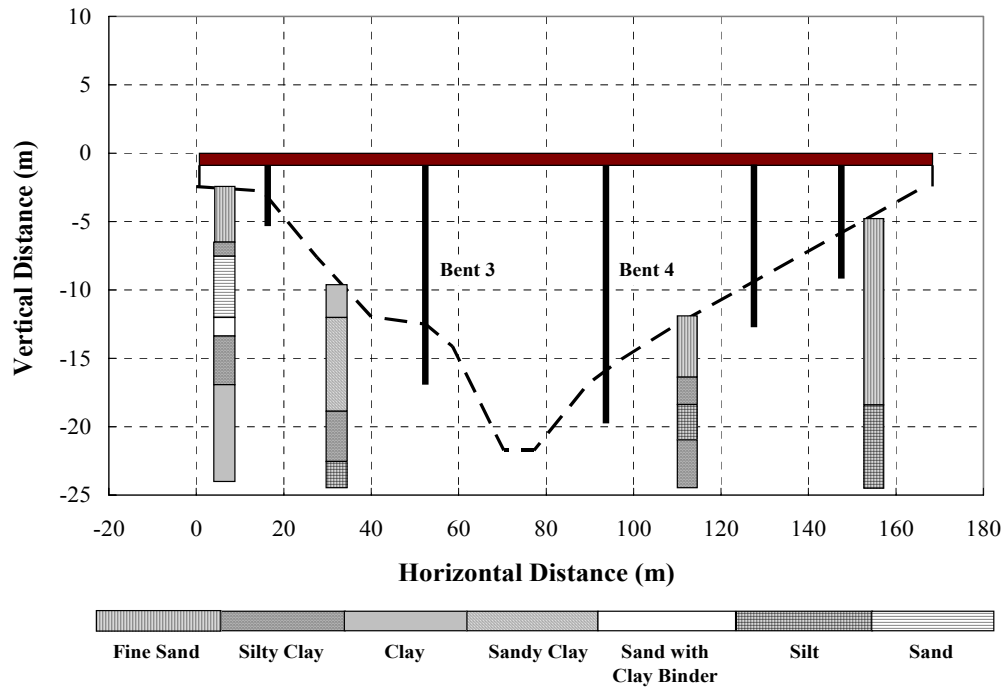


Figure 5.6: Profiles of Trinity River Bridge at FM 787 in 1976

- **The San Marcos River Bridge at SH 80**

The San Marcos River Bridge at SH 80 is located approximately 1.4 km south of the city of Luling, Texas. This bridge has 11 pre-stressed concrete spans with an overall length of 176.2m. The channel profile is shown in Figure 5.7.

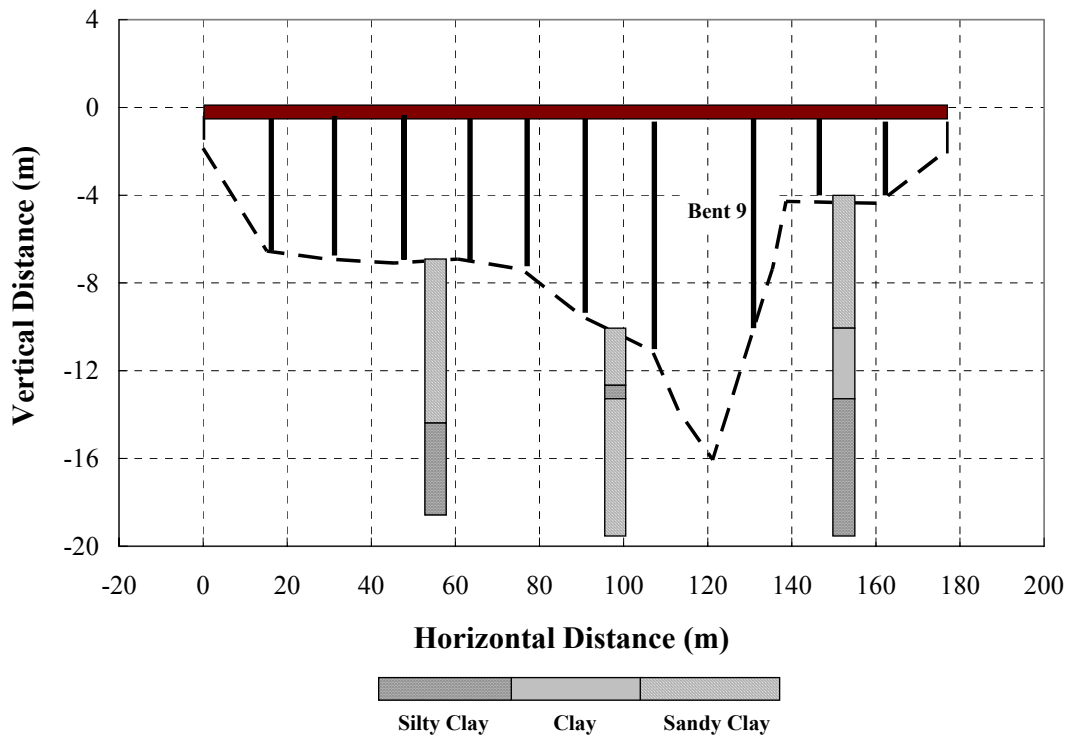


Figure 5.7: Profile of San Marcos River Bridge at SH 80 in 1939

- **The Sims Bayou Bridge at SH 35**

The Sims Bayou Bridge at SH 35 is located approximately 3.2 km south of the IH 45 in Harris County, Texas. The bridge has 5 spans, which are supported on 4 interior bents and the overall length is 85.3m. Each bent consists of 4 round drilled concrete shafts. Soil borings show mostly clay layers with a significant sand layer 7.6 to 10.7 m thick at approximately 3 to 4.6 m underneath the channel bed. The channel profile measurements indicate that the channel is stable and aggradation is dominant. The channel profile is shown in Figure 5.8.

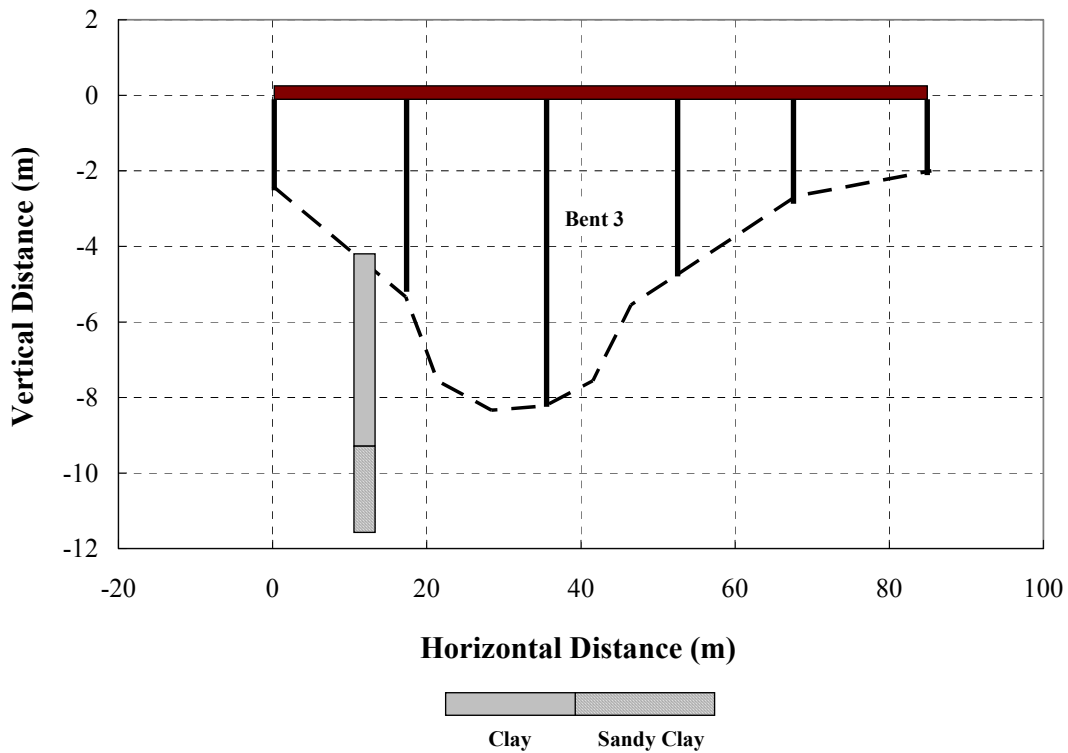


Figure 5.8: Profile of Sims Bayou Bridge at SH 35 in 1993

- **The Bedia Creek Bridge at US 75**

The Bedia Creek Bridge at US 75 is located approximately 14.4 km south of the city of Madisonville, Texas. The bridge consists of 29 concrete steel I-beam spans on concrete pile bents in the approach spans and concrete piers founded on spread footings at bent 26 and 27 on either side of the main channel and the overall bridge length is 271.9m. The channel profile measurements indicate that the channel bed has not changed significantly since the bridge was built in 1947. The channel profile is shown in Figure 5.9.

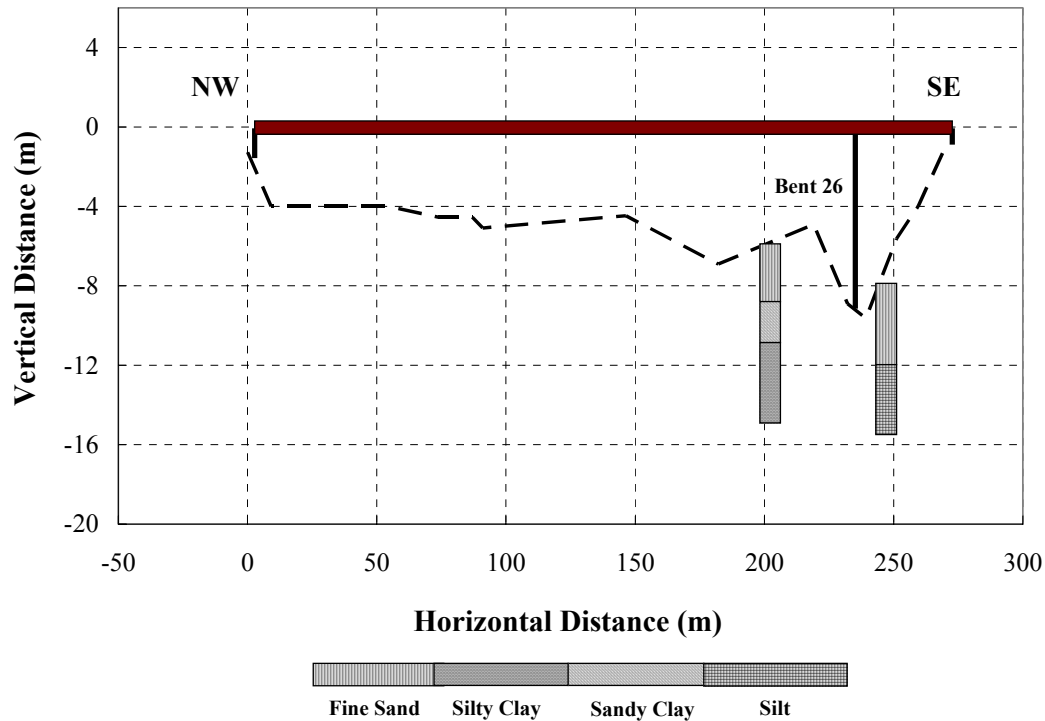


Figure 5.9: Profile of Bedias Creek Bridge at US 75 in 1947

5.3.3 DISCHARGE HYDROGRAPHS FOR CASE HISTORIES

The most basic and important hydrologic parameters involved in the scour calculations are discharge, water depth and velocity. Usually, the discharge hydrograph is used in the SRICOS-EFA method because it can be obtained from USGS (US Geological Survey) website easily and directly. The discharge hydrograph is a plot of discharge data over time. Discharge hydrograph can be determined in the gaging station by the water-stage recorder, which provides a record of water surface elevation with respect to time. The water surface elevation can be transformed to the discharge hydrograph by certain relationships between the water surface elevation and discharge.

The relationship between these two values is based on field measurements or calculated by a computer program like HEC-RAS. Once obtained, a best fitting curve will be applied on the data of water surface elevation versus discharge, so that the regression equation for these two parameters can be established. The discharge hydrographs for the 6 selected bridges in this study, which show the daily mean discharge, are shown in following figures, 5.10 to 5.15. All the hydrographs data were found and downloaded from the USGS website.

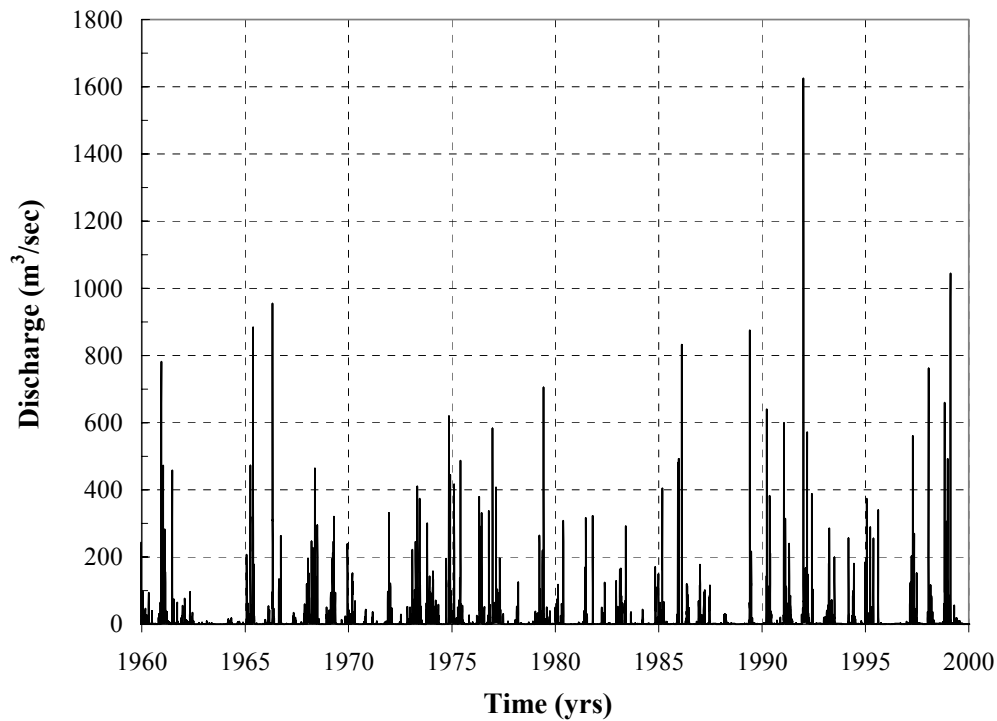


Figure 5.10: Discharge Hydrograph of Navasota River Bridge at SH 7

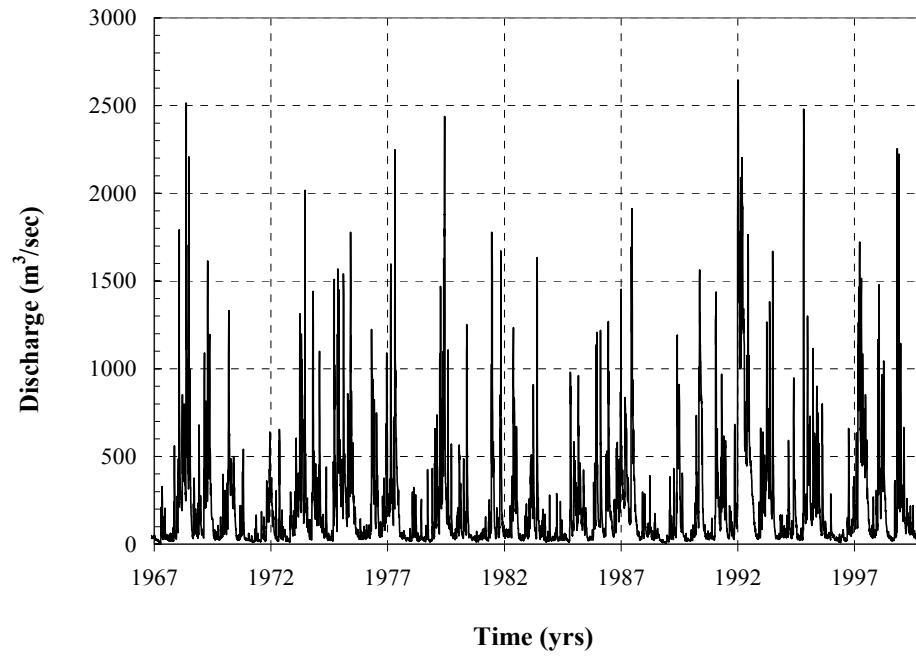


Figure 5.11: Hydrograph of Brazos River Bridge at US 90A

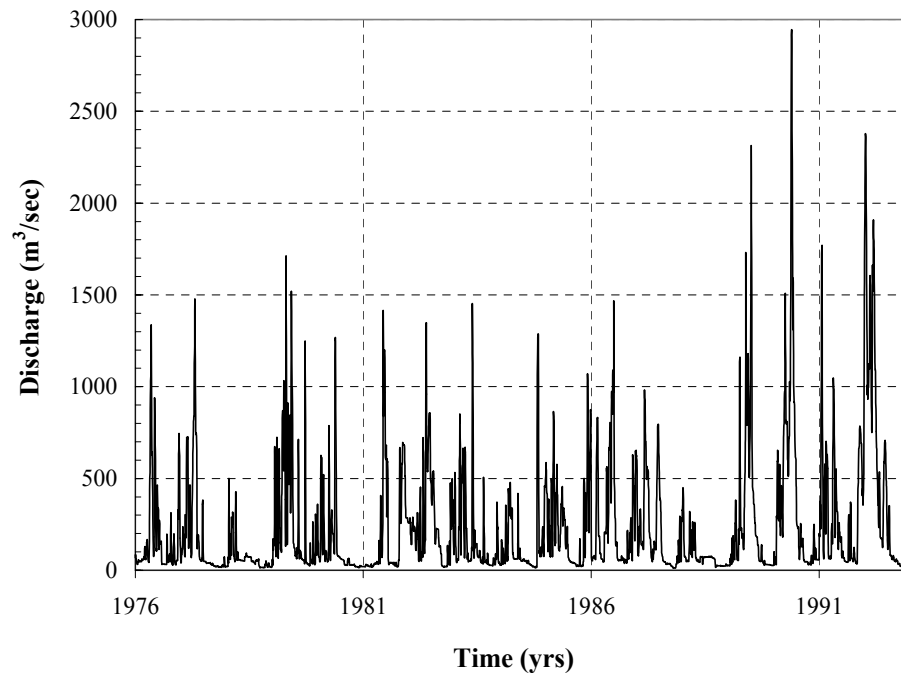


Figure 5.12: Hydrograph of Trinity River Bridge at FM 787

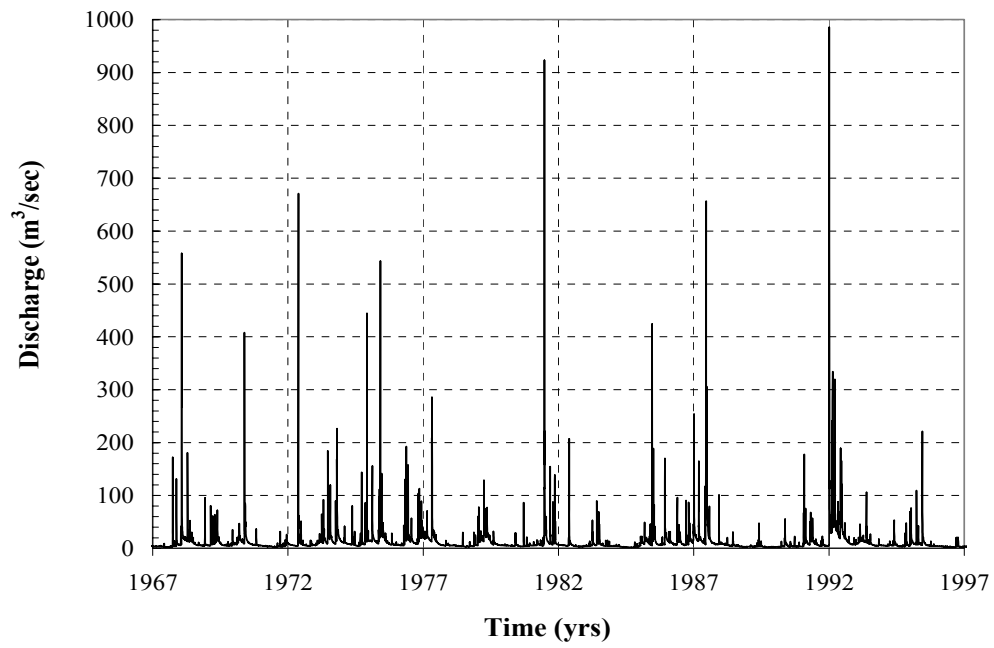


Figure 5.13: Hydrograph of San Marcos River Bridge at SH 80

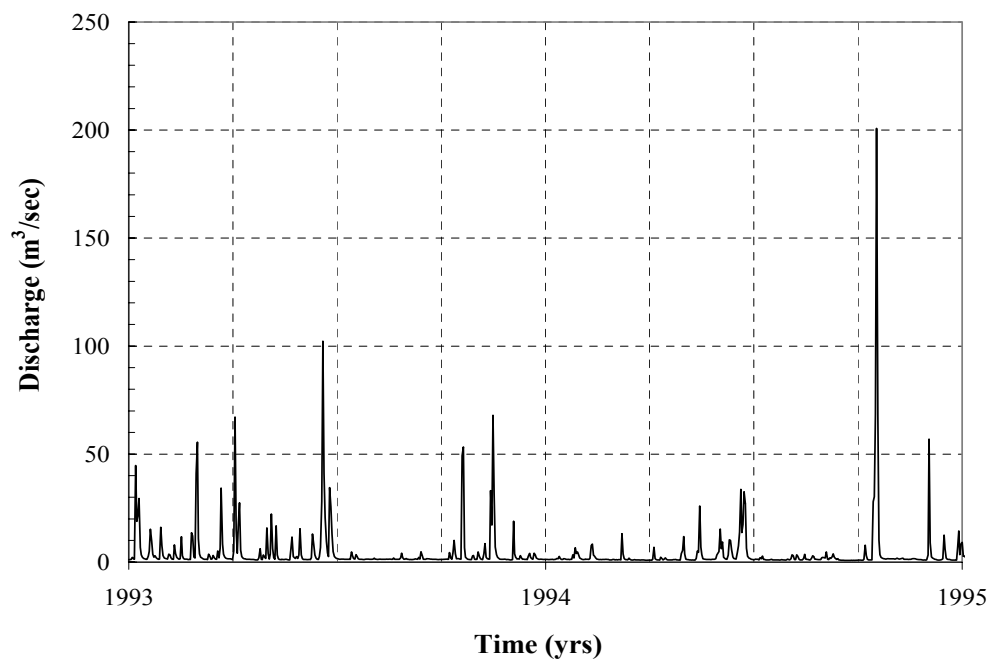


Figure 5.14: Hydrograph of Sims Bayou Bridge at SH 35

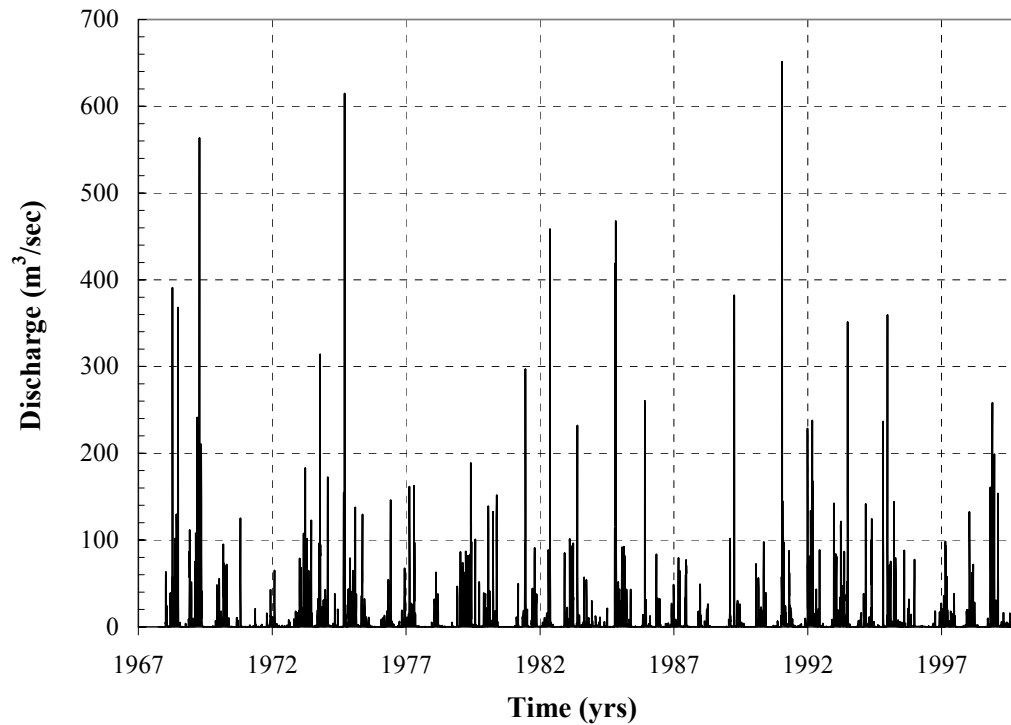


Figure 5.15: Hydrograph of Bedia Creek Bridge at US 75

5.3.4 VELOCITY TRANSFORM

The scour process is a soil and water interaction process. The driving force contributing to the scour is provided by flow and the resistant force is provided by soil. Basically, the occurrence happens when the shear stress generated by flow is larger than the critical shear stress of soil at the soil-water interface. As it was discussed before, the most influential hydrologic parameter in scour was assumed to be the velocity of flow. The direct parameter related to scour is the mean water depth velocity. Hence, it is necessary to transform the discharge hydrograph to velocity hydrograph during the scour analysis period.

In this research, the computer program called Hydrologic Engineering Center's River Analysis System (HEC-RAS, 1997), which was developed by United States Army Corps of Engineers, was used for flood analysis to obtain the relationship between the discharge hydrograph and velocity hydrograph for case histories. Some necessary hydraulic parameters and geographical features need to be entered into the program. The flow will be assumed as the uniform flow in HEC-RAS analysis. Manning's equation is the governing equation for uniform flow in the analysis.

$$V = \frac{1}{n} R^{\frac{2}{3}} S^{\frac{1}{3}} \quad (5.4)$$

where n is Manning's coefficient

R is length of wetted perimeter of the channel

S is channel energy slope

So the necessary inputs of hydraulic parameters for HEC-RAS are Manning's coefficient and energy slope of channel.

5.3.4.1 MANNING'S COEFFICIENT

Manning's coefficient ($\text{s/m}^{1/3}$) is used to describe the friction characteristics of channel; it is an empirical value and usually obtained from experiments. Young (1997) summarized the values of Manning's coefficient in different conditions and it is shown in Table 5.2. In this research, the Manning's coefficients were 0.035.

Table 5.2: Typical Values of Manning's Coefficient (after Young et al., 1997)

Categories		Manning's Coefficient
Natural Channel	Clean and straight	0.030
	Sluggish with deep pools	0.040
	Major rivers	0.035
Floodplains	Pasture, farmland	0.035
	Light brush	0.050
	Heavy brush	0.075
	Trees	0.150
Excavated earth channels	Clean	0.022
	Gravelly	0.025
	Weedy	0.030
	Stony, cobbles	0.035
Artificially lined channels	Glass	0.010
	Brass	0.011
	Steel, smooth	0.012
	Steel, painted	0.014
	Steel, riveted	0.015
	Cast, iron	0.013
	Concrete, finished	0.012
	Concrete, unfinished	0.014
	Planned wood	0.012
	Clay tile	0.014
	Brickwork	0.015
	Asphalt	0.016
	Corrugated metal	0.022
	Rubble masonry	0.025

5.3.4.2 AVERAGE SLOPE OF STREAMBED

Kwak (2000) used the site investigations and topographic maps, which were drawn to a scale of 1:24,000 to obtain the average slopes of the 6 selected object channels. The values are shown in Table 5.3.

Table 5.3: Average Slopes of Selected Channels (After Kwak, 2000)

Object Channel	Average Bed Slope
Navasota River at SH 7	0.0010
Brazos River at US 90A	0.0011
Trinity River at FM 787	0.0011
San Marcos River at SH 80	0.0010
Sims Bayou at SH 35	0.0001
Bedias Creek at SH 90	0.0005

5.3.4.3 COMPUTATIONS RESULTS FROM HEC-RAS

After inputting hydraulic and geographical features into HEC-RAS, the relationships between velocity and discharge and the relationships between discharge and channel water depth were defined. These relationships can be used to convert the discharge hydrograph to velocity hydrograph and discharge hydrograph to water depth hydrograph. These velocities and water depths were the velocities and water depths found in the upstream of channels. The relationships are plotted into charts, which are shown from Figure 5.16 to Figure 5.27.

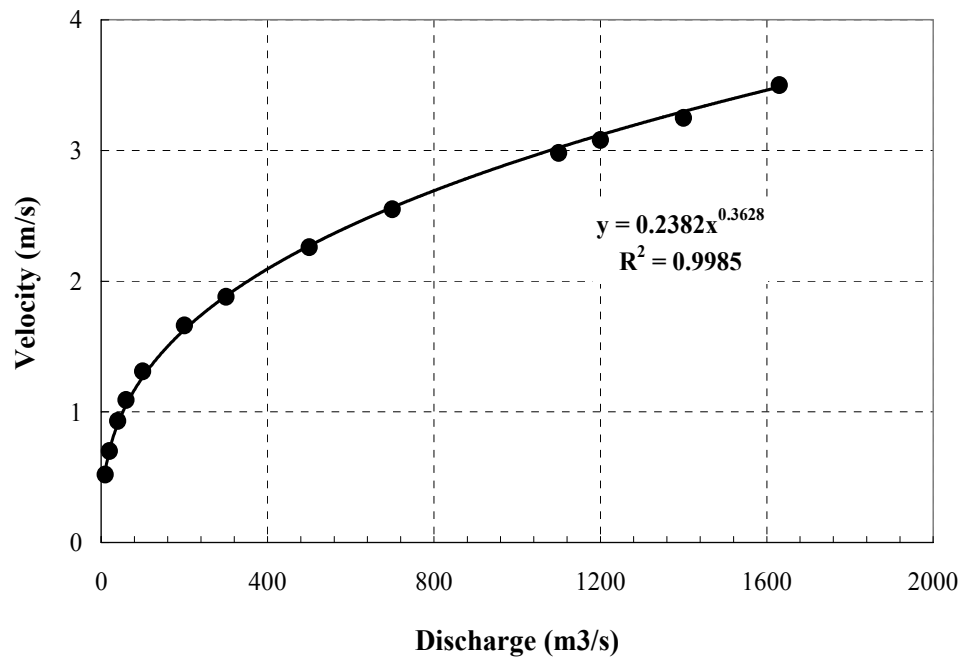


Figure 5.16: Relationship between Discharge and Velocity – Navasota River

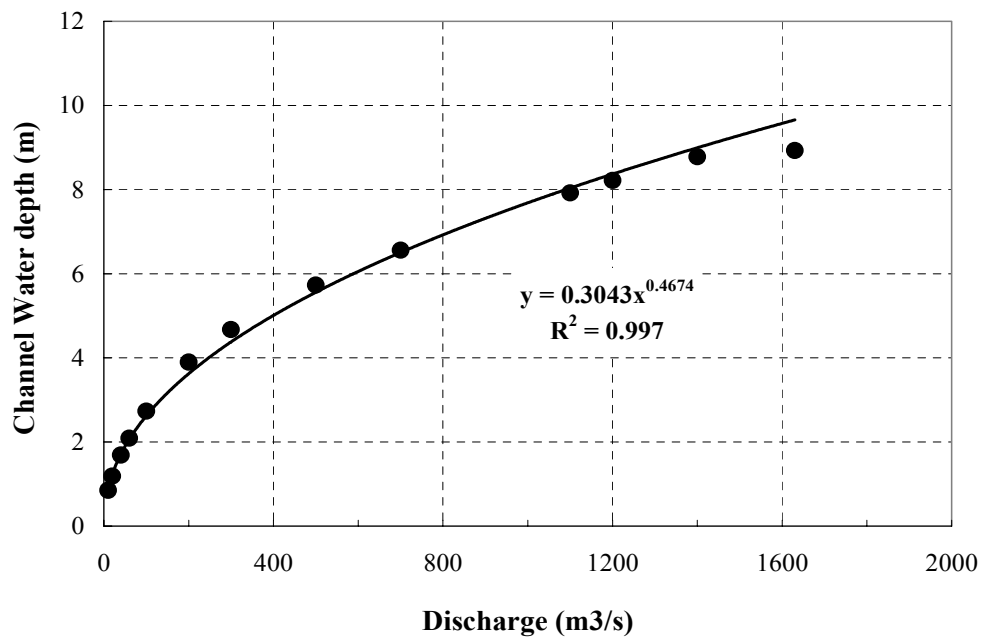


Figure 5.17: Relationship between Discharge and Water Depth - Navasota River

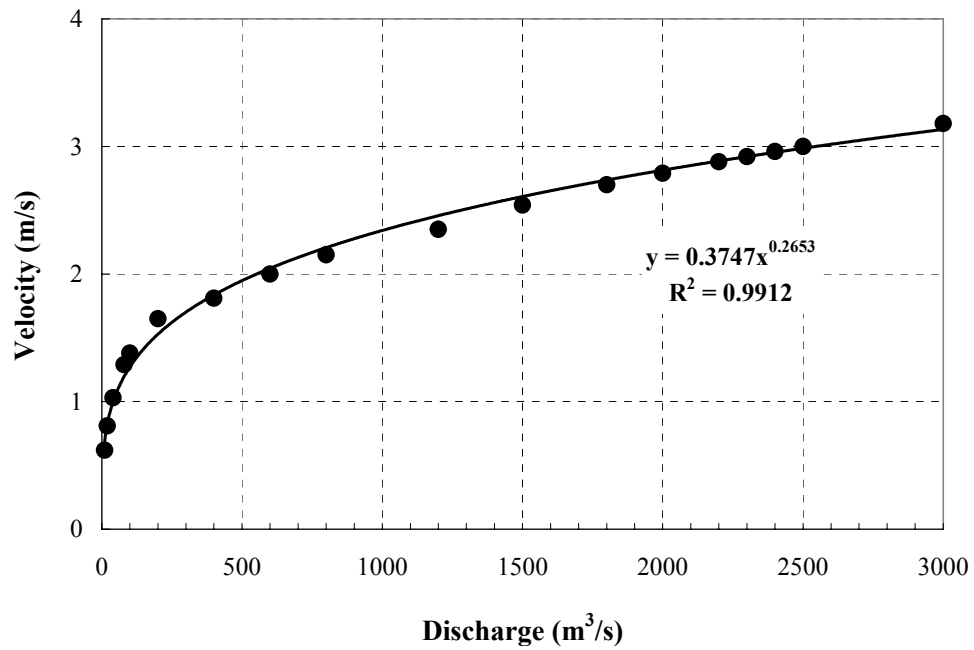


Figure 5.18: Relationship between Discharge and Velocity – Brazos River

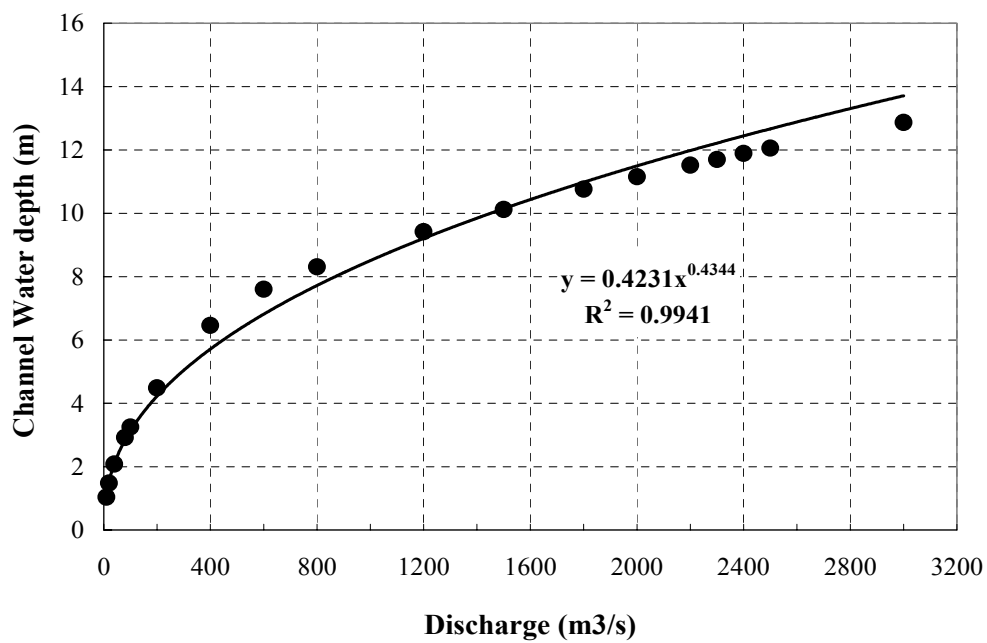


Figure 5.19: Relationship between Discharge and Water Depth – Brazos River

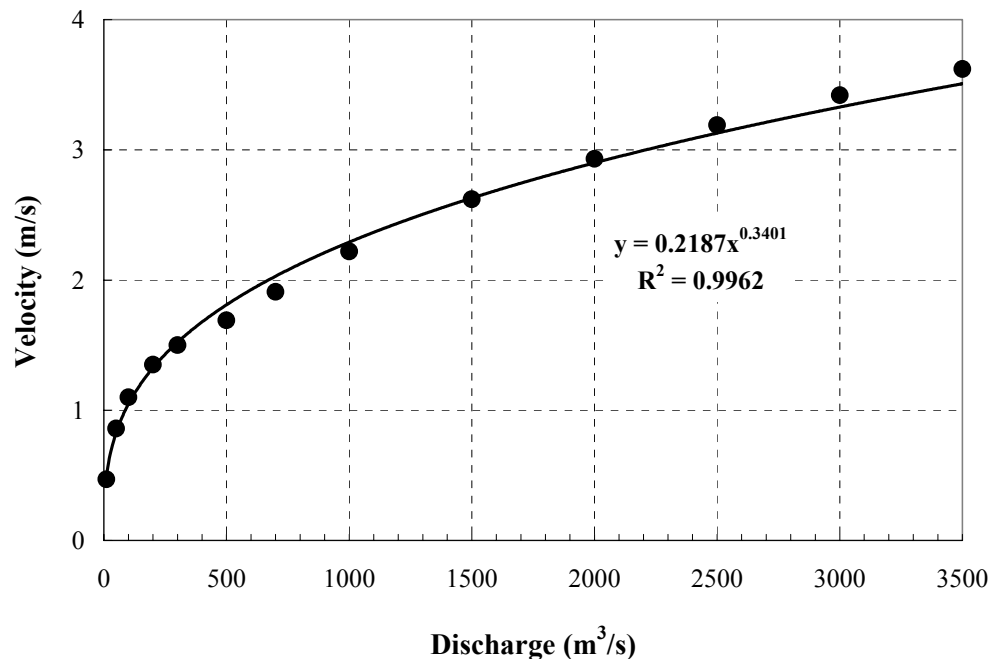


Figure 5.20: Relationship between Discharge and Velocity – Trinity River

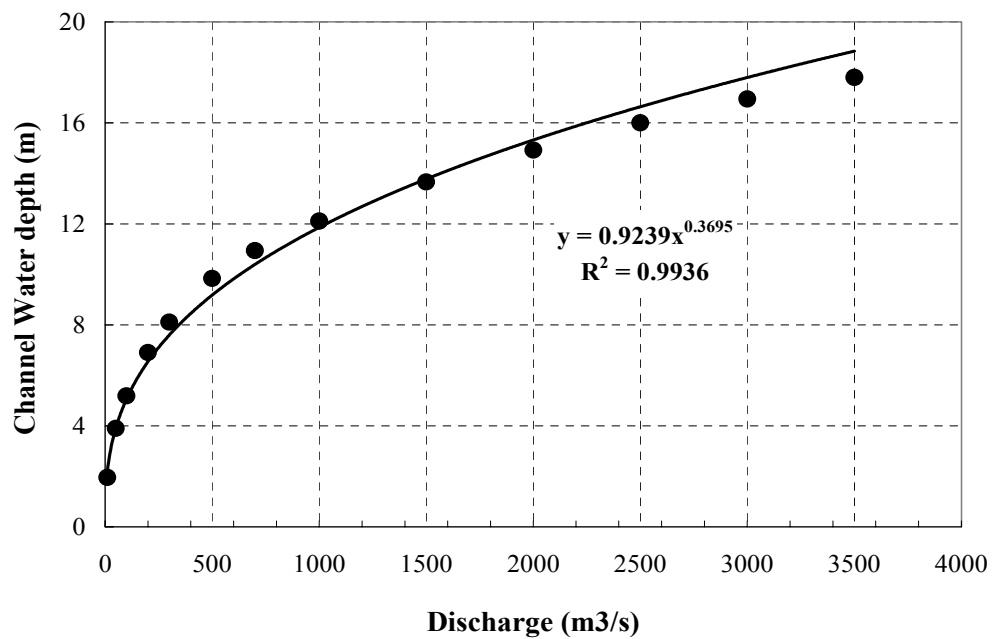


Figure 5.21: Relationship between Discharge and Water Depth – Trinity River

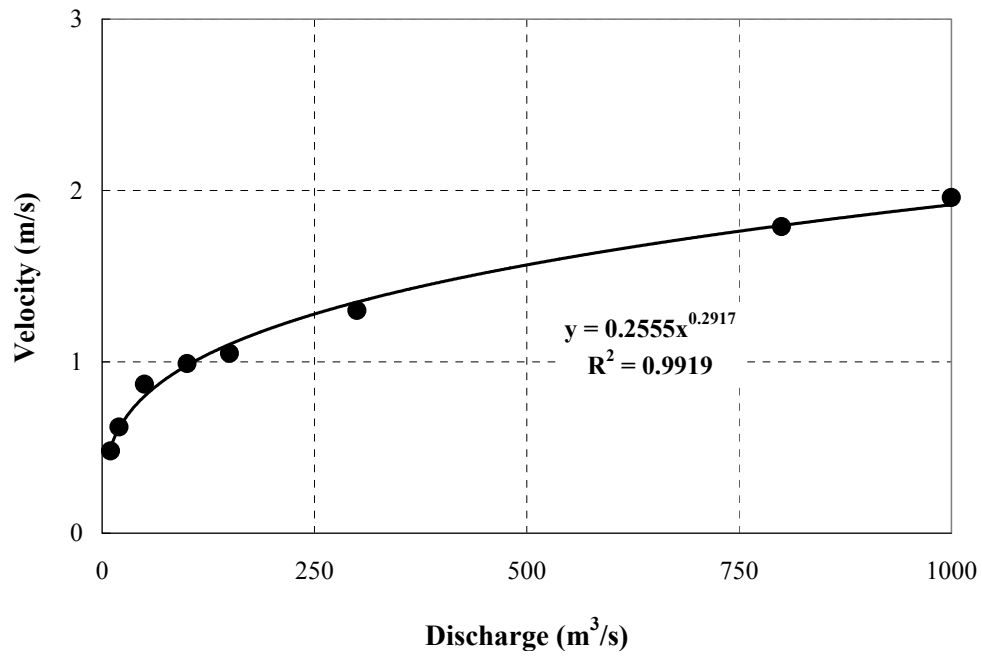


Figure 5.22: Relationship between Discharge and Velocity – San Marcos River

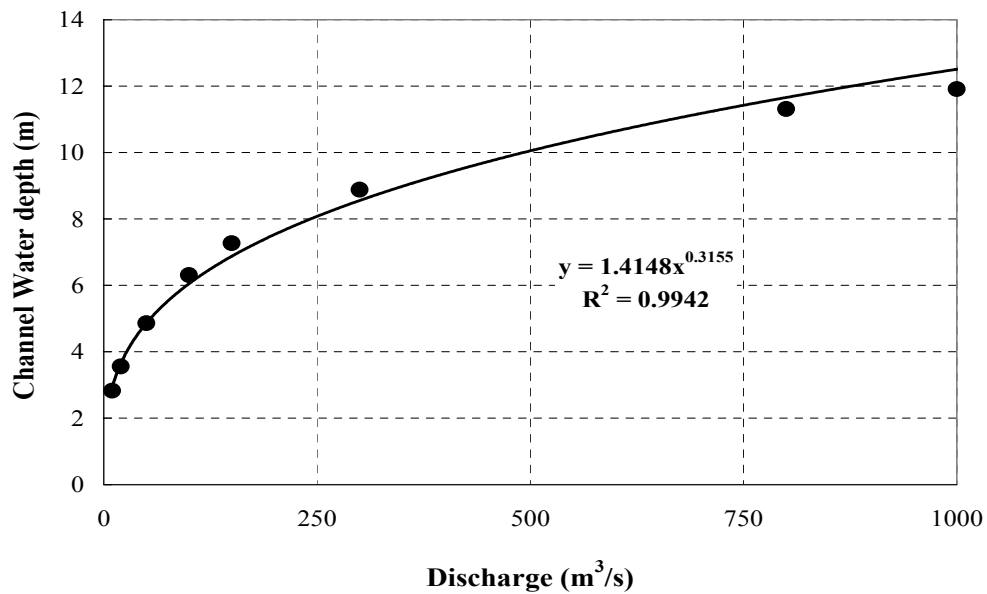


Figure 5.23: Relationship between Discharge and Water Depth – San Marcos River

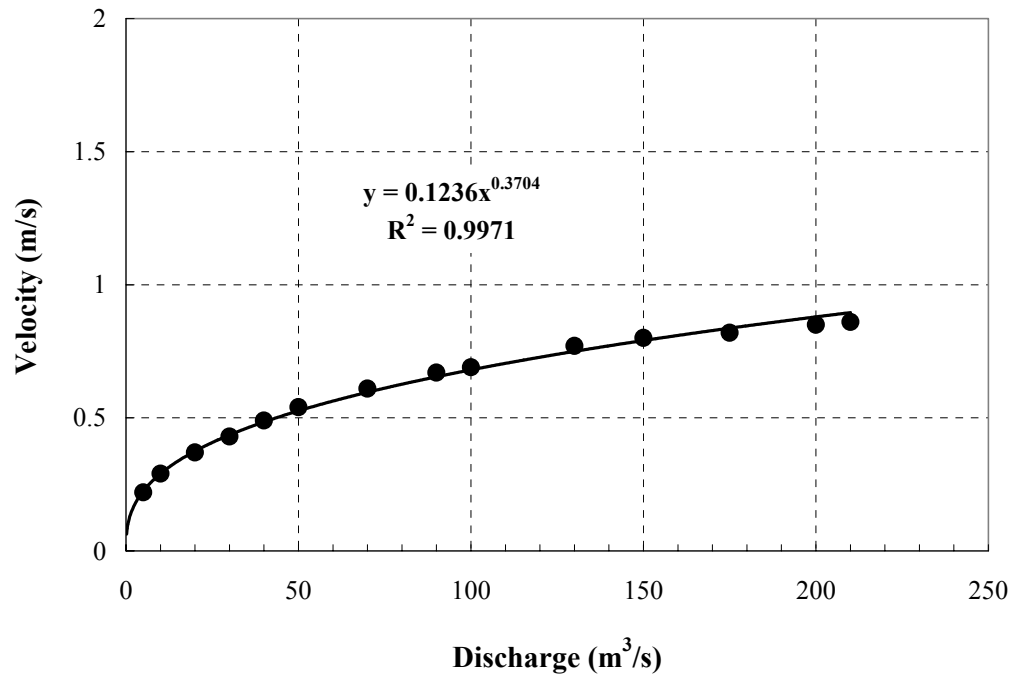


Figure 5.24: Relationship between Discharge and Velocity – Sims Bayou

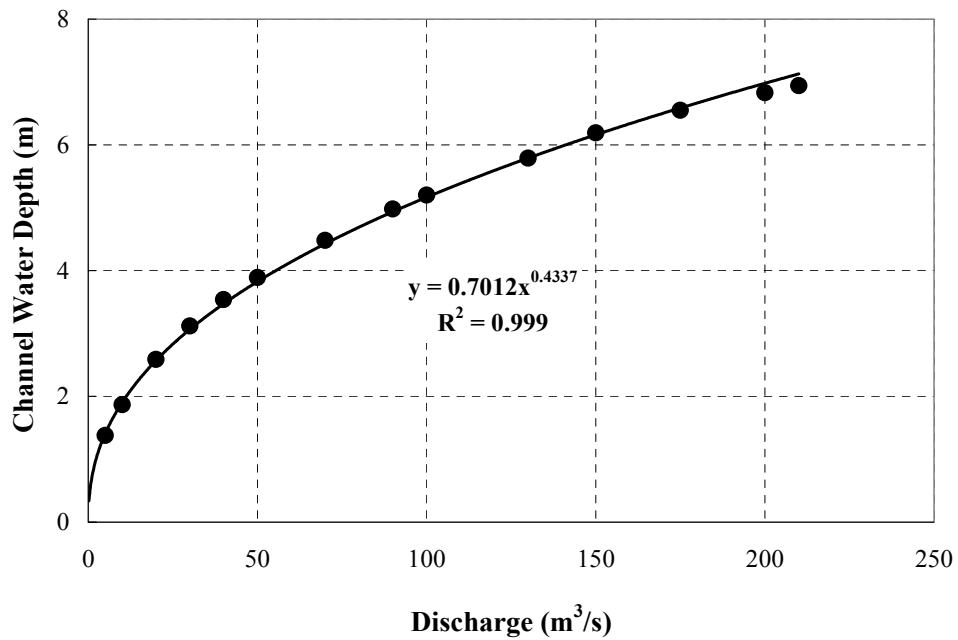


Figure 5.25: Relationship between Discharge and Water Depth - Sims Bayou

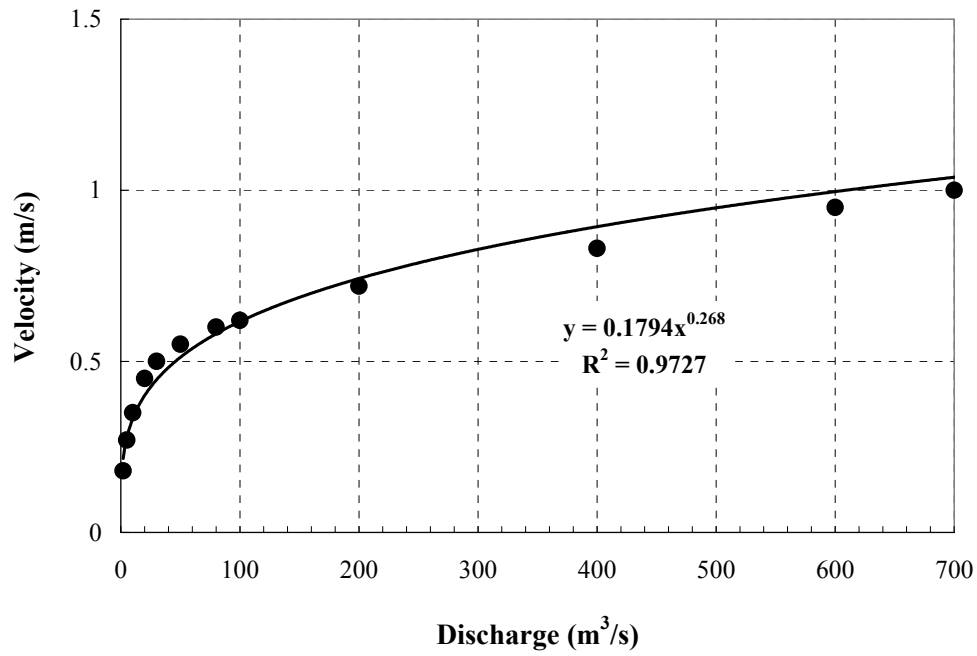


Figure 5.26: Relationship between Discharge and Velocity – Bedia Creek

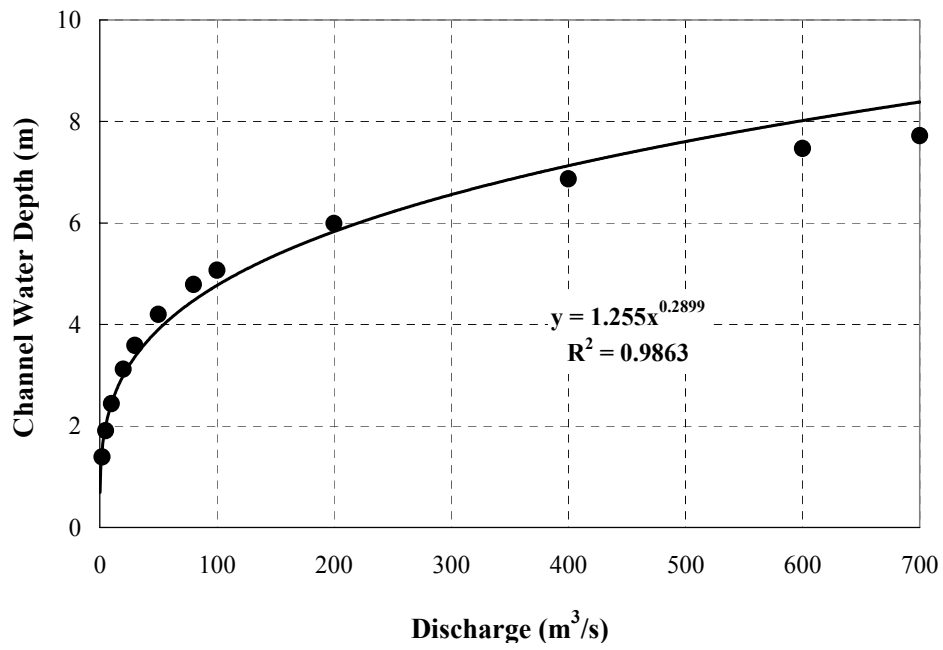


Figure 5.27: Relationship between Discharge and Water Depth – Bedia Creek

5.3.5 GEOTECHNICAL AND EROSION PROPERTIES OF SOIL IN SELECTED CHANNELS

Soil samples were taken and site explorations were performed to determine the stratification and engineering properties of soils in the channels. Some conventional geotechnical engineering tests were performed by Kwak (2000). The purpose of doing some geotechnical testing is to keep accurate documentation on the testing and help us to find out the potential relationships between soil erodibility and soil properties. The relationship between the soil erodibility and soil properties will be discussed in Chapter VIII. The method of soil sampling will be the drilling technique, which is commonly used in geotechnical engineering. All the soil property tests were conducted by following American Society for Testing and Materials (ASTM) standards. The results of soil properties tests are shown in Table 5.4.

The EFA tests were performed for each Shelby tube sample taken from the bridge sites. During performing the scour calculation by the SRICOS-EFA method, the interpolation technique will be used to obtain the initial scour rate from the soil erodibility function. However, when the maximum shear stress τ_{\max} that occurs during the analysis period exceed the range of the EFA test results, in some cases, the regression equation from the data points on the EFA curve will be used to cover all the range of τ_{\max} values. If the soils in the bridge sites consist of several different layers, the EFA curve will be plotted individually for each layer. The EFA results presented as the shear stress vs. scour rate curve for the 6 selected channels are shown in figures from Figure 5.28 to Figure 5.37.

Table 5.4: Soil Properties of 6 Selected Channels

Channel		Depth (m)	Liquid Limit (%)	Plastic Limit (%)	Plasticity Index (%)	Water Content (%)	D50 (mm)	Shear Strength (Kpa)	Unit Weight (KN/m ³)	% Passing #200 sieve
Navasota	Layer1	1.8-2.4	27.72	14.29	13.43	19.80	0.125	43.10	19.20	26.20
	Layer 2	4.9-5.5	26.42	6.25	20.17	26.60	-	32.10	18.80	57.70
Brazos	Layer 1	13.0-13.7	24.49	9.41	15.08	17.32	0.265	45.69	20.20	30.09
Trinity	Layer 1	10.7-11.4	-	-	-	7.67	6.00	9.57	22.00	11.52
	Layer 2	13.0-13.7	42.24	8.7	33.54	22.22	-	11.48	22.10	68.40
San	Layer 1	6.1-6.6	41.34	16.67	24.67	22.00	-	27.30	19.60	78.30
Marcos	Layer 2	7.0-7.5	40.31	19.18	21.13	24.40	-	29.67	20.20	73.40
Sims	Layer 1	3.0-3.7	84.16	16.05	68.11	25.25	0.0012	23.00	19.60	99.07
Bedias	Layer 1	6.1-6.9	47.86	13.56	34.30	18.07	0.048	10.00	20.04	86.81
	Layer 2	6.9-7.6	-	-	-	17.50	0.130	32.00	21.30	35.14

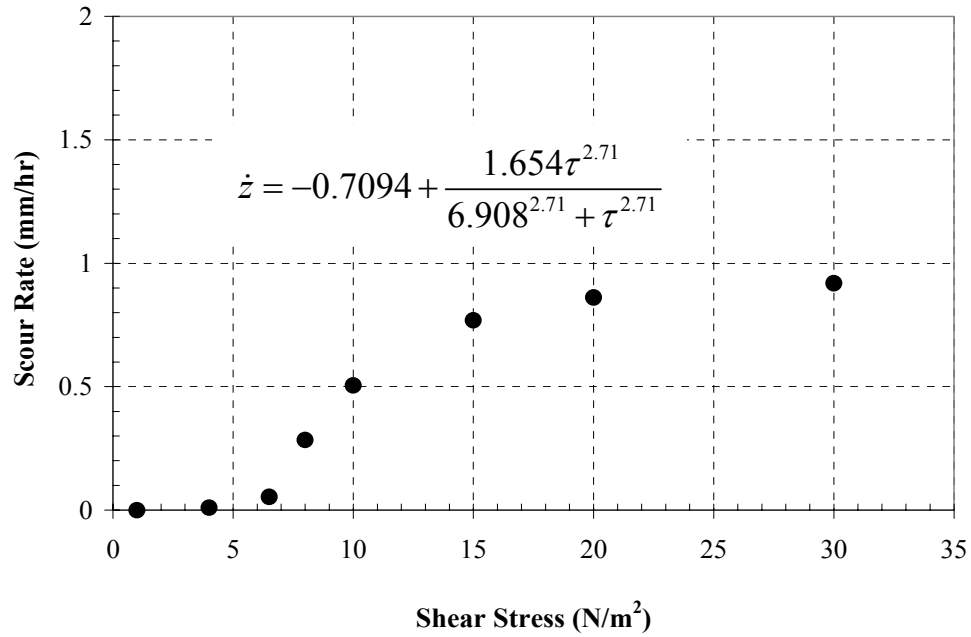


Figure 5.28: Scour Rate vs. Shear Stress –Navasota River Layer 1

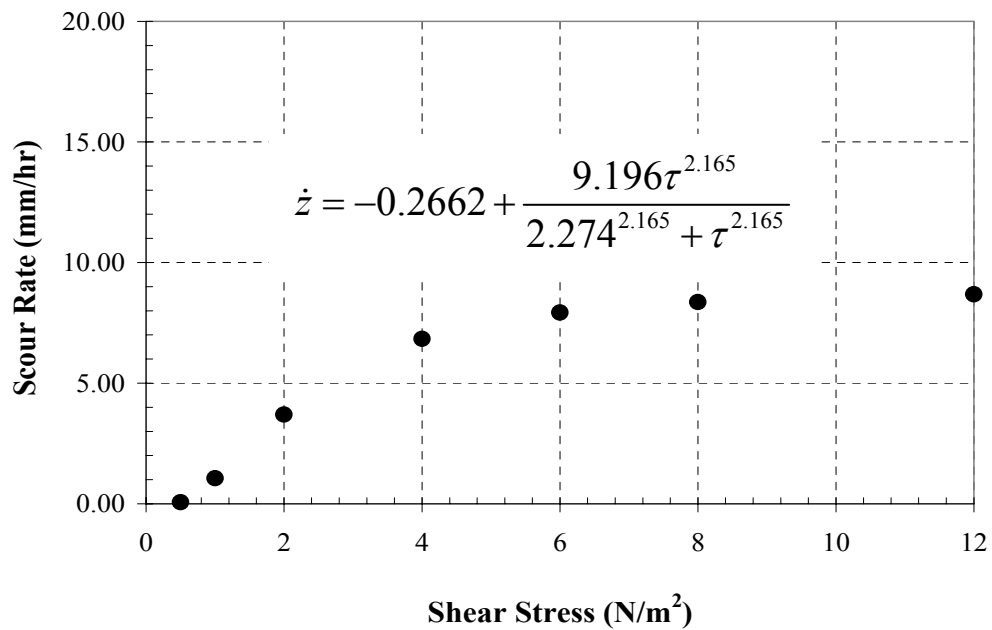


Figure 5.29: Scour Rate vs. Shear Stress –Navasota River Layer 2

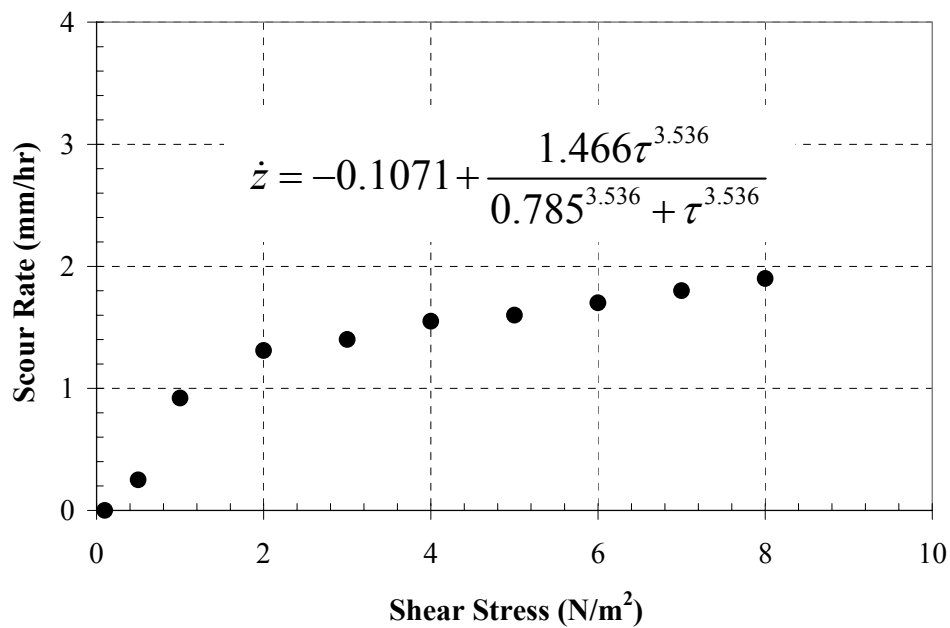


Figure 5.30: Scour Rate vs. Shear Stress –Brazos River Layer 1

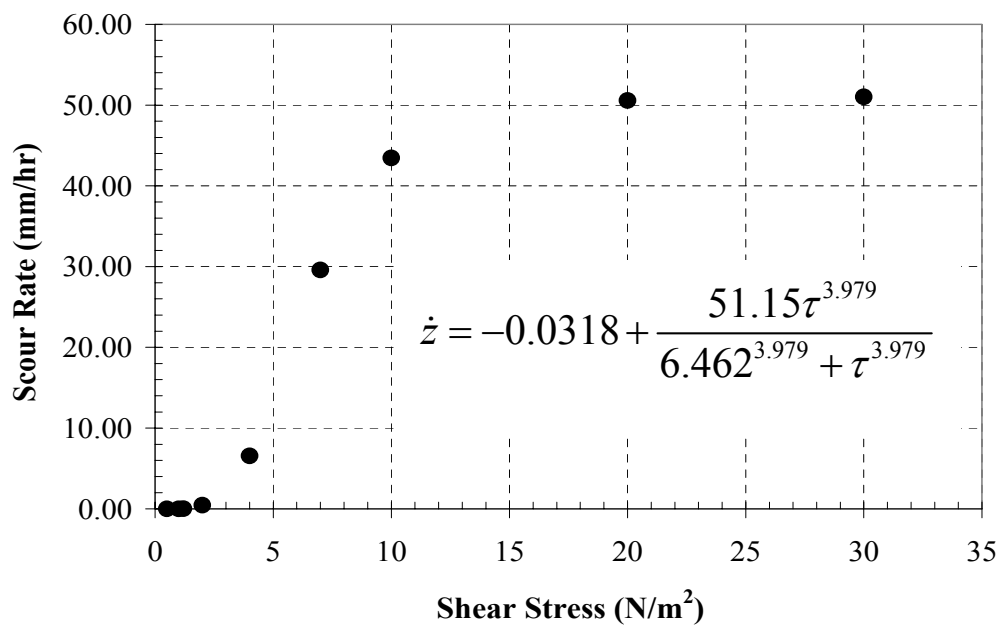


Figure 5.31: Scour Rate vs. Shear Stress –Trinity River Layer 1

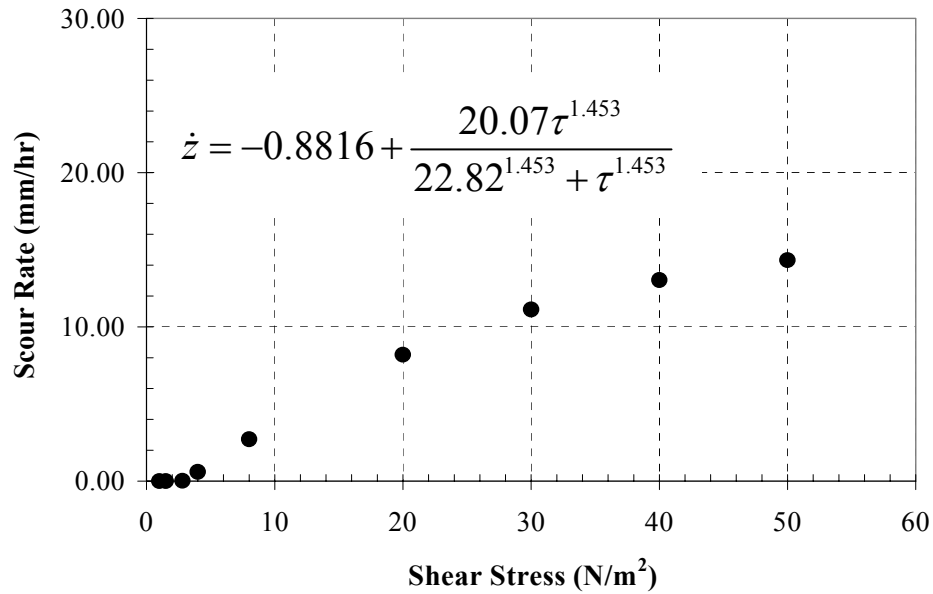


Figure 5.32: Scour Rate vs. Shear Stress –Trinity River Layer 2

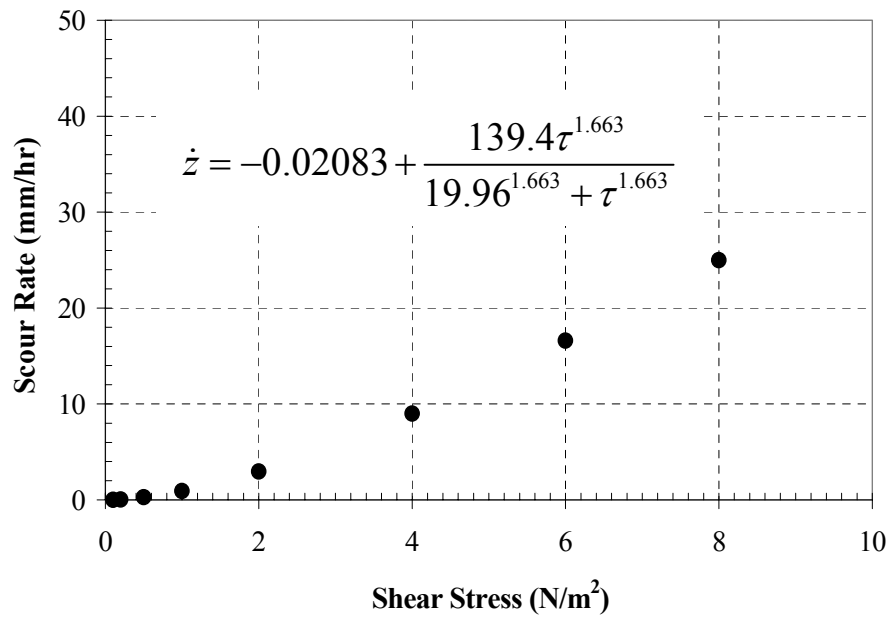


Figure 5.33: Scour Rate vs. Shear Stress –San Marcos River Layer 1

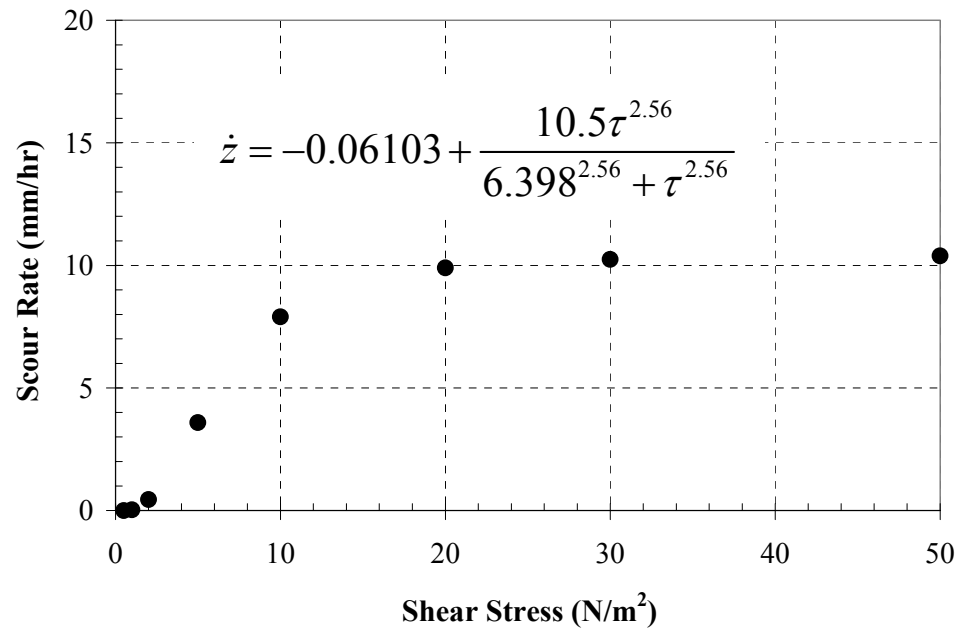


Figure 5.34: Scour Rate vs. Shear Stress –San Marcos River Layer 2

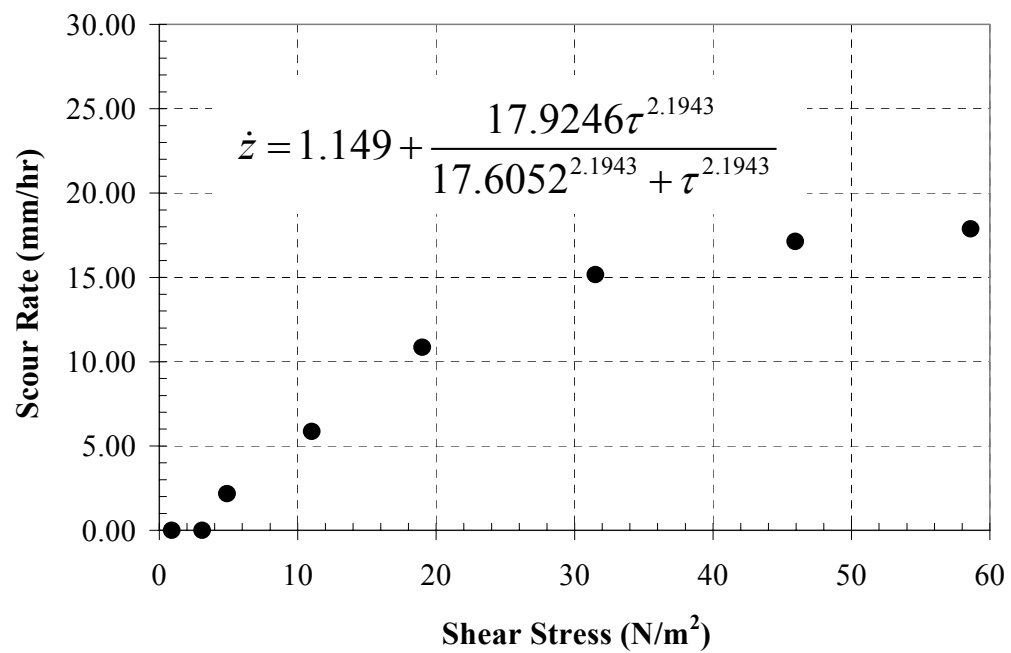


Figure 5.35: Scour Rate vs. Shear Stress –Sims Bayou Layer 1

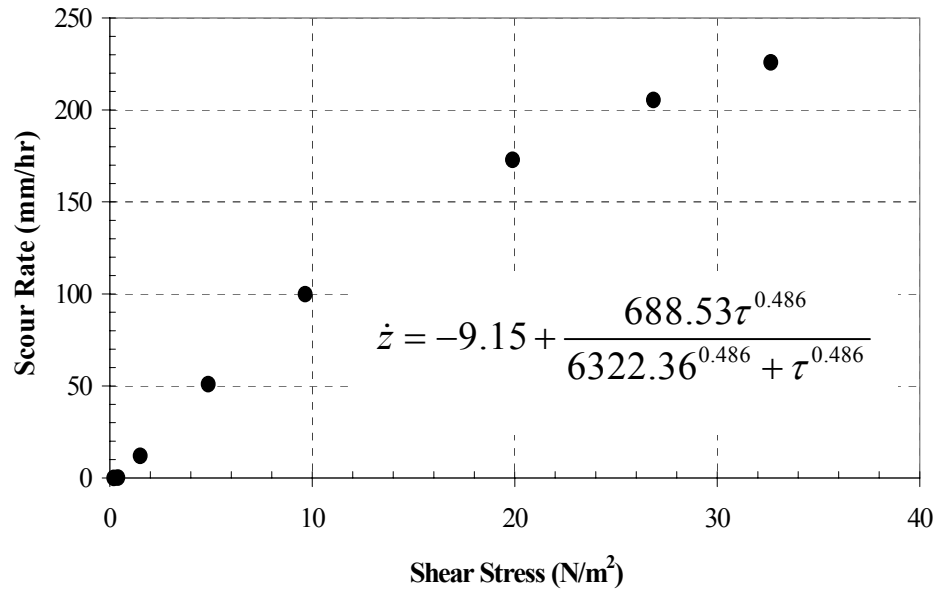


Figure 5.36: Scour Rate vs. Shear Stress –Bedia Creek Layer 1

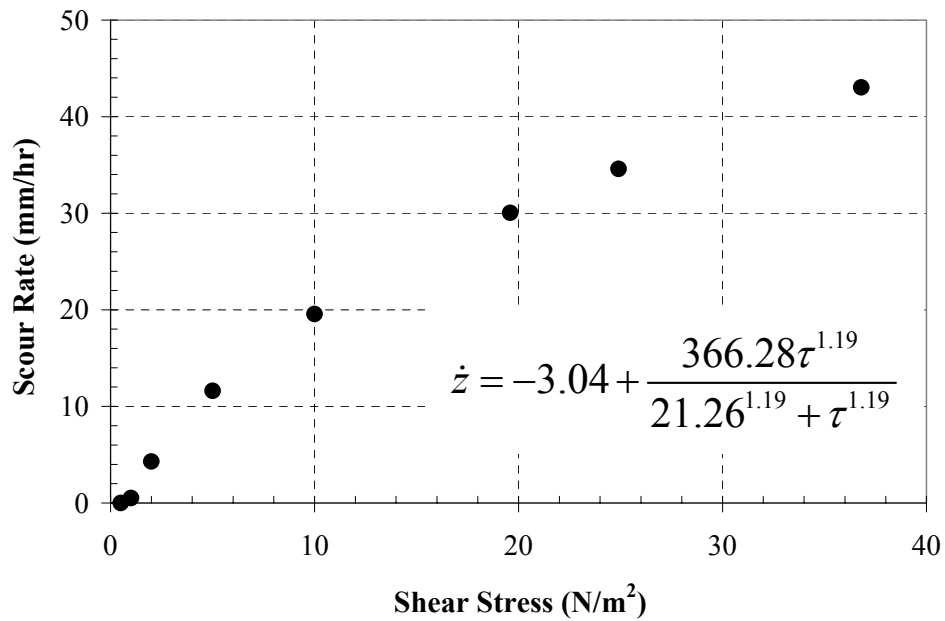


Figure 5.37: Scour Rate vs. Shear Stress –Bedia Creek Layer 2

5.3.6 EQUIVALENT TIME FOR CONTRACTION SCOUR

Once the parameters to calculate the contraction scour by using the SRICOS-EFA program have been prepared, then the analysis period will be separated into small time durations, for example 5 years. It is helpful to generate more case histories and make more data points in the regression analysis. During the process to calculate the equivalent time for each case, it was found that the duration of hydrograph t_{hyd} , flow velocity V_{max} and the mean initial scour rate Z_i affect the equivalent time t_{equiv} significantly. Hence the parameters in the equivalent time equation will contain t_{hyd} (duration of hydrograph), V_{max} (maximum velocity) and $Z_{i,mean}$ (mean initial scour rate). The values of mean initial scour rates $Z_{i,mean}$ were determined by weighting the average values of initial scour rates based on the thickness of different soil layers.

Following are the steps of equivalent time's calculation for each case:

Step 1: Calculate the contraction scour with whole hydrograph for each channel by SRICOS-EFA method,

Step 2: Break the whole hydrograph into small hydrographs with 5, 10, 20.. years duration,

Step 3: Find the maximum velocity through the analysis period for each case,

Step 4: Calculate the contraction scour with V_{max} instead of the whole hydrograph,

Step 5: Find the equivalent time by comparing the contraction scour depths obtained in Step 1 and Step 4.

The results of equivalent times for the 6 selected channels for contraction scour are shown in Table 5.5.

Table 5.5: Equivalent Time t_{equiv} (Contraction Scour) and Selected Parameters

River	t_{hyd} (Years)	V_{max} (m/s)	Scour Rate (mm/hr)	t_{equiv} (Hours)
Trinity River	5	2.76	46.97	860.8
	10	2.76	44.88	1111.2
Navasota River	5	2.68	0.95	3988.0
	10	2.75	2.63	4788.7
	15	2.82	3.33	5147.3
	20	2.82	3.33	5247.6
	25	2.82	3.50	5448.3
	30	2.82	3.51	5465.7
	35	2.82	3.90	6089.2
San Marcos River	5	1.48	131.88	123.17
	10	1.48	131.88	126.22
	15	1.7	127.72	324.00
	20	1.7	127.20	343.60
	25	1.7	126.60	366.40
Bedias River	5	0.93	49.37	126.2
	10	0.96	51.04	146.4
	15	0.96	51.04	160.9
	20	0.96	51.04	184.7
	25	0.97	51.6	205.4
	30	0.97	51.6	209.2
Brazos River	5	3.1	1.36	8477.7
	10	3.1	1.36	10229.2
	15	3.1	1.36	12790.4
	20	3.1	1.36	13519.9
	25	3.1	1.36	14417.9
	30	3.1	1.36	20558.1
	35	3.1	1.36	21479.6
Sims Bayou	2	0.85	17.13	125.7

The equivalent time equation for contraction scour was obtained by multi-regression technique, which is shown in the following:

$$t_{equiv}(hrs) = 644.32 g_{hydr}^{0.4242} (yrs) g_{max}^{1.648} \left(\frac{m}{s} \right) g_{t,mean}^{-0.605} \left(\frac{mm}{hr} \right) \quad (5.5)$$

Compare equivalent time t_{equiv} from Equation 5.5 and the results from Table 5.5. The relationship is shown in the following Figure 5.38.

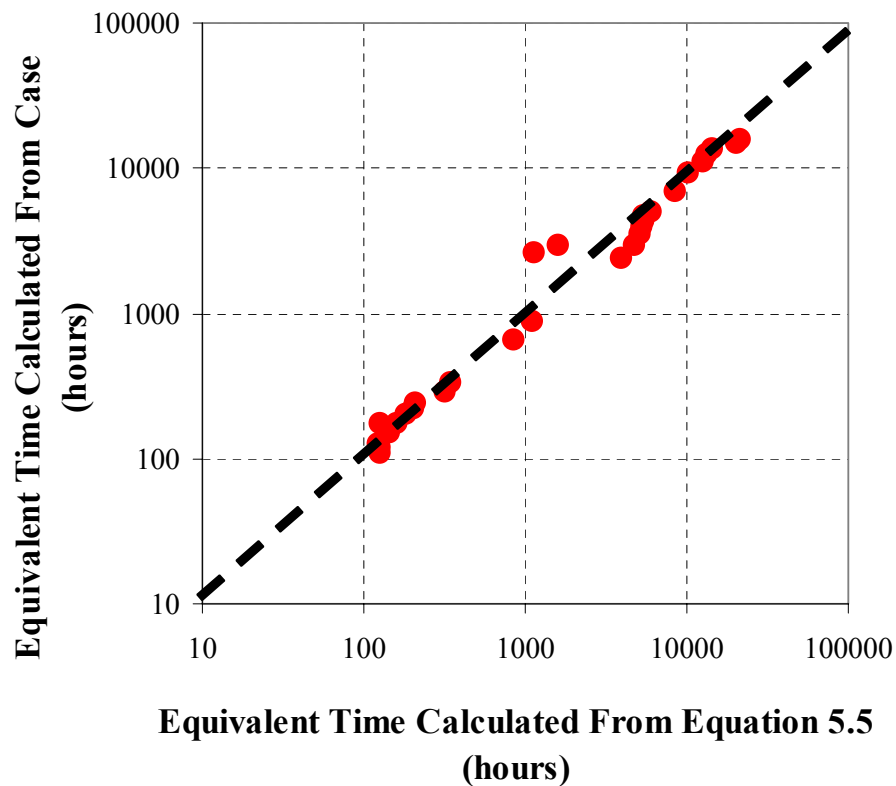


Figure 5.38: Comparison of Equivalent Time t_{equiv}

The equivalent time equation shows the reasonable tendency. The tendency can be described as higher equivalent time t_{equiv} with increasing duration of the hydrograph t_{hyd} and increasing the maximum velocity V_{max} . On the other hand, lower equivalent time t_{equiv} will occur with increasing the mean initial scour rate $\alpha_{t,mean}$. The statistic coefficient of determination R^2 in the comparison of equivalent time from case calculations and equivalent time from Equation 5.5 (Figure 5.38) was 0.97.

The contraction scour depths calculated by using the simple SRICOS-EFA method with the parameters of the equivalent time t_{equiv} from Equation 5.5, the mean initial scour rate $\alpha_{t,mean}$, the hydrograph time t , and the maximum scour depth calculated by Equation 4.26 will be compared to the contraction scour depths calculated from SRICOS-EFA method by inputting the whole hydrographs. The results are shown in following Table 5.6 and Figure 5.39.

Table 5.6: Comparison of Results by Simple SRICOS-EFA and SRICOS-EFA Method

River	t_{hyd.} (Year)	t_{equiv.} (hours)	Simple SRICOS-EFA (mm)	SRICOS-EFA (mm)
Sims Bayou	2	125.7	1420.9	1421.8
Bedias River	5	126.2	2457.0	2654.5
	10	146.4	2944.6	2935.3
	15	160.9	3138.5	3043.1
	20	184.7	3270.3	3195.8
	25	205.4	3438.1	3359.9
	30	209.2	3517.0	3379.5
Brazos River	5	8477.7	6975.9	7601.9
	10	10229.2	8456.8	8569.4
	15	12790.4	9377.1	9775.1
	20	13519.9	10046.2	10080.7
	25	14417.9	10571.1	10437.2
	30	20558.1	11002.1	12410.1
	35	21479.6	11366.9	12651.0
Navasota River	5	3988.0	6372.3	6211.7
	10	4788.7	8007.8	8236.8
	15	5147.3	8998.0	9108.0
	20	5247.6	9409.3	9261.5
	25	5448.3	9724.5	9548.2
	30	5465.7	9968.2	9572.3
	35	6089.2	10189.2	10314.6
San Marcos River	5	123.17	6042.0	5976.4
	10	126.22	6637.4	6030.0
	15	324.00	8305.2	6719.5
	20	343.60	8552.3	6750.0
Trinity River	5	860.8	12424.3	12536.9
	10	1111.2	13762.9	13135.1

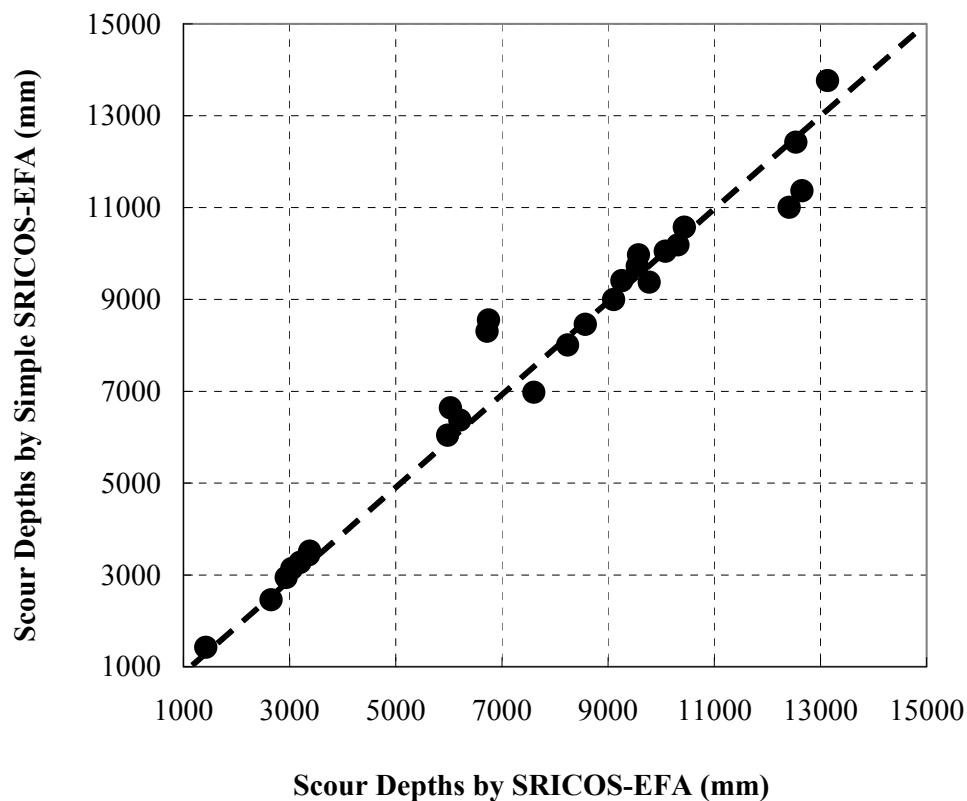


Figure 5.39: Comparison of Results by Using SRICOS-EFA and Simple SRICOS-EFA

As the results are shown in Table 5.6 and Figure 5.39, the values of contraction scour depths by using these two methods are very close in most cases. The statistic coefficient of determination R^2 is 0.965. Therefore it is indicated that the simple SICOS-EFA method for contractions scour calculation is reasonable and applicable.

CHAPTER VI

SRICOS-EFA METHOD FOR COMPLEX PIER AND

CONTRACTION SCOUR AND SRICOS-EFA

COMPUTER PROGRAM

6.1 INTRODUCTION

The new SRICOS-EFA method for complex pier and contraction scour can be used to handle the complex pier, and contraction scour alone, or it can handle the superposition of complex pier scour and contraction scour (integrated SRICOS-EFA method). Since the abutment scour is not one of the research parts in this project, the method cannot solve all the bridge scour problems. But the final target of this method will include the abutment scour to solve the bridge scour problems in different conditions. A method to predict the bridge scour was developed in HEC-18. This method will compute the magnitude of contraction scour, the local scour at piers, and the local scour at abutments. Then account the bridge scour as adding them together. It should be noted that the results of HEC-18 are conservative, which has been often stated by engineers. The SRICOS-EFA integrated method is not just only adding the complex pier scour and contraction scour together. The method was developed based on considering the time factor, the soil properties and most importantly, the interactions between the contraction scour and pier scour. In following sections, the principle, accumulation algorithm and the step-by-step procedure of SRICOS-EFA method will be presented.

6.2 INTEGRATED SRICOS-EFA METHOD

6.2.1 GENERAL PRINCIPLE

This method integrates the pier scour and the contraction scour into a set of calculations. In the integrated SRICOS-EFA method for calculating bridge scour, the scour process is separated into two imaginary stages: (1) calculation of the total contraction scour, (2) calculation of pier scour. The followings are the assumptions for the integrated SRICOS-EFA method development:

1. Contraction scour is uniformly scoured.

Li (2002) performed a series of contraction flume tests in a hydraulic laboratory at Texas A&M University. Three types of scour profiles were identified in the tests, which are shown in Figure 6.1.

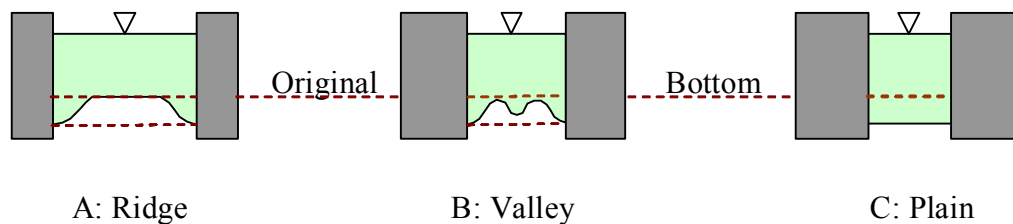


Figure 6.1: Three types of contraction scour profiles (after Li, 2002)

In the integrated SRICOS-EFA method, the contraction scour is assumed to occur uniformly along the entire river channel bottom and the contraction scour depth is the same in the different locations along the bridge cross section.

2. Contraction is assumed to occur first and pier scour occur afterward.

The scour shape of pier scour usually can be defined as a hole around the pier (Herbich, 1984). The profile of contraction scour has been assumed uniformly in the bridge cross section. If the contraction scour is assumed to occur first, the contraction scour depth is uniform, which makes it easier and more logical to superpose the pier scour depth on the contraction scour. This procedure doesn't mean that the piers are not influencing the contraction scour; indeed the piers are considered in the contraction scour calculations because their total projection width of piers is added to the abutment projection width to calculate the total contraction ratio. Hence in integrated SRICOS-EFA method, the contraction scour is calculated for a given hydrograph firstly, and then the pier scour is calculated afterward.

3. If contraction scour doesn't occur, the velocity to calculate the pier scour will be the mean depth velocity in the pier location without pier presence.

If the contraction scour calculations indicate that there is no occurrence of contraction scour at the bridge site, then the pier scour is calculated by following the SRICOS-EFA complex pier scour calculation procedure. In this case, HEC-RAS, for example, can be used to calculate the water depth and the approach velocity in the contracted section after removing the piers obstructing the flow. The removal of the piers is necessary because the velocity used for pier scour calculations is the mean depth velocity at the location of the pier if the pier were not there.

- 4. If contraction scour occurs, the velocity to calculate the pier scour will be V_c (the critical velocity of soil).**

If the calculations indicate that the contraction scour occurs at the bridge site, then the pier scour calculations are made by using the critical velocity, not the actual velocity, because when contraction scour has stopped (Z_{\max} (cont) is reached), the velocity in the contracted zone is critical velocity V_c . The value of V_c can be obtained from the EFA tests for cohesive soil or the equations presented in the HEC-18 for non-cohesive soil.

- 5. If contraction scour occurs, the water depth for pier scour calculation will be the original water depth plus the maximum contraction scour depth.**

When the contraction scour has stopped, the velocity has reached the critical velocity in the river and the water depth in contraction section has become deeper than in the original one. So after contraction scour occurrence, the water depth is the total water depth of the original water depth and the calculated maximum contraction scour depth in the contracted section.

This approach is valid for the calculations of maximum scour depth in combined scour case. For the time stepping process, the maximum scour depth is not reached at each step, but the maximum scour depth (Z_{\max}) will be one of the essential parameters to build the hyperbola model to describe the scour development curve. Therefore the above technique is included in each time step. The other parameter calculated at each time step is initial maximum shear stress τ_{\max} ; this shear stress is used to read the initial scour rate \dot{z}_i on the erosion function obtained from EFA tests. Both parameters Z_{\max} and \dot{z}_i are

used to generate the scour depth versus time curve. The actual scour depth is read on that curve at the value equal to the time. The details of the procedure are presented in the next section.

6.2.2 THE INTEGRATED SRICOS-EFA METHOD PROCEDURES

Step I: Input Data Collection (Figure 6.2)

Water: flow (mean velocity V_1 , and water depth H_1) at bridge upstream where the flow is not noticeably influenced by the existence of bridge contractions and piers.

Geometry: bridge contraction parameters and pier geometry.

$$\text{Total Contraction Ratio: } B_2/B_1 = (w_1 + w_2 + w_3 + w_4)/B_1 \quad (6.1)$$

Soil: Critical shear stress and erosion function.

All the parameters are defined in Figure 6.2.

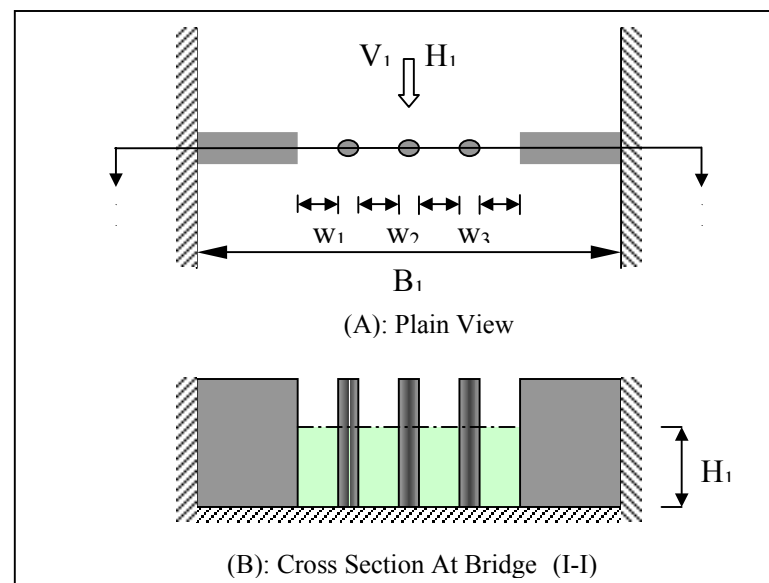


Figure 6.2: Step I - Bridge Scour Input Data and Primary Calculation

Step II: Maximum Contraction Scour Calculation (Figure 6.3)

Based on the upstream flow condition, the soil properties and the total bridge contraction ratio calculated in Step I, the maximum contraction scour can be obtained directly by Equation 6.2:

$$Z_{\max}(cont) = K_{\theta}K_L 1.90 \left(\frac{1.38 \left(V_1 \frac{B_1}{B_2} \right) - \left(\frac{\tau_c}{\rho} \right)^{0.5}}{\sqrt{gH_1} - \frac{1}{gnH_1^{1/3}}} \right) H_1 \geq 0 \quad (6.2)$$

$Z_{\max}(cont)$ (m) is the maximum contraction scour, K_{θ} is the factor for the influence of the transition angle (K_{θ} is equal to 1), K_L is the factor for the influence of the length of the contracted channel (K_L is equal to 1), V_1 is the velocity in the uncontracted channel (m/s), B_1 is the width of the uncontracted channel (m), B_2 is the width of the contracted channel as defined in Equation 6.1 and Figure 6.2 (m), g is the acceleration due to gravity (m/s^2), H_1 is the water depth in the uncontracted channel (m), τ_c is the critical shear stress of the soil (KN/m^2), ρ is the density of water (kg/m^3), and n is the Manning's coefficient ($s/m^{1/3}$).

The engineers may prefer to calculate the velocity V_{hec} in the contracted channel using width B_2 as calculated according to Equation 6.1 and Figure 6.2 by using a program like HEC-RAS. In this case, the engineer needs to use Equation 6.3.

$$Z_{\max}(cont) = K_{\theta}K_L 1.90 \left(\frac{1.49V_{hec} - \left(\frac{\tau_c}{\rho} \right)^{0.5}}{\sqrt{gH_1} - \frac{1}{gnH_1^{1/3}}} \right) H_1 \geq 0 \quad (6.3)$$

Where, V_{hec} is the maximum velocity in the middle of the contracted channel. If the value of maximum contraction scour $Z_{max} (cont)$ is negative, the flow and contraction is not severe enough to cause any contraction scour and the maximum contraction scour is zero. If there is contraction scour, the shear stress reached on the river bottom at the time of maximum contraction scour $Z_{max} (cont)$ is the critical shear stress of the soil τ_c . The scour at the bridge site is shown in Figure 6.3.

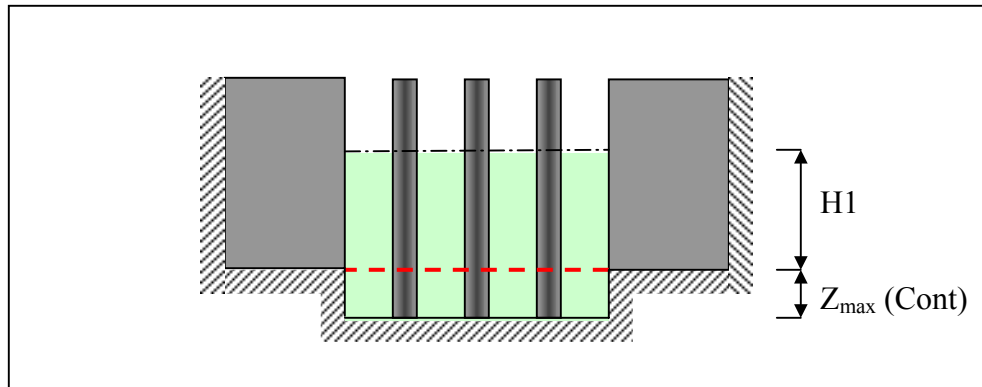


Figure 6.3: Step II - Contraction Scour Calculation and Distribution

Step III: Pier Scour Calculation

- (1) If Step II leads to no contraction scour, the pier scour is calculated by using velocity V and water depth H at the location of the pier in the contracted channel assuming that the bridge piers are not there. The velocity and water depth can be calculated directly using the upstream flow inputs and the bridge abutment contraction through a program like HEC-RAS for example.

(2) If Step II leads to a maximum contraction scour depth Z_{\max} (cont), then the maximum pier scour depth is calculated by using the critical velocity for the soil and the water depth including the contraction scour depth. These are:

$$H_2 = H_1 + Z_{\max}(Cont) \quad (6.4)$$

$$V = \begin{cases} V_c = \sqrt{\frac{\tau_c H_2^{\frac{1}{3}}}{\rho g n^2}} & Z_{\max}(Cont) > 0 \\ V_{hec} & Z_{\max}(Cont) = 0 \end{cases} \quad (6.5)$$

Where H_2 is the water depth to use in the pier scour calculation after contraction scour calculation, H_1 is the water depth before contraction scour starts, V_c is the critical velocity at a water depth H_2 of the bed material.

Then the maximum pier scour depth Z_{\max} (pier) can be calculated by following equation:

$$Z_{\max}(Pier) = 0.18 K_w K_{sp} K_{sh} R_e^{0.635} \quad (6.6)$$

Where K_w is the correction factor for pier scour water depth, given by:

$$\begin{aligned} \text{For } H/B \leq 1.6 & \quad K_w = 0.85 (H/B)^{0.34} \\ \text{For } H/B > 1.6 & \quad K_w = 1 \end{aligned} \quad (6.7)$$

K_{sp} is the correction factor for the pier spacing effect on the pier scour depth, when n piers of diameter B are installed in a row, given by:

$$K_{sp} = \frac{B_1}{(B_1 - nB)} \quad (6.8)$$

K_{sh} is the correction factor for the pier shape effect on pier scour. K_{sh} is equal to 1.1 for rectangular piers with length to width ratios larger than 1. R_e is the Reynolds number:

$$\text{Re} = \frac{VB'}{\nu} \quad (6.9)$$

where V is the mean depth average velocity at the location of the pier if the pier is not there when there is no contraction scour, or the critical velocity V_c (equation 6.5) of the bed material if contraction scour occurs, B' is the pier diameter or projected width ($L\sin\alpha + B\cos\alpha$), B and L are the pier width and length respectively, α is the flow attack angle and ν is the kinematic viscosity of water.

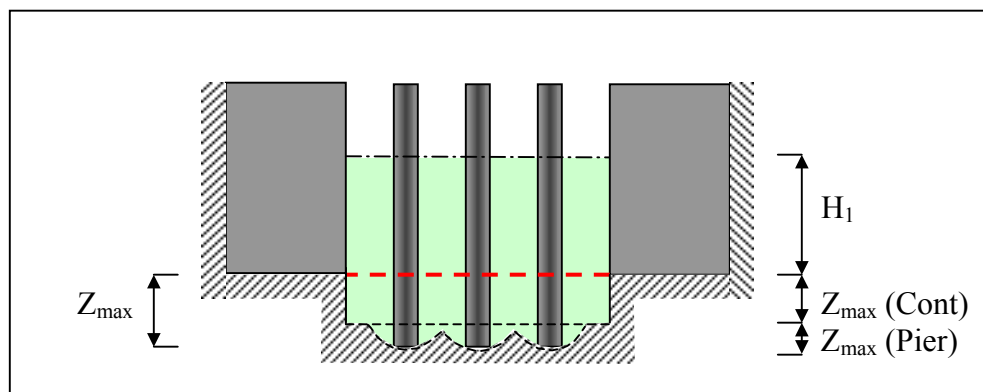


Figure 6.4: Steps III and IV – Calculations of Pier Scour and Superposition

Step IV: Total Bridge Scour Calculation

The maximum bridge scour is (Figure 6.4):

$$Z_{\max} = Z_{\max}(\text{Cont}) + Z_{\max}(\text{Pier}) \quad (6.10)$$

Step V: Maximum Shear Stress Around the Bridge Pier (Figure 6.5)

In the calculations of the initial development of the scour depth, the shear stress τ_{\max} is needed. This maximum shear stress is the one that exists around the bridge pier

since the pier is the design concern. Step V describes how to obtain τ_{\max} . Figure 6.5 gives the definition of parameters.

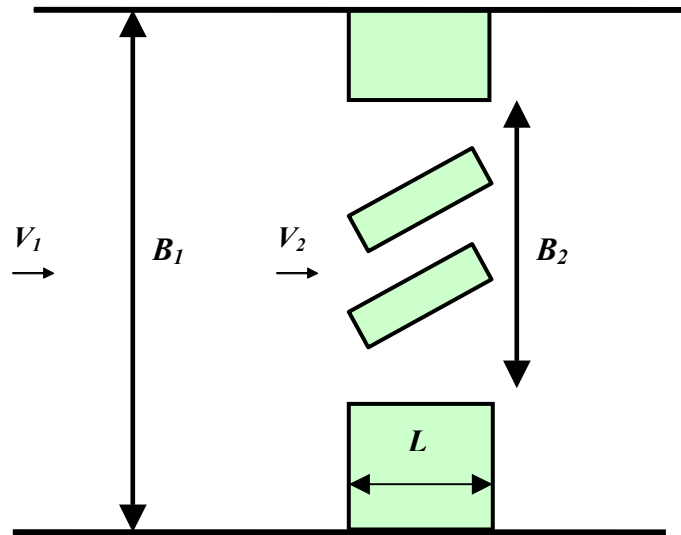


Figure 6.5: Plan-view of Complex Pier Scour and Contraction Scour

In this case of an uncontracted channel (no abutments), the maximum bed shear stress τ_{\max} around the pier is given by:

$$\tau_{\max} = k_w k_{sh} k_{sp} k_{\alpha} \cdot 0.094 \rho V_1^2 \left[\frac{1}{\log R_e} - \frac{1}{10} \right] \quad (6.11)$$

where ρ is the water density (kg/m^3), V_1 is the approach velocity (m/s), R_e is the Reynolds number based on pier diameter and approach velocity, k_w , k_{sh} , k_{sp} , k_{α} are the correction factors for water depth, shape, pier spacing and attack angle, respectively.

$$k_w = \frac{\tau_{\max}}{\tau_{\max}(\text{deep})} = 1 + 16 e^{-\frac{4H}{B}} \quad (6.12)$$

$$k_{sp} = \frac{\tau_{\max}}{\tau_{\max}(\text{single})} = 1 + 5 e^{-1.1 \frac{S}{B}} \quad (6.13)$$

$$k_{sh} = \frac{\tau_{\max}}{\tau_{\max}(\text{circle})} = 1.15 + 7 e^{-4 \frac{L}{B}} \quad (6.14)$$

$$k_{sh} = 1 \text{ for circular shape}$$

$$k_a = \frac{\tau_{\max}}{\tau_{\max}(0 \text{ deg})} = 1 + 1.5 \left(\frac{\alpha}{90} \right)^{0.57} \quad (6.15)$$

where H is the water depth, B is the pier diameter or projected width, S is the pier center to center spacing, L is the pier length, and α is the angle between the direction of the flow and the main direction of the pier.

In the case of a contracted channel (Figure 6.5), the maximum bed shear stress around pier is given by Equation 6.16 with exception that the velocity at the contracted section V_2 is used instead of the approach velocity V_1 . The equation can be written as:

$$\tau_{\max} = k_w k_{sh} k_{sp} k_{\alpha} 0.094 \rho V_2^2 \left[\frac{1}{\log \text{Re}} - \frac{1}{10} \right] \quad (6.16)$$

where V_2 is the mean depth velocity in the contracted channel at the location of the pier without the presence of the pier (m/s). The velocity V_2 can be obtained from HEC-RAS or from mass conservation for a rectangular channel

$$V_2 = 1.14 V_1 \left(\frac{B_1}{B_2} \right) \quad (6.17)$$

Step VI: Time History of the Bridge Scour

This part of the method proceeds like the original SRICOS-EFA method. The initial shear stress τ_{\max} around the pier is calculated from Equation 6.16. The corresponding erosion rate dz/dt (initial) is obtained from the erosion function (measured

in the EFA), and the maximum scour depth due to contraction scour and pier scour is calculated from Equation 6.10. With these two quantities defining the tangent to the origin and the asymptotic value of the scour depth versus time curve, a hyperbola is defined to describe the entire curve.

$$Z(t) = \frac{t}{\frac{1}{\dot{z}_i} + \frac{t}{Z_{\max}}} \quad (6.18)$$

where $Z(t)$ is the scour depths due to flood, t is the floods duration, \dot{z}_i is the initial erosion rate, Z_{\max} is the maximum scour depth due to flood, which can be calculated by Equation 6.10. In the case of a complete hydrograph and of a multi-layer soil system, the accumulation algorithms will be described as follows.

6.2.3 MULTI-FLOOD SYSTEM

The true hydrograph of a river contains the continuous floods as a function of time. The fundamental basis of the accumulation algorithms is that the velocity histogram is a time step function with a constant velocity value for each step. Usually the velocity hydrograph will be a constant value in everyday because the daily basis records are kept from gaging station maintained by USGS (US Geological Survey). The case of a sequence of two different constant velocity floods scouring a uniform soil is considered in Figure 6.6a.

In this case the flood 1 has velocity V_1 and lasts a time t_1 while flood 2 has velocity V_2 and lasts a time t_2 . After flood 1, a scour depth Z_1 is reached at time t_1 (Point A on Figure 6.6b), which can be calculated using the following equation:

$$Z_1 = \frac{t_1}{\frac{1}{\dot{z}_{i1}} + \frac{t_1}{Z_{\max 1}}} \quad (6.19)$$

For flood 2, the scour depth will be:

$$Z_2 = \frac{t_2}{\frac{1}{\dot{z}_{i2}} + \frac{t_2}{Z_{\max 2}}} \quad (6.20)$$

The scour depth Z_1 also can be created in a time t_e by flood 2 (Point B on Figure 6.6c). The time t_e is called the equilibrium time, which is the time required for a flood in the hydrograph to create the same scour depth as the one created by the previous flood in the hydrograph. So the time t_e can be obtained by using Equation 6.19 and 6.20 with $Z_2 = Z_1$ and $t_2 = t_e$.

$$t_e = \frac{t_1}{\frac{\dot{z}_{i2}}{\dot{z}_{i1}} + t_1 \dot{z}_{i2} \left(\frac{1}{Z_{\max 1}} - \frac{1}{Z_{\max 2}} \right)} \quad (6.21)$$

When flood 2 starts, even though the scour depth Z_1 was due to flood 1 over a time t_1 , the situation is equivalent to having had flood 2 for a time t_e . Therefore when flood 2 starts, the scour depth versus time curve proceeds from point B on Figure 6.6c to point C after time t_2 . The z versus t curve for the sequence of flood 1 and 2 follows the path OA on the curve for flood 1 then switches to BC on the curve for flood 2. This is shown as the curve OAC on Figure 6.6d.

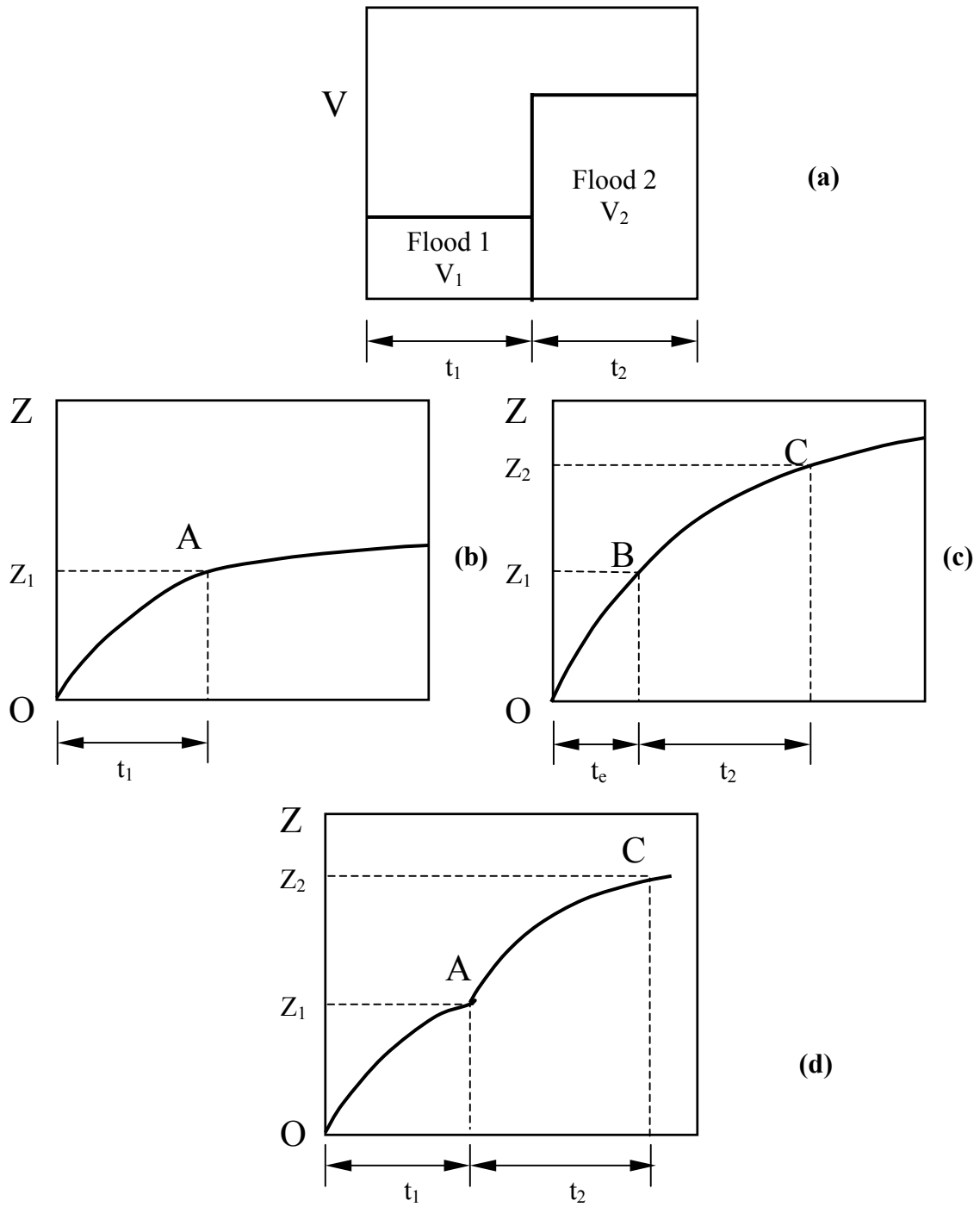


Figure 6.6: Scour due to a Sequence of Two Flood Events

The procedure discussed above describes the case in which the following velocity V_2 is higher than the previous velocity V_1 . In the opposite case, the following velocity V_2 is less than the previous velocity V_1 . After a time t_1 , flood 1 creates a scour depth. This depth should be compared with $Z_{\max 2}$ due to flood 2. If Z_1 is larger than $Z_{\max 2}$ it means that when flood 2 starts the scour hole has been already larger than the flood 2 can be created. Hence, the flood 2 cannot add any additional scour depth and the scour depth versus time curve remains flat during flood 2. If Z_1 is less than $Z_{\max 2}$, the procedures of Figure 6.6d should be followed.

In general, the complete velocity hydrograph will be broken into a series of partial flood events, each of which will last Δt . The scour depth due to the first two floods (flood 1 and flood 2) in the hydrograph will be handled by following procedures of Figure 6.6d. Then the process will consider the time increments and regard the following flood as a new “flood 2” at each step. The time Δt is typically one day and the velocity hydrograph can be 70 years long.

6.2.4 MULTI-LAYER SOIL SYSTEM

The soil is assumed to be uniform in the multi-flood system analysis. In reality, the soil usually involves different layers and the soil characteristics vary significantly with soil depth. It is necessary to have the accumulation procedure in the multi-layer soil system.

The soil model considered here consists of two layers, the first layer with ΔZ_1 thickness and the second layer with ΔZ_2 thickness. The riverbed is subject to a constant velocity V (Figure 6.7a). The scour depth z versus time curves for Layer 1 and

Layer 2 are given by Equation 6.18 (Figure 6.7b, Figure 6.7c). If the thickness of Layer 1 ΔZ_1 is larger than the maximum of scour depth $Z_{\max 1}$, which is calculated by Equation 6.10, then the scour process only involves the Layer 1 and the scour depth will not reach the Layer 2. On the other hand, the maximum of scour depth $Z_{\max 1}$ may exceed the thickness ΔZ_1 , in which the Layer 2 will involve the scour process as well. When this occurs, the scour depth ΔZ_1 (Point A on Figure 6.7b) over a time t_1 , at that time the situation is equivalent to having had Layer 2 scoured over an equivalent time t_e (Point B on Figure 6.7c). Therefore when the Layer 2 starts to erode, the scour depth versus time curve will proceed from Point B to Point C on Figure 6.7c. The combined scour process for the two-layer system will be the OAC curve on Figure 6.7d.

In most cases, there will be a series of soil layers with different erodibilities in the actual bridge sites. The computations proceed by stepping forward in time. The time steps are Δt long, the velocity is the one for the corresponding flood event, and the erosion function (\dot{z} vs τ) is the one for the soil layer corresponding to the current scour depth (bottom of the scour hole). When Δt is such that the scour depth enters to a new soil layer, the computations follow the process described in Figure 6.7d.

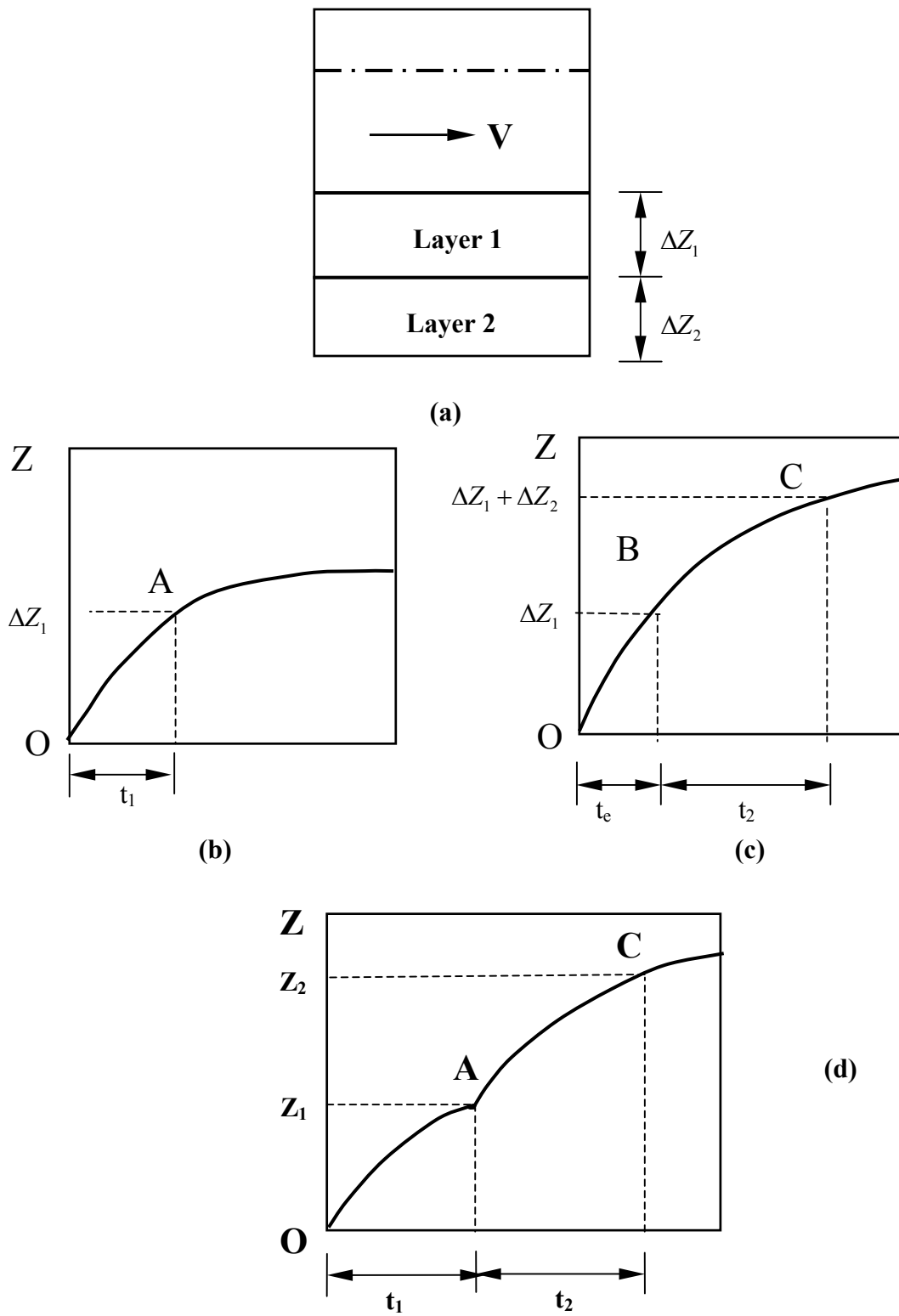


Figure 6.7: Scour of a Two-Layer Soil System

6.3 THE SRICOS-EFA METHOD PROGRAM

6.3.1 GENERAL INFORMATION

The SRICOS-EFA program is associated with the SRICOS-EFA method. This program includes all the procedures of the SRICOS-EFA method except the experiment parts. It contains calculations of the parameters such as maximum shear stresses for different scours, maximum scour depth, the scour depth vs. time curve, and transformation of discharge into velocities etc. In addition, the techniques to handle multi-flood and multi-layer systems are combined in this program. The old SRICOS-EFA program was written in FORTRAN by using Visual FORTRAN 5.0. The flow chart of the program in Figure 6.8 gives an overall view of the SRICOS-EFA method. It shows the general process and all the equations used in the program. We are implementing this flow chart into the SRICOS-EFA program. As the chart shows, there is one branch to handle complex pier scour alone, one branch to handle contraction scour alone, and one branch to handle the concurrent occurrence of complex pier scour and contraction scour.

For the input hydrograph, the number of velocity or discharge data points can reach several thousand for the time duration corresponding to the design life of bridges if the velocity data is given on a daily basis. The velocity or discharge data should be prepared in the format of an ASCII file or a text document before running the program. The input data can be either in the Metric System or the U.S. Customary System; the output can be in either system.

Because the DOS version of the program was very difficult for users to operate and took long time to input the parameters, it was transformed to WINDOWS version in November 2003. The old FORTRAN program code is the main engine to implement the SRICOS-EFA method. The interfaces of the new WINDOWS program were written by using C++. The new SRICOS-EFA program is a user friendly, interactive code that lets the users operate the program very easily and directly. The interfaces of the program include the main screen, the geometry data input screen, the soil data input screen, the water data input screen and the output screen etc. From Figure 6.9 to Figure 6.14 show the interfaces of that WINDOWS version SRICOS-EFA program:

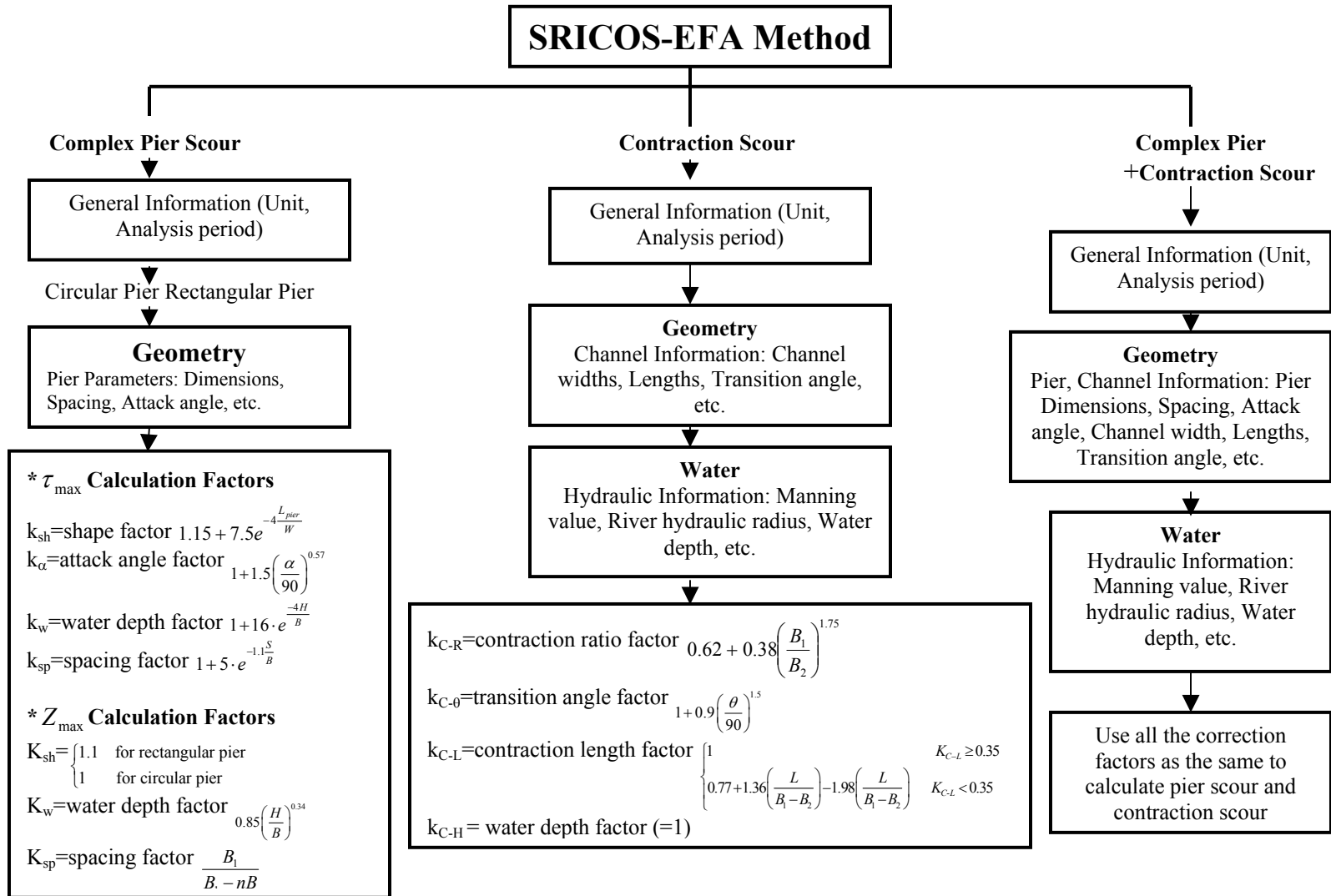
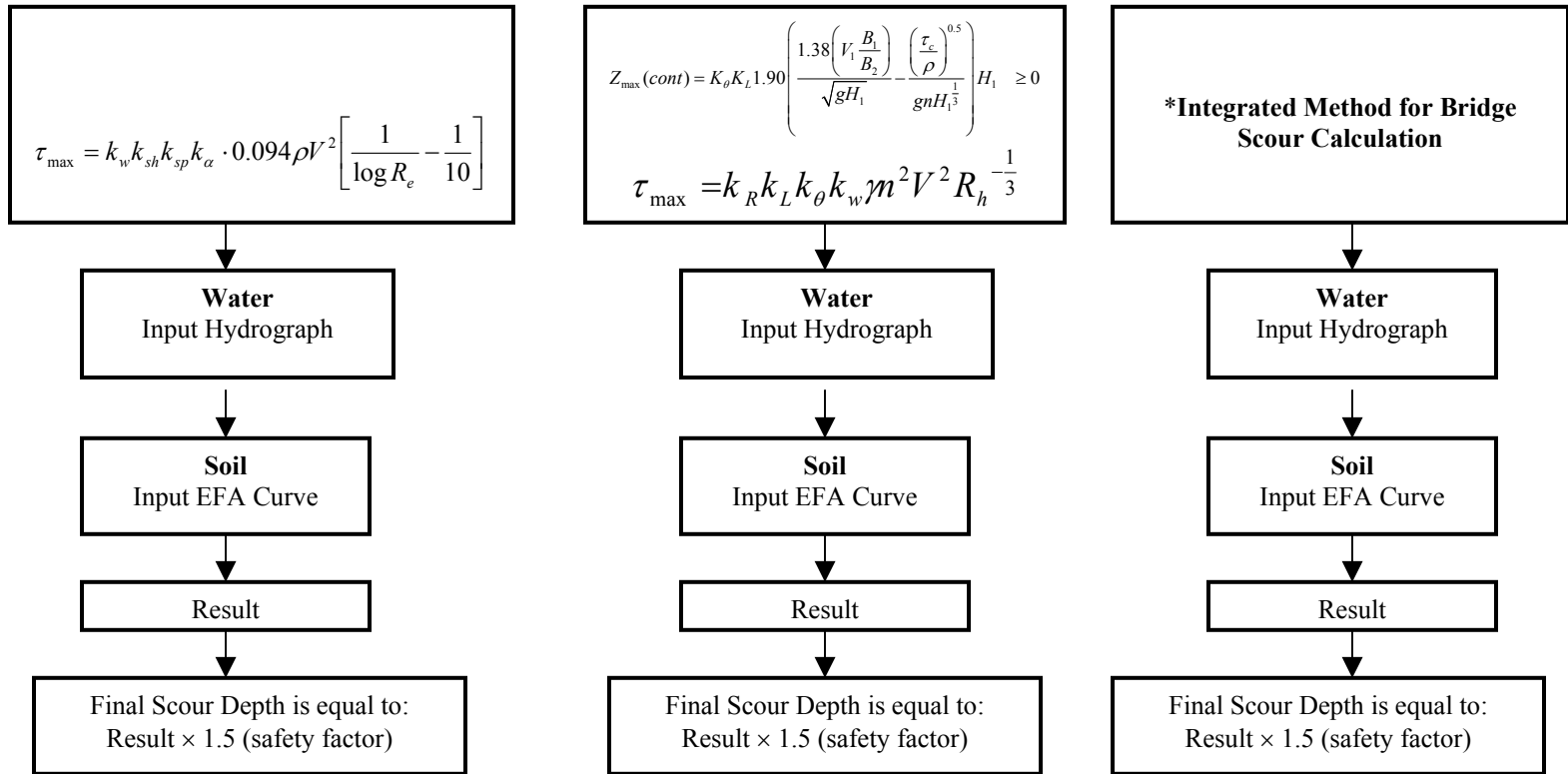


Figure 6.8: Flow Chart of SRICOS-EFA Method



***Integration Method for Bridge Scour Calculation is presented detailed in Section 6.2.**

Note:

- | | | | |
|--|--|------------------------------|--|
| L_{pier} : Length of rectangular pier | S: Spacing of group piers | V_1 : Approaching velocity | ρ : unit mass of water at 20°C |
| W: Width of rectangular pier | B_1 : Width of un-contracted channel | n: Manning's value | g: acceleration of gravity |
| B: Diameter of pier | B_2 : Width of contracted channel | R_e : Reynolds number | τ_c : Critical shear stress of riverbed |
| H: Approaching water depth | L: Length of contracted channel | R_h : Hydraulic radius | |

Figure 6.8: Continued

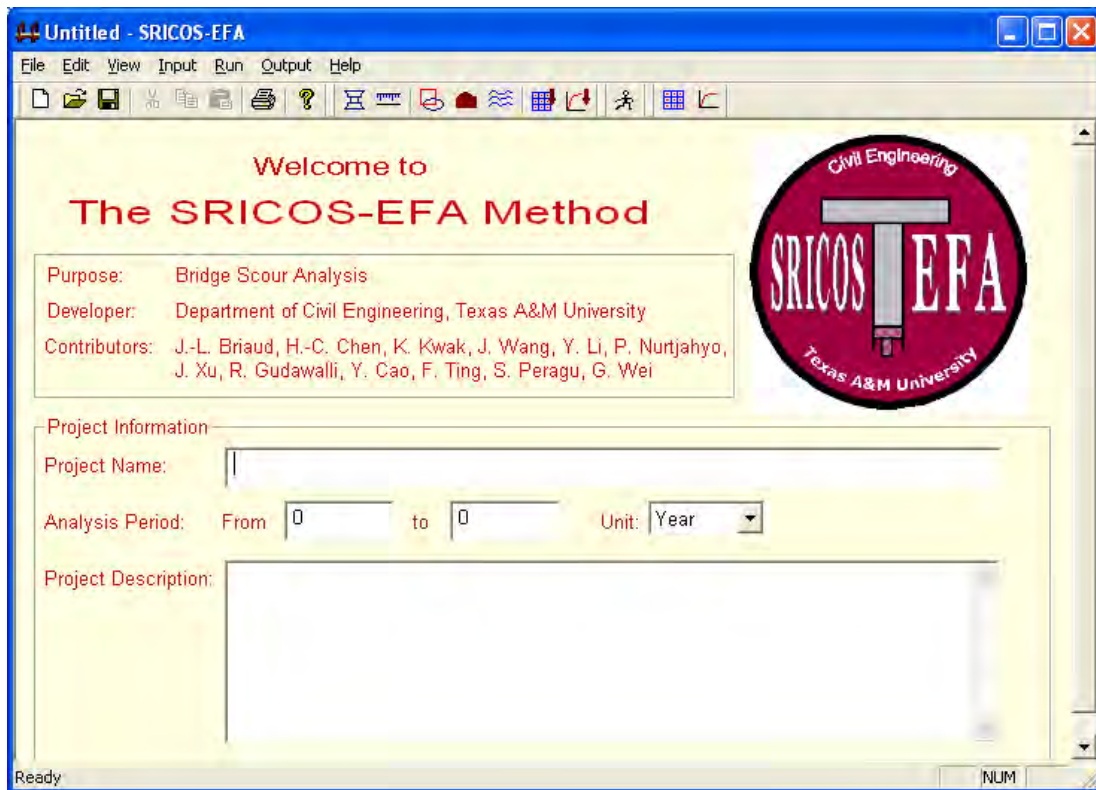


Figure 6.9: The Main Window of SRICOS-EFA Program

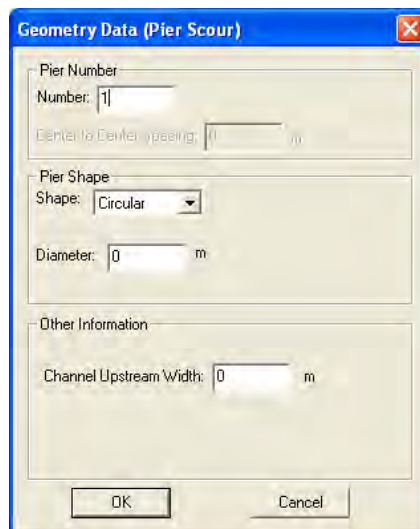


Figure 6.10: The Geometry Data (Pier Scour) Input Screen

Soil Data (Pier Scour)

Number of Layers: 1

Current Layer: Layer 1

Erodibility Properties (Layer 1)

Layer Thickness: 0 m

Critical Shear Stress: 0 N / m²

Points on EFA Curve: 0

Point No	Shear Stress (N/m ²)	Scour Rate (mm/hr)

OK Cancel

Figure 6.11: The Soil Data (Pier Scour) Input Screen

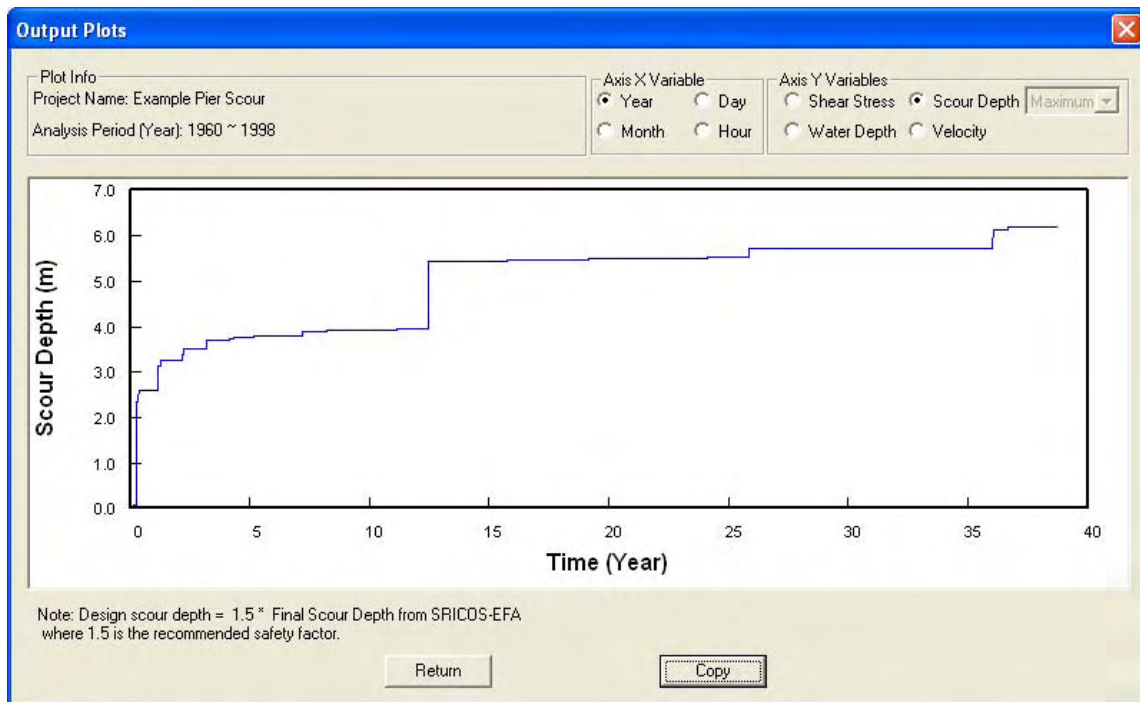


Figure 6.14: The Output Plots Screen

Several new features were added into the WINDOWS version of the program, which the DOS version didn't contain. One feature is the 100 year flood, Q_{100} , or 500 year flood, Q_{500} , insertion into the existing hydrograph. Currently, most bridge designs are based on the Q_{100} or Q_{500} flood as the essential parameters. Many scour prediction methods in the bridge design, like HEC-18, use the Q_{100} , Q_{500} flood as the hydrologic parameter. Also the insertion of Q_{100} , Q_{500} flood can show the influence of these floods on the scour depth development as the function of time. This function will ask the user to input the values of Q_{100} or Q_{500} flood, then the program will automatically insert the value into the middle of the prepared existing hydrograph file if only one of the Q_{100} or Q_{500} flood is the input. If users want to insert both Q_{100} and Q_{500} , then the Q_{100} will be

inserted into 1/3 of the hydrograph file and Q_{500} will be inserted into 2/3 of the hydrograph. Another exciting new feature of the WINDOWS version program is the risk analysis. The risk analysis includes two portions: future hydrograph prediction and scour depths risk analysis. As you know, the SRICOS-EFA method predicts the scour depth as a function of time, one of the inputs is the hydrograph. This hydrograph should cover the period over which the scour depth must be predicted. The principles and the prediction models of the future hydrograph will be presented in Chapter VII. Once the future hydrographs have been predicted, the scour depths can be calculated by SRICOS-EFA method corresponding to these future hydrographs. For each future hydrograph, the SRICOS-EFA program generates a scour depth history including a final depth of scour at the end of the projected life. These values of the final depth of scour can be organized in a frequency distribution to show the possibility for different scour depths. Then the WINDOWS version program will calculate the level of risk associated with the choice of different design values of scour depth and project lives. By definition, the risk level is the probability that the design conditions will be exceeded in the course of the life of the structure. The risk analysis of the scour depths is also presented in Chapter VII.

6.4 THE INPUT OF SRICOS-EFA PROGRAM

6.4.1 INTRODUCTION OF PARAMETERS

Since scour process is a soil-water interaction, the input of the SRICOS-EFA program will be the soil properties, the water conditions and the geometry of the bridge and river.

- **Soil properties:** In SRICOS-EFA method, the soil properties of the bridge site are presented by the soil erosion function. Generally speaking, the erosion function is a measure of the erodibility of the soil. The soil erosion function is the relationship between the erosion rate \dot{z} of the soil and the hydraulic shear stress τ applied on the bottom of the riverbed, which can be obtained by performing the EFA tests on the soil samples. The values of the data points on the EFA curve will be the input for the program. When performing the scour calculation by the SRICOS-EFA program, the interpolation technique will be used to obtain the initial scour rate from the soil erodibility function. However, when the maximum shear stress τ_{\max} occurs during the analysis period exceed the range of the EFA test results in some case, the regression equation from the data points on the EFA curve will be used to cover all the range of τ_{\max} values. Figure 6.15 shows a typical example of EFA test result.

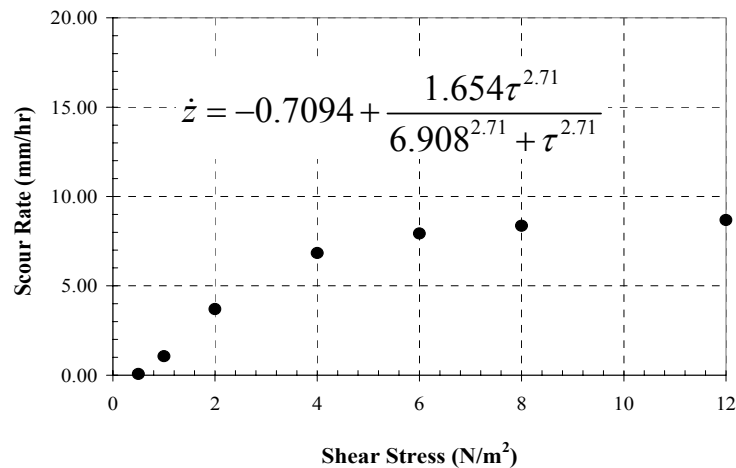


Figure 6.15: Example of EFA Test Result

- Hydrologic data:** The water flow is represented by the velocity hydrograph. This hydrograph can be obtained from a gauge station nearby the bridge site. The hydrograph should last as long as the required period of prediction. Furthermore, if the hydrograph obtained from the gauge station does not contain a 100-year flood or 500-year flood, it can be spiked artificially to include such a large event if required by the design. The hydrograph is typically in the form of discharge as a function of time. Because the input for scour calculations is the velocity and not the discharge, it is necessary to transform the discharge data at the gauge station into velocity data at the bridge site. This can be done by using a program such as HEC-RAS (Hydrologic Center's River Analysis System, HEC-RAS, 1997), which was developed by the US Army Corps of Engineers. In order to run HEC-RAS, several geographical features are necessary such as the average slope of channel bed, the channel cross-section, and the roughness coefficient of the riverbed. Figure 6.16 shows the discharge hydrograph, the discharge versus velocity curve (HEC-RAS results), and the mean depth velocity at one of the piers versus time

(velocity hydrograph) for the Woodrow Wilson Bridge on the Potomac River in Washington DC between 1960 and 1998.

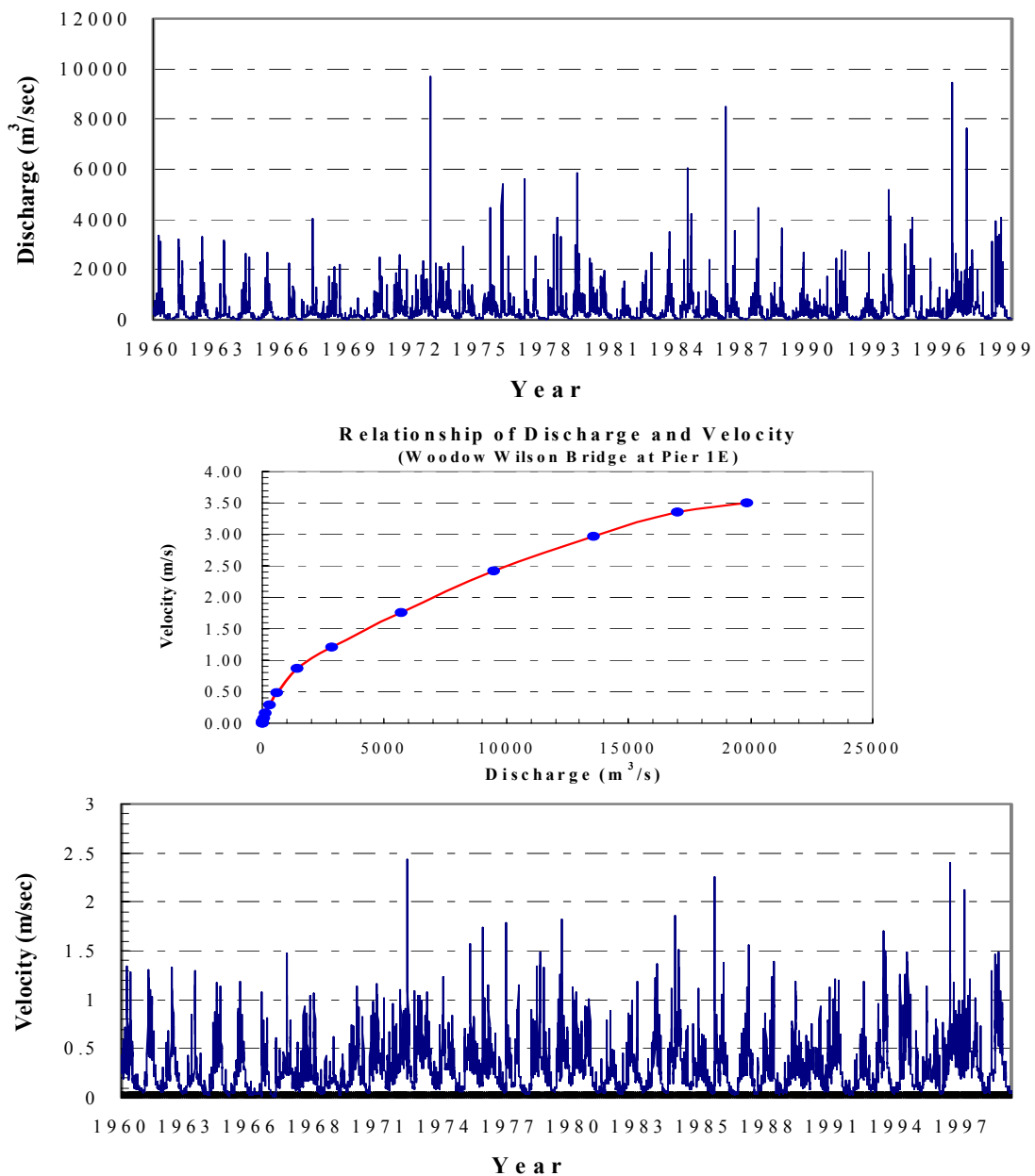


Figure 6.16: Example of Hydrograph Transforming for Pier 1E of the Woodrow Wilson Bridge on the Potomac River in Washington D.C.

- **Geometry:** The geometry includes the channel geometry and the bridge geometry. The input values of geometry can be used to define the characteristics of the channel and bridge in quantity levels such as contraction ratio, the pier size, shape, spacing and angle of attack etc. Table 6.1 is the summary table for the geometry factors.

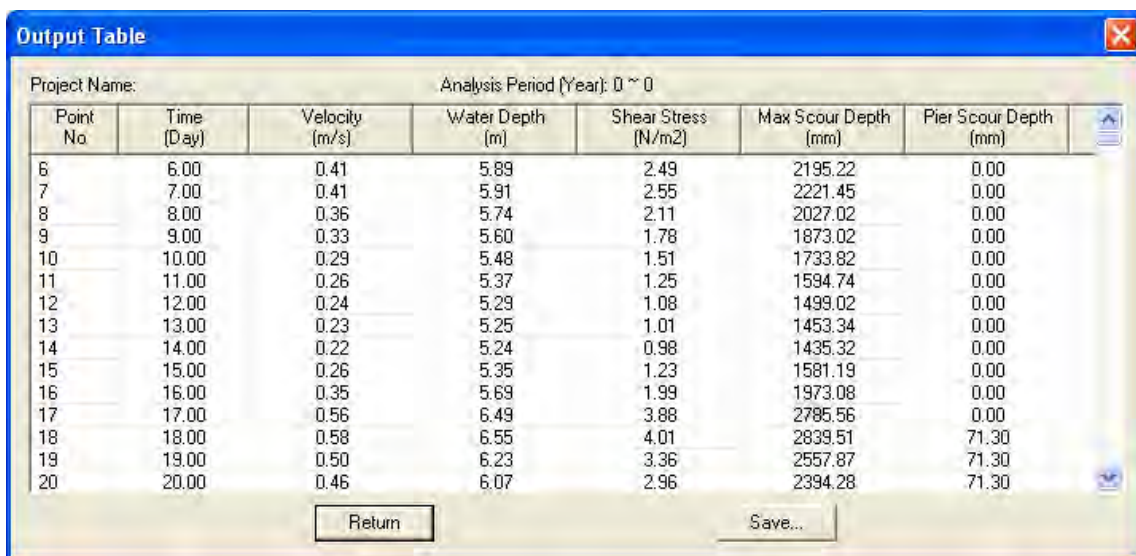
Table 6.1: Summary of Geometry Factors

Bridge Geometric Factors		Channel Geometric Factors	
Bridge opening	Bridge contraction ratio	Channel characteristics	Channel contraction ratio
	Bridge contraction length		Channel contraction length
Bridge piers	Type, shape		Channel water depth
	Attack angle		Manning coefficient
	Size, length, width (diameter)		Channel hydraulic radius
	Pier spacing		Soil stratigraphy
	Number of piers		

6.5 THE OUTPUT OF SRICOS-EFA PROGRAM

Once the program finishes all of the computations successfully, the output tables and plots are automatically created. The output table includes the following columns: time, flow velocity, water depth, shear stress, maximum scour depth (pier scour, contraction scour, or combined scour), and instantaneous scour depth (pier scour, contraction scour, or combined scour). The first few days of a typical output table of the program are shown in Figure 6.17. For this example the critical shear stress was 4 N/m^2 ; as the figure shows no scour occurred until the velocity was high enough to overcome the critical shear stress on day 18. The output plots will provide the following most

commonly plotted curves: water velocity vs. time, water depth vs. time, shear stress vs. time, and scour depth vs. time. The scour depth versus time curve indicates whether the final scour depth Z_{final} (scour depth at the end of the hydrograph) is close to the maximum scour depth for the biggest flood in the hydrograph $Z_{max(max)}$ or not. Typically in sand the answer is yes but in low erodibility clays the difference is significant enough to warrant the initial analysis. Kwak et al. (2001) showed the results of a parametric analysis indicating the most important parameters in the prediction process. Typical output plots of the program are shown in Figure 18.



Point No.	Time (Day)	Velocity (m/s)	Water Depth (m)	Shear Stress (N/m ²)	Max Scour Depth (mm)	Pier Scour Depth (mm)
6	6.00	0.41	5.89	2.49	2195.22	0.00
7	7.00	0.41	5.91	2.55	2221.45	0.00
8	8.00	0.36	5.74	2.11	2027.02	0.00
9	9.00	0.33	5.60	1.78	1873.02	0.00
10	10.00	0.29	5.48	1.51	1733.82	0.00
11	11.00	0.26	5.37	1.25	1594.74	0.00
12	12.00	0.24	5.29	1.08	1499.02	0.00
13	13.00	0.23	5.25	1.01	1453.34	0.00
14	14.00	0.22	5.24	0.98	1435.32	0.00
15	15.00	0.26	5.35	1.23	1581.19	0.00
16	16.00	0.35	5.69	1.99	1973.08	0.00
17	17.00	0.56	6.49	3.88	2785.56	0.00
18	18.00	0.58	6.55	4.01	2839.51	71.30
19	19.00	0.50	6.23	3.36	2557.87	71.30
20	20.00	0.46	6.07	2.96	2394.28	71.30

Figure 6.17: Example of SRICOS-EFA Program Output Table

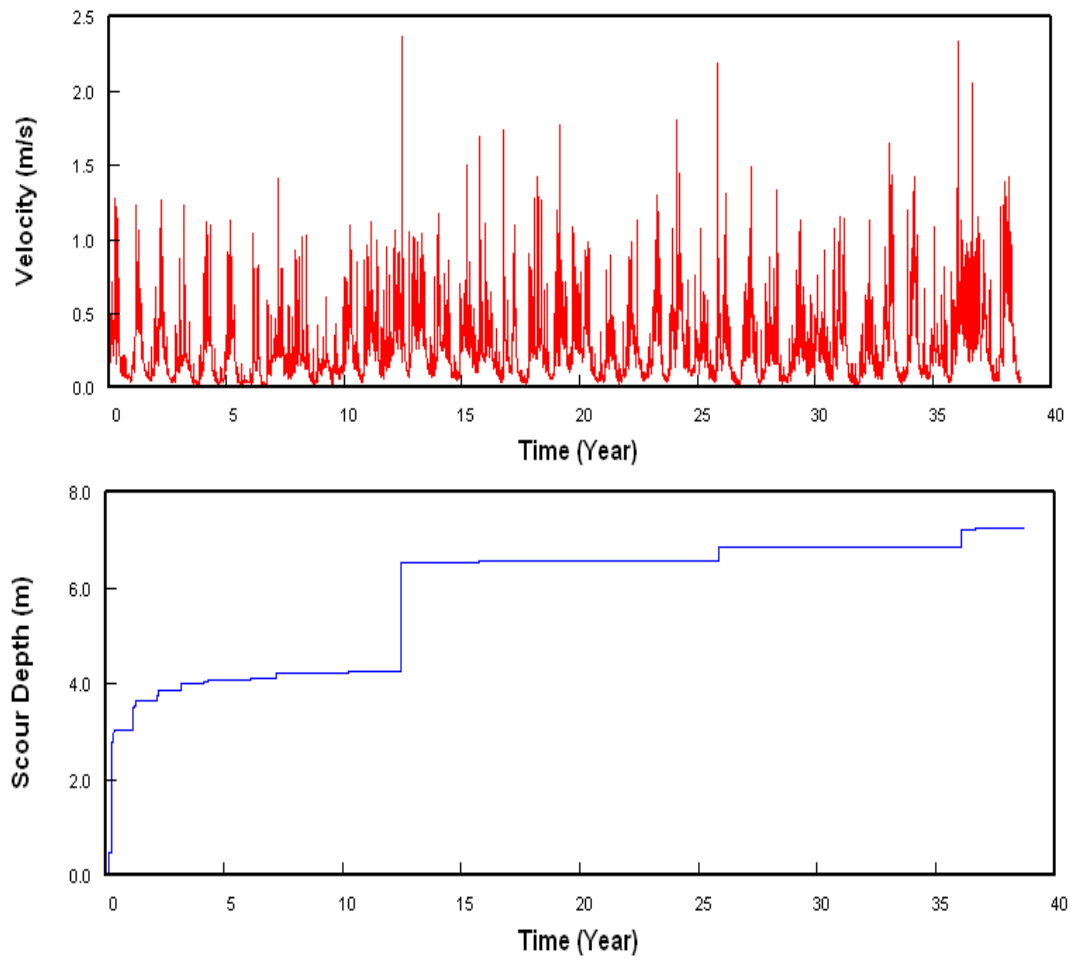


Figure 6.18: Example of Plot from Output Plots in SRICOS-EFA Program

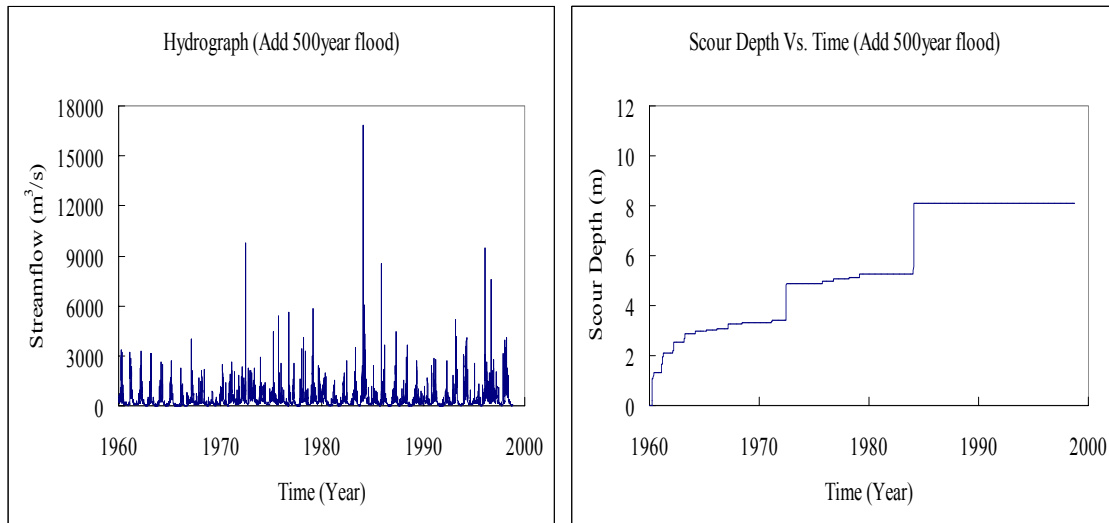
CHAPTER VII

FUTURE HYDROGRAPHS & SCOUR RISK ANALYSIS

7.1. BACKGROUND

Since the SRICOS-EFA method predicts the scour depth as a function of time, one of the inputs is the velocity versus time curve or hydrograph at the foundation location. This hydrograph should cover the period over which the scour depth must be predicted. A typical bridge is designed for 75 years. Therefore the design for a new bridge requires the knowledge of the hydrograph from the year of construction until year plus 75 years. The question is: how can one obtain the future hydrograph covering that long period of time? This requires predicting the future over a 75-year period!

One solution is to use a hydrograph recorded at a nearby gauge station over the last 75 years and assume that the future hydrograph will be equal to the past hydrograph. If the gauge is not at the future bridge location, the discharge can be multiplied by the ratio of the drainage area at the bridge site over the drainage area at the gauge site. If the record at the gauge station is not 75 years long, one can simply repeat the recorded hydrograph until it covers the 75-year period. If the recorded hydrograph does not include the design flood (100 year flood or 500 year flood), one can spike the hydrograph with one or more of those floods before running the SRICOS program (Figure 7.1).



(a) Hydrograph

(b) Scour Depth vs. Time Curve

Figure 7.1: Woodrow Wilson Measured Hydrograph Spiked with a 500-year Flood

Another solution is to use the new technique which is presented here by using the existing hydrograph and the 100 year flood and 500 year flood from the historical data from the site. Furthermore the future hydrograph prediction is repeated 10,000 times and, for each hydrograph, a final scour depth (the depth reached after 75 years of flow) is generated. These 10,000 final depths of scour are organized in a frequency distribution plot with a mean and a standard deviation. That plot can be used to quote a scour depth with a corresponding probability of occurrence, or better, to choose a risk level and quote the corresponding final depth of scour.

7.2. PREPARATION OF THE FUTURE HYDROGRAPHS

The SRICOS-EFA method determines the scour depth at the end of the bridge life as a progressive process driven by a given sequence of daily stream-flow values throughout the life, L_t , of the structure. The randomness of the hydrologic forcing suggests combining the scour model with some hydrological and statistical analyses. If the stream-flow sequence (or *hydrograph*) is modeled as a stochastic process, it is possible to set up a Monte Carlo procedure. This requires sampling from different realizations of the hydrograph (of length L_t), and estimating (SRICOS-EFA method) for each of them the scour depth, d , at the end of the bridge life. Thus, d is regarded as a random variable and its statistics can be studied in detail to determine the risk of failure associated with different choices of the design value of the scour depth.

- Existing Hydrograph Method

One approach to predict the future hydrograph is using the existing hydrograph. This technique consists of using a past hydrograph, preparing the frequency distribution plot for the floods within that hydrograph, sampling the distribution randomly and preparing a future hydrograph, for the required period, which has the same mean and standard deviation as the measured hydrograph.

The modeling of daily stream-flow, Q , can be tackled using different approaches (e.g., Bras and Rodriguez-Iturbe, 1986; Montanari et al., 1997; 2000) corresponding to various levels of complexity. A first simple analysis suggested here considers Q as a random, uncorrelated variable. A suitable distribution is fitted to the data and the hydrographs are then generated as series of values sampled from such a distribution.

Ongoing research is also applying other stochastic models to account for both the autocorrelation and the memory of the process. The current research is also assessing whether the temporal structure (i.e. both autocorrelation and memory) of the stream-flow sequences is able to affect the statistical properties of the scour-depth probability distribution.

The theoretical distribution used to model daily stream-flow observations needs to be defined only for positive values of Q , to have a positive skewness, and to be able to provide an accurate representation of the extreme values (i.e. good fit at the upper tail of the distribution). As expected, the extreme values are found to greatly affect the scour depth estimates and an imprecise modeling of stream-flow maxima could easily lead to unrealistic estimations of the scour depth statistics. Logarithmic transformations are frequently used to study stream-flow extremes (e.g., Chow et al., 1988; Benjamin and Cornell, 1970); therefore, a log-normal distribution can be a good candidate for modeling the daily stream-flows. The method of moments is used to determine the parameters of the distribution. The mean and standard deviation can be expressed as:

$$\mu_y = \frac{1}{2} \text{Log} \left[\frac{\mu_Q^2}{1 + \left(\frac{\sigma_Q}{\mu_Q} \right)^2} \right] \quad (7.1)$$

$$\sigma_y = \sqrt{\text{Log} \left[1 + \left(\frac{\sigma_Q}{\mu_Q} \right)^2 \right]} \quad (7.2)$$

with μ_Q and σ_Q being the mean and the standard deviation of daily stream flow, respectively.

The basic procedures of existing hydrograph approach are:

1. Calculate the mean μ_Q and standard deviation σ_Q of the daily stream flow values in existing hydrograph.
2. Calculate the log-normal mean μ_y and standard deviation σ_y of the daily stream flow values by using Equation 7.1 and 7.2.
3. Q_f (future daily stream flow) is expressed as the exponential of a normally distributed random variable.

$$Q_f = \exp(\mu_y + \text{random} \times \sigma_y) \quad (7.3)$$

where Q_f is predicted future daily stream flow, μ_y is the mean value of log-normal distribution, σ_y is the standard deviation of log-normal distribution, random is random value from a normal distribution with $\mu = 0$ and $\sigma = 1$.

- 100 Year Flood and 500 Year Flood Method

Another approach to predict the future hydrograph is using the 100 year flood and 500 year flood values. As it was discussed in the Existing Hydrograph Approach, the Lognormal Distribution will be a good model to simulate the daily stream flow. If the Q_{100} and Q_{500} are known values, the parameters of the Lognormal Distribution (mean value and standard deviation) can be calculated using the conditions:

$$\text{Prob}[Q > Q_{100}] = 0.01(\text{per year}) = 1/36500 \text{ (per day)} \quad (7.4)$$

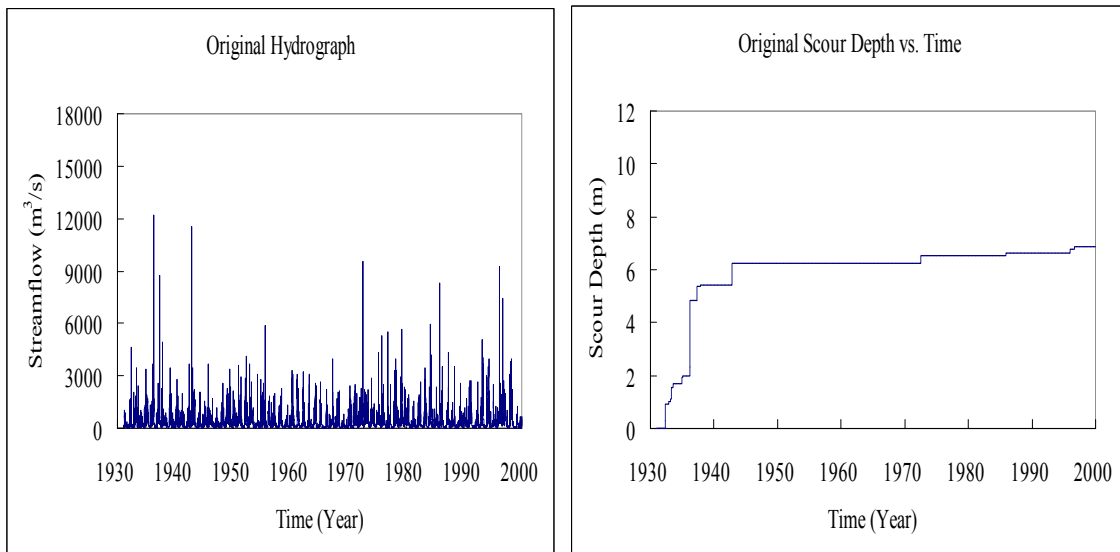
$$\text{Prob}[Q > Q_{500}] = 0.002 (\text{per year}) = 1/182500 (\text{per day}) \quad (7.5)$$

Two conditions with two unknowns and the parameters of the Lognormal Distribution can be defined.

Hence, the basic procedures of Q_{100} and Q_{500} approach will be:

1. Calculate the log-normal mean μ_y and standard deviation σ_y of the daily stream flow values by using Equation 7.5 and 7.6.
2. Q_f (future daily stream flow) is expressed as Equation 7.3: the exponential of a normally distributed random variable.

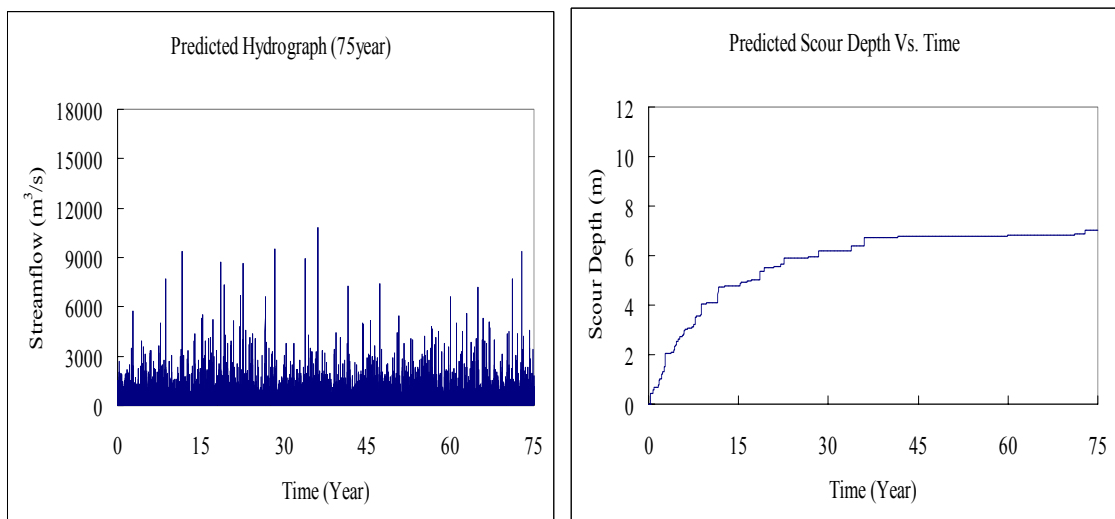
In the case of the Woodrow Wilson Bridge, stream-flow data is available at the Little Falls station (USGS #01646500) on the Potomac River, approximately 13 km upstream from the bridge. Correction of the measured stream flow is applied by multiplying the values by the drainage area ratio. The correction is of the order of 3%. Figure 7.2 shows the original hydrograph and the corresponding prediction of scour depth history using the SRICOS-EFA method. The mean and standard deviation of Q of the period from 1931-2001 are $\mu_Q = 327 \text{ m}^3\text{s}^{-1}$, and $\sigma_Q = 467 \text{ m}^3\text{s}^{-1}$, respectively, while the maximum discharge in the 70-year-long record was $12,056 \text{ m}^3\text{s}^{-1}$. Figure 7.3 shows the synthetic hydrograph of the same length generated by using the existing hydrograph approach and the predicted scour depth development from SRICOS-EFA method. Figure 7.4 shows the synthetic hydrograph of the same length generated by using the Q_{100} and Q_{500} approach and the predicted scour depth development from SRICOS-EFA method.



(a) Hydrograph

(b) Scour Depth vs. Time

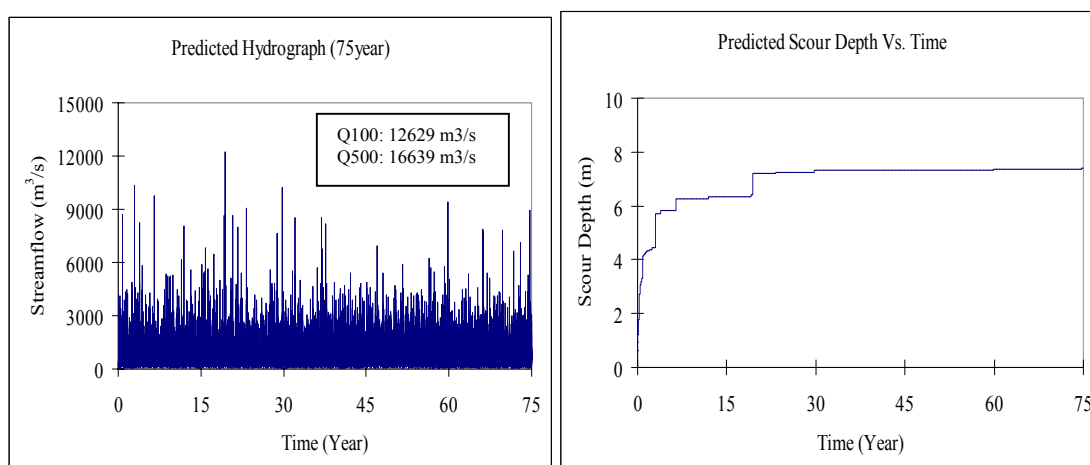
Figure 7.2: Original Hydrograph & Scour Depth vs. Time near Woodrow Wilson Bridge Site



(a) Hydrograph

(b) Scour Depth vs. Time

Figure 7.3: Predicted Hydrograph and Scour Depth vs. Time Curve near Woodrow Wilson Bridge Site Using Existing Hydrograph Approach (Projected Time = 75 Years)



a) Hydrograph

(b) Scour Depth vs. Time

Figure 7.4: Predicted Hydrograph and Scour Depth vs. Time Curve near Woodrow Wilson Bridge Site Using Q_{100} and Q_{500} Approach (Projected Time = 75Years)

7.3. RISK APPROACH TO SCOUR PREDICTIONS

Many equally possible future hydrographs such as the one in Figure 7.3 and Figure 7.4 are generated by the random sampling process. For each hydrograph, the SRICOS program generates a scour depth history including a final depth of scour, d , at the end of the project life. These values of the final depth of scour can be organized in a frequency distribution. Figure 7.5 shows the probability distributions obtained for the example of the Woodrow Wilson Bridge at the end of a chosen bridge life, L_t .

This analysis can be used to estimate the level of risk, R , associated with the choice of different design values of scour depth and project lives. By definition, the risk level is the probability that the design conditions are exceeded in the course of the life of the structure. Thus, from the probability distribution of d (Figure 7.5) it is possible to determine the cumulative distribution function (CDF) of d (Figure 7.6). The risk is then

estimated as the probability of exceedence (Figure 7.6). Table 7.1 reports the risk level associated with different project lives and design values of d . It is observed that R is a non-linear function of d and L_t . This analysis provides a statistical framework that can be used in a cost-benefit study of bridge foundation design.

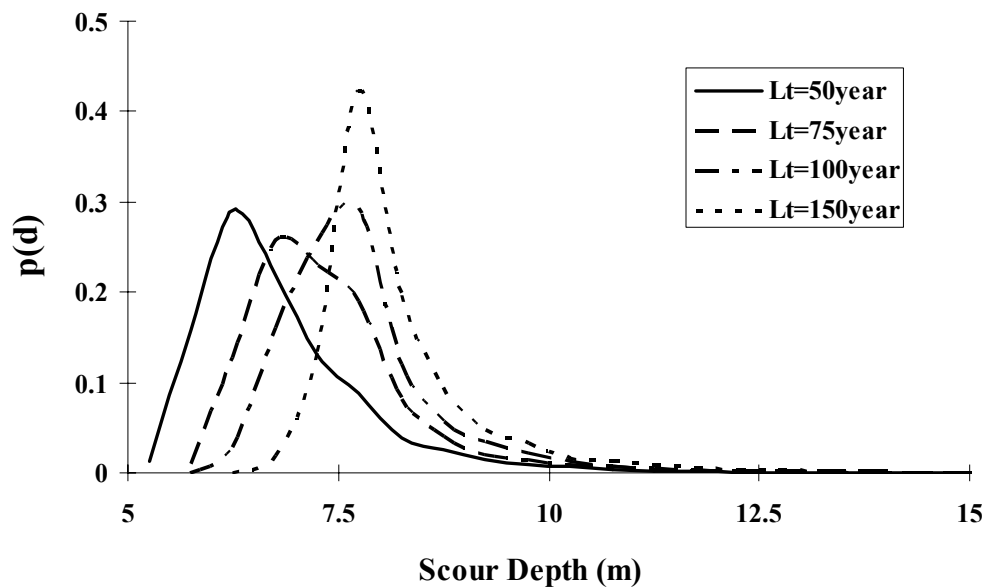


Figure 7.5: Probability Distribution of Scour Depth, d , for Different Lengths of the Projected Life, L_t

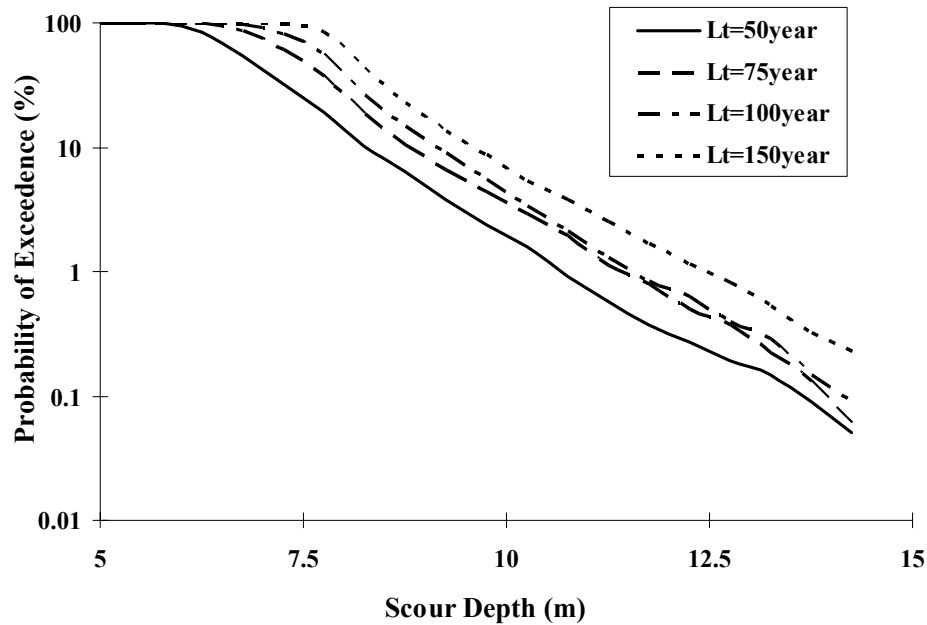


Figure 7.6: Risk Associated with Different Design Values of the Final Scour Depth, d , and Different Lengths of the Projected Life, L_t

Commonly accepted methods of scour analysis in noncohesive soils refer to a single peak-flow value selected on the basis of its return period, T_r , as well as the associated level of risk. Such an approach does not account for the contribution to bridge scour due to smaller (and more frequent) floods. The SRICOS-EFA method can be used to include the effect of the entire hydrograph. The Monte Carlo procedure outlined in this section represents a possible new probabilistic approach to scour analysis. Ongoing research is developing an extended version of this approach using different stochastic hydrologic models able to account for the daily-flow distribution, and for the autocorrelation of the stream-flow series. This study will show whether the scour depth

is sensitive to the temporal structure of stream-flow sequences and will indicate the level of detail that is necessary to include in the hydrologic stochastic model.

7.4. OBSERVATIONS ON CURRENT RISK LEVELS

A direct comparison between the risk results obtained here with the SRICOS method (Table 7.1) and traditional approaches based on single peak-flow values is not easy. Nevertheless, an example is provided here. The peak flow value associated with a given return period can be determined through a flood-frequency analysis (e.g., Chow et al., 1988; pp 375-378). Figure 7.7 shows the result of such an analysis for the Woodrow Wilson measured hydrograph. As can be seen on that figure, the 100 year flood has a discharge of 12,629 m³/s and the 500 year flood has a value of 16,639 m³/s. If the design life of the bridge is L_t , the probability of exceedence or risk R for a flood having a return period T_r is given by:

$$R = 1 - (1 - 1/T_r)^{L_t} \quad (7.6)$$

If the design life of the bridge is 75 years, the probability that the flood with a return period of 100 year will be exceeded during the 75 year design life is 53% according to Equation 7.6. The risk that the 100 year flood will be exceeded during the 75 years is 53% or about one chance out of two. For the 500 year flood, and for the same 75 year design life, the risk is 14% or about one chance in 7.

Even if a bridge designed for a 100 or 500 year flood experiences a 1000 year flood, this bridge may not collapse. Indeed, collapse of the bridge is based on a different criterion than just exceedence of the design flood. There are numerous inherent redundancies in the design of a bridge and many design parameters must be exceeded

before collapse occurs. Nevertheless, the risk level associated with the floods used in everyday design appears very high compared to risk levels in other disciplines within Civil Engineering. For example the structural engineers have based their codes on a risk level of about 0.1%. The geotechnical engineers probably operate at about 1%. The scour engineers seem to operate at a much higher risk level. This is particularly worrisome since there is no factor of safety on the depth of scour passed on from the scour engineer to the geotechnical engineer for him to calculate the pile length.

One useful approach in this respect is to conduct a sensitivity analysis by varying the input parameters and monitoring the impact of the parameter variation on the final scour depth. This would help in realizing how important each parameter is and give a range of scour depth values. Note that the proposed method is a prediction method not a design method. Indeed the equations were derived from a number of best-fit regressions against the experimental data. The proposed method becomes a design method when a factor of safety is added. The recommended factor of safety is 1.5. In other words, the predicted final depth of scour should be multiplied by 1.5 before it becomes a design scour depth.

Table 7.1: Risk of Failure Associated with Different Design Values of Scour Depth and Projected Life

Design value of Scour depth (m)	Project Life			
	50 yrs	75 yrs	100 yrs	150 yrs
6.5	42%	74%	91%	99.8%
7.0	25%	48%	70%	93%
7.5	14%	27%	40%	65%

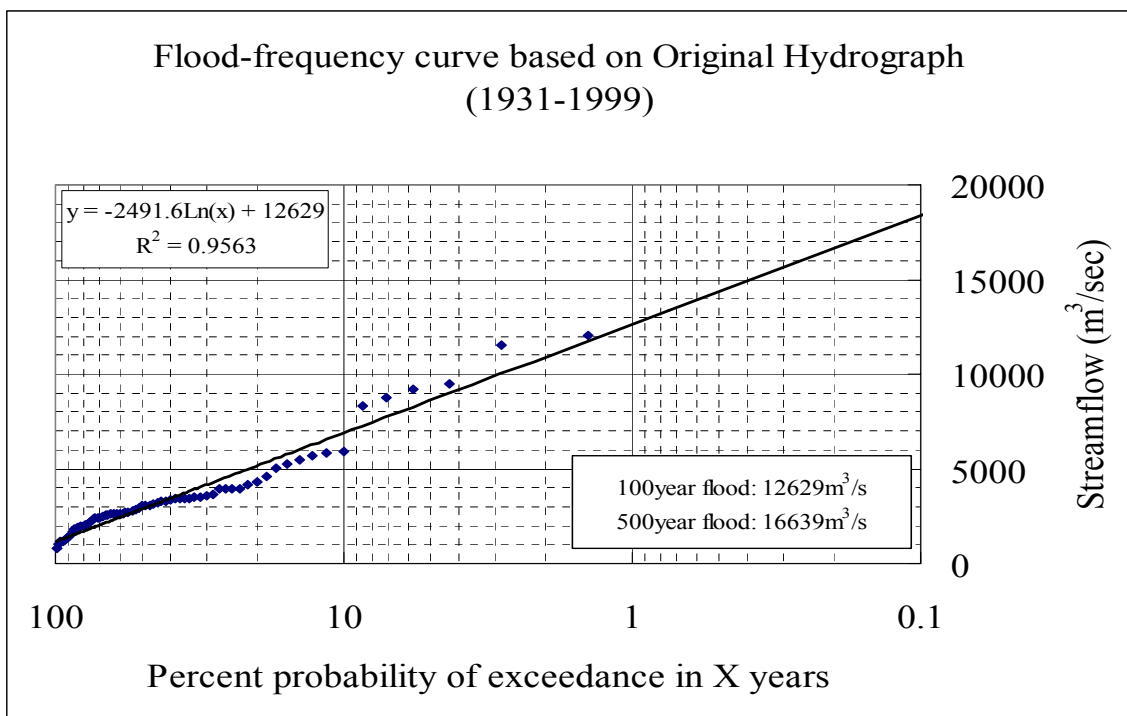


Figure 7.7: Flood-frequency Curve for the Potomac River at the Woodrow Wilson Bridge

CHAPTER VIII

INFLUENCING FACTORS OF SCOUR RATE IN COHESIVE SOILS ON EFA TESTS

8.1 INTRODUCTION

The erosion behavior in cohesive soils is a very complicated process. Gravitational and frictional laws control the erosion process of non-cohesive soils while physicochemical laws control the erosion process in cohesive soil. Scour process is a soil-water interaction, which involves a lot of factors. The erodibility of soils is characterized by the erosion function, which is the scour rate \dot{z} versus shear stress τ curve. It requires many curve-fitting parameters to describe the nonlinear relationship between the \dot{z} and τ . One of the curve-fitting parameters concerning the erodibility of a cohesive soil is the critical shear stress τ_c (Briaud et al. 2001). Critical shear stress τ_c is an important factor that relates to the scour rate. For sand, HEC-18 has provided some equations to calculate the critical shear stress by using the size of the grains represented by D_{50} . For clay it is difficult to use a formula to get the τ_c value directly. τ_c involves various forces such as electromagnetic and electrostatic forces found in the chemistry of the soil and water particles, which lead to many influencing factors for τ_c . Briaud et al. (1999) summarized the influencing factors for τ_c on basis of a literature review. The factors include the soil water content, the soil unit weight, the soil plasticity, the soil shear stress, the soil void ratio, the soil swell, the soil mean grain size, the soil percentage passing the No. 200 sieve, the soil clay mineral, the soil dispersion ratio, the

soil cation exchange capacity, the soil sodium absorption ratio, the soil pH, the soil temperature and the water chemical composition.

In order to find the correlation between these influencing factors and the erosion of cohesive soils, two major factors concerning water chemical composition were selected and a series tests were run in the EFA. These major factors include: pH value and salinity levels in eroding water.

8.2 pH TESTS

8.2.1 GENERAL

The purpose of the pH test is to study the possible influence of the pH level on the erodibility of porcelain clay.

The soil in the scour site is usually soaked in water. The soil and water have some chemical interactions in the soil water interface. Some of the hydrogen ions absorbed in the soil surface will be hydrated and remain in the water. From the literature review it was found many researchers have studied the influences of the water pH value or the soil pH value on the erodibility of the cohesive soil. Alizadeh (1970) found that the pH value in the eroding water and the pH value in the soil are very important parameters to the erodibility of the cohesive soil. Arulanandan et al. (1975) also mentioned that the pH value of the eroding fluid and soil pH value were the critical factors to the erodibility of cohesive soil. Sherard et al. (1972) found that the erodibility of Ca-Montmorillonite of an embankment, which was severely damaged by rainfall, could be reduced by using sodium salt, such as Na_2CO_3 . Shaikh et al. (1988) used a series of flume tests with three different types of clay; his results showed that the soil

pore water chemistry is the most important parameter affecting the erodibility of unsaturated compacted clays. The pore water chemistry was characterized by SAR and TDS, where SAR is the ratio of dissolved sodium ions to other main basic cations, such as Ca and Mg in pore water; and TDS is total dissolved salt, or total dissolved solids concentration. The erosion rate of the Ca-Montmorillonite (TDS=7.8 and SAR=0.4) was 300 times greater than that of the Na-Montmorillonite (TDS=20.5 and SAR=19.8).

8.2.2 EXPERIMENTAL PARAMETERS

The soils adopted in the EFA pH tests were Armadillo Porcelain Clay. The predominant component of this commercial clay is Kaolinite. The chemical formula for Kaolinite is $\text{Si}_2\text{Al}_2\text{O}_5(\text{OH})_4$. The layers of Kaolinite are composed of one silica tetrahedral sheet and one alumina octahedral sheet (gibbsite). Kaolinite is the most prominent member of this group, which also includes halloysite, nacrite and dickite. Tap water was used as the eroding water. The chemical material used to bring the pH value down was sodium bisulfate (NaHSO_3). It is the main component of pH minus, which contains 94.5% of NaHSO_3 and 5.5% of inter ingredients. The chemical material used to raise the pH value was soda ash or sodium carbonate (Na_2CO_3), the main component of pH plus. It contains 99.6% of Na_2CO_3 and 0.4 % of the inter ingredients. Before the tests started, the water tank was filled with tap water. Then the pH plus or pH minus was gradually added into the tank. A pH probe (OAKTON pH Tester 3) was used to measure the pH value when the chemical material was absolutely dissolved into the water. Once the desired pH value was reached, the EFA tests were started immediately. During the

tests, neither fresh water or chemical material was added, nor was water pumped out of the tank. Table 8.1 shows some selected chemical properties of eroding water.

Table 8.1: Chemical Properties of Eroding Water in pH Test

Properties	Tap water	Acid	Alkalinity
Molar Concentration (M/L)	N/A	0.0077	0.463
pH Value	8.39	5	10.79
TDS (mg/L)	536	1210	>19900
SAR (ppm)	500	1200	44300
Conductivity (millisiemens)	1.1	2.4	65.40

8.2.3 GENERAL PROCEDURES OF pH TEST ON EFA

1. Push a standard Shelby tube (ASTM) with a perpendicular direction into a porcelain clay block to get the soil sample. Then label the tube properly.
2. Fill the water tank and gradually add pH minus or pH plus into water. Make sure that the desired pH value of water has been reached before the test start.
3. Start the pump and achieve an initial low water velocity in the flume. The water flows over the sample at the chosen velocity and 1mm of soil sample is pushed into the flow.
4. Continue pushing the soil sample in the Shelby tube to maintain the protrusion of the soil sample between 0mm and 1mm in the flow until 50mm height of soil has been eroded or 1 hour is reached, whichever comes first. The scour rate can be calculated as the total soil push divided by the time it takes to be eroded.
5. Stop the pump, take out the tube and trim the clay surface to be flush with the edge

of the Shelby tube. Then repeat Step 2 to 4 with a higher flow velocity.

- Once 6 to 8 velocities have been performed, the scour rate vs. velocity curve can be obtained. Then the scour rate vs. shear stress curve can be calculated by using Moody Chart.

8.2.3 EXPERIMENTAL RESULTS

Figure 8.1 and Figure 8.2 show the EFA test results for different pH values.

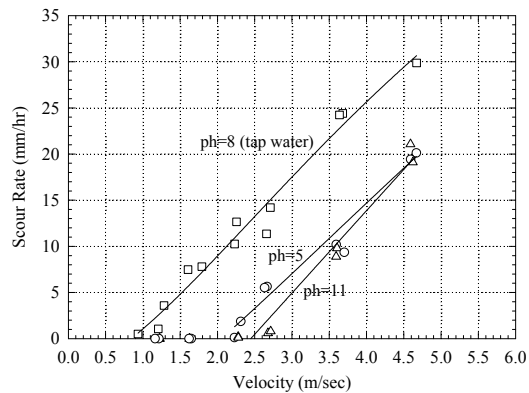


Figure 8.1: Relationship between Erosion Rate and Velocity for Different pH Values

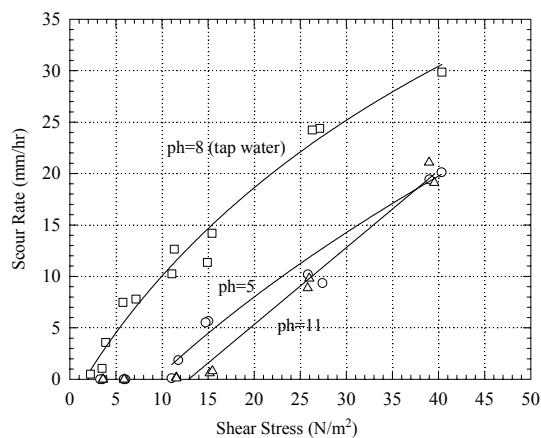
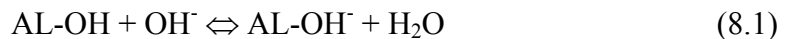


Figure 8.2: Relationship between Erosion Rate and Shear Stress for Different pH Values

8.2.5 DATA ANALYSIS

The results from the pH tests show that whenever the pH value was away from neutral (the tap water was assumed to be neutral), the scour rate of porcelain clay decreased and the critical shear stress τ_c increased. From the results we found that the initial slope S_i of scour rate vs. shear stress did not change a lot with pH value changing. The surface charges of some soil, such as porcelain clay, are dependent on the soil properties (Brady, 1990). As the pH value increases, more and more OH^- is introduced into the environment, which results in increasingly negative charges at porcelain clay surface in a high pH environment. The following equation illustrates this phenomenon (Brady, 1990).



It was found that this chemical equation could occur in double directions. We found that when it is high pH environment, the OH^- concentration is high, which will lead the equation to right hand side. The porcelain clay surface has more negative charges; these negative charges will attract more and more Na^+ (introduced by adding pH plus) in the eroding water to adhere to the porcelain clay surface. So the porcelain clay proves to be more scour resistant in the alkalinity case than tap water case. When it is low a pH environment, the H^+ concentration is high; this leads the equation to left hand side. The negative charges on the porcelain clay surface will decrease, which can drop the electronegativity on the porcelain clay surface. An electronegativity decrease will result in a reduction of repulsive force between the soil particles and cause the soil particles hold more tightly. This is the reason why when the eroding water in an acidic

environment, the scour rate decreases and critical shear strength increases compared to the tap water case.

8.2.6 CONCLUSIONS OF pH TEST

1. The TDS of the eroding water is an important factor to determine the erodibility of cohesive soils. The TDS affects the erodibility of cohesive soil directly, however the pH influences it indirectly.
2. The scour rate of porcelain clay decreases with increasing TDS. The critical shear stress of porcelain clay increases with increasing TDS.
3. The relationship between TDS and the erodibility of cohesive soils is non-linear.
4. When the eroding water is in neutral state ($\text{pH} = 7$), it has the largest scour rate and smallest critical shear stress. When the pH of eroding water drops down to acid conditions, the cohesive soil will be strengthened against erosion.
5. Cations in the eroding water tend to neutralize the surface electronegativity of porcelain clay, which causes the salinity of the eroding water to make clay more scour resistant.
6. The initial slope S_i doesn't change with pH of eroding water or TDS.
7. In the EFA test, it is more conservative to use tap water as the eroding water compared to using acid.
8. A site-specific EFA test using water from the scour site will be ideal.

8.3 SALINITY TESTS

8.3.1 GENERAL

In delta areas, where the river flows into the sea or bridges cross sea, the salt concentration in river can range from 0% to 100%. It is necessary to study the scour behaviors of soil as influenced by the salinity of water. Salinity tests simulate the conditions where bridges are founded in delta areas.

Sherard et al. (1972) carried out extensive research work on piping in earth dams of dispersive clay in Australia. It was found that two major factors would influence the erosion rate of dispersive clay. As we described in pH test, these two factors are SAR and TDS. Sherard (1972) reported that the lower the TDS concentration in eroding water, the higher erosion observed in clay soils. Arulanandan (1975) performed a series of erosion tests in Yolo Loam in a Rotating Cylinder Test Apparatus with different concentration of NaCl in the eroding water. The samples were tested at three different NaCl levels, distilled water, 0.001N NaCl and 0.005N NaCl (N: The number of equivalents of acid or base solute in one liter of solution). Figure 8.3 presents the results of his tests. At the same shear stress, the order of erodibility of the soil sample is distilled water > 0.001N NaCl > 0.005N NaCl. The shear stresses versus erosion rate curves are almost linear for all three NaCl levels. The values of critical shear stress of soil increase with increasing salinity in eroding water. The slopes of curves decrease with increasing salt concentration.

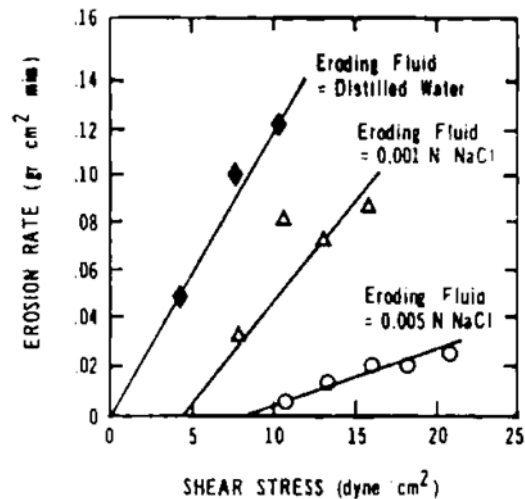


Figure 8.3: Relationship between Erosion Rate and Shear Stress for Different Concentrations of Eroding Fluid (after Arulanandan, 1975)

Liou (1970), Sherard et al. (1972) and Sargunan et al. (1973) researched the effect of chemical composition of pore water on the soil erosion rate. It was investigated that cations in the pore water tend to make soil more scour resistant, because of the reduction of repulsive forces. Therefore, the strength of soil can be increased with the valences increasing due to the absorbed cations.

8.3.2 EXPERIMENTAL PARAMETERS

The porcelain clay was the tested soils in the EFA. The tap water was used as the eroding water in three different salt concentrations: 1: 500ppm salinity (tap water); 2: 17500ppm salinity (50% seawater); 3: 35000ppm salinity (100% seawater). From the tests, the possible influence of the salinity levels on cohesive soil erodibility was investigated. The salt used in the salinity tests was table salt, 99% of which was NaCl. Before the test, table salt was gradually added into the water tank with some mechanical

agitation, which was filled by the tap water. A salinity probe (ORION Model 115) was used to measure and monitor the changing of salinity value. As the same in the pH tests, there was neither salt added nor water filled-in or water pumped out of the tank during the tests. The following table shows the selected chemical properties of eroding water for the salinity test.

Table 8.2: Chemical Properties of Eroding Water in Salinity Test

Properties	Tap water	50% seawater	100% seawater
Salinity (ppm)	500	17500	35000
TDS (mg/l)	536	15900	>19900
PH Values	8.39	8.12	7.96
Conductivity (millisiemens)	1.15	28.3	52.9

8.3.3 GENERAL PROCEDURES OF SALINITY TESTS ON EFA

The procedures of the salinity tests were similar to the procedures of the pH tests. Please refer to the corresponding section of the pH test and replace table salt with pH plus or pH minus at the appropriate places.

8.3.4 EXPERIMENTAL RESULTS

Figure 8.4 and Figure 8.5 show the EFA test results for different salinity levels.

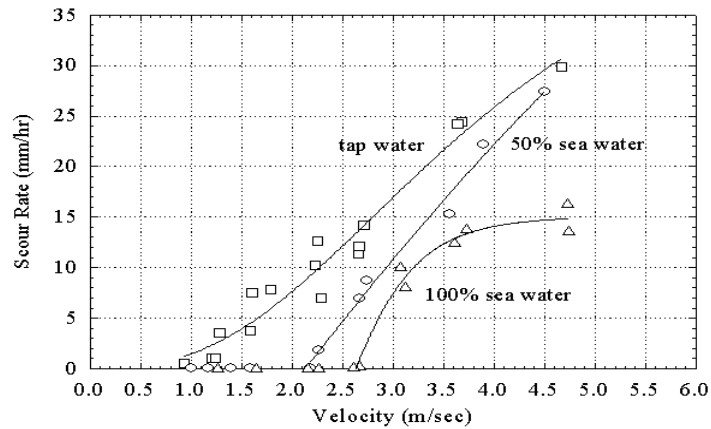


Figure 8.4: Relationship between Erosion Rate and Velocity for Different Concentrations of Salinity of Eroding Fluid

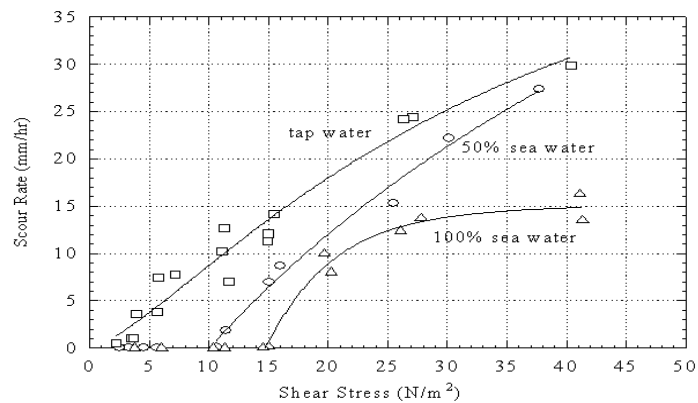


Figure 8.5: Relationship between Erosion Rate and Shear Stress for Different Concentrations of Salinity of Eroding Fluid

8.3.5 DATA ANALYSIS

The results of the salinity tests showed that the scour rate decreased with increasing salinity, while critical shear stress increased with increasing salinity. The

influence of salinity on scour rate and critical shear stress seems significant. When the eroding water had low or medium salinity level, the scour rate vs. shear stress curve exhibited linear behavior. The phenomenon of the salinity tests indicated that the results of tests are similar to Arulanandan's test (1975) results (Figure 8.3). Some differences between Arulanandan's test and EFA salinity test were also found. First, the initial slope of the scour rate vs. shear stress curve in Arulanandan's tests decreased with increasing salinity, while it was the opposite in the EFA salinity tests. Second, at high salinity levels in EFA Salinity tests, the scour rate vs. shear stress curves lost linearity and converged to a maximum value. We noted that curves from Arulanandan's test were linear with the increasing shear stress. The reason for this is because the shear stress levels of Arulanandan's test are quite low compared to the EFA salinity tests we conducted. The maximum shear stress for Arulanandan's test is only about 2 N/m^2 , while the maximum shear stress in EFA Salinity tests is 40 N/m^2 . It is possible that the Arulanandan's test results may be convergent in the high shear stress region.

The possible mechanism of the salinity test can be described as following: It was found that the existence of cations in the eroding water would strengthen the surface soil and make it more scour resistant (Liou, 1970; Sherard et al, 1972; Sargunan et al, 1973). In EFA salinity tests, the surface of porcelain clay has negative charges, which can attract the Na^+ cations to adhere its surface. The Na^+ cations concentration can be increased by adding more salt (NaCl) to the water. When more and more Na^+ cations adhere to the surface of porcelain clay, the overall surface electronegativity decreases. The decrease results in a reduction of repulsive force between the soil particles. The

more Na^+ cations attached to the porcelain clay surface, the more reduction of the repulsive force between the two adjacent soil particles. So the porcelain clay proved more scour resistant.

Arulanandan (1975) found that the difference of salt concentration in water and soil would cause osmotic pressure and generate a swelling towards the side with high salt concentration. The swelling can cause the soil particles in the surface to move and finally these particles will detach themselves from the soil surface. According to Arulanandan's comments, the higher the differences of cation concentration between the soil-water interfaces, the higher the rate of change in erosion rate. When water is 100% seawater, the highest salt concentration difference exists in the interface between soil and water. This difference contributes to the high initial slope of scour rate vs. shear stress curve in 100% seawater. As tests going on, the difference of the salt concentration between eroding water and soil decreases due to cations exchanging between them. So the slope of scour rate vs. shear stress curve gradually decreases and finally flattens.

8.3.6 CONCLUSIONS OF SALINITY TESTS

1. The cations in the eroding water tend to neutralize the surface electronegativity of porcelain clay so that the salinity of the eroding water can make clay more scour resistant.
2. The scour rate of porcelain clay decreases with increasing salinity.
3. The critical shear stress of porcelain clay increases with increasing salinity.
4. The initial slope S_i of scour rate vs. shear stress curve increases with increasing salinity.

In the EFA test, it will be more conservative to use tap water as the eroding water compared to the use of salinity water.

8.4 OTHER INFLUENCING FACTORS OF SCOUR RATE IN COHESIVE SOILS ON EFA TEST

A lot of efforts have been done in scour research to find out the direct relationship between soil geotechnical properties and soil erodibility. If some relationships between these two sides can be established, it will simplify the scour prediction process significantly and strengthen the connection of Geotechnical Engineering to scour study. Recently, studies by Briaud et al. (2000) at Texas A&M University pointed out that the scour of cohesive soil is a soil-structure-water interface problem. There are usually more than 10 factors from cohesive soil and more than 5 factors from water involved in the scour problem for cohesive soil. One simple formula is much less likely to be developed for this problem than the same problem in cohesionless soils, which have a much shorter list of parameters (Briaud et al. 2000). From a practical point of view, even if the formula does exist, the amount of experimental data and analytical work on the data will be too massive. A lot of EFA tests have been finished on various types of soil and various eroding water conditions at Texas A&M University and our research team is continuing work on the establishment of EFA scour databases. There is the possibility of determining these relationships, but massive experimental data is needed. As of now more than 100 EFA tests have been conducted on different cases. Based on the data we have, a scour database will be set up for different soil properties and eroding water conditions. The following soil parameters

have been studied in order to find any possible correlations between soil critical shear stress & initial slope of scour rate vs. shear stress curve and water content (w%), undrained shear strength (Su), plastic index (PI), and fine clay percentage. The EFA results for different parameters are shown in the figures from Figure 8.6 to Figure 8.9.

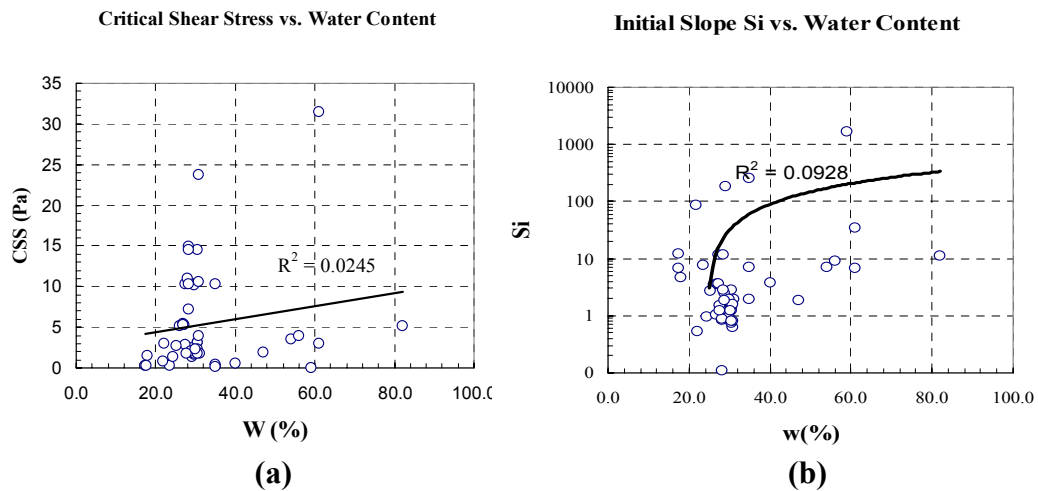


Figure 8.6: (a) Relationship between Critical Shear Stress vs. Water Content;
(b) Relationship between Initial Slope Si vs. Water Content

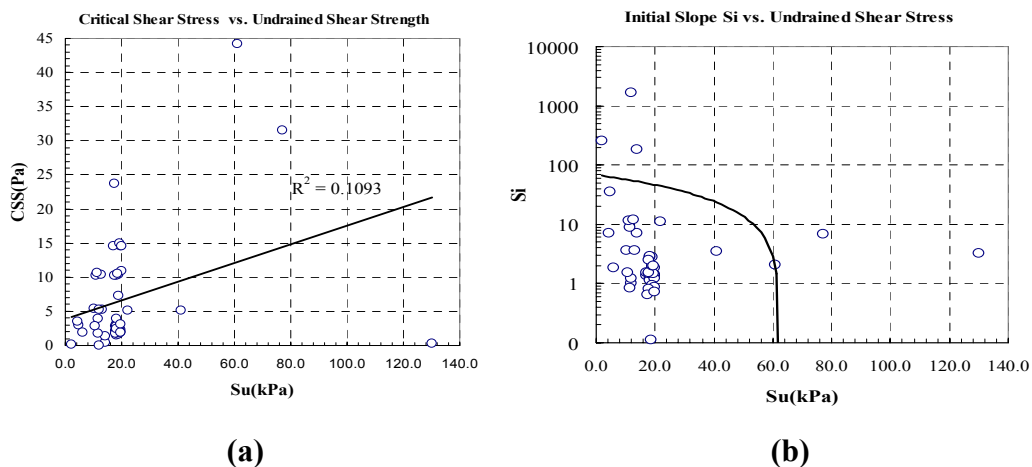


Figure 8.7: (a) Relationship Between Critical Shear Stress vs. Undrained Shear Strength;
(b) Relationship Between Initial Slope Si vs. Undrained Shear Strength

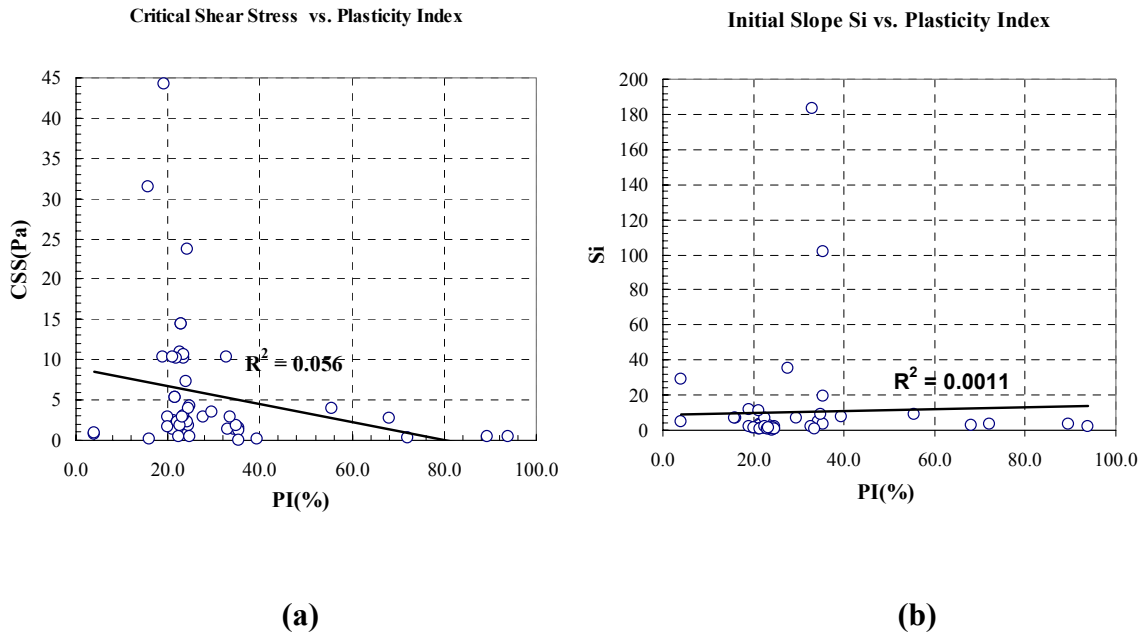


Figure 8.8: (a) Relationship between Critical Shear Stress vs. Plasticity Index; (b) Relationship between Initial Slope Si vs. Plasticity Index

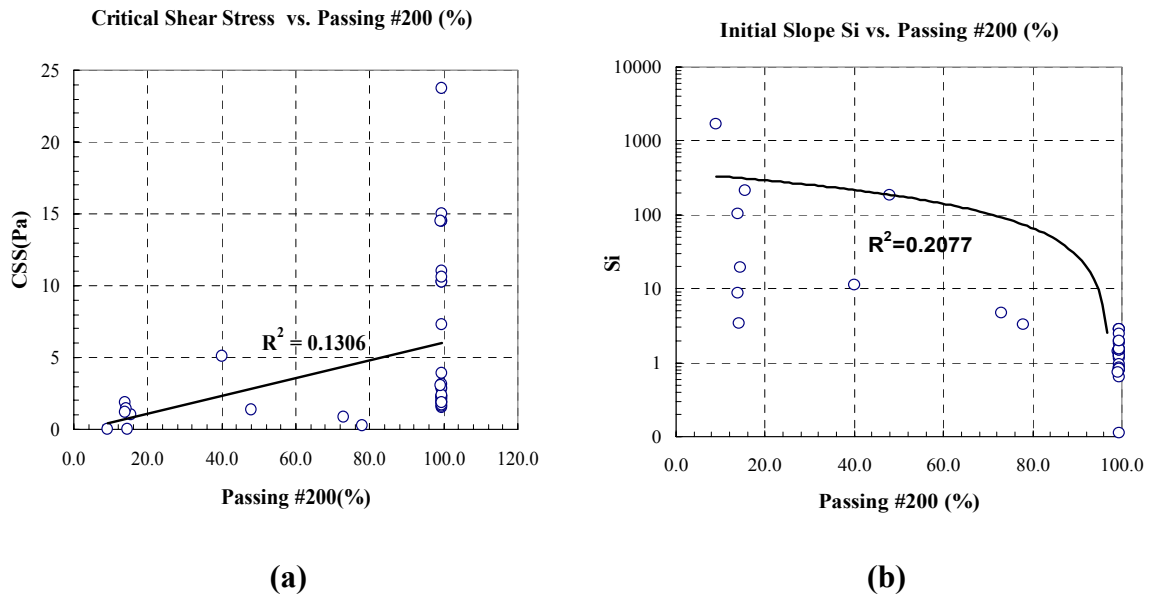


Figure 8.9: (a) Relationship Between Critical Shear Stress vs. Percentage Passing #200 Sieve; (b) Relationship Between Initial Slope Si vs. Percentage Passing #200 Sieve

From the results, no strong relationships can be found. These results lead us to believe that it is tough to find a simple relationship between the soil erodibility and soil properties. However these research practices give us a much better understanding about the influence of soil properties on soil erosion rate.

8.5 CONCLUSIONS

This chapter presents two kinds of EFA tests designed to study the influence of pH values and salinity levels in eroding water on the erodibility of soil.

- **For pH Tests:** The pH value of eroding water affected the erosion process indirectly. TDS (total dissolved salt) is the direct factor that influences the erodibility of cohesive soil. The scour rate of porcelain clay decreased with increasing TDS. The critical shear stress increased with increasing TDS. The relationship between TDS and the erodibility of cohesive soils was non-linear. When the eroding water was in neutral (pH=7, lowest TDS) state, it had the largest scour rate and smallest τ_c . When the pH of eroding water dropped down to acidity, the TDS would increase, and thus the cohesive soil would be strengthened against erosion. Cations in the eroding water tended to neutralize the surface electronegativity of porcelain clay which caused the clay to be more scour resistant. The initial slope S_i of scour rate vs. shear stress curve did not change with the pH of eroding water or TDS. If tap water is used as the eroding water, it will be more conservative compared to the use of low pH values for eroding water.

- **For Salinity Tests:** Erosion in brackish water was less severe than that of fresh water. The cations in the eroding water tended to neutralize the surface electronegativity of porcelain clay which caused the clay to be more scour-resistant. The scour rate of

porcelain clay decreased with increasing salinity. The critical shear stress increased with increasing salinity. The initial slope S_i of scour rate vs. shear stress curve increased with increasing salinity. If tap water is used as the eroding water, it will be more conservative compared to salty eroding water.

Since the scour process is a complicated soil-water interaction, it is quite difficult to find a simple equation to describe the relationship between the erodibility of cohesive soil and the soil properties. Considering these problems, direct measurement of scour parameters in EFA for specific soils is favorable. From the Texas A&M University EFA test database, we chose various parameters and tried to find a possible relationship between these parameters and the erodibility of porcelain clay. The parameters were: water content (w%), undrained shear strength (S_u), plastic index (PI), and fine clay percentage. From the results, unfortunately only poor relations were found. There are two possible reasons for this finding: (1) there are relationships between the erodibility and soil parameters, but our EFA database is not sufficient enough to perform such kind of study. (2) the relationship between the soil erodibility and soil parameters is not one-to-one relationships. It is more likely a relationship related to various soil parameters. Further research is still required on this issue.

CHAPTER IX

VERIFICATION CASE STUDIES

9.1 GENERAL

The SRICOS-EFA method was developed based on the flume tests for the maximum scour depth equation establishment and numerical simulations for the maximum initial shear stress equation establishment. As a new method developed based on experimental conditions, it was necessary to verify it by using case histories and other data resources. Verification is very important for method development because it can check whether the method is good enough to provide sound results in real cases. And the verification process can provide more feedback for method development to improve the methodology. Two kinds of data resource will be used for the method verification. One is real full-scale bridge cases and the other is existing scour databases. Several criteria were set up to find the qualified case histories:

1. A bridge with piers in the water;
2. A gauge station which gives the whole hydrograph over the analysis period, or provides field hydrologic data measurements;
3. The site can be accessed with a drill rig for soil sampling;
4. The river cross-sections were documented at the beginning and at the end of the analysis period;

A survey for searching the case histories was conducted with the help of the Department of Transportation in different states. After much effort, eight bridge sites were found which satisfied the requirements for full-scale bridge cases selection:

1. The Woodrow Wilson Bridge over the Potomac River in Washington D.C. for pier scour
2. The Sloop Channel Bridge over the Sloop Channel on Wantagh Parkway for bridge scour
3. 6 selected Texas bridges for pier scour

Obviously 8 case histories are not quite enough for verification purposes. Two other bridges were also adopted for the verification, although these two bridges did not satisfy all the selection criteria. However, performing the scour analysis for these kinds of cases can provide supplementary verification. These two bridges are: The Indian Inlet over Indian River in Delaware for contraction scour, and the Goose Creek Bridge over Goose Creek in Wantagh Parkway for bridge scour.

Meanwhile it was decided to do more literature reviews and try to find some existing scour database as another supplement. The following databases were found and will be used in this study:

1. Mueller (1996) Database for complex pier scour
2. Froehlich (1988) Database for complex pier scour
3. Gill (1981) Database for contraction scour

These databases were primarily for non-cohesive soils, but it was felt that it would be useful to compare the SRICOS-EFA method with the measurements in non-cohesive soils. These are good cases to be regarded as references for the SRICOS-EFA method, which is considered applicable in non-cohesive soil conditions. Note that since the data pertains to non-cohesive soils and since it is not possible to gather all the soil samples

and perform the EFA tests for each case in the databases, the comparison is limited to evaluating the equations for maximum scour depth Z_{\max} (complex pier scour and contraction scour).

9.2 VERIFICATION CASE STUDY 1: THE WOODROW WILSON BRIDGE OVER THE POTOMAC RIVER

9.2.1 INTRODUCTION

The existing Woodrow Wilson Bridge is located in Prince George County in Maryland, Alexandria, Virginia, and Washington D.C. It carries interstate Routes 95 and 459 over the Potomac River. The Woodrow Wilson Bridge is an essential element of the I-495/95 beltway around Washington D.C. The Woodrow Wilson Bridge is a draw bridge, which is 6 lanes wide, 58 spans in length and is approximately 1,800 m long. It was built and opened in 1961 with a design traffic capacity of 75,000 vehicles per day. At the bridge site, the Potomac River can be divided in three areas: the main channel, the secondary channel, and the median area between the two channels. The main channel is near the west shore and is approximately 275 m wide. The main piers of the existing bridge are all founded on piles.

In 1998, approximately 190,000 vehicles were using the bridge each day. A new bridge needs to be built to increase the daily traffic volume and release the stressed traffic intensity. The replacement bridge will be built at the south side of the existing bridge. The proposed bridge will have two parallel six-lane bridges to replace the existing single six-lane bridge, and it will incorporate a drawbridge to enable ships to pass through. The new bridge will have fewer but wider piers. The piers are designed to

have exposed pile foundations and to be capped near the water surface. The two bascule piers that support the drawbridges will be protected from vessel impact by a fender system. The pier locations and the soil stratigraphy profile for the existing and the replacement Woodrow Wilson Bridges are shown in Figure 9.1. In this study, only the existing bridge will be analyzed.

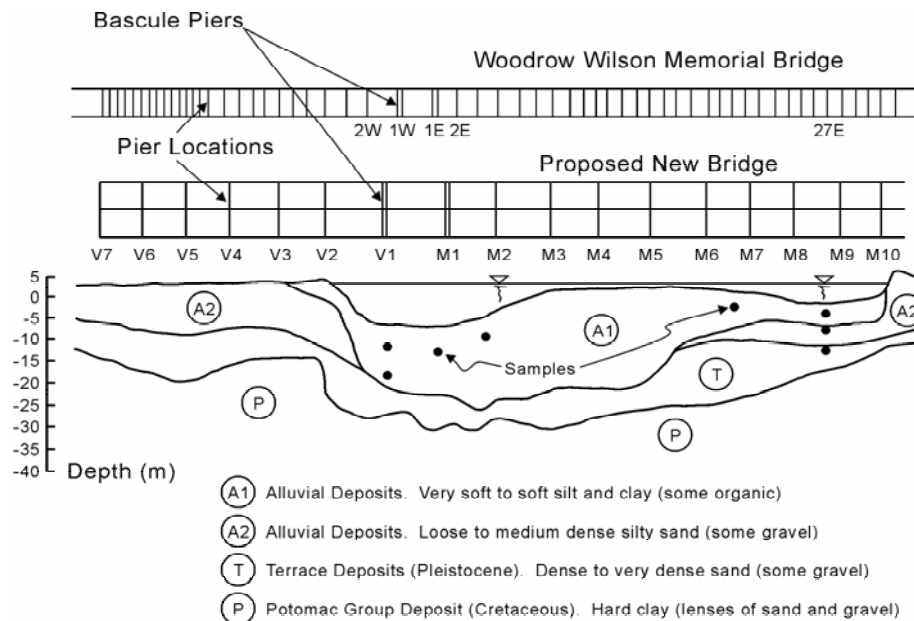


Figure 9.1: Pier Locations and Soil Stratigraphy Profile for Woodrow Wilson Bridges (after Kwak, 2002)

9.2.2 HYDROGRAPH DATA FOR THE WOODROW WILSON BRIDGE

The drainage basin area of the Woodrow Wilson Bridge at the Potomac River is 30,742 km². The drainage basin is comprised of portions of Pennsylvania, West Virginia, Virginia, Maryland, and Washington D.C. The nearest gaging station was

found at the USGS website, which is numbered as 01646500. The gaging station is located on Potomac River near the Little Falls pump station, approximately 13 km upstream from the Woodrow Wilson Bridge, and has a drainage area of 29,965 km². The discharge hydrograph at the bridge site was calculated by the downloaded discharge from the USGS website multiplied the drainage ratio (30742/29965). The bridge discharge hydrograph is shown in Figure 9.2. The maximum discharge was 9850 m³/s, which occurred in 1972.

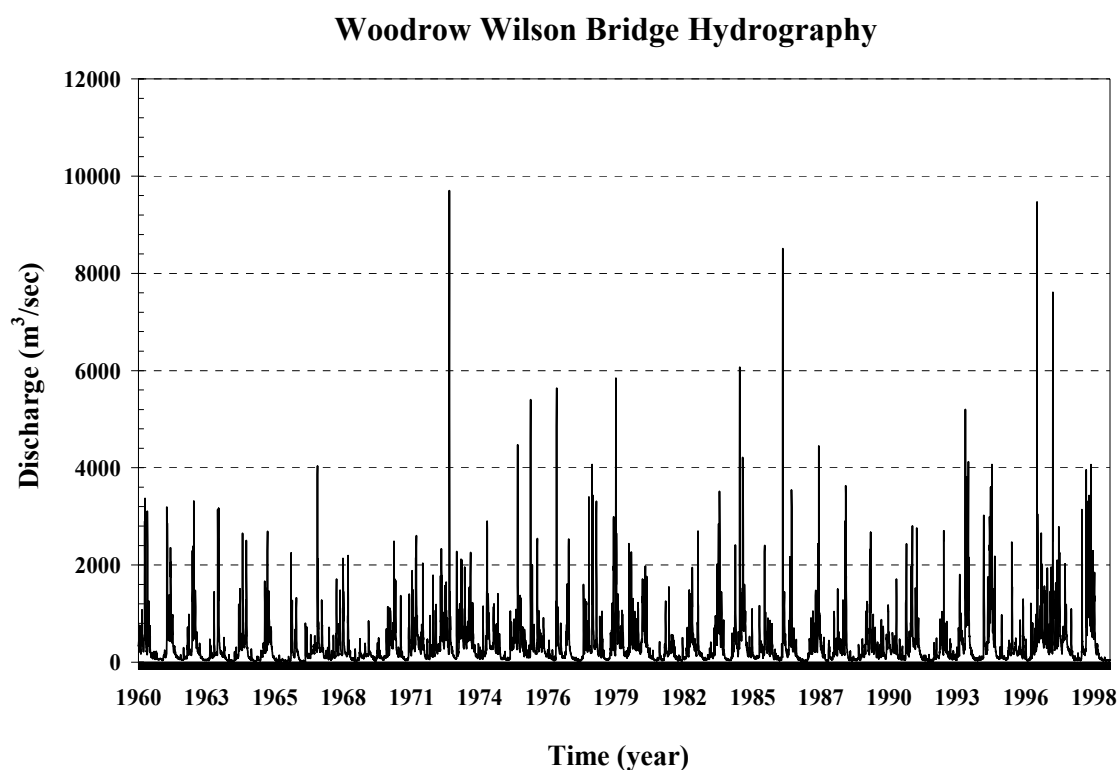


Figure 9.2: Woodrow Wilson Bridge Hydrograph from 1960 to 1998

A computer program titled HEC-RAS, standing by the Hydrologic Engineering Center's River Analysis System, and developed by the United States Army Corps of Engineers, was used for the flood analysis. The basic input for HEC-RAS consists of the riverbed cross-section profiles, Manning's coefficient, the average channel slope, and some selected discharges, which cover the values from 0 to the maximum discharge. The output of HEC-RAS consists of the velocities and water depths at the specific pier locations corresponding to the input discharges. This is important for the pier scour calculations in the SRICOS-EFA method because the velocities to calculate the pier scour depth is the velocities in the pier locations calculated without piers being present. The details of the input and output of HEC-RAS have been discussed in Chapter V. The curves of the relationships between the discharge vs. velocity and the discharge vs. water depth can be obtained by the data regression. The bridge discharge hydrograph can be transformed into the velocity hydrograph and the water depth hydrograph by using these regression relationships. For example, the relationships between discharge vs. velocity and discharge vs. water depth in the location of Pier 1E are shown in Figure 9.3 and Figure 9.4.

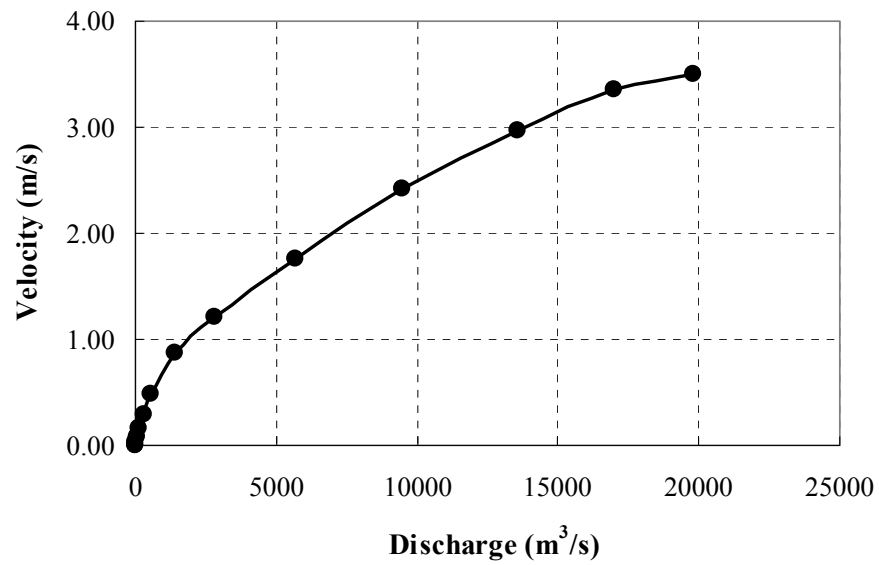


Figure 9.3: Relationship between Discharge and Velocity at Pier 1E Location

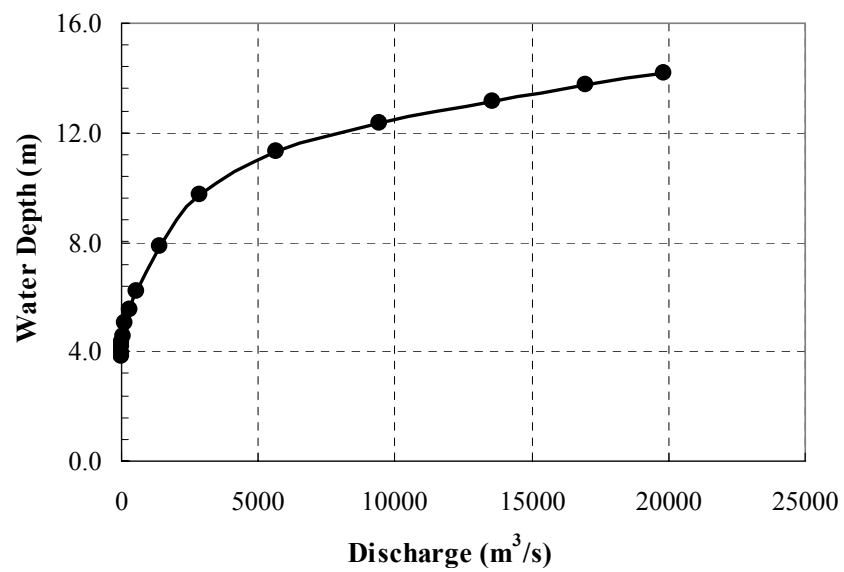


Figure 9.4: Relationship between Discharge and Water Depth at Pier 1E Location

9.2.3 SOIL DATA FROM THE WOODROW WILSON BRIDGE SITE

The Woodrow Wilson Bridge over the Potomac River in Washington D.C. is located within the Atlantic Coastal Plain, which consists of a broad belt of flat-lying sediments over deep bedrock. Throughout the whole area, the ground surface has been altered over time by man-made fills, especially in low lying areas and along rivers and streams. The soils below the main channel bed are mostly alluvial deposits, which contain soft clay, silt, and silty sand, extending down to approximately 25 m over the layer of Pleistocene deposits, which contain dense sand, silt and gravel.

The soil samples for EFA tests were taken near the locations of piers 1W, 1E, and 4E in the main channel, and pier 21E and 27E in the secondary channel by using standard Shelby tubes with a 76.2 mm outside diameter. The drilling locations are shown in Figure 9.1. The soil properties were obtained according to the standard of the American Society for Testing and Materials (ASTM) by performing laboratory tests. The soil properties from laboratory testing results are shown in the following Table 9.1.

The EFA tests were conducted for all the soil samples by Kwak (2000). The erosion functions for all the soil samples, presented as a scour rate \dot{z} versus shear stress τ curve, were obtained. The EFA testing results for the soil samples located in a depth of 4 m – 4.6 m and in a depth of 10 m – 10.6 m near Pier 1E are shown in Figure 9.5 and Figure 9.6 respectively. The EFA testing results for the soil samples located in a depth of 2.6 m – 3.2 m and in a depth of 11.2m – 11.7m near Pier 27 are shown in Figure 9.7 and Figure 9.8 respectively. From the EFA test results, it was found that the bigger undrained shear stress values don't refer to a higher critical shear stress of soil, while smaller undrained shear stress values don't refer to a lower critical shear stress of soil. For example, 22 Kpa (undrained shear stress) is relatively low for the soil sample at pier 27E (2.6 m ~ 3.2 m), however, the critical shear stress is 5.09 N/m². 130 Kpa (undrained shear stress) is relatively high for the soil sample at pier 27E (11.2 m ~ 11.7 m), however, the critical shear stress is only 0.16 N/m². This observation confirmed that the soil erodibility is unlikely to have a direct relationship to the single soil property, which has been studied in Chapter VIII.

Table 9.1: Geotechnical Soil Properties Testing Results (after Kwak, 2000)

Sample Location	Pier 1W	Pier 1W	Pier 2E	Pier 4E	Pier 21E	Pier 27E	Pier 27E	Pier 27E	Pier 27E
Depth (m)	4.0-4.6	10.1-10.6	5.5-6.1	5.5-6.1	2.1-2.7	2.6-3.2	5.2-5.6	11.2-11.7	11.9-12.5
Soil Type	Clay	Clay	Clay	Sandy Clay	Clay	Organic	Silt	Clay	Sand
Undrained Shear Stress	11.5	19.0	14.0	14.1	6.1	22.0	-	130.0	12.0
Bulk Density (KN/m ³)	18.1	15.6	18.5	16.3	15.4	15.2	15.2	21.3	17.1
% Passing #200	57	71	48	64	86	40	73	78	9
Liquid Limit (%)	53	51	47	37	68	-	43	86	-
Plastic Limit (%)	12	18	14	14	13	-	39	14	-
Water Content (%)	56	35	29	35	47	82	66	24	59
Critical Shear Stress	3.90	10.20	1.30	0.43	1.92	5.09	3.80	0.16	0.025
Initial Erodibility (mm/hr)	4.0	1.9	182.9	9.0	2.7	11.2	91.0	3.2	1665.2

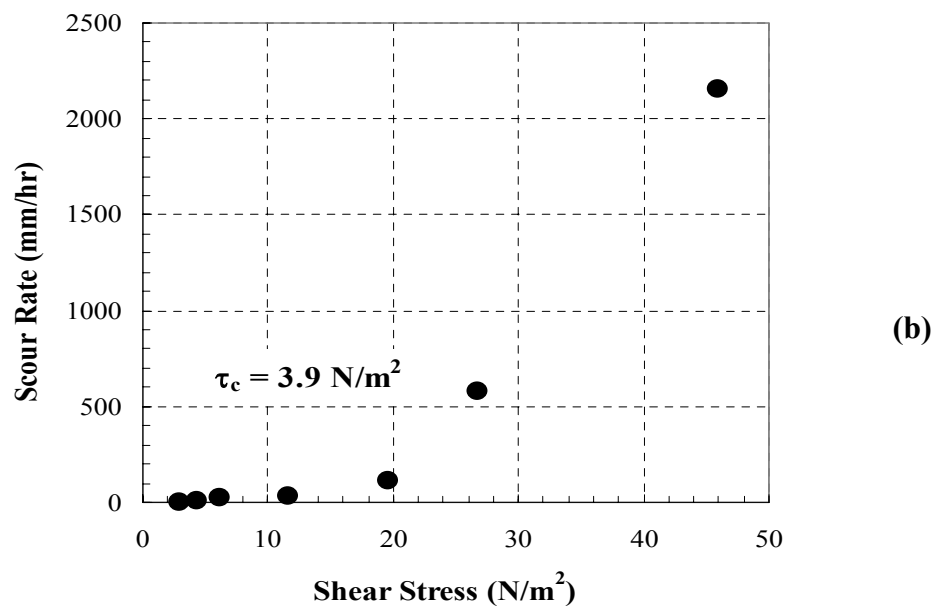
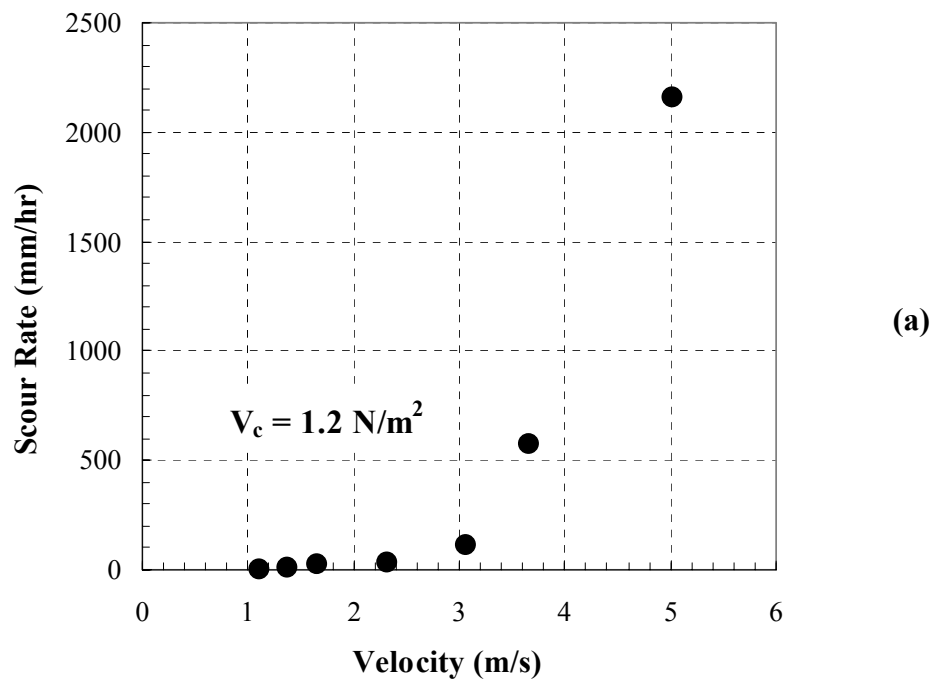


Figure 9.5 Erosion Function for a Soil Sample Taken near Pier 1E of the Existing Woodrow Wilson Bridge (4.0 – 4.6 m depth)
 (a) Scour Rate vs. Velocity, (b) Scour Rate vs. Shear Stress

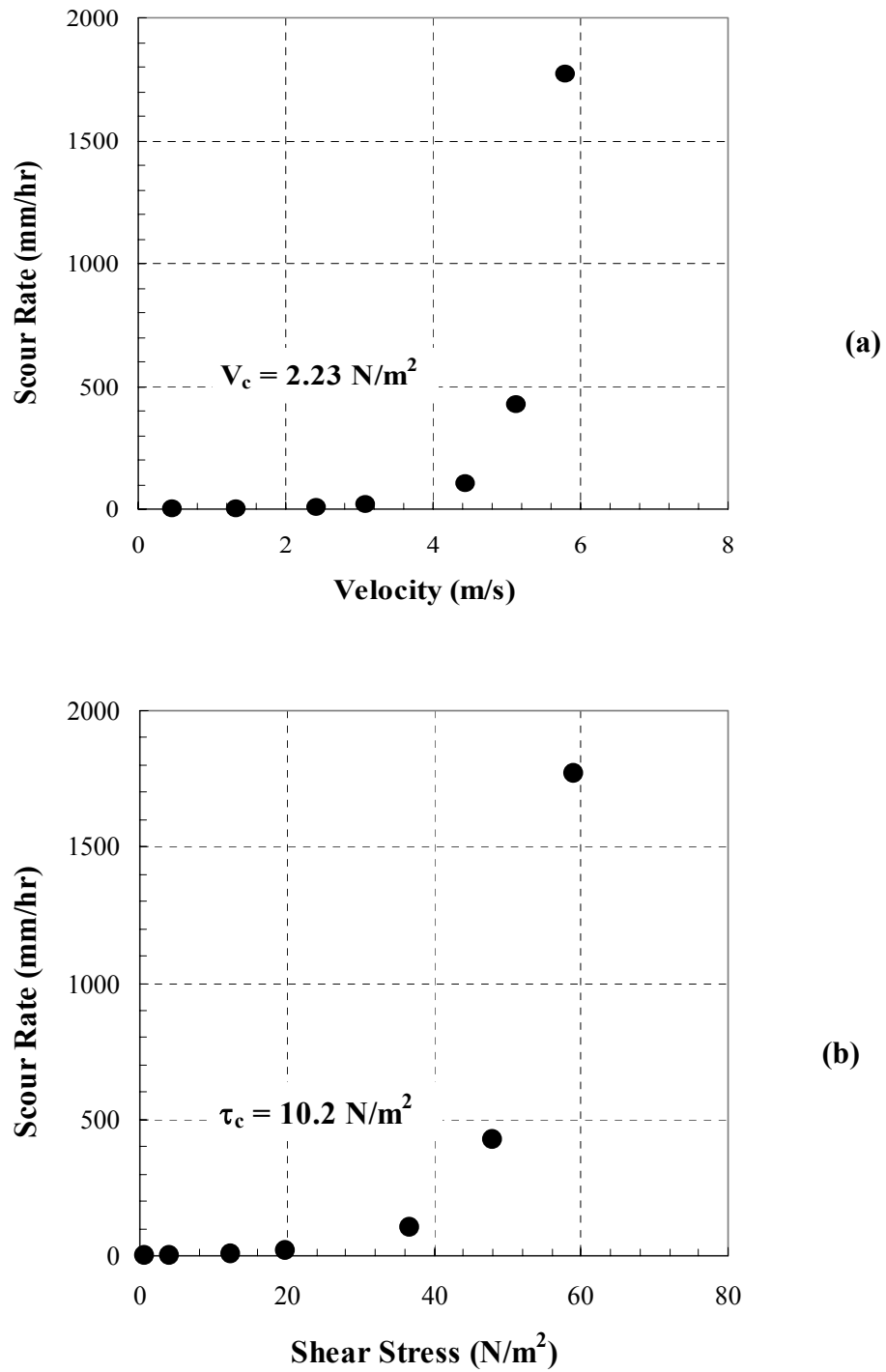


Figure 9.6 Erosion Function for a Soil Sample Taken near Pier 1E of the Existing Woodrow Wilson Bridge (10.0 – 10.6 m depth)
 (a) Scour Rate vs. Velocity, (b) Scour Rate vs. Shear Stress

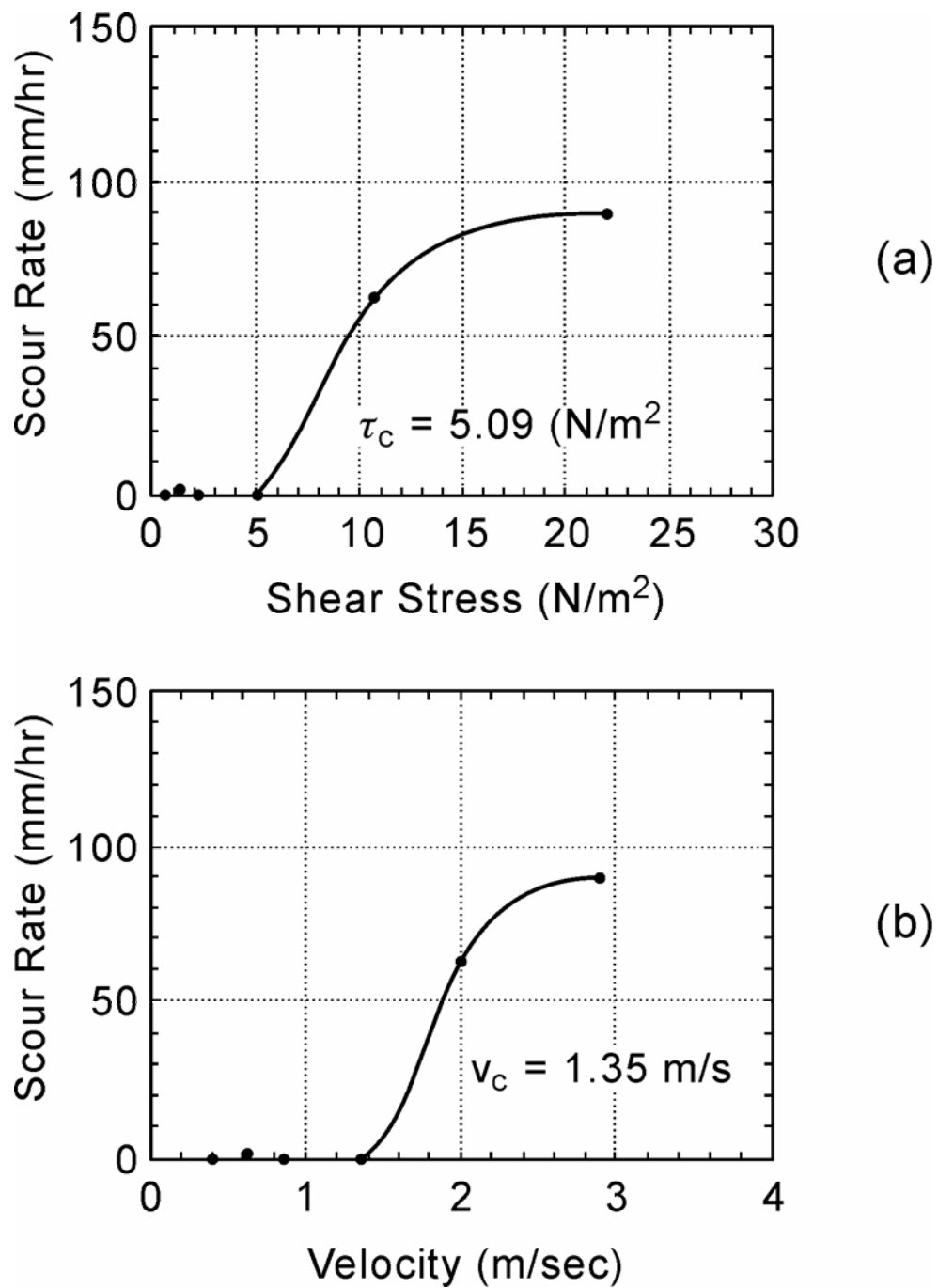


Figure 9.7: Erosion Function for a Soil Sample Taken near Pier 27E of the Existing Woodrow Wilson Bridge (2.6 – 3.2 m depth)

(a) Scour Rate vs. Shear Stress, (b) Scour Rate vs. Velocity

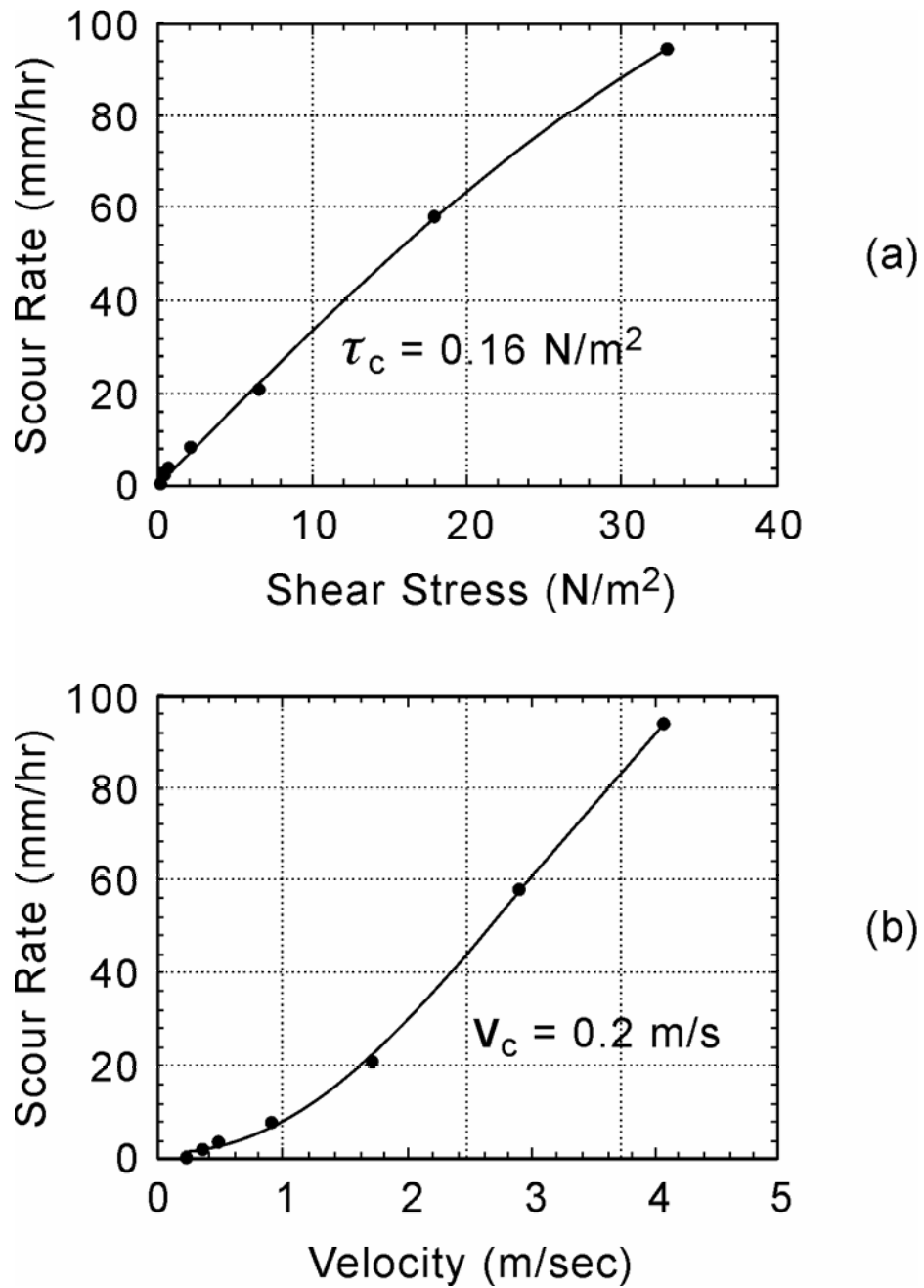


Figure 9.8: Erosion Function for a Soil Sample Taken near Pier 27E of the Existing Woodrow Wilson Bridge (11.2 – 11.7 m depth)
 (a) Scour Rate vs. Shear Stress, (b) Scour Rate vs. Velocity

9.2.4 MEASURED PIER SCOUR DEPTHS

The existing Woodrow Wilson Bridge is about 1,800 m long with 58 spans. The piers are numbered beginning at the center of the bascule section in the main channel and the number of piers increases as they approach each shore (Figure 9.1). Piers 1W through 26W are on the west side of the bridge and Piers 1E through 31E are on the east side of the bridge. All the piers and abutments are built as reinforced concrete and are supported by drilled piles. The junctions connecting the pier and piles are below the surface of the river bottom, so the pier width to be considered in the pier scour analysis is the width of the pier, not the width of the piles. Piers from 4W to 26W on the west side of the bridge and Piers from 6E to 23E were not considered in the scour analysis because these piers were not in water.

The channel bed has been monitored since 1998. The depths of pier scour were defined as the differences between the river bottom elevations at the piers and the channel bed elevations as the reference level of the pier scour, which should be far enough away from the pier. The reference level is practically taken as the average level of several points measured around the unscoured region. In the scour depth measurements, it is necessary to interpret the scour profiles because it is not possible to measure all the points around the scour hole. Hence, it was decided to use the range of values to describe the scour depths in most cases. An example Pier 5E scour profile is shown in the Figure 9.9, which has the maximum and minimum scour depth values. The measurements of the scour depths for the Piers are shown in Table 9.2.

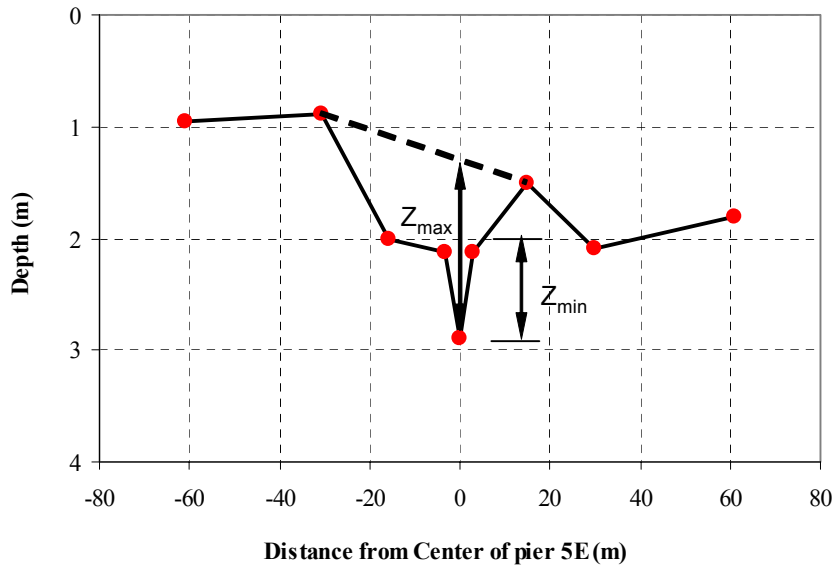


Figure 9.9: Scour Depth Measurements in Pier 5E (after Kwak, 2000)

Table 9.2: Measured Pier Scour Depths in the Existing Woodrow Wilson Bridge

Pier	Shape	Width (m)	Measured Scour Depth (m)	
			<i>Min.</i>	<i>Max.</i>
3W	Square	2.51	1.31	2.72
2W	Square	2.51	0.97	1.46
1W	Square	9.75	0.92	2.14
1E	Square	9.75	1.22	1.79
2E	Square	2.51	0.76	3.13
3E	Square	2.51	1.53	2.80
4E	Square	2.51	1.98	3.28
5E	Circle	1.68	0.77	1.72
24E	Circle	1.22	0.37	0.60
25E	Circle	1.22	1.01	1.50
26E	Circle	1.22	0.76	0.88
27E	Circle	1.22	0.73	1.15
28E	Circle	1.22	0.61	0.73
29E	Circle	1.22	0.31	0.52

9.2.5 PIER SCOUR PREDICTIONS

The scour depths z versus time t curves were calculated for each analysis pier of the Existing Woodrow Wilson Bridge over the time period from 1960 to 1998. This period covers from the time the bridge was built to the date of scour measurements.

It was not possible to take soil samples in each pier location, so limited EFA tests were performed on the soil samples located in the specific piers. The soil erosion function inputs in the SRICOS-EFA program were the EFA results of the nearest soil samples taken from the bridge site. Table 9.3 shows an example (Pier 1E) of the input parameters requested by the SRICOS-EFA program for the pier scour depth calculation.

Results Pier 1E:

After the 39 years period of the flood, the final pier scour is:

$$\mathbf{Z = 7.26\ m}$$

Figure 9.10 illustrates the scour depth development over time at the Pier 1E location.

Table 9.3: Summary of Data Input (Pier 1E)

Input Unit	SI Unit	1
Output Unit	SI Unit	1
First Date of Analysis		01-01-1960
Last Date of Analysis		09-30-1998
No. Of Hydrologic Data		14153
Upstream Channel Width		480
Type of Pier		Rectangular Pier
Pier Width	(m)	9.75
Pier Length	(m)	9.75
Attack Angle	(degree)	0
Number of Piers		1
Time Step	Hours	24
Input Hydrologic Data	Type of Hydrologic Input	Discharge vs. Time
	Number of Regression Points	Discharge vs. Velocity 8
	Values of Regression Points	Discharge, Velocity (m ³ /s) (m/s) 1.42, 0 14, 0.02 57, 0.07 141, 0.16 566, 0.49 1415, 0.87 5663, 1.75 13592, 2.97
	Values of Regression Points	Discharge, Water Depth (m ³ /s) (m) 1.42, 3.86 14, 4.18 57, 4.55 141, 5.02 566, 6.18 1415, 7.83 5663, 11.33 13592, 13.15
No. Of Layers		1
Properties of 1st Layer	Thickness (m)	7.62
	Critical Shear Stress (N/m ²)	3.9
Estimate Initial Scour Rate	Number of Regression Points	Shear Stress vs. Scour Rate 7
	Value of Regression Points	Shear Stress, Scour Rate (N/m ²) (mm/hr) 2.99, 0.02 4.36, 4.10 6.17, 20.31 11.69, 33.09 19.56, 110.66 26.71, 575.05 45.93, 2153.77

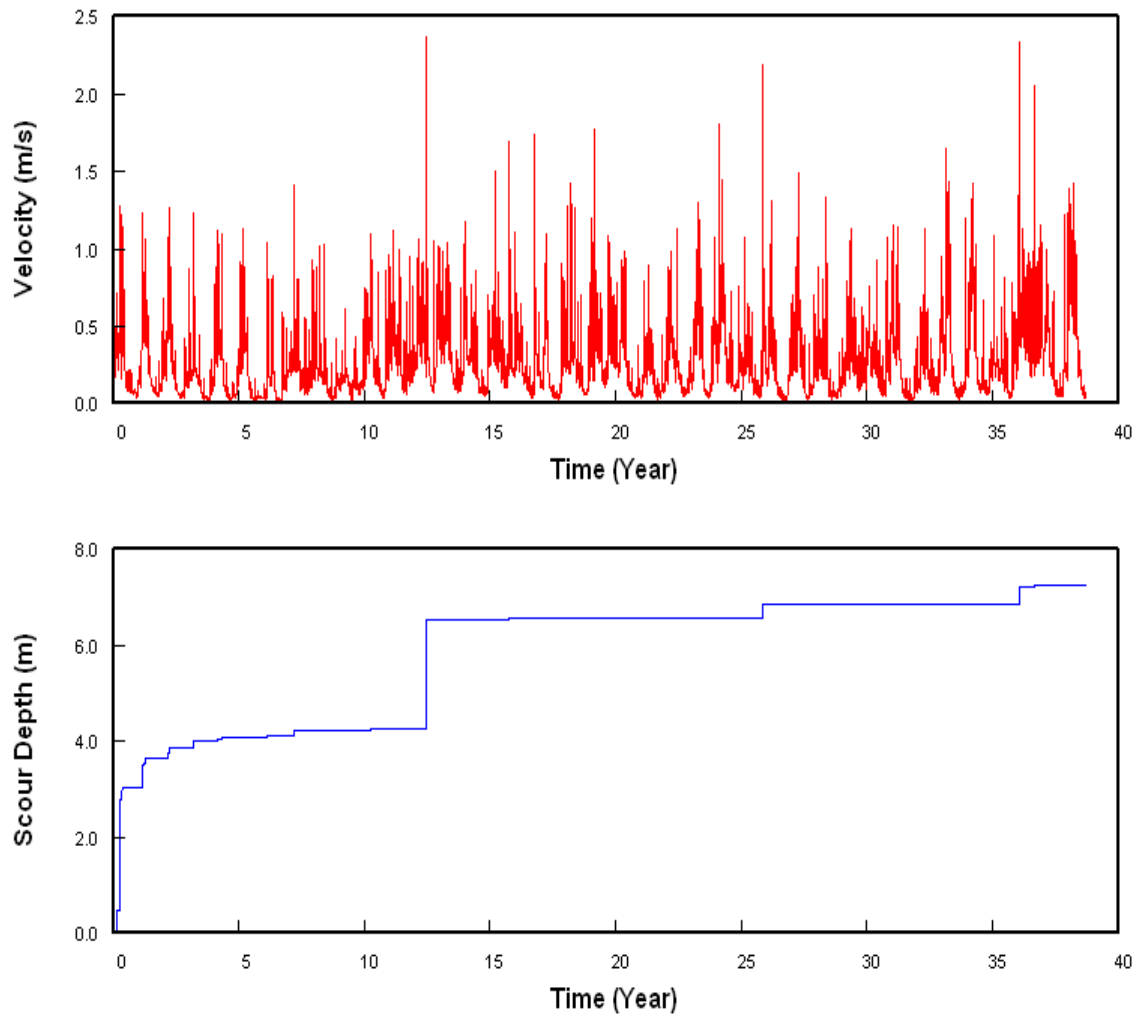


Figure 9.10: Scour Depth vs. Time in Pier 1E of Existing Woodrow Wilson Bridge over the Potomac River

The results of scour calculations for other piers by using the SRICOS-EFA method are shown in Table 9.4.

Table 9.4: Predicted Pier Scour Depths at the Existing Woodrow Wilson Bridge by Using the SRICOS-EFA Method from the 1960 to 1998 Period

Pier No.	Max. Discharge Q_{\max} (m ³ /s)	Max. Velocity V_{\max} (m/s)	Pier Width B (m)	Water Depth H (m)	K _w	K _{sp}	K _{sh}	Max. Scour Depth Z_{\max} (mm)	Predicted Scour Depth z(t) (m)	$\frac{z(t)}{Z_{\max}}$ (%)
Pier 3W	9457.8	1.39	2.51	8.1	1	1	1.1	2.83	1.94	68.6
Pier 2W	9457.8	2.09	2.51	12.03	1	1	1.1	3.66	3.20	87.4
Pier 1W	9457.8	2.3	9.75	12.34	0.92	1	1.1	8.48	6.78	79.9
Pier 1E	9457.8	2.43	9.75	12.34	0.92	1	1.1	8.79	7.25	82.5
Pier 2E	9457.8	2.37	2.51	11.73	1	1	1.1	3.97	3.64	91.8
Pier 3E	9457.8	2.01	2.51	10.81	1	1	1.1	3.57	3.03	84.8
Pier 4E	9457.8	1.75	2.51	10.2	1	1	1.1	3.27	2.50	76.4
Pier 5E	9457.8	1.27	1.68	3.8	1	1	1	1.88	1.20	63.8
Pier 24E	9457.8	0.87	1.22	2.58	1	1	1	1.21	0.30	24.9
Pier 25E	9457.8	0.91	1.22	4.41	1	1	1	1.24	0.42	33.8
Pier 26E	9457.8	1.26	1.22	5.63	1	1	1	1.53	1.04	68.1
Pier 27E	9457.8	1.53	1.22	6.54	1	1	1	1.73	1.33	77.0
Pier 28E	9457.8	1.54	1.22	6.54	1	1	1	1.73	1.34	77.3
Pier 29E	9457.8	1.48	1.22	5.93	1	1	1	1.69	1.28	75.7

Note: Maximum scour depths Z_{\max} were calculated based on the maximum discharge of the hydrograph.

- K_w: correction factor for water depth
- K_{sp}: correction factor for pier spacing
- K_{sh}: correction factor for pier shape

In order to compare the HEC-18 method and SRICOS-EFA method, scour analysis for a 100 year flood and a 500 year flood were also performed for the selected piers in the Existing Woodrow Wilson Bridge by using SRICOS-EFA and HEC-18. The values of 100 year and 500 year floods, obtained from the Maryland State Highway Administration, are shown in Table 9.5.

Table 9.5: 100 Year and 500Year Flood Discharges for the Potomac River at the Woodrow Wilson Bridge

Flood Type	Discharge (m ³ /s)
100 year flood	13592
500 year flood	19822

The pier scour results from HEC-18 are the scour depths without considering the time effect, so the maximum pier scour depths from the SRICOS-EFA method will be the values compared by HEC-18. The results are shown in Table 9.6 (100 year flood) and Table 9.7 (500 year flood).

Table 9.6: Predicted Maximum Pier Scour Depths at the Existing Woodrow Wilson Bridge Using the SRICOS-EFA Method and HEC-18 for a 100Year Flood Event

Pier No.		3W	2W	1W	1E	2E	3E	4E
Velocity (m/s)		1.77	2.58	2.83	2.97	2.9	2.49	2.2
Water Depth (m)		8.9	12.84	13.15	13.15	12.54	11.63	11.0 2
Scour Depth (m)	SRICOS-EFA Z_{max}	3.30	4.19	9.89	10.20	4.51	4.09	3.78
	HEC-18 Z_{max}	4.63	5.72	14.41	14.72	5.99	5.55	5.23
Pier No.		5E	24E	25E	26E	27E	28E	29E
Velocity (m/s)		1.67	1.24	1.27	1.65	1.95	1.96	1.9
Water Depth (m)		4.61	3.4	5.22	6.44	7.36	7.36	6.75
Scour Depth (m)	SRICOS-EFA Z_{max}	2.24	1.51	1.53	1.81	2.02	2.02	1.98
	HEC-18 Z_{max}	2.89	1.98	2.12	2.44	2.67	2.68	2.61

Table 9.7: Predicted Maximum Pier Scour Depths at the Existing Woodrow Wilson Bridge Using the SRICOS-EFA Method and HEC-18 for a 500Year Flood Event

Pier No.		3W	2W	1W	1E	2E	3E	4E
Velocity (m/s)		2.66	3.2	3.47	3.5	3.55	3.09	2.78
Water Depth (m)		9.9	13.8 8	14.19	14.19	13.58	12.66	12.05
Scour Depth (m)	SRICOS-EFA Z_{max}	4.27	4.80	11.55	11.61	5.13	4.69	4.39
	HEC-18 Z_{max}	5.59	6.34	15.90	15.96	6.61	6.16	5.85
Pier No.		5E	24E	25E	26E	27E	28E	29E
Velocity (m/s)		2.18	1.71	1.76	2.16	2.5	2.5	2.44
Water Depth (m)		5.65	4.43	6.26	7.48	8.4	8.4	7.79
Scour Depth (m)	SRICOS-EFA Z_{max}	2.65	1.85	1.89	2.15	2.36	2.36	2.32
	HEC-18 Z_{max}	3.33	2.36	2.50	2.80	3.03	3.03	2.97

9.2.6 RESULT ANALYSIS AND COMPARISON

Kwak (2000) indicated that the shape of the scour depth z versus time t curve depends on the scour rate of the soil as well as the shape and intensity of the hydrograph. As an example, the scour depth of Pier 1E increased gradually and the big floods, for example the flood in 1986, didn't generate a sudden increasing scour depth, because a certain amount of the scour depth had already developed by the pervious hydrograph (see Figure 9.10). In the case of Pier 27E, the maximum velocity in 1972 generated a big scour depth development. The reason for this occurrence is the very low velocities in the pier location prior to 1972, which couldn't develop the scour depth since the shear stresses due to the flowing water were below the critical shear stress of channel materials in the most time prior to 1972 (see Figure 9.11).

In 1996 Mueller compared 22 scour equations using field data prepared by Landers and Mueller (1996), and indicated that compared to the other methods the HEC-18 equation frequently grossly over-predicted the observed scour. It was found that in the comparison between HEC-18 and SRICOS-EFA had the same tendency. HEC-18 gave larger predictions than the predictions given by the SRICOS-EFA method. Figure 9.12 shows the comparison between the measured pier scour depths and the prediction results from the SRICOS-EFA method. Figure 9.13 shows the comparison between the results from the SRICOS-EFA and HEC-18 methods.

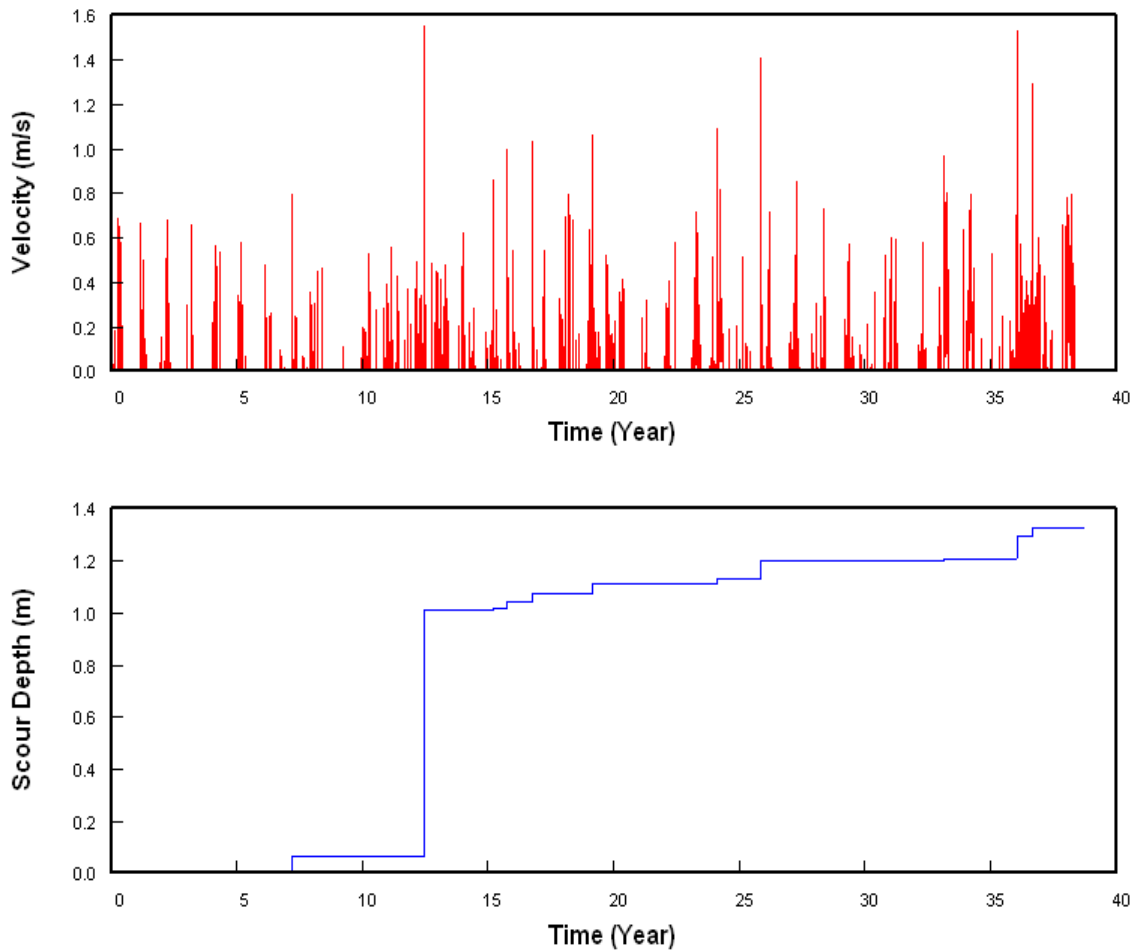


Figure 9.11: Scour Depth vs. Time in Pier 27E of the Woodrow Wilson Bridge over the Potomac River

A clear tendency can be observed from the comparison that, with the increasing of the pier widths, the differences between the results from these two methods increase as well. Although HEC-18 usually overestimated the scour depth as stated by Mueller (1996), it is a good design method, which rarely under-predicts the scour depths. SRICOS-EFA is a research method and its target is to predict the scour depths as close to the measured values in the sites as possible. Compared to HEC-18, in some cases,

SRICOS-EFA probably will underestimate the scour depths. Hence under such circumstances, a safety factor should be applied to the predicted scour depths to minimize the risk of having an actual scour depth larger than the predicted values. The recommended value of a safety factor is 1.5.

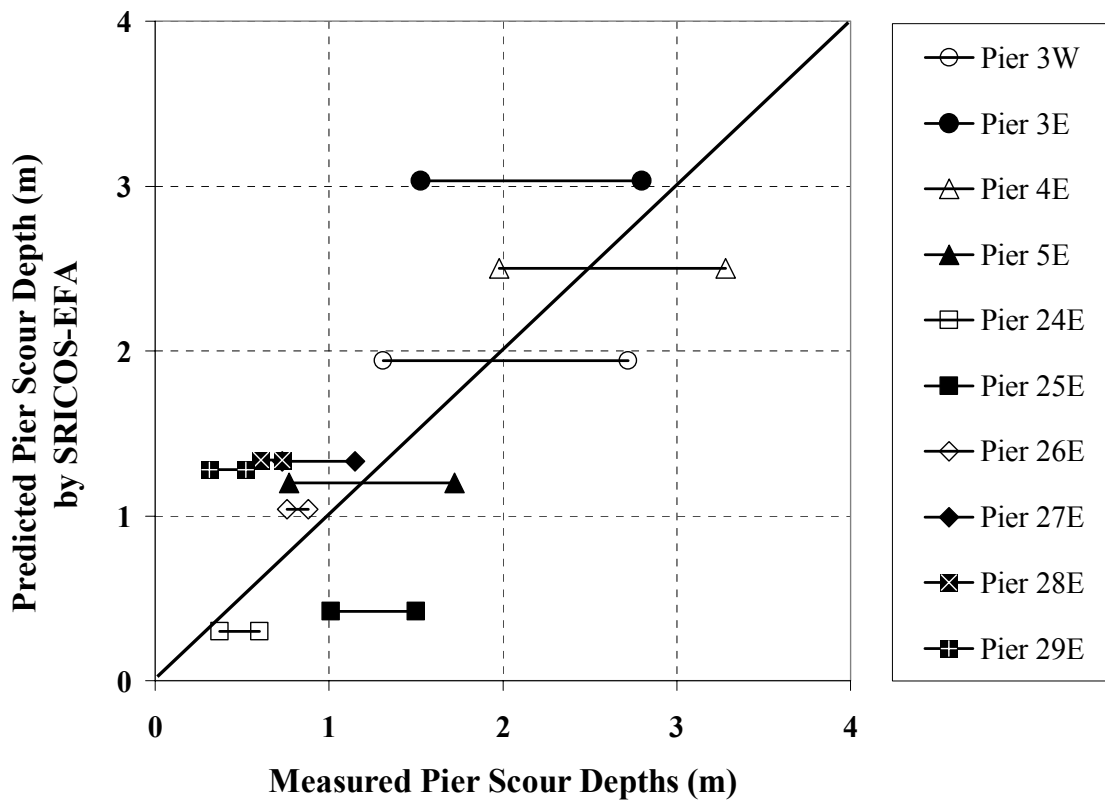


Figure 9.12: Comparison of Measured and Predicted Pier Scour Depths

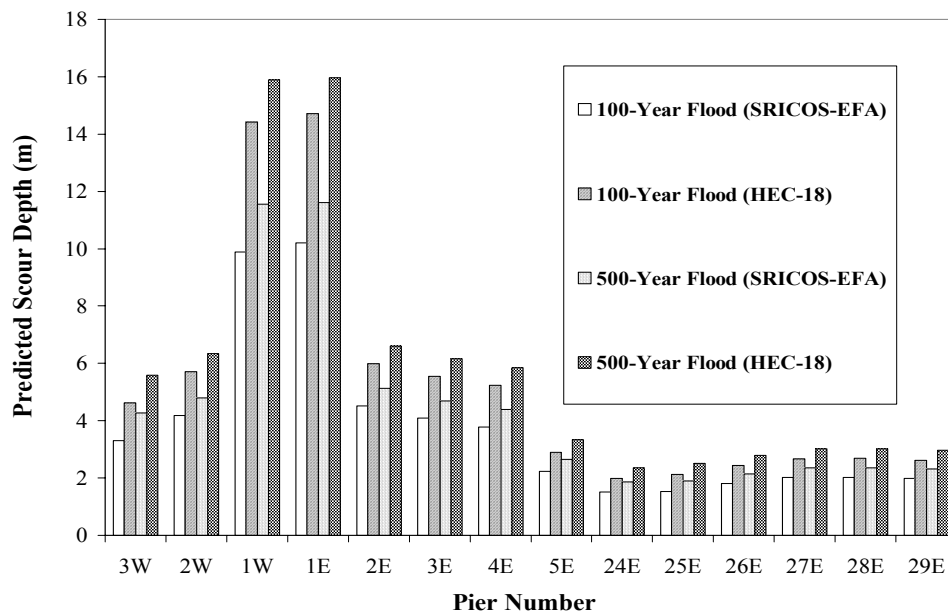
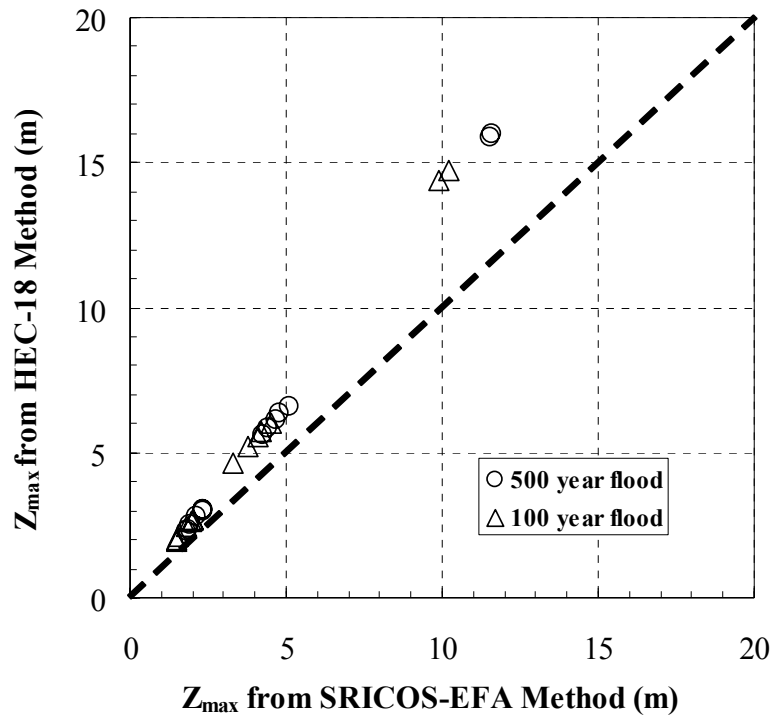


Figure 9.13: Comparisons between the Predictions for 100 and 500 Year Floods from SRICOS-EFA and HEC-18 in the Woodrow Wilson Bridge Case

9.3 VERIFICATION CASE STUDY 2: THE NEW SLOOP CHANNEL BRIDGE ON SLOOP CHANNEL ON WANTAGH PARKWAY

9.3.1 INTRODUCTION

Wantagh Parkway was built in 1929, and is an important roadway link providing access from mainland Long Island to the Jones Beach recreational area. The bridges over Sloop Channel are the southernmost structures carrying the Wantagh Parkway, crossing several small, level, grassy islands and the tidal inlets between them. The Sloop Channel Bridge is located in southeastern Nassau County, New York State. The Sloop Channel Bridge connects Green Island (an undeveloped island) to Jones Beach Island (the major barrier island that contains the Jones Beach State Park). Figure 9.14 is an aerial photograph which shows the location of the Existing Sloop Channel Bridge.

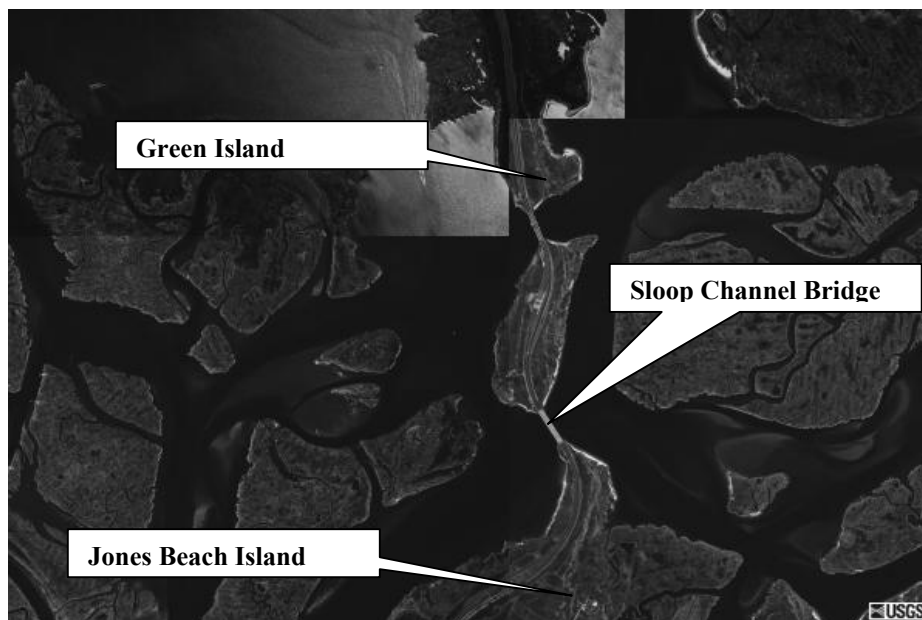


Figure 9.14: Location of the Existing Sloop Channel Bridge over Sloop Channel on Wantagh Parkway

The US Geological Survey (USGS) with the New York State Department of Transportation (NYSDOT) investigated the scour problem at the Sloop Channel Bridge in 1998. The results of the investigation indicated that two scour holes were nearly parallel to the Sloop Channel Bridge. One was along the east side and the other along the west side, while the bridge is oriented north-south. The scour holes located on both sides of the bridge are due to the tidal flow in the Long Island area. The scour depths are as much as 14.3 m below sea level and average more than 12.2 m below sea level. The historic streambed elevations for different years are illustrated in Figure 9.15.

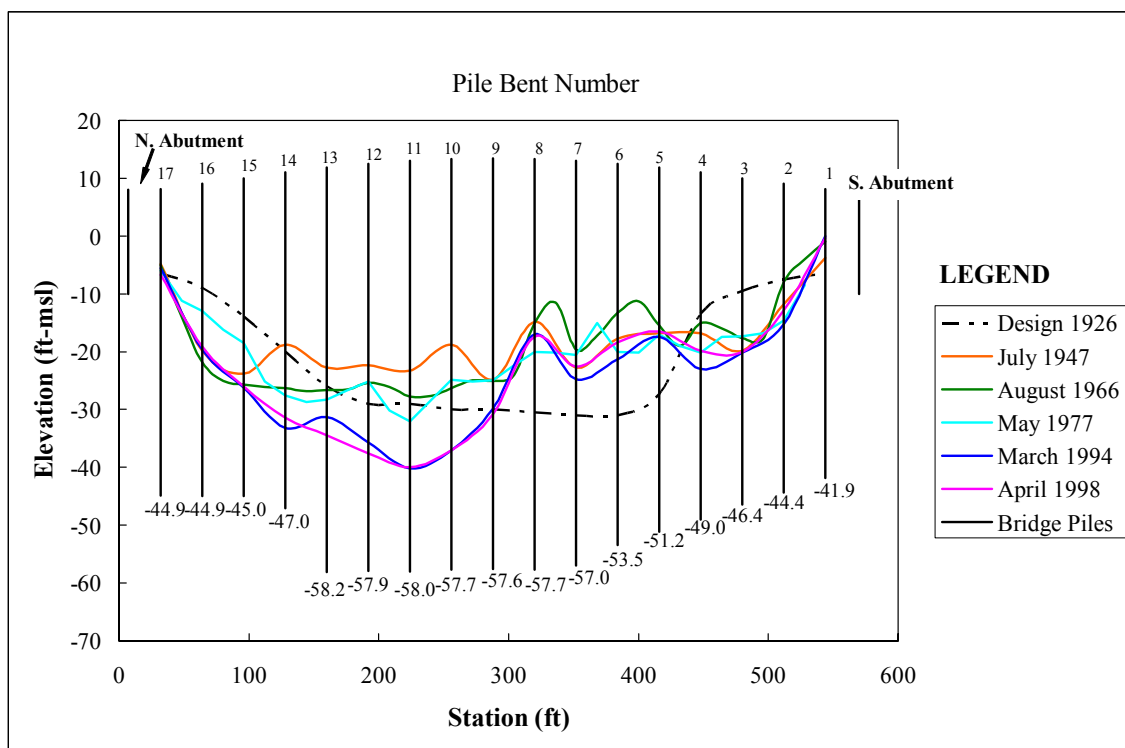


Figure 9.15: Sloop Channel Bridge Historic Streambed Elevations in Different Years

The existing scour-holes at the Sloop Channel Bridge promoted the NYSDOT to embark on a project to replace the Sloop Channel Bridge. The NYSDOT plans to construct a new permanent draw span for the replacement Sloop Channel Bridge in order to provide more direct east-west access for marine traffic using the state boat channel. The existing Sloop Channel Bridge will be demolished and the replacement Sloop Channel Bridge will be constructed in the same location. The new Sloop Channel Bridge will consist of two large round-nose bascule piers and 8 normal piers. From the north side to the south side of the bridge, the piers will be numbered from Pier 1 to Pier 10. Two bascule piers will be labeled as Pier 4 and Pier 5. The bascule piers are 8.2 m in width, 47.5 m in length and 5.2 m in the thickness of the pier cap. The normal piers are 1.76 m in width and 32.1 m in length. The bascule span between the two bascule piers is 32.0 m; the franking spans between the bascule pier and normal pier are 16.9 m; the distance between two adjacent normal piers are 19.0 m. The bascule piers (Pier 4 and Pier 5) will be supported by 22 steel pipe piles 1.524 m in diameter, distributed in two rows under the large pier cap. These steel piles will be driven into soil layers approximately 48.8 m deep. The normal piers will be supported by 6 prestressed concrete cylinder piles 1.37m in diameter, located in a single row. The length of the supporting piles for Pier 1 and Pier 10 will be 39 m; for Pier 2 and Pier 9, the pile lengths will be 43 m; for Pier 3 and Pier 4, the pile lengths will be 48 m; for Pier 7, the length of piles will be 42 m; for Pier 8, the length of piles will be 47 m. The overview and cross section of the New Sloop Channel Bridge are shown in Figure 9.16.

9.3.2 HYDROLOGIC DATA ON THE SLOOP CHANNEL BRIDGE

Three basic hydraulic events will be featured in the scour analysis for the Sloop Channel Bridge in this dissertation. The first one is a 100 year flood, the second one is a 500 year flood and the last one is a normal tidal hydrograph. The discharges of a 100 year flood and a 500 year flood in the approach channel of the Sloop Channel are 3460 m³/s and 4685 m³/s respectively. The upstream mean velocity values for 100-year and 500-year floods for the Sloop Channel Bridge are 1.35 m/s and 1.72 m/s respectively. The discharge and velocity values were given in the Ayres report (Ayers Associates, 2000). Ayres Associates Inc., located in Fort Collins, Colorado, conducted a hydraulic analysis for bridges along the south shore of Long Island, New York in 2000. The scope of this analysis included a system-wide hydraulic computer model that was capable of representing the tidal waterways during normal and extreme events: 100 year floods and 500 year floods. A total of 19 bridges in that area were studied. The Sloop Channel Bridge was one of them.

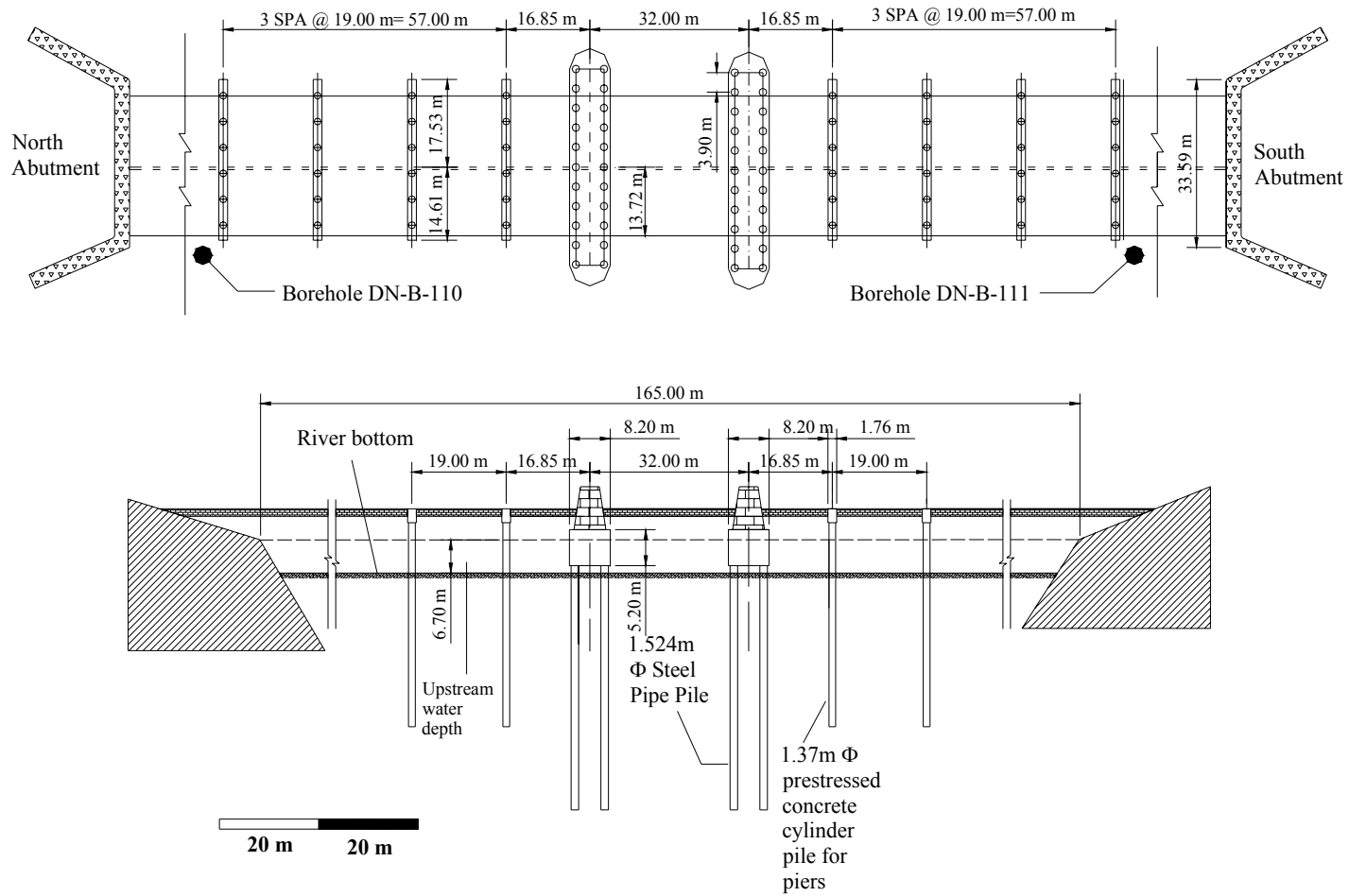


Figure 9.16: Overview and Cross Section of the New Sloop Channel Bridge over Sloop Channel on Wantagh Parkway

The normal tide cycle will be prepared in measured velocities, which were provided by Hardesty & Hanover Inc. These velocities were measured every hour from 6am to 6pm (a 12 hour period) in two different locations near the bridge site. In each measured point, three velocities were recorded at 10%, 50% and 100% of water depth. These three values were averaged and led to the mean depth velocities in the calculations. The variations of mean depth velocity were from 0.1 m/s to 0.9 m/s. The measured values in the 12 hour period at two different locations formed the basic one day velocity cycle, which would be repeated in 75 years to establish the normal tidal hydrograph. Table 9.8 and Figure 9.17 shows the measured velocity values at the Sloop Channel Bridge.

The Sloop Channel Bridge is located in the coastal region, so the direction of the flow will be reversed. A typical tidal cycle should involve a complete rise and fall of the tide. The measured velocities listed in Table 9.8 are in two directions: East to West and West to East. This caused two big scour holes, one on either side of the bridge. These were found during the scour investigation in 1998. Since SRICOS-EFA couldn't calculate the scour depths under the tidal flow condition, an assumption will be applied in this case: the flow going through the bridge cross section will be assumed to go in only one direction. This assumption will allow the scour prediction be more conservative, because the entire flow will contribute to the scour development on one side.

Table 9.8: Measured Velocities during One Day Period in Two Different Locations near the Sloop Channel Bridge

Time	10% of Water Depth (m/s)	50% of Water Depth (m/s)	90% of Water Depth (m/s)	Flow Direction	Mean Velocity (m/s)
Location A					
6:00 AM	0.73	0.98	0.61	W→E	0.8
7:00 AM	0.79	0.91	0.58	W→E	0.8
8:00 AM	0.49	0.82	0.64	W→E	0.7
9:00 AM	0.37	0.24	0.03	W→E	0.2
10:00 AM	0.18	0.21	0.15	E→W	0.2
11:00 AM	0.40	0.46	0.49	E→W	0.4
12:00 PM	0.64	0.58	0.49	E→W	0.6
1:00 PM	0.67	0.67	0.46	E→W	0.6
2:00 PM	0.61	0.61	0.52	E→W	0.6
3:00 PM	0.34	0.34	0.09	E→W	0.3
4:00 PM	0.27	0.06	0.15	W→E	0.2
5:00 PM	0.46	0.61	0.15	W→E	0.4
6:00 PM	0.52	0.82	0.58	W→E	0.6
Time	10% of Water Depth (m/s)	50% of Water Depth (m/s)	90% of Water Depth (m/s)	Flow Direction	Mean Velocity (m/s)
Location B					
6:00 AM	0.79	0.94	0.82	W→E	0.9
7:00 AM	0.70	0.76	0.64	W→E	0.7
8:00 AM	0.49	0.76	0.61	W→E	0.6
9:00 AM	0.34	0.30	0.09	W→E	0.2
10:00 AM	0.03	0.15	0.24	E→W	0.1
11:00 AM	0.37	0.40	0.27	E→W	0.3
12:00 PM	0.52	0.46	0.21	E→W	0.4
1:00 PM	0.67	0.49	0.37	E→W	0.5
2:00 PM	0.64	0.52	0.34	E→W	0.5
3:00 PM	0.30	0.06	0.09	E→W	0.2
4:00 PM	0.18	0.15	0.03	W→E	0.1
5:00 PM	0.52	0.73	0.49	W→E	0.6
6:00 PM	0.67	0.70	0.64	W→E	0.7

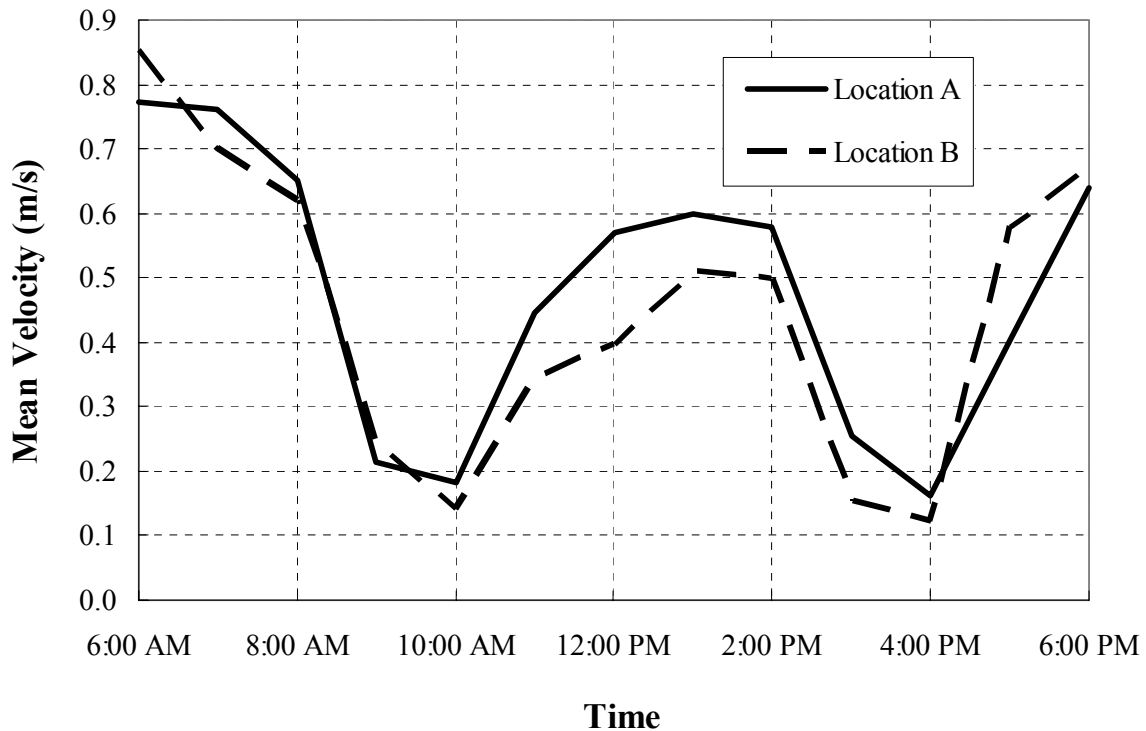


Figure 9.17: Measured Velocities during a 12 Hour Period in Two Different Locations near the Sloop Channel Bridge

The following will describe the techniques used to form the 500 year flood hydrograph. The 500 year flood will be inserted in the middle of the normal 75 years hydrograph to establish the 500 year flood hydrograph. The velocity values of the normal hydrograph will be increased gradually to 1.72 m/s (the 500 year flood velocity). Then the velocity will be decreased from 1.72 m/s to 1m/s, and after that, the velocity will be increased again to 1.72 m/s to reach another 500 year flood peak value. Finally the velocity values will be decreased from 1.72 m/s to the normal velocity hydrograph cycle. The duration of all velocity increments and decrements is 1 hour. One part of the 500 year flood hydrograph is illustrated in Figure 9.18.

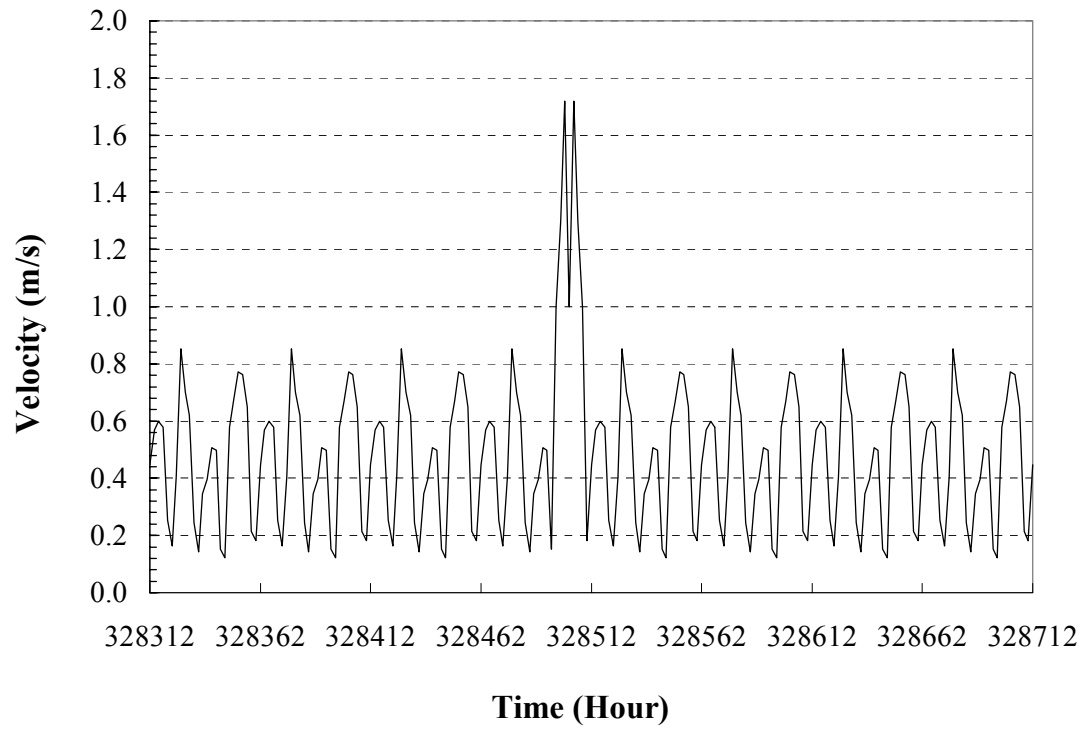


Figure 9.18: One Part of the 500 Year Flood Hydrograph for the Sloop Channel on Wantagh Parkway

9.3.3 SOIL DATA FROM THE SLOOP CHANNEL BRIDGE SITE

Six soil samples were sent to Texas A&M University by NYSDOT (New York State Department of Transportation). These were taken from the Sloop Channel Bridge site by using the standard Shelby tubes with a 72.6 mm outside diameter. These soil samples were from two boreholes labeled as DN-B-110 and DN-B-111. Four soil samples were from Borehole DN-B-110, which was located near the north abutment of the bridge. Two soil samples were from Borehole DN-B-111, which was near the south abutment of the bridge. According to the site investigation and the soil sample descriptions provided by NYSDOT, 4 underlying soil layers were identified under the channel bottom. The soil properties of the different layers were obtained under the standards of the American Society for Testing and Materials (ASTM) by performing the laboratory tests. There were only two soil samples taken from Borehole DN-B-111 in order to keep the data continuity. So the EFA testing results and soil properties of these two soil samples will be just the reference of the results from the soil samples in Borehole DN-B-110. The erosion functions and soil properties from Borehole DN-B-110 will be adopted as the input of SRICOS-EFA method. The soil properties from laboratory testing are shown in Table 9.9. All six soil samples from NYSDOT were tested by the EFA at Texas A&M University on March 2002. These EFA tests were performed according to the standard procedure. The following figures show the erosion functions for different soil samples. All the results will be presented as scour rate vs. velocity curve and scour rate vs. shear stress curve.

Table 9.9: General Subsurface Information & Laboratory Test Data for the Sloop Channel

Layer 1 (DNB-110-T3) Dark gray clayey slit with organics	Thickness	(m)	7.2
	Critical Shear Stress	(N/m ²)	0.5
	Water content	(%)	36
	Density	(KN/m ³)	18.2
	Liquid Limit	(%)	49
	Plastic Limit	(%)	22
	Plastic Index		27
Layer 2 (DNB-110-T4) Layered gray silty clay/ clayed silt with fine sand & Organics	Thickness	(m)	0.61
	Critical Shear Stress	(N/m ²)	1.5
	Water content	(%)	37
	Density	(KN/m ³)	18.8
	Liquid Limit	(%)	41
	Plastic Limit	(%)	19
	Plastic Index		22
Layer 3 (DNB-110-T5-T6) Layered gray silty clay with organics & fine sand	Thickness	(m)	2.4
	Critical Shear Stress	(N/m ²)	1.9
	Water content	(%)	33.5
	Density	(KN/m ³)	18.6
	Liquid Limit	(%)	46.5
	Plastic Limit	(%)	24
	Plastic Index		22.5
Layer 4 (DNB-110-T7) Layered gray sandy slit/ silty sand with organics	Thickness	(m)	30
	Critical Shear Stress	(N/m ²)	0.19
	Water content	(%)	27
	Density	(KN/m ³)	20.1
	Liquid Limit	(%)	35
	Plastic Limit	(%)	18
	Plastic Index		17

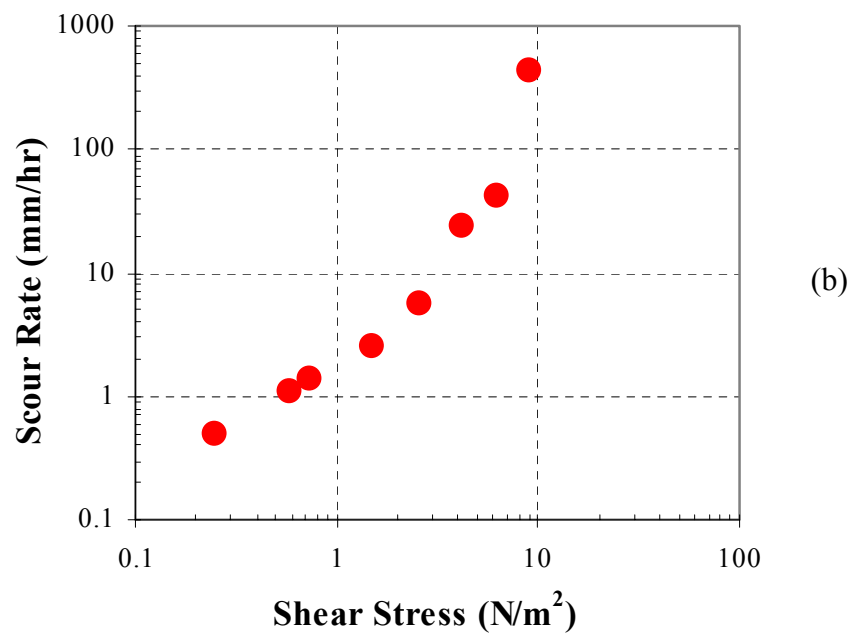
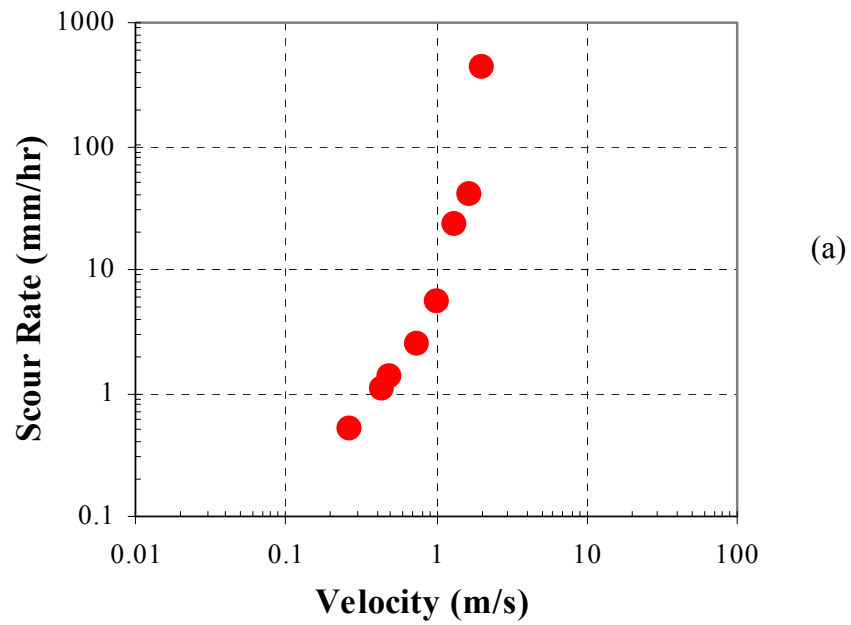


Figure 9.19: Erosion Function for Soil Sample (DB-N-110, Tube 3) of the Sloop Channel (21.49 – 21.79 m depth)

(a) Scour Rate vs. Velocity, (b) Scour Rate vs. Shear Stress

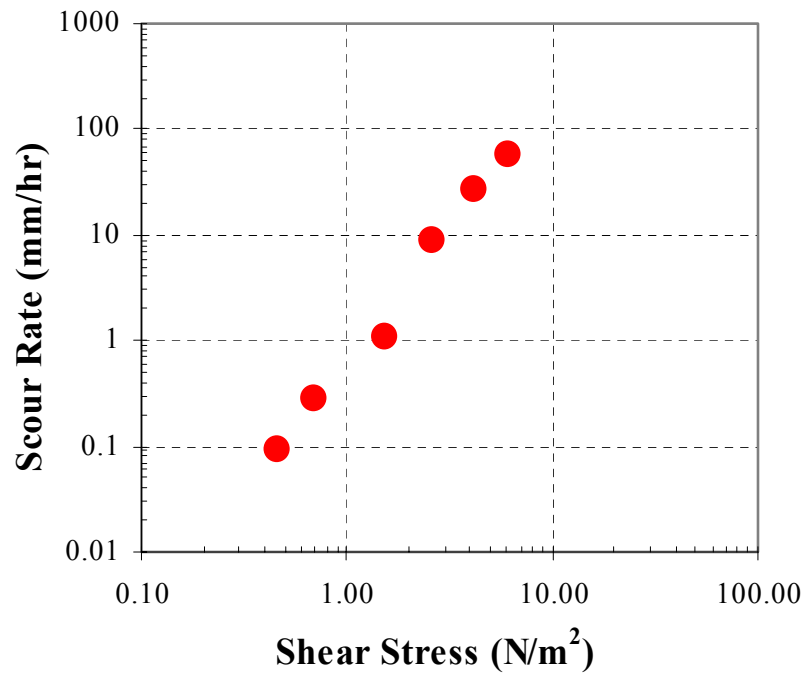
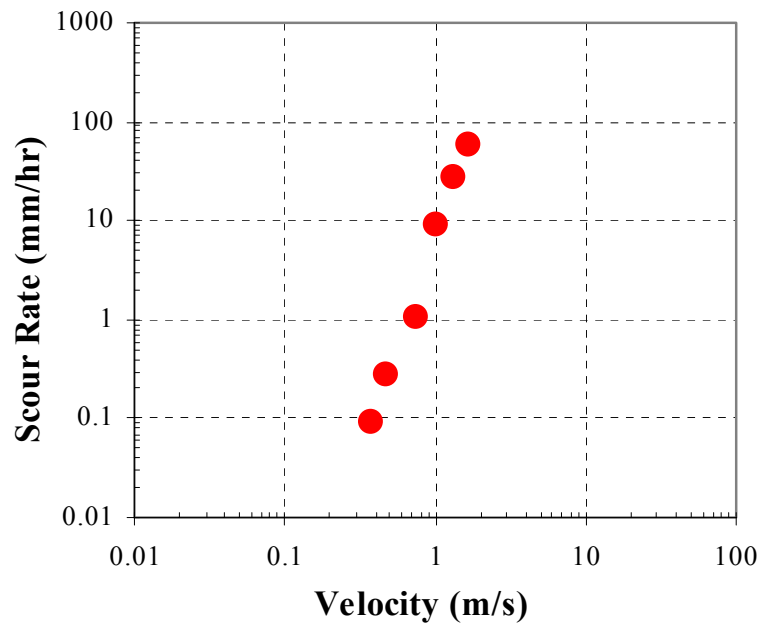


Figure 9.20: Erosion Function for Soil Sample (DB-N-110, Tube 4) of the Sloop Channel (22.10 – 22.40 m depth)
 (a) Scour Rate vs. Velocity, (b) Scour Rate vs. Shear Stress

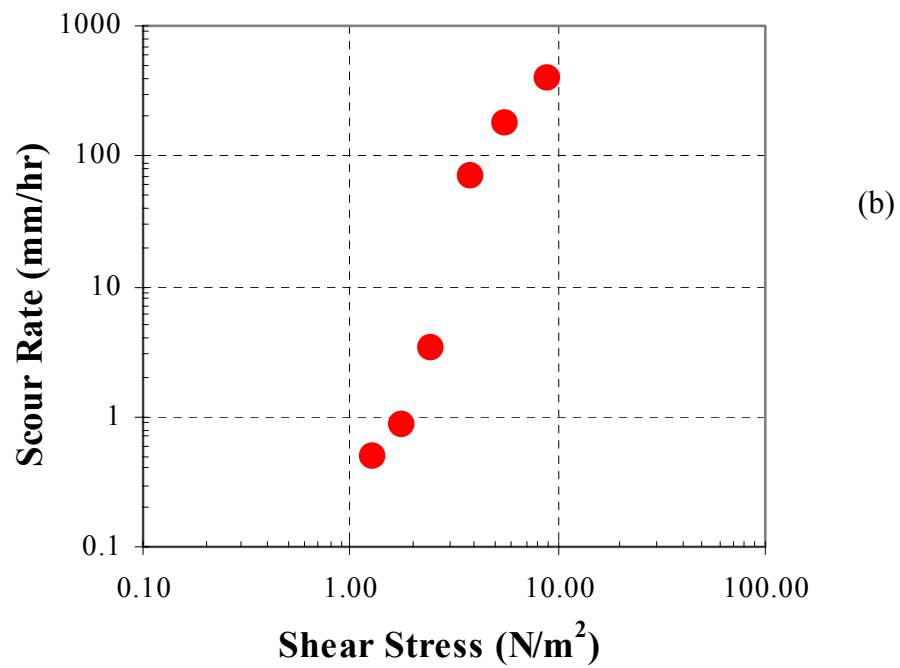
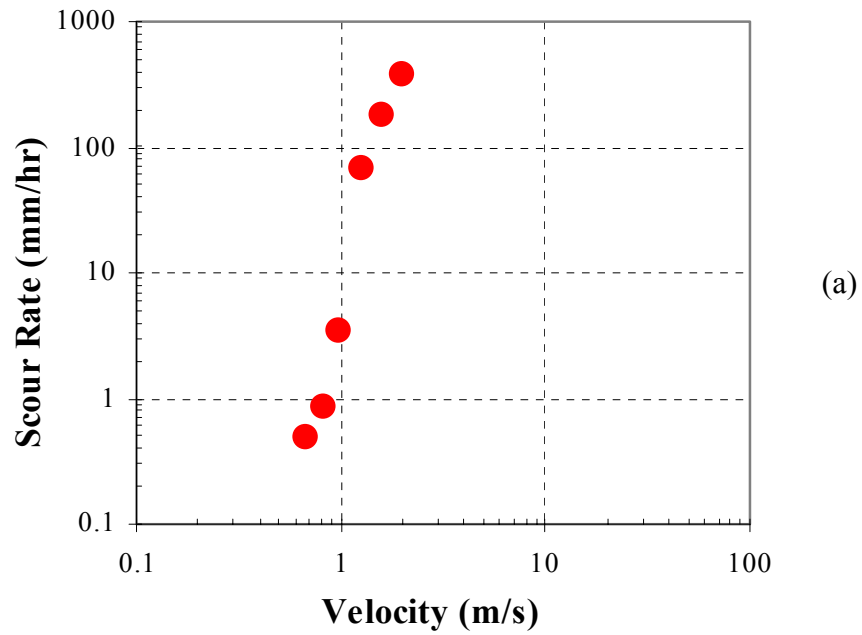


Figure 9.21: Erosion Function for Soil Sample (DB-N-110, Tube 5) of the Sloop Channel (22.71 – 23.01 m depth)

(a) Scour Rate vs. Velocity, (b) Scour Rate vs. Shear Stress

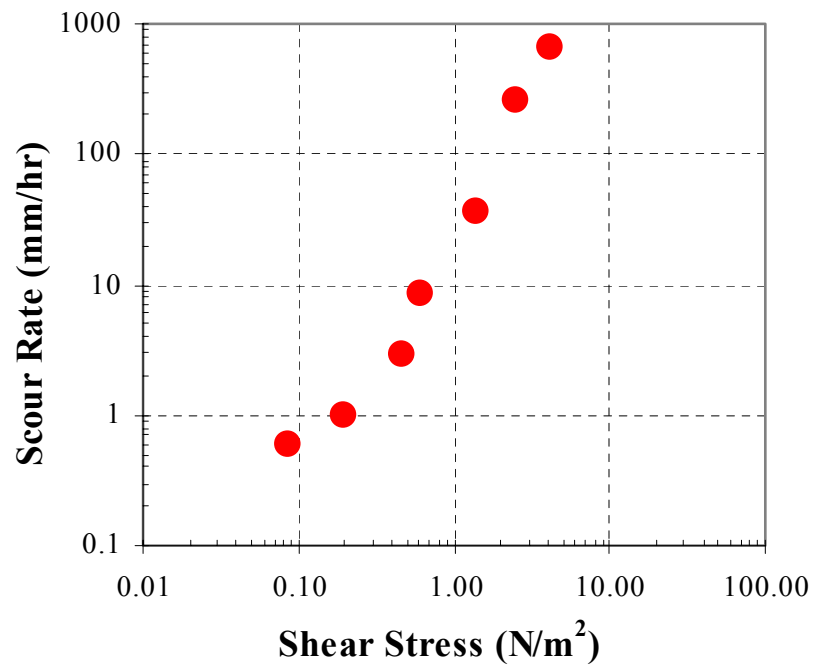
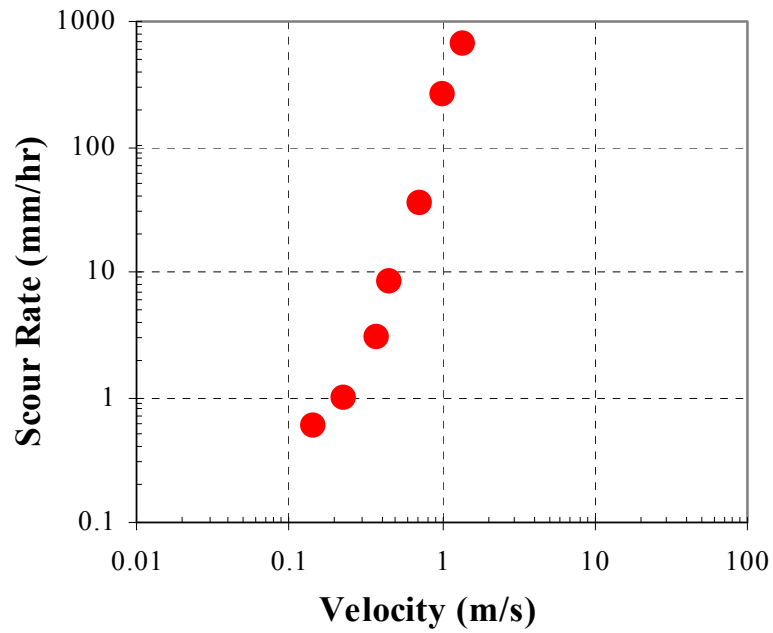


Figure 9.22: Erosion Function for Soil Sample (DB-N-110, Tube 7) of the Sloop Channel (26.21 – 26.51 m depth)

(a) Scour Rate vs. Velocity, (b) Scour Rate vs. Shear Stress

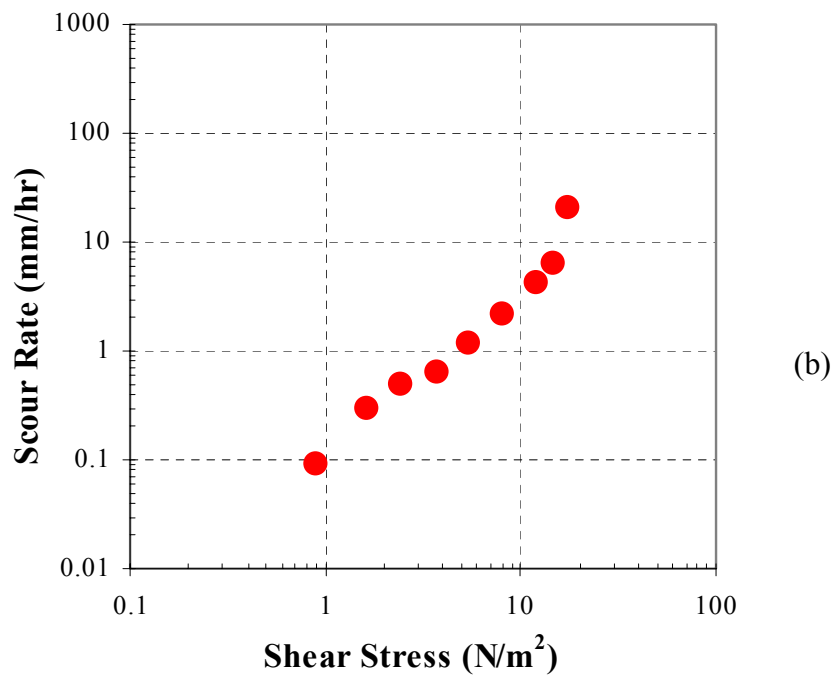
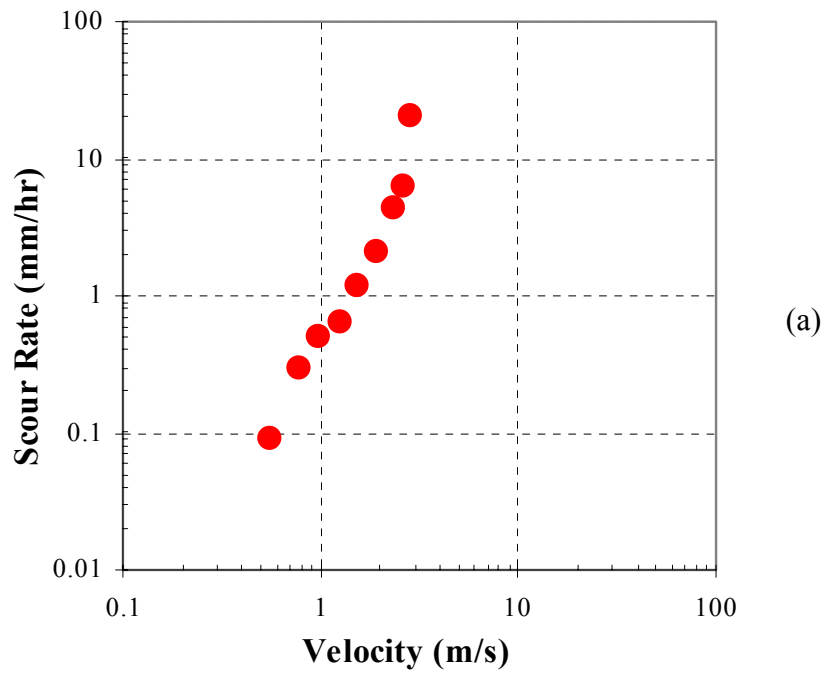


Figure 9.23: Erosion Function for Soil Sample (DB-N-111, Tube 2) of the Sloop Channel (21.60 – 22.10 m depth)
 (a) Scour Rate vs. Velocity, (b) Scour Rate vs. Shear Stress

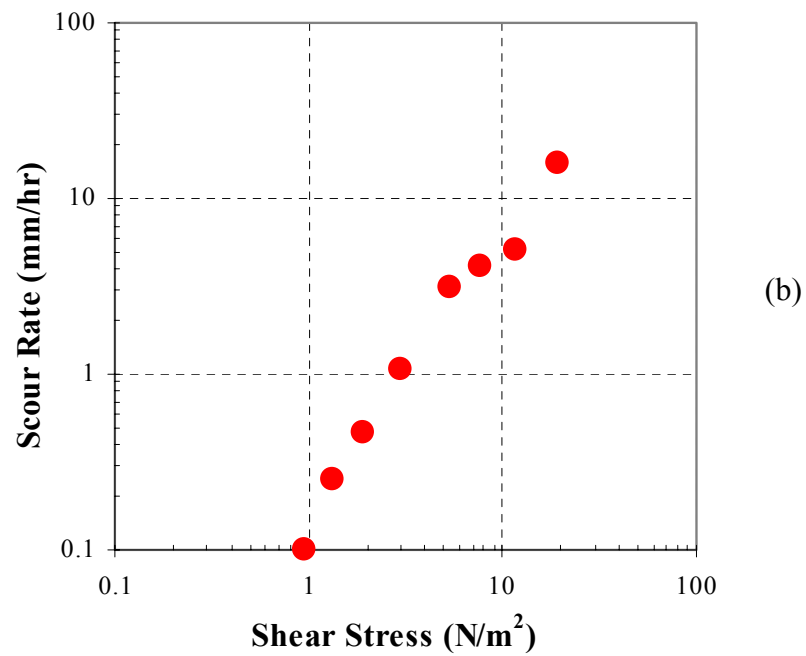
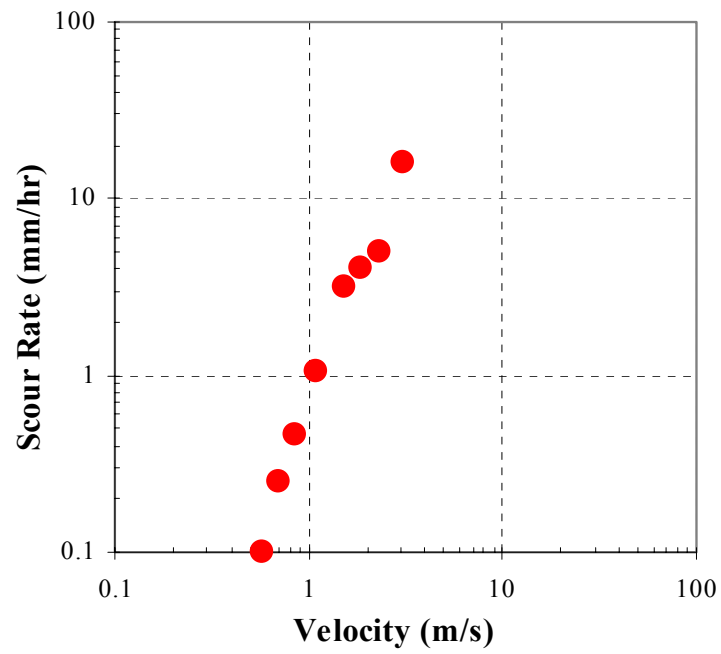


Figure 9.24: Erosion Function for Soil Sample (DB-N-111, Tube 4) of the Sloop Channel (28.00 – 28.70 m depth)
 (a) Scour Rate vs. Velocity, (b) Scour Rate vs. Shear Stress

9.3.4 PIER SCOUR PREDICTIONS

The pier scour depths will be calculated for different piers of the new Sloop Channel Bridge by using the SRICOS-EFA method. The analysis period will be 6 hours for a short term flood or the 75 year hydrograph. Velocity values in the 6 hour short term flood will be constant. The velocity values will be 0.9 m/s (the maximum velocity in the normal hydrograph), 1.35 m/s (100 year flood), 1.72 m/s (500 year flood). The 75 year velocity hydrographs will include two types: one is the normal tidal velocity hydrograph and the other is the 500 year flood associated with the normal tidal velocity hydrograph. These have been described in detail in Section 9.3.2 (Hydrologic Data of the Sloop Channel Bridge). Input from the soil erosion function in the SRICOS-EFA Program will be the EFA results of the soil samples in Borehole DN-B-110. Two bascule piers (Pier 5 and Pier 6) and two franking piers adjacent to the bascule piers (Pier 4 and Pier 7) will be analyzed (Figure 9.16). The details of the bascule pier and franking piers are shown in Figure 9.25 and Figure 9.26.

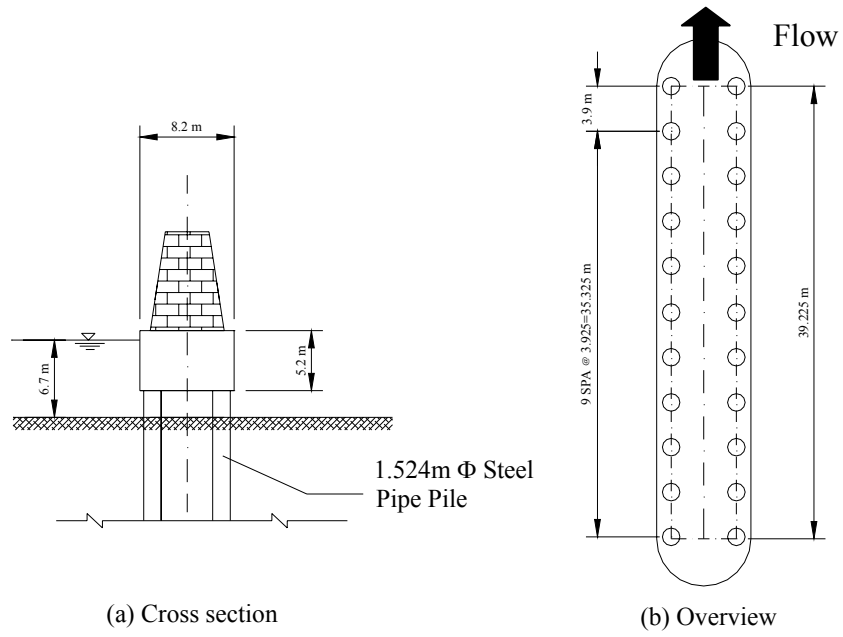


Figure 9.25: Geometry of the Bascule Pier at the New Sloop Channel Bridge

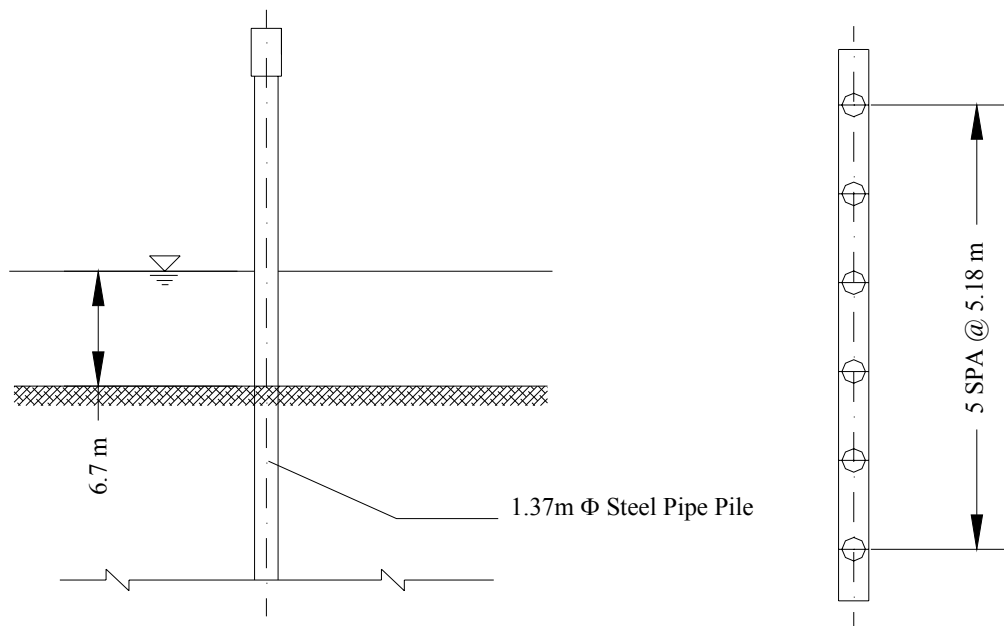


Figure 9.26: Geometry of the Franking Pier at the New Sloop Channel Bridge

In this case, the bascule piers should be treated as the complex pier case in HEC-18. In Richardson and Davis (2001), the total scour depth consists of 3 scour depth components:

- Scour component for the pier stem in the flow
- Scour component for the pier cap
- Scour component for the piles of pier exposed to the flow

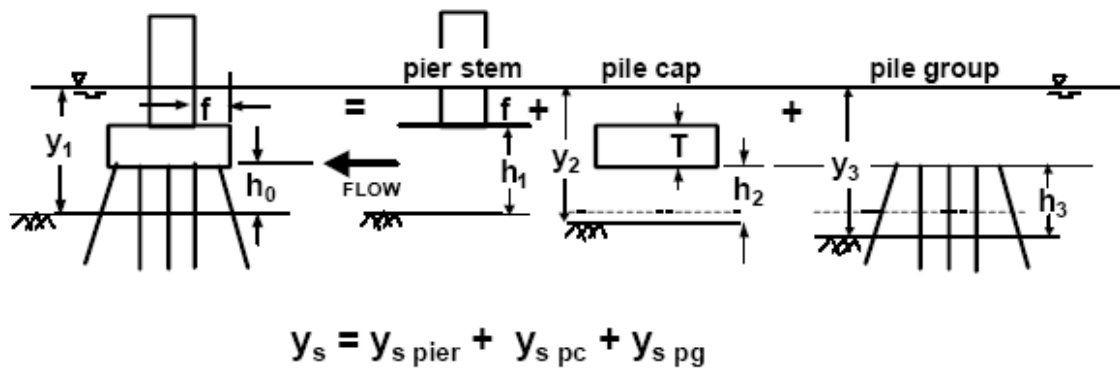


Figure 9.27: Definition Sketch for Scour Components for a Complex Pier Case (Richardson and Davis, 2001)

Where f is the distance between the front edge of the pile cap or footing and the pier, m (ft), h_0 is the height of the pile cap above the bed at the beginning of computation, m (ft), $h_1 = h_0 + T$ is the height of the pier stem above the bed before scour, m (ft), $h_2 = h_0 + y_{s \text{ pier}}/2$ is the height of the pile cap after the pier stem scour component has been computed, m (ft), $h_3 = h_0 + y_{s \text{ pier}}/2 + y_{s \text{ pc}}/2$ is the height of the pile group after the pier stem and pile cap scour components have been computed, m (ft), S is the spacing between the columns of piles, pile center to pile center, m (ft), T is the thickness of the

pile cap or footing, m (ft), y_1 is the approach flow depth at the beginning of computations, m (ft), $y_2 = y_1 + y_{\text{spier}}/2$ is the adjusted flow depth for pile cap computations m (ft), $y_3 = y_1 + y_{\text{spier}}/2 + y_{\text{spc}}/2$ is the adjusted flow depth for pile group computations, m (ft), V_1 is the approach velocity used at the beginning of computations, m/sec (ft/sec), $V_2 = V_1(y_1/y_2)$ is the adjusted velocity for pile cap computations, m/sec (ft/sec), $V_3 = V_1(y_1/y_3)$ is the adjusted velocity for pile group computations, m/sec (ft/sec). y_{spier} is the scour component for the pier stem in the flow, m (ft), y_{spc} is the scour component for the pier cap or footing in the flow, m (ft), y_{spg} is the scour component for the piles exposed to the flow, m (ft). Each of the scour component from the basic pier equations use the equivalent sized pier to represent the irregular pier components, adjusted flow depths and velocities, and height adjustments for pier stem and pier group. The total scour depth y_s will be the sum of these three components.

The complex pier case in the SRICOS–EFA method is different from the complex pier case described in HEC-18. The SRICOS-EFA method considers pier shape, group piers and flow attack angle as the main parameters in the complex pier case. In this circumstance, some simplifications will be adopted for the Pier 5 and Pier 6 analysis. Three cases will be analyzed on the basis of the different widths of the bascule piers. The most conservative case will be the width of pile cap 8.2 m as the pier width in the scour depth calculation. The second case will be adding the widths of two steel pipe piles together, and the total width (3.05 m) will be considered as the equilibrium pier width. The last case will only consider the diameter of the single pile as the width of the pier. The widths of the franking piers (Pier 4 and Pier 7) are 1.37 m in the calculation.

From the information given by NYSDOT, the flow attack angle for all cases is zero. Due to the lack of information about the relationship between upstream velocity and upstream water depth for the Sloop Channel Bridge, the water depth will be assumed to stay constant for variable velocities. The constant value of the water depth will be 6.7 m, which is the upstream water depth of the 500 year flood in the Sloop Channel provided by the Ayres Report (2000). The constant water depth of 6.7 m will lead to conservative results, because deeper water depth cases will increase the maximum shear stress and maximum scour depth.

The following tables are the calculation results for different pier scour cases. Table 9.10 displays the results from 6 hour floods by using the SRICOS-EFA method. 0.9 m/s is the maximum velocity from the basic daily hydrograph cycle, 1.35 m/s is the velocity of the 100 year flood and 1.72 m/s is the velocity of the 500 year flood. Pier scour analyses for maximum velocity of the normal hydrograph, 100 year flood and 500 year flood, also were performed by using the HEC-18 method. The results are shown in Table 9.11.

Table 9.10: Pier Scour Predictions by SRICOS-EFA
for Short Duration Flood Events in the Sloop Channel Bridge

Pier No.	Pier Width (m)	Flow Velocity (m/s)	Water Depth (m)	Attack Angle (degree)	Flood Period (hours)	τ_{\max} (N/m ²)	Scour Rate (m/hr)	Z _{max} (m)	Z(t) (m)
Pier 5 and Pier 6	8.2	0.9	6.7	0	6	5.6	0.040	3.28	0.23
		1.35	6.7	0	6	11.6	0.716	4.25	2.14
		1.72	6.7	0	6	17.8	3.458	4.95	4.00
	3.05	0.9	6.7	0	6	4.2	0.023	2.21	0.13
		1.35	6.7	0	6	8.8	0.264	2.85	1.02
		1.72	6.7	0	6	13.6	1.293	3.33	2.33
	1.524	0.9	6.7	0	6	4.8	0.030	1.42	0.16
		1.35	6.7	0	6	10.0	0.422	1.84	1.07
		1.72	6.7	0	6	15.5	2.082	2.14	1.83
Pier 4 and Pier 7	1.37	0.9	6.7	0	6	4.9	0.031	1.33	0.16
		1.35	6.7	0	6	10.2	0.454	1.72	1.05
		1.72	6.7	0	6	15.8	2.240	2.01	1.74

Table 9.11: Pier Scour Predictions by HEC-18
for Short Duration Flood Events in the Sloop Channel Bridge

Pier No.	Pier Width (m)	Flow Velocity (m/s)	Water Depth (m)	Attack Angle (degree)	K ₁	K ₂	K ₃	K ₄	Fr	HEC-18 Z _{Max} (m)
Pier 5 and Pier 6	8.2	0.9	6.7	0	1.0	1.0	1.1	1.0	0.11	6.53
		1.35	6.7	0	1.0	1.0	1.1	1.0	0.17	7.78
		1.72	6.7	0	1.0	1.0	1.1	1.0	0.21	8.63
	3.05	0.9	6.7	0	1.0	1.0	1.1	1.0	0.11	3.43
		1.35	6.7	0	1.0	1.0	1.1	1.0	0.17	4.09
		1.72	6.7	0	1.0	1.0	1.1	1.0	0.21	4.54
	1.524	0.9	6.7	0	1.0	1.0	1.1	1.0	0.11	2.19
		1.35	6.7	0	1.0	1.0	1.1	1.0	0.17	2.60
		1.72	6.7	0	1.0	1.0	1.1	1.0	0.21	2.89
Pier 4 and Pier 7	1.37	0.9	6.7	0	1.0	1.0	1.1	1.0	0.11	2.04
		1.35	6.7	0	1.0	1.0	1.1	1.0	0.17	2.43
		1.72	6.7	0	1.0	1.0	1.1	1.0	0.21	2.70

Note

K₁: Correction factor for pier nose shape K₂: Correction factor for angle of attack of flow
 K₃: Correction factor for bed condition K₄: Correction factor for armoring by bed material size
 Fr: Froude Number directly upstream of the pier

The pier scour predictions in the long term hydrographs conditions were also performed by using the SRICOS-EFA method. Two kinds of hydrographs were used: the 75 year normal tide hydrograph and the 75 year normal tide hydrograph, including inserting the 500 year flood at the middle of the hydrograph. Table 9.12 presents the pier scour predictions by SRICOS-EFA method for different hydrographs.

Table 9.12: Pier Scour Predictions by SRICOS-EFA for Different Hydrographs

Pier No.	Pier Width (m)	Flood Period (years)	Hydrograph Type	Z(t) (m)
Bascule Pier Pier 5 Pier 6	8.2	75	Normal Tide	3.28
			Normal tide With 500 flood	4.95
	3.05	75	Normal Tide	2.20
			Normal tide With 500 flood	3.21
	1.524	75	Normal Tide	1.42
			Normal tide With 500 flood	2.14
Pier 4 and Pier 7	1.37	75	Normal Tide	1.33
			Normal tide With 500 flood	2.00

9.3.5 CONTRACTION SCOUR AND COMBINED SCOUR PREDICTIONS

The contraction scour depth will be calculated by means of the SRICOS-EFA method for the Sloop Channel Bridge cases. The flood events in contraction scour and combined scour are the same as the calculations in the pier scour case, so the analyses include short term flood events and long term hydrographs lasting 75 years. The soil erosion functions will be the same as the input for the pier scour cases. The upstream channel width (407 m) and contracted channel width (165 m) of the Sloop Channel are provided by the Ayres report (2000). The transition angle and the length of the

contraction are 73.5° and 33.6 m, measured from the new bridge overview plan given by NYSDOT. The chosen Manning's coefficient was 0.035 as a reasonable value in the absence of other data. The water depth will be kept at a constant value of 6.7 m for the different case. 6.7 m is the upstream water depth of the 500 year flood in the Sloop Channel provided by Ayres Report (2000). This will bring conservative results, since the larger water depth values will lead to a larger maximum shear stress and a larger maximum scour depth in the SRICOS-EFA method. In order to calculate the hydraulic radius, a rectangular channel was assumed to exist at the bridge site. Using the upstream width and water depth, the average hydraulic radius was found to be 6.49 m.

Table 9.13 shows the contraction scour predictions by using the SRICOS-EFA method with 3 constant velocities in the 6 hour flood period. 0.9 m/s is the maximum velocity in the basic daily hydrograph cycle, 1.35 m/s is the velocity of the 100 year flood and 1.72 m/s is the velocity of the 500 year flood. The long term contraction scour predictions from the SRICOS-EFA method are shown in Table 9.14. Two kinds of long term hydrographs used in the contraction scour calculation are the same as those used in the pier scour cases. These two long term hydrographs are: the 75 year normal tide hydrograph and the 75 year normal tide hydrograph, inserting the 500 year flood at the middle of the hydrograph.

The integrated SRICOS-EFA method (introduced in Section 6.2) is used to study the combined scour problem (pier scour + contraction scour) in this case study as well. Two combined scour cases with 1.37m and 8.2 m pier widths are predicted. Table 9.15 shows the results for combined scour cases. Table 9.16 shows the summary of results.

Table 9.13: Contraction Scour Predictions by SRICOS-EFA for Short Duration Flood Events

Upstream Velocity (m/s)	Upstream Width (m)	Contracted Width (m)	Transition Angle (degree)	Contraction Length (m)	Water Depth (m)	Hydraulic Radius (m)	Flood Period (hours)	τ_{max} (N/m ²)	Scour Rate (m/hr)	Z _{max} (m)	Z(t) (m)	
0.9	407	165	73.5	33.6	6.7	6.49	6	21.8	7.21	4.37	3.97	
1.35	407	165	73.5	33.6	6.7	6.49	6	49.1	137.2	6.78	6.77	
1.72	407	165	73.5	33.6	6.7	6.49	6	79.8	L1	798	8.75	8.33
									L2	65.9	8.43	
									L3	316	8.33	

Note:

- L1, L2, L3 represent the layers of soils.
- Thickness and critical shear stress for different soil layers
 Layer 1: 7.20 m, 0.5 N/m²; Layer 2: 0.61 m, 1.5 N/m²
 Layer 3: 2.40 m, 1.9 N/m²; Layer 4: 10 m, 0.19 N/m²

Table 9.14: Contraction Scour Predictions by SRICOS-EFA for Different Hydrographs

Upstream Width (m)	Contracted Width (m)	Contraction Ratio	Transition Angle (degree)	Contraction Length (m)	Hydraulic Radius (m)	Flood Period (years)	Hydrograph Type	Z(t) (m)
407	165	2.47	73.5	33.6	6.49	75	Normal Tide	4.37
							Normal tide With 500 flood	8.32

Table 9.15: Pier Scour + Contraction Scour Predictions (SRICOS-EFA Integrated Method) for Different Hydrographs

Pier Width (m)	Attack Angle (degree)	Upstream Width (m)	Contracted Width (m)	Contraction Ratio	Transition Angle (degree)	Contraction Length (m)	Hydraulic Radius (m)	Flood Period	Hydrograph Type	Z(t) (m)
1.37	0	407	165	2.47	73.5	33.6	6.49	75 years	Normal Tide	5.04
									Normal tide With 500 flood	9.44
								6 hours	500 year flood	9.43
8.2	0	407	165	2.47	73.5	33.6	6.49	75 years	Normal Tide	6.33
									Normal tide with 500 flood	10.92
								6 hours	500 year flood	10.90

Table 9.16: Summary Table of the Sloop Channel Bridge Scour Analysis

Scour Type	Pier Width (m)	500 year Flood 6 Hours (m)	500 year Flood Hydrograph 75 years (m)
Pier Scour	8.2	4.00	4.95
	1.37	1.74	2.00
Contraction Scour	N/A	3.96 (8.33-4.37)	3.96(8.33-4.37)
Pier + Contraction (Superposition)	8.2	7.96 (4.00+3.96)	8.91 (4.95+3.96)
	1.37	5.70 (1.74+3.96)	5.96 (2.00+3.96)
Pier + Contraction (Integrated)	8.2	6.53 (10.90-4.37)	6.55 (10.92-4.37)
	1.37	5.06 (9.43-4.37)	5.07 (9.44-4.37)

9.3.6 RESULT ANALYSIS AND COMPARISON

For pier scour, the soil classification of this layer of soil is clayey silt, which was demonstrated by the EFA test to be very erodible. Even small τ_{\max} has a very high scour rate in the scour process. This characteristic of soil brings out the pier scour predictions of the 75 years normal tide hydrograph and the normal hydrograph with the 500 year flood, which were very close to the maximum pier scour depths calculated with the maximum velocities in the hydrographs. Compared to the results of the normal hydrograph and the normal hydrograph with the 500 year flood, it was found that the large flood has a big impact on the final scour depth in the SRICOS-EFA method. The 500 year flood hydrograph created approximately 50% more pier scour depths than created by the normal hydrograph in the 75 years. Figure 9.28 shows the plotted comparison of pier scour predictions between SRICOS-EFA and HEC-18. Clearly the HEC-18 predictions give the bigger results. They are very similar to the comparisons in the Woodrow Wilson Bridge case. Furthermore a tendency can be observed from Figure 9.28 showing that with increasing the pier widths, the differences between the predictions from these two methods increase as well. The HEC-18 method appears more conservative in the pier scour predictions than the SRICOS-EFA method.

For contraction scour, from the results of the short term flood event (6 hour period), it was found that the contraction scour depths for the larger velocities almost reached to the maximum scour depths in a short time. According to the maximum shear stress equations for pier scour and contraction scour, regardless of geometry, the shear stress in contraction scour generates higher shear stress than in pier scour with the same

velocity, so contraction scour can reach the maximum scour depth faster than pier scour in this case.

Usually the occurrence of contraction scour is due to the embankments imposing a restriction on the width of flowing water. In this case the upstream channel width of 407 m and the contracted width of channel (165 m) provide a significant channel width reduction for contraction scour to take place. The channel restriction has been there from the formation of the channel, so it is reasonable to conclude the contraction scour occurred long ago. The contraction scour was estimated in this site for the 75 year normal tide hydrograph to be up to 4.37 m. According to the occurrence time, this scour can be regarded as long-term contraction scour in the site. In the SRICOS-EFA method, uniform scouring in the entire riverbed is assumed in the calculation. So if the long-term contraction scour occurred, the final scour predictions related to the contraction scour will be deducted by 4.37 m (the long-term contraction scour depth).

In most methods, the way to predict the combined scour of pier and the contraction scour will be: first compute the magnitude of contraction scour, the local scour at piers individually, second add them together for the combined scour. It should be noted, as often stated by engineers, that the results would be conservative. The SRICOS-EFA integrated method considers the time factor, the soil properties, and especially the interactions between contraction scour and pier scour, so that it will not overestimate the scour depths compared to simply adding the different scour components together. The results in the Sloop Channel Bridge scour analysis prove this point. The comparison between the superposition method and the integrated method is shown in

Figure 9.29. Table 9.16 shows the summary of the scour analysis on the new Sloop Channel Bridge, and Figure 9.30 shows the scour profiles in new Sloop Channel Bridge on Wantagh Parkway.

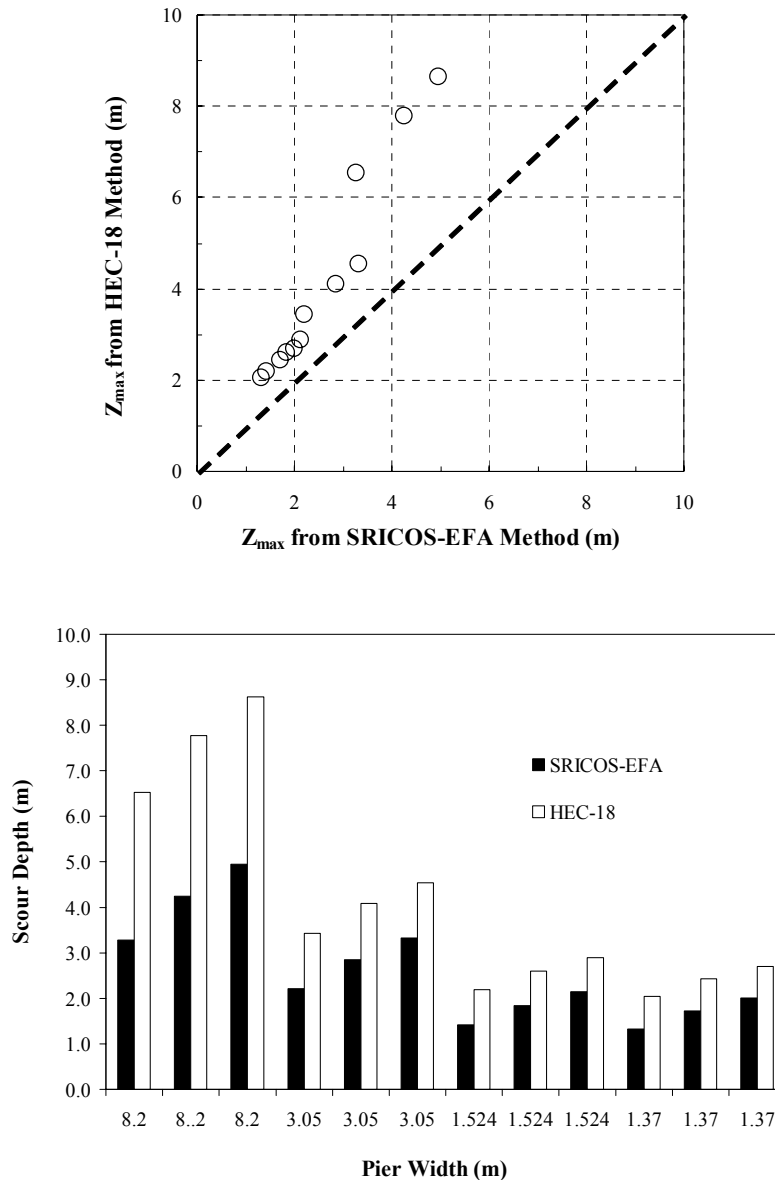


Figure 9.28: Comparison of Pier Scour Predictions between SRICOS-EFA and HEC-18 for the Sloop Channel Bridge Case

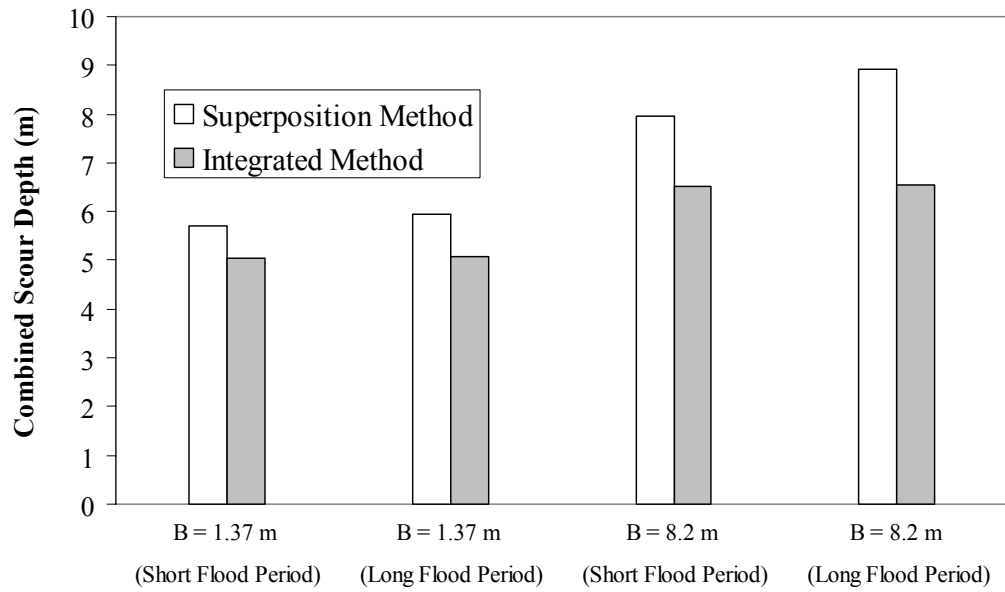


Figure 9.29: Comparison of Combined Scour Depths between the Superposition Method and the Integrated Method in the Sloop Channel Bridge Case

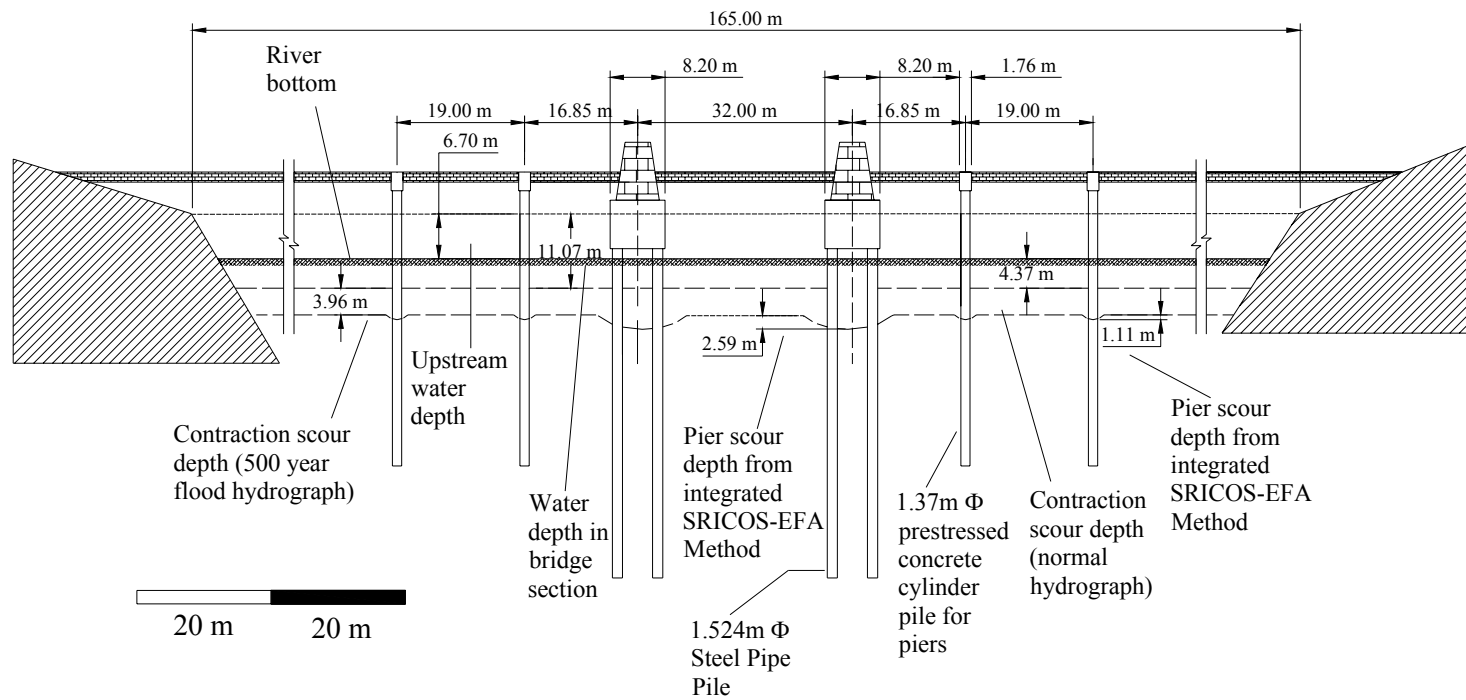


Figure 9.30: Scour Profiles for the New Sloop Channel Bridge on Wantagh Parkway

9.4 VERIFICATION CASE STUDY 3: THE NEW GOOSE CREEK BRIDGE ON GOOSE CREEK ON WANTAGH PARKWAY

9.4.1 INTRODUCTION

Goose Creek Bridge is located on the south shore of New York's Long Island and carries the Wantagh State Parkway over a tidal waterway named Goose Creek. Goose Creek and Sloop Channel are major conduits for tidal currents between South Oyster Bay and the Atlantic Ocean. Goose Creek Bridge connects Long Island to Jones Beach State Park on Jones Island, a major barrier island along the south-central shore of Long Island through Low and Green Islands in the bay. The Wantagh Parkway provides access to the extremely popular beaches and recreation areas of Jones Beach State Park. Goose Creek Bridge is just 0.5 mile north of Sloop Channel Bridge. The location of Goose Creek Bridge is shown in Figure 9.31.

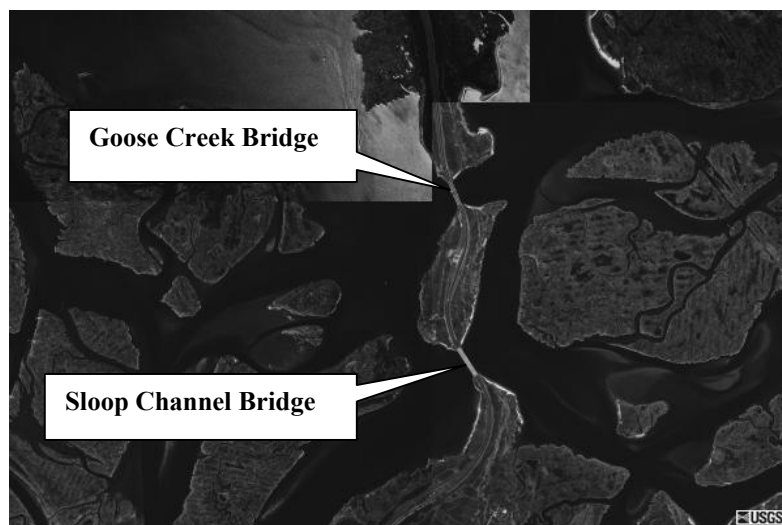


Figure 9.31: Location of the New Goose Creek Bridge on Wantagh Parkway

Inspection of the Goose Creek Bridge in southeastern Nassau County in April 1998 by the New York State Department of Transportation (NYSDOT) indicated a separation of bridge piers from the road bed as a result of pier instability due to apparent seabed scouring by tidal currents. 1.83-meter underwater holes adjacent to two piles supporting the bridge were discovered. Heavy rains during the first three months of 1998 washed sand away from the supports of the bridge, prompting NYSDOT to immediately close the Wantagh Parkway south of Merrick Road. Work crews quickly filled the underwater hole with large stones, while state engineers conducted sand tests and inspected for additional damage to the bridge supports. Soon thereafter, the NYSDOT embarked on a \$75 million project to replace the Goose Creek Bridge by a new bridge. In this research, the scour analysis for the new Goose Creek Bridge will use the SRICOS-EFA method and will be compared to the predictions from HEC-18.

The new Goose Creek Bridge is a bascule bridge 170 m long. Two bascule piers are at the center and there are six adjacent concrete piers in both sides. The bridge span has a closed vertical clearance of 7.3 m above mean high water. When open, this bridge has a 22.9-meter-wide unobstructed horizontal clearance. At the north side of the bridge, from north to south, the piers are numbered from Pier 1N to Pier 3N, and the north bascule pier is called N. Tower. At the south side of the bridge, from south to north, the piers are numbered from Pier 1S to Pier 3S, and the south bascule pier is called S. Tower. The span length between normal piers is approximately 18.3 m. The span between the two bascule piers is approximately 28.3 m. The width and length of the bascule pier caps are 4.21 m and 31.7 m respectively. It is unknown how many piles

under the pier cap of the two bascule piers, but it didn't have much influence on the pier scour calculations, because the piles were totally embedded in soil and the pier cap was partially embedded in soil as well. So the width of the bascule piers in the scour analysis will be the same as the pier cap width. The width and length of Pier 1N, Pier 2N, Pier 1S and Pier 2S are the same, which are 1.37 m and 8.22 m respectively. The width and length of Pier 3N and Pier 3S are the same, which are 1.87 m and 8.22 m respectively. All the normal piers are individually supported by six 1.37-m diameter prestressed concrete cylinder piles. The pile embedment is as deep as 30.5 m below the surface of the river bottom. A cross section view of the new Goose Creek Bridge is shown in Figure 9.32.

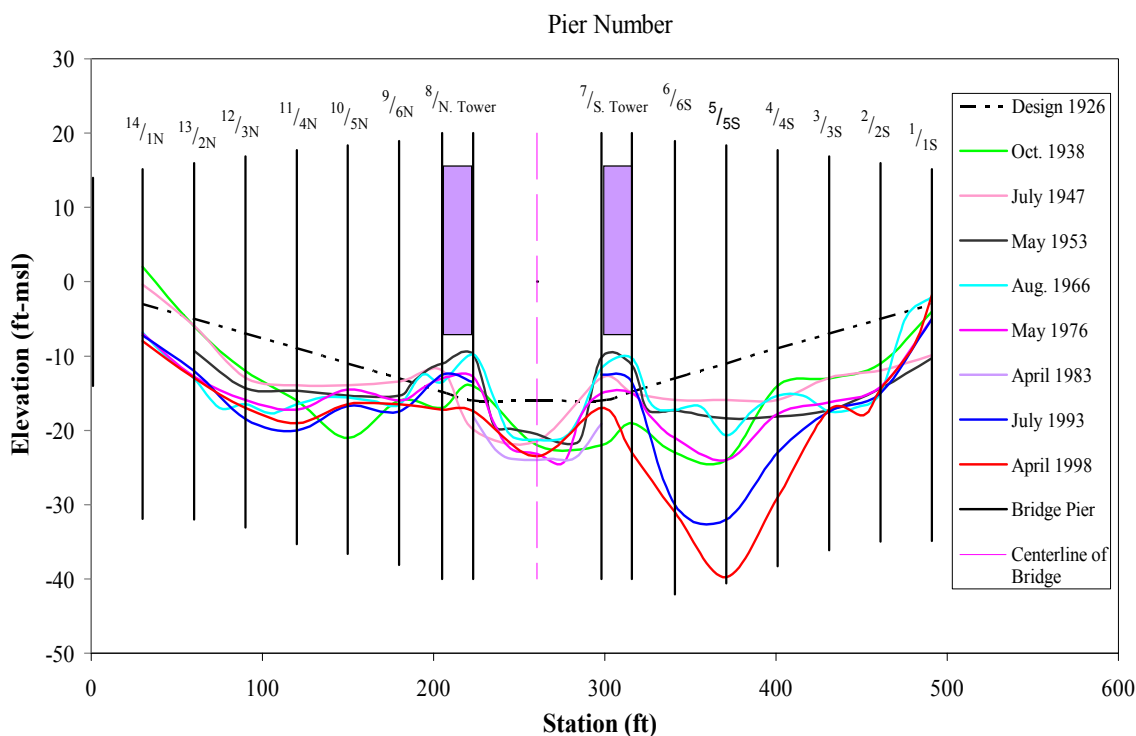


Figure 9.32: Cross Section View of the New Goose Creek Bridge and Historical Streambed Elevations

9.4.2 HYDROLOGIC DATA OF GOOSE CREEK BRIDGE

Ayres Associates conducted a hydraulic analysis of Sloop Channel Bridge and Goose Creek Bridge on Wantagh Parkway in 1998. 100 year and 500 year flood discharges in the approach channel of Goose Creek were calculated in the Ayres Report, which are 1514 m³/s and 1810 m³/s respectively. The main upstream water depths are 5.08 m for a 100 year flood and 5.59 m for a 500 year flood. The water depth in the scour calculations will be a constant value of 5.59 m for a 500 year flood. As discussed in the Sloop Channel Bridge case, the deeper water depth leads to more conservative predictions. The upstream mean velocity values for 100-year and 500-year floods in the Goose Creek Bridge are 0.89 m/s and 0.97 m/s respectively. The Ayres analysis provided the 100 year flood and 500 year flood data for both bridges, but there was no information for the hydrographs at the bridge sites. In the Sloop Channel Bridge case, the velocity hydrograph was established by the velocities measured near the Sloop Channel Bridge by Hardesty & Hanover. Unfortunately, there were no field velocity measurements at the Goose Creek Bridge. In this circumstance, the hydrologic data for the Goose Creek Bridge site was the same as the Sloop Channel Bridge data, except for applying the deduction factor on all the velocity values in the hydrograph, which is the average ratio of the 100 year flood and the 500 year flood between these two bridges. The deduction factor is approximately 0.61. In the Goose Creek Bridge scour analysis, the following three flood events were applied: the short term floods (100 year flood and 500 year flood) lasting 6 hours, normal tidal hydrograph lasting 75 years and normal tidal hydrograph associated with the 500 year flood lasting 75 years. The techniques for

establishing the 500 year flood hydrograph for the Goose Creek Bridge are the same as those adopted in the Sloop Channel Bridge case. The following Figure 9.33 shows one part of the 500 year flood hydrograph at the Goose Creek Bridge.

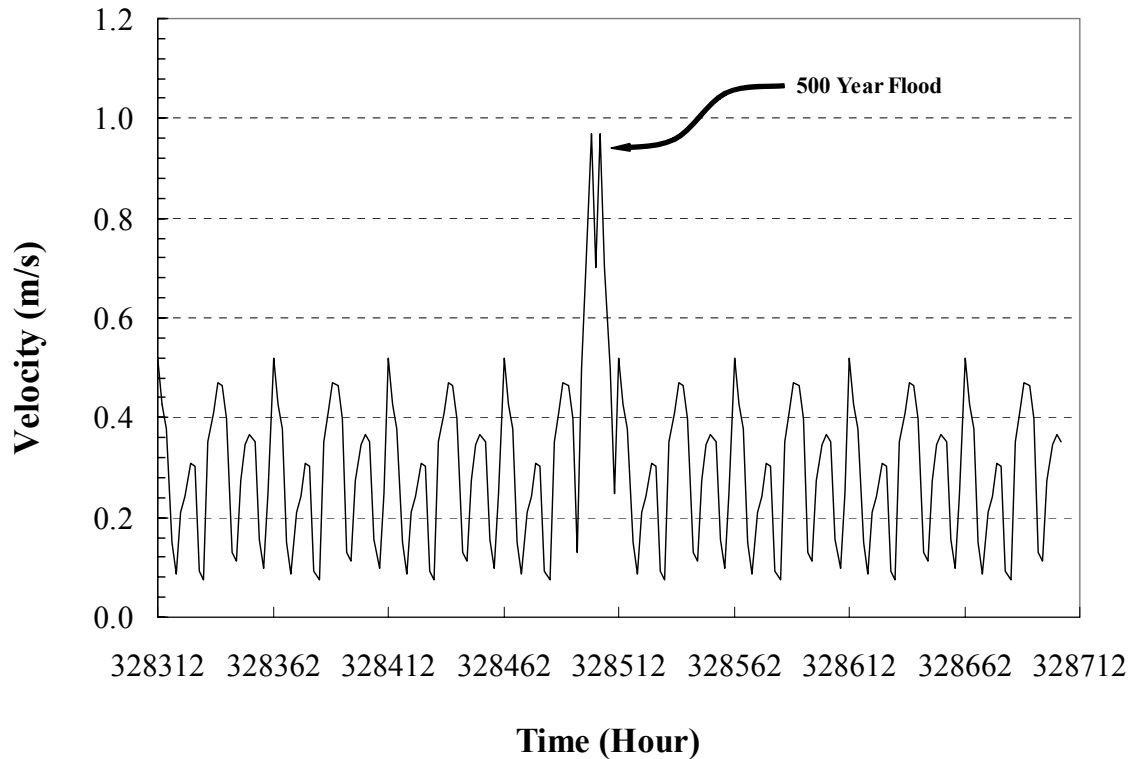


Figure 9.33: One Part of the 500 Year Flood Hydrograph for the Goose Creek on Wantagh Parkway

9.4.3 SOIL DATA FOR THE GOOSE CREEK BRIDGE SITE

For some reason, NYSDOT did not send soil samples to us for EFA testing. In order to do the scour analysis at the Goose Creek Bridge, the distance between the Sloop Channel Bridge and Goose Creek was estimated only about 0.5 mile. So as an

alternative, the EFA soil test results from the Sloop Channel will be used in the Goose Creek case. For information on the EFA test results, please refer to Section 9.3.3 (Figure 9.19 ~ Figure 9.22).

9.4.4 PIER SCOUR PREDICTIONS

Pier scour depths will be calculated for different piers at the new Goose Creek Bridge by using the SRICOS-EFA method. The analysis period will be 6 hours for short term flood and 75 years for multi-flood hydrographs. The velocity for 6 hour short term floods will be constant, being obtained from different flood events. The 75 year velocity hydrographs will include two kinds of hydrograph, one is a normal tidal velocity hydrograph and the other is the 500 year flood associated with the normal tidal velocity hydrograph. The input of the soil erosion function for the SRICOS-EFA Program will be the EFA results of the soil samples in Borehole DN-B-110 at the Sloop Channel Bridge site. Due to the symmetry of the bridge and the river bottom profile, only the piers in one side of the bridge (Pier 1N, Pier 2N, Pier 3N and N. Tower) will be calculated. Table 9.17 shows the geometric information on the piers at the Goose Creek Bridge.

Table 9.17: Information on Piers at the New Goose Creek Bridge

Pier	Shape	Width (m)	Length (m)	Flow Attack Angle
Pier 1N	Round Nose	1.37	8.22	0
Pier 2N	Round Nose	1.37	8.22	0
Pier 3N	Round Nose	1.87	8.22	0
N. Tower	Round Nose	4.21	31.7	0
S. Tower	Round Nose	4.21	31.7	0
Pier 3S	Round Nose	1.87	8.22	0
Pier 2S	Round Nose	1.37	8.22	0
Pier 1S	Round Nose	1.37	8.22	0

The following tables show the calculation results for different pier scour cases. Table 9.18 displays the results from 2 constant velocities for a 6 hour flood period by using the SRICOS-EFA method. 0.89 m/s is the velocity of the 100 year flood and 0.97 m/s is the velocity of the 500 year flood. Pier scour analyses for the 100 year flood and the 500 year flood also used the HEC-18 method. The results are shown in Table 9.19. Table 9.20 shows the pier scour predictions by using the SRICOS-EFA method for the normal tide hydrograph and the normal tide hydrograph with the 500 year flood inserted in the middle of the normal hydrograph.

Table 9.18: Pier Scour Predictions by SRICOS-EFA for Short Duration Flood Events at the Goose Creek Bridge

Pier No.	Pier Width (m)	Flow Velocity (m/s)	Water Depth (m)	Attack Angle (degree)	Flood Period (Days)	τ_{\max} (N/m ²)	Scour Rate (m/hr)	Z _{max} (m)	Z(t) (m)
Pier 1N	1.37	0.89	5.59	0	6	4.79	0.030	1.32	0.16
		0.97	5.59	0	6	5.60	0.051	1.39	0.25
Pier 2N	1.37	0.89	5.59	0	6	4.79	0.030	1.32	0.16
		0.97	5.59	0	6	5.60	0.051	1.39	0.25
Pier 3N	1.87	0.89	5.59	0	6	4.52	0.028	1.61	0.15
		0.97	5.59	0	6	5.29	0.042	1.70	0.22
North Tower	4.21	0.89	5.59	0	6	4.19	0.026	2.52	0.15
		0.97	5.59	0	6	4.89	0.031	2.66	0.18

Table 9.19: Pier Scour Predictions by HEC-18 for Short Duration Flood Events at the Goose Creek Bridge

Pier No. (m)	Pier Width (m)	Flow Velocity (m/s)	Water Depth (m)	Attack Angle (degree)	K ₁	K ₂	K ₃	K ₄	Fr	Z(t) (m)
Pier 1N	1.37	0.89	5.59	0	1	1	1.1	1	0.120	1.98
		0.97	5.59	0	1	1	1.1	1	0.131	2.06
Pier 2N	1.37	0.89	5.59	0	1	1	1.1	1	0.120	1.98
		0.97	5.59	0	1	1	1.1	1	0.131	2.06
Pier 3N	1.87	0.89	5.59	0	1	1	1.1	1	0.120	2.43
		0.97	5.59	0	1	1	1.1	1	0.131	2.52
North Tower	4.21	0.89	5.59	0	1	1	1.1	1	0.120	4.11
		0.97	5.59	0	1	1	1.1	1	0.131	4.27

Note

K₁: Correction factor for pier nose shape
 K₃: Correction factor for bed condition

K₂: Correction factor for angle of attack of flow
 K₄: Correction factor for armoring by bed material size

Fr: Froude Number directly upstream of the pier

Table 9.20: Pier Scour Predictions by SRICOS-EFA for the Normal Hydrograph and the Normal Hydrograph with the 500Year Flood

Pier No.	Pier Width (m)	Flood Period (years)	Hydrograph Type	Z(t) (m)
Pier 1N	1.37	75	Normal Tide	0.91
			Normal tide With 500 year	0.93
Pier 2N	1.37	75	Normal Tide	0.91
			Normal tide With 500 year	0.93
Pier 3N	1.87	75	Normal Tide	1.11
			Normal tide With 500 year	1.13
North Tower	4.21	75	Normal Tide	1.73
			Normal tide With 500 year	1.74

9.4.5 CONTRACTION SCOUR AND COMBINED SCOUR PREDICTIONS

The contraction scour depths will be obtained by the SRICOS-EFA method for the new Goose Creek Bridge case. It is the same as the calculations in the pier scour case, so the analyses include short term flood events lasting 6 hours and long term hydrographs lasting 75 years. The soil erosion functions will be the same as the input for the pier scour cases. The upstream channel width (335 m) and the contracted channel width (145 m) of Goose Creek are provided by the Ayres Report (2000). The transition angle and the length of the contraction are 90° and 25.7 m, measured from the new bridge overview plan given by NYSDOT. Manning's coefficient of 0.035 was chosen as a reasonable value in the absence of other data. The water depth will be kept at a constant value of 5.59 m for different cases. 5.59 m is the upstream water depth of the 500 year flood at Goose Creek provided by the Ayres Report (2000), which will lead to conservative predictions in the SRICOS-EFA method. In order to calculate the hydraulic

radius, a rectangular channel was assumed to exist at the bridge site. Using the upstream width and the water depth, the average hydraulic radius was found to be 5.41 m.

Table 9.21 shows the contraction scour predictions by using the SRICOS-EFA method with 2 constant velocities in the 6 hours flood period. 0.89 m/s is the velocity of the 100 year flood and 0.97 m/s is the velocity of the 500 year flood.

For comparison purposes, the contraction scour analysis calculated by HEC-18 will also be used in this case study. There are two types of contraction scour equations from HEC-18: live-bed equation and clear-water equation. Choosing which equation depends on the competence of the uncontracted approach flow to transport bed material into the contraction. Live-bed scour occurs when there is streambed sediment being transported into the contracted section from upstream. Clear water scour occurs when the bed sediment material transport in the uncontracted approach flow is negligible or the material being transported in the upstream reach is transported through the downstream reach at less than the capacity of the flow. To determine which contraction scour applies in the actual case, calculate the critical velocity for the beginning of motion V_c of the D_{50} size of the bed material being considered for movement and compare it with the mean velocity V of the flow in the main channel or over the bank area upstream of the bridge opening. If the critical velocity of the bed material is larger than the mean velocity ($V_c > V$), then clear-water contraction scour will occur. If the critical velocity is less than the mean velocity ($V_c < V$), then live-bed contraction scour will occur. The following equation is recommended by HEC-18 for V_c calculation.

$$V_c = 6.19y^{\frac{1}{6}}D_{50}^{\frac{1}{3}} \quad (9.1)$$

where V_c is the critical velocity above which bed material of size D and smaller will be transported, m/s (ft/s); y is the average depth of flow upstream of the bridge, m (ft); D_{50} is the size in a mixture of which 50 percent are smaller, m (ft). In this case, V_c was found as 0.50 m/s for D_{50} equal to 0.0002 m (D_{50} provided by NYSDOT). Obviously, the mean flow velocities are larger than V_c , so the scour equation to be used is the live-bed equation of HEC-18 in this case. Table 9.22 shows the predictions obtained from the HEC-18 equation.

The long term contraction scour predictions from the SRICOS-EFA method are shown in Table 9.23. Two kinds of long term hydrographs used in the contraction scour calculation for the SRICOS-EFA method are the same as those used in the pier scour cases. These two long term hydrographs are: 75 years normal tide hydrograph and 75 years normal tide hydrograph inserting the 500 year flood in the middle of the normal hydrograph.

The integrated SRICOS-EFA method (introduced in Section 6.2) is used to calculate the combined scour problem (pier scour + contraction scour) in this case study as well. Three combined scour cases with 1.37 m, 1.87 m and 4.21 m pier widths will be predicted. Table 9.24 shows the results for combined scour cases. Table 9.25 is the summarized table of calculation results.

Table 9.21: Contraction Scour Predictions by SRICOS-EFA for Short Duration Flood Events

Upstream Velocity (m/s)	Upstream Width (m)	Contracted Width (m)	Transition Angle (degree)	Contraction Length (m)	Water Depth (m)	Hydraulic Radius (m)	Flood Period (hours)	τ_{max} (N/m ²)	Scour Rate (m/hr)	Z _{max} (m)	Z(t) (m)
0.89	335	145	90	25.7	5.59	5.41	6	23.34	9.17	3.68	3.45
0.97	335	145	90	25.7	5.59	5.41	6	27.72	17.15	4.05	3.89

Table 9.22: Contraction Scour Predictions by HEC-18 for Short Duration Flood Events

Velocity (m/s)	Upstream Width (m)	Contracted Width (m)	Upstream Discharge (m ³ /s)	Contracted Discharge (m ³ /s)	Upstream Water Depth (m)	Contracted Water Depth (m)	ω Fall Velocity (m/s)	s ₁ Energy slope (m/m)	V* (m/s)	V*/ ω	K ₁	Z _{max} (m)
0.89	335	145	1514	1996	5.08	9.7	0.025	3.63E-05	0.043	1.70	0.64	1.30
0.97	335	145	1810	2639	5.59	10.16	0.025	3.78E-05	0.046	1.82	0.64	3.04

Note:

Contraction scour calculations using live-bed scour equation from HEC-18

V*: shear velocity in the upstream section = $(g s_1)^{1/2}$, m/s

ω : median fall velocity of the bed material based on the D₅₀, m/s

s₁: slope of energy grade line of main channel, m/m

g: acceleration of gravity (9.81 m/s²)

K₁: exponents determined below depending on the

Table 9.23: Contraction Scour Predictions by SRICOS-EFA for Different Hydrographs

Upstream Width (m)	Contracted Width (m)	Contraction Ratio	Transition Angle (degree)	Contraction Length (m)	Hydraulic Radius (m)	Flood Period (years)	Hydrograph Type	Z(t) (m)
335	145	2.31	90	25.7	5.41	75	Normal Tide	1.90
							Normal tide With 500 flood	4.18

Table 9.24: Pier + Contraction Scour Predictions by SRICOS-EFA Integrated Method for Different Hydrographs

Pier Width (m)	Attack Angle (degree)	Upstream Width (m)	Contracted Width (m)	Contraction Ratio	Transition Angle (degree)	Contraction Length (m)	Hydraulic Radius (m)	Flood Period	Hydrograph Type	Z(t) (m)
1.37	0	335	145	2.1	90	25.7	5.41	75 years	Normal Tide	2.54
									Normal tide With 500 flood	4.83
								6 hours	500 year flood	4.89
1.87	0	335	145	2.1	90	25.7	5.41	75	Normal Tide	2.67
									Normal tide with 500 flood	4.98
								6 hours	500 year flood	5.07
4.21	0	335	145	2.1	90	25.7	5.41	75	Normal Tide	3.20
									Normal tide with 500 flood	5.52
								6 hours	500 year flood	5.75

Table 9.25: Summary Table for the Goose Creek Bridge Scour Analysis

Scour Type	Pier Width (m)	500 year Flood 6 Hours (m)	500 year Flood Hydrograph 75 years (m)
Pier Scour	4.21	0.18	1.74
	1.87	0.22	1.13
	1.37	0.25	0.93
Contraction Scour	N/A	1.99 (3.89-1.90)	2.28 (4.18-1.9)
Pier + Contraction (Integrated)	4.21	3.76 (5.75-1.90)	3.62 (5.52-1.90)
	1.87	3.17 (5.07-1.90)	3.08 (4.98-1.90)
	1.37	2.99 (4.89-1.90)	2.93 (4.83-1.90)

9.4.6 RESULTS ANALYSIS AND COMPARISON

For pier scour, the result shows a similar tendency found in the Sloop Channel Bridge case. The HEC-18 predictions give the bigger results. Figure 9.34 shows the plotted comparison of pier scour predictions between SRICOS-EFA and HEC-18 and shows that with increasing pier widths, the differences between the predictions from these two methods increase as well. The HEC-18 method appears more conservative in the pier scour predictions than the SRICOS-EFA method.

For contraction scour, Briaud et al. (2002) used the Gill (1981) contraction scour database, compared the SRICOS-EFA and HEC-18 methods, and found that SRICOS-EFA matched the measured depths quite well, while HEC-18 severely underestimated the contraction scour depths. This case has the same observations as their finding. The predictions from SRICOS-EFA and HEC-18 have a contrary tendency compared to the pier scour predictions. The SRICOS-EFA method gives larger Z_{\max} predictions than the predictions of Z_{\max} from HEC-18. Figure 9.35 shows a plotted comparison in pier scour between SRICOS-EFA and HEC-18 predictions in contraction scour cases.

As it was discussed in the Sloop Channel case, the restriction for contraction scour occurrences in Goose Creek has been there from the formation of the channel, so it is reasonable to conclude that contraction scour occurred a long time ago. The contraction scour was estimated at this site for the 75 year normal tide hydrograph as up to 1.90 m. According to the occurrence time, this scour can be regard as a long-term contraction scour at the site. In the SRICOS-EFA method, uniform scouring in the entire riverbed is assumed in the calculation, so if long-term contraction scour occurred, the

final scour predictions related to the contraction scour will be deducted by 1.90 m (the long-term contraction scour depth). Table 9.25 shows the summary of the scour analysis in the Goose Creek Bridge case.

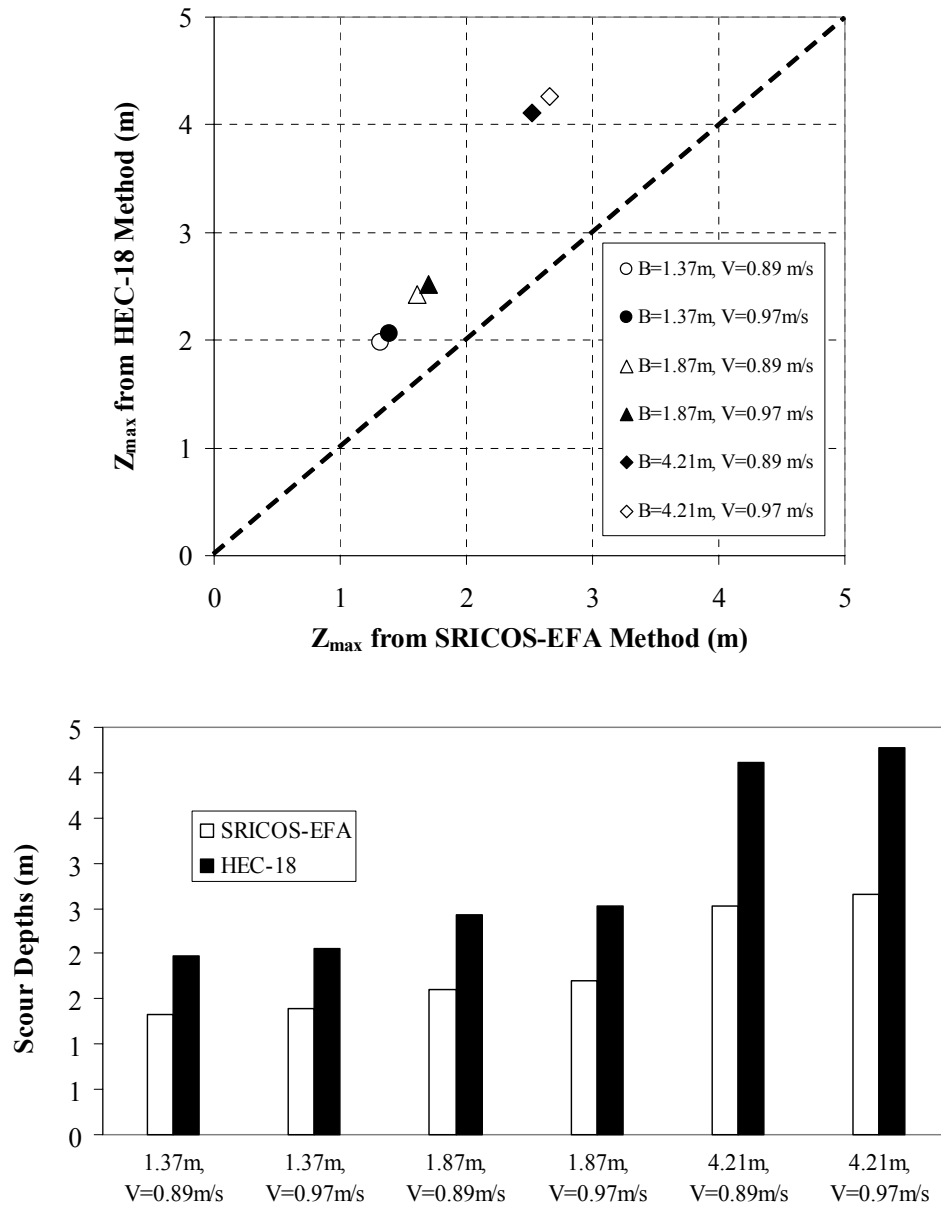


Figure 9.34: Comparison of Pier Scour Predictions between SRICOS-EFA and HEC-18 in the Goose Creek Bridge Case

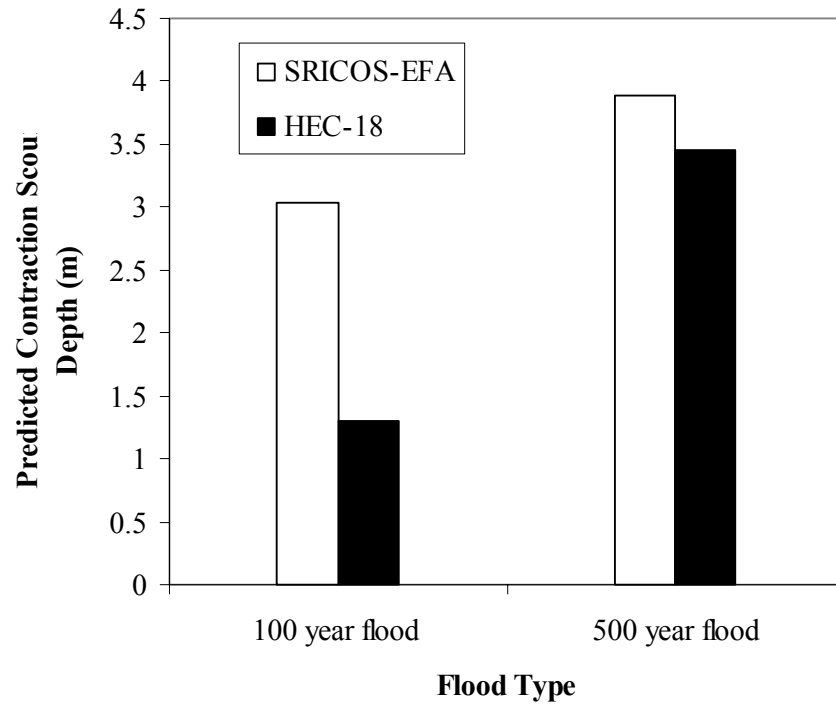


Figure 9.35: Comparison of Contraction Scour Predictions between SRICOS-EFA and HEC-18 in the Goose Creek Bridge Case

9.5 VERIFICATION CASE STUDY 4: CONTRACTION SCOUR STUDY AT THE INDIAN RIVER BRIDGE ON INDIAN BAY, DELAWARE

9.5.1 INTRODUCTION

The Indian River Inlet is part of the Delaware Seashore State Park system, an area that comprises over six miles of ocean and bay line. The inlet was constructed in 1939 by the federal government to stabilize the area. It consists of two areas: the North side and the South side. There are campgrounds in both areas and campers can walk a short distance from their campsite to the inlet fishing area. The Indian River Bridge, located on Indian River Inlet, links the towns of Lewes and Rehoboth Beach on the north side of the inlet with the towns of Bethany Beach, South Bethany and Fenwick Island to the south. The current Indian River Inlet Bridge on SR 1 provides a critical link on the Eastern seaboard between Bethany Beach and Dewey Beach, Sussex County, Delaware, and the bridge currently accommodates 16,000 to 18,000 vehicles daily. Since the 1970s, strong currents in the man-made inlet that links the inland bays to the Atlantic Ocean have gouged deep holes in the channel. Due to severe tidal conditions experienced in the area, the bridge is scheduled for replacement with a new structure that will have a main span of approximately 1,000 feet. This longer main span will allow the bridge to cross the inlet without any piers in the water and provides for a potential future widening of the inlet. Figure 9.36 shows an overview of the Indian River Inlet. A simplified overview of Indian River Inlet is shown in Figure 9.37. Details of the geometric data of the channel and a scour survey contour (Figure 9.38) are provided by the Delaware Department of Transportation (DLDOT).



Figure 9.36: Aerial Photo of Indian Inlet

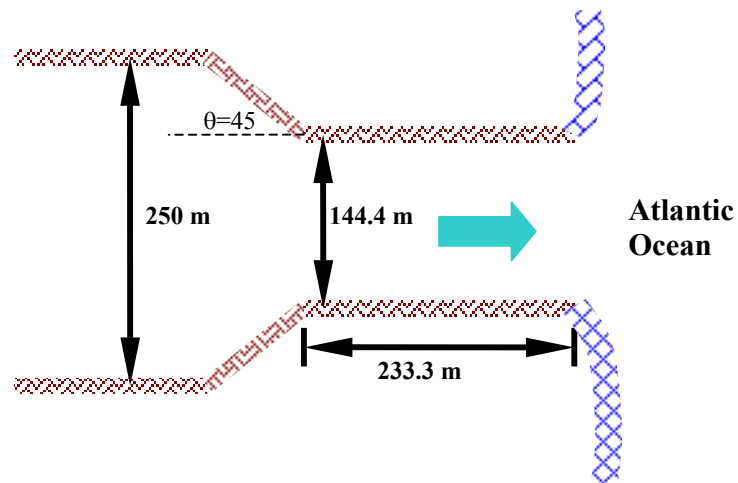


Figure 9.37: Overview of Indian River Inlet

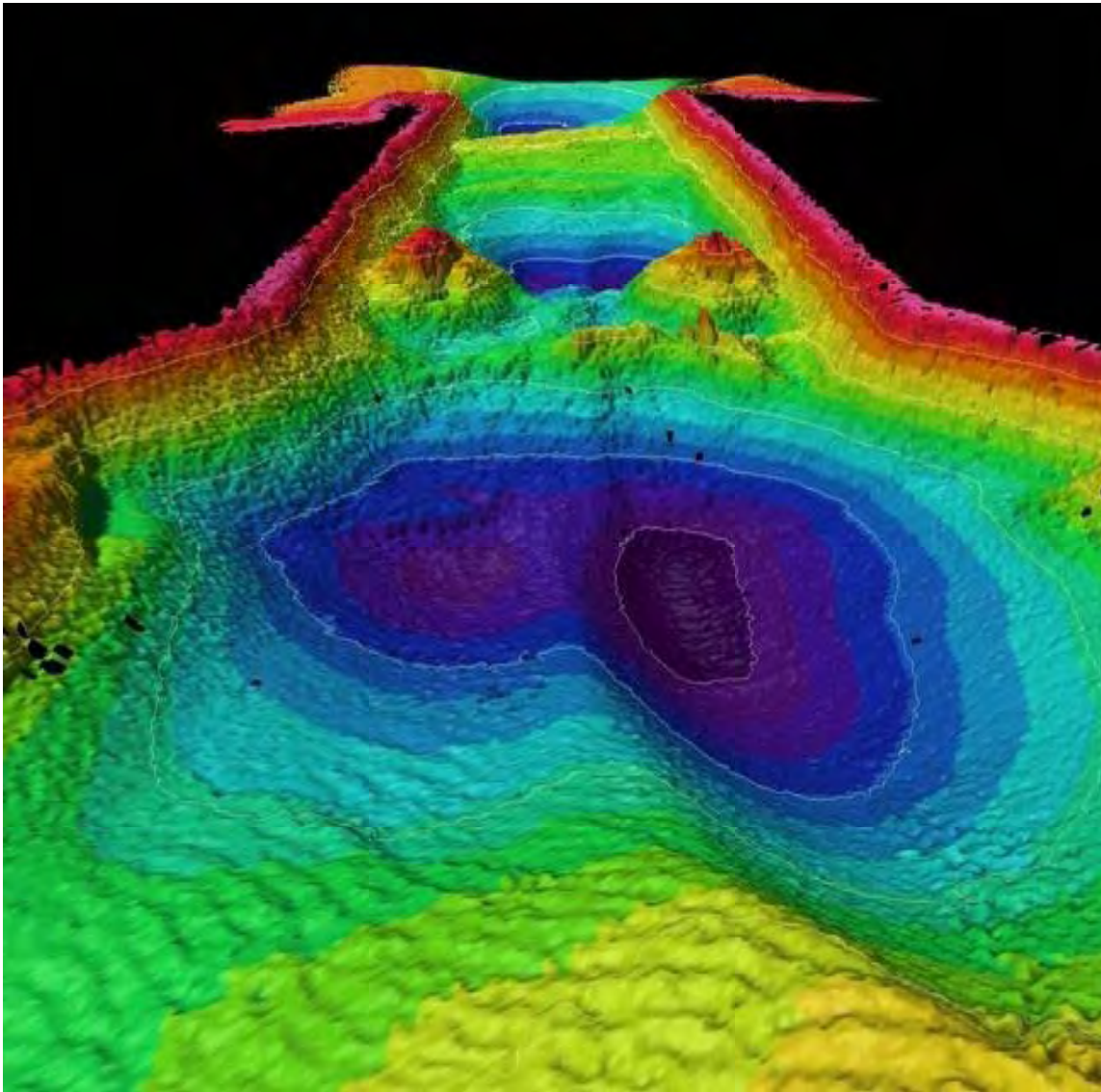


Figure 9.38: River Bottom Profile from Indian River Bay, Looking from East

9.5.2 HYDROGRAPH DATA OF THE INDIAN RIVER CHANNEL

The nearest gaging station to the Indian River Inlet was found at the USGS website, which is numbered as 01484525. The gaging station is located at latitude $38^{\circ}35'40.4''$, longitude $75^{\circ}17'27.7''$, and about 3m upstream from the bridge on State Highway 24, at Millsboro, Sussex County, Delaware. The location of this gaging station is shown in Figure 9.39.

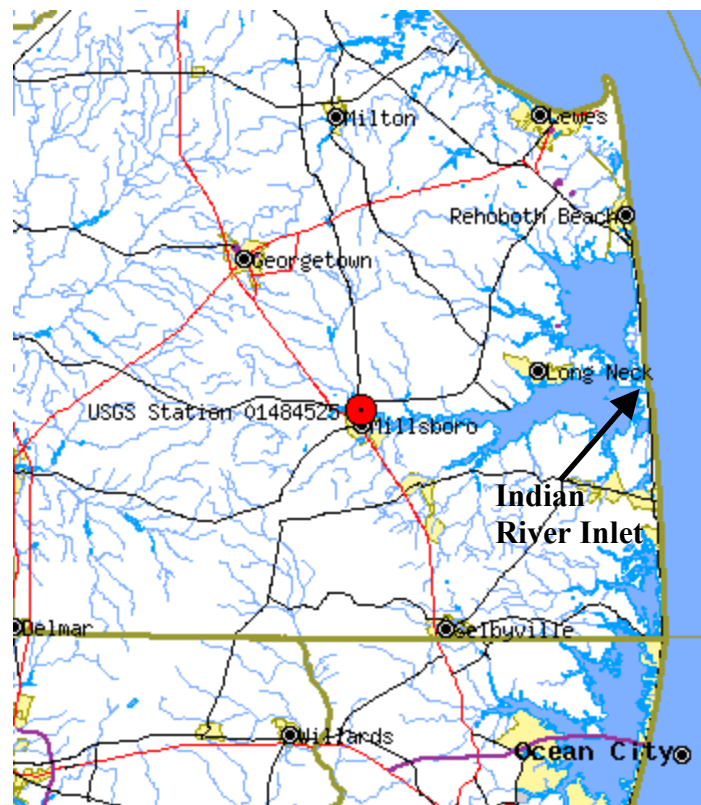


Figure 9.39: Location of USGS Gaging Station 01484525

The discharge hydrograph at the gaging station was downloaded from the USGS website. The record shows that the gaging station was not in operation from 09/31/1988 to 03/15/1991, so that the hydrograph data is missing for this period. The downloaded hydrograph is shown in the Figure 9.40 (discarding the period of missed data):

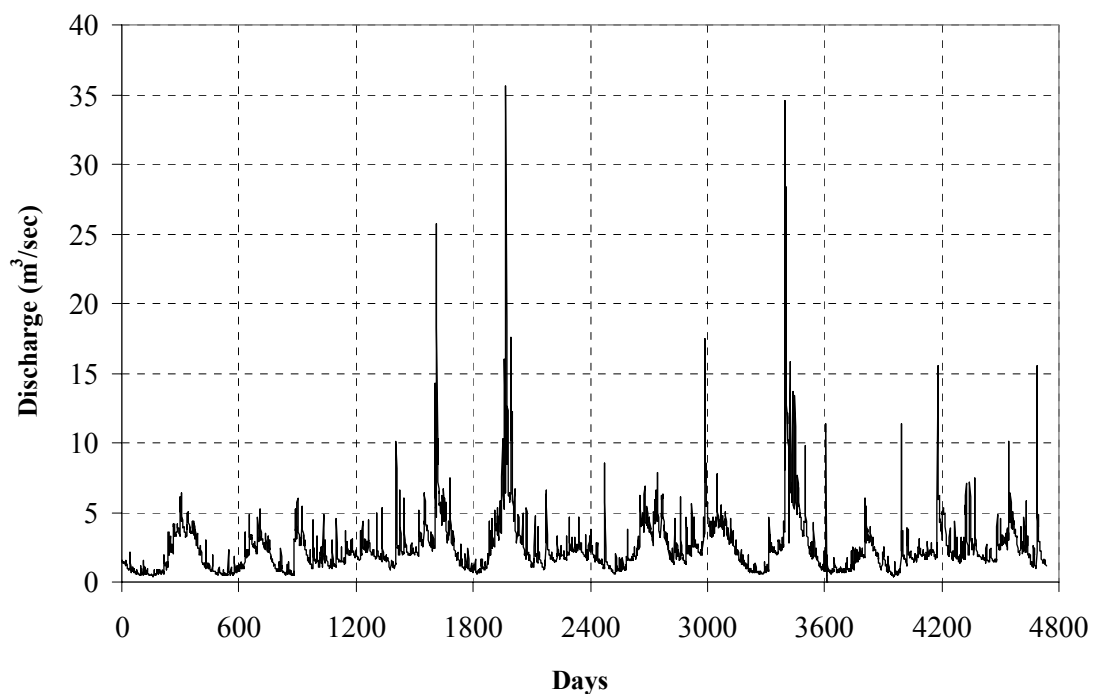


Figure 9.40: Downloaded Hydrograph from Gaging Station 0148425

Since the distance between Gaging Station 01484525 and the Indian River Inlet is approximately 20 km, the hydrograph recorded from the gaging station is not the same as the hydrograph for the location of Indian River Inlet. Hence, it is necessary to find a way to predict the hydrograph at Indian River Inlet based on the existing data from the

gaging station. One piece of important information is the water depth for the 100 year flood in the Indian River Inlet, which is 20 m, obtained from the Delaware Department of Transportation. In this research, HEC-RAS, which was developed by The United States Army Corps of Engineers, was used for flood analysis to obtain the relationship between the hydrologic parameters for Indian River Inlet. For details on the program, please refer to Section 5.3.4. The necessary input from HEC-RAS is Manning's coefficient and the average slope of the streambed. In this case, Manning's coefficient 0.035 was chosen based on Manning's coefficient Table from Young et al. (1997). The average slope of streambed 0.001 was calculated based on the topographic map of Sussex County in Delaware. In the calculation, due to a lack of detailed information about the cross section of the inlet, the Indian River was assumed to be a rectangular channel. Doing trial and error calculation in HEC-RAS, it was found that the discharge is $14460\text{m}^3/\text{s}$ when the water depth is 20 m. So the discharge value of the 100 year flood in Indian River Inlet is $14460\text{m}^3/\text{s}$. Once we know the discharge value of the 100 year flood $Q_{100\text{inlet}}$ in the inlet, and if the discharge of the 100 year flood $Q_{100\text{gaging}}$ in the gaging station can be calculated as well, then the hydrograph for the inlet can be calculated by multiplying the ratio of $\frac{Q_{100\text{inlet}}}{Q_{100\text{gaging}}}$ on the downloaded hydrograph for the gaging station. The following steps (Flood Frequency Analysis) were implanted to find the value of $Q_{100\text{gaging}}$.

1. Find the maximum discharge data for each year in the hydrograph.

2. Rank the maximum discharge data from the largest to the smallest values. If two or more observations have the same value, assume that they have slightly different values and assign each a different rank. Do not omit any years during the period of record since it will have a biasing effect. The data can be excluded when the cause of the data interruption is known to be independent of the flow condition.
3. Calculate the plotting position from the following equation.

$$P_m = \frac{m}{n+1}(100) \quad (9.2)$$

Where, n: the number of peak discharge data; m: discharge ranking

4. Plot the flood magnitude on the ordinate and the corresponding plotting position on the abscissa, representing the probability of exceedence as one side of the scale and the return period on the other side.

Figure 9.41 shows the flood-frequency curve for USGS Gaging Station 01484525.

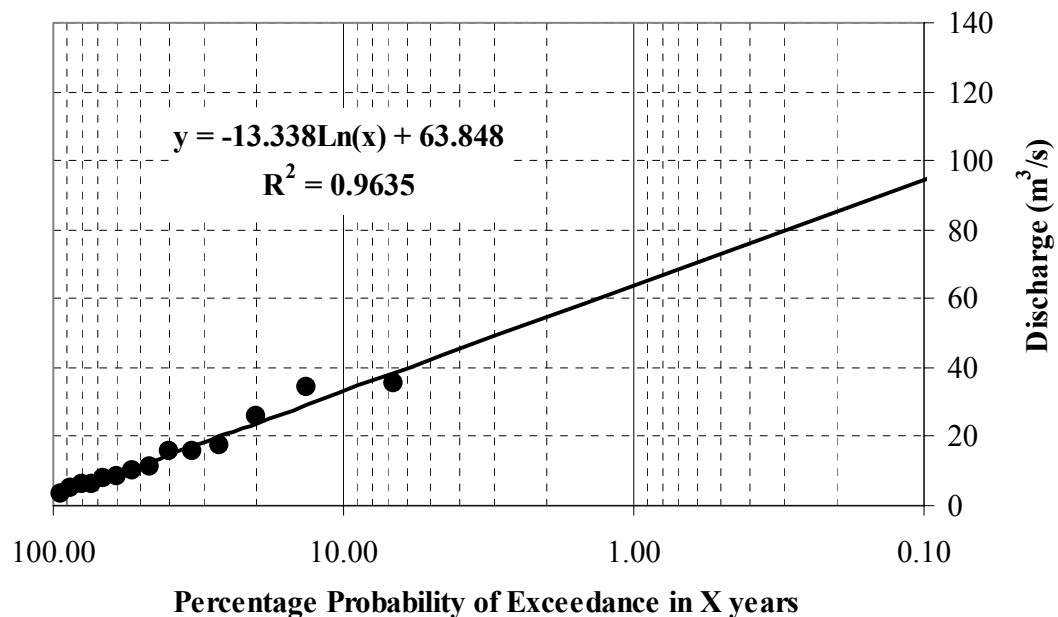


Figure 9.41: Flood-frequency Curve of USGS Gaging Station 01484525

Before trying to find the 100-year (Q_{100}) and the 500-year flood (Q_{500}), it is necessary to define these terms first. Q_{100} and 500-year flood Q_{500} are probabilistic assessments. Q_{100} means a given event has a one-in-one hundred chance (1 percent) of occurrence in any given year. Q_{500} means a given event has a one-in-five hundred chance (0.2 percent) of occurrence in any given year. Such assessments are based on the statistical frequency of collected data. The term "100-year flood" is misleading because it leads people to believe that it happens only once every 100 years. The truth is that an unusually big flood can happen any year. The term "100-year flood" is actually a statistical designation, and there is a 1-in-100 chance that a flood this size will happen during any year. Perhaps a better term would be the "1-in-100 chance flood." (USGS, 1996)

From Figure 9.41, Q_{100} can be read on a curve corresponding to 1% in the X axis or using the regression equation. Q_{100} is found as $63.85 \text{ m}^3/\text{s}$ and Q_{500} is found as $85.31 \text{ m}^3/\text{s}$. So the ratio of the discharges between the gaging station and the inlet is:

$$R_Q = \frac{Q_{100\text{inlet}}}{Q_{100\text{gaging}}} = 226.47.$$

The $Q_{500\text{inlet}}$ can be calculated by the 500-year flood in the gaging station and R_Q , which is equal to $19321 \text{ m}^3/\text{s}$. The discharge hydrograph at the inlet was the values downloaded from the USGS website multiplied by the discharge ratio 226.47, which is shown in Figure 9.42.

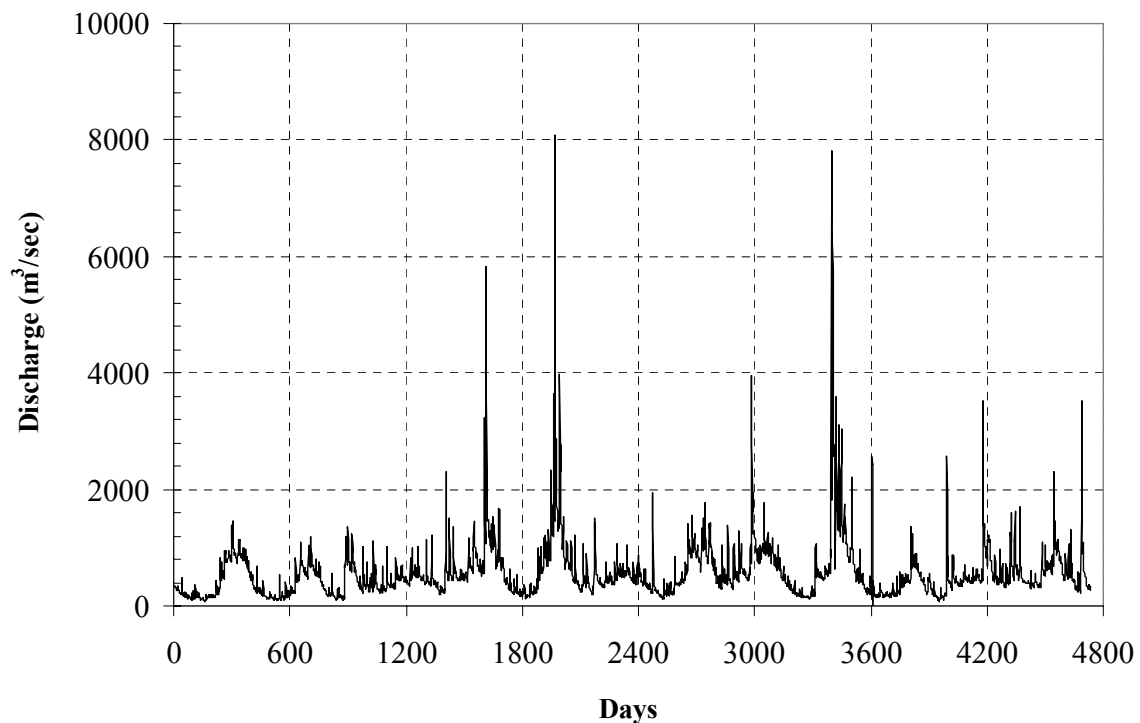


Figure 9.42: Discharge Hydrograph at Indian River Inlet

The calculation results of HEC-RAS also provide the relationship between discharge vs. upstream velocity and discharge vs. upstream water depth of Indian River Inlet. The following Figure 9.43 shows the relationship between the discharge vs. upstream velocity and the discharge vs. upstream water depth of the Indian River Inlet, which are calculated from HEC-RAS.

The velocity and water depth in the upstream channel corresponding to the 100-year flood are 2.89 m/s and 20 m. The velocity and water depth in the upstream channel corresponding to the 500-year flood are 3.23 m/s and 23.54 m. Manning's coefficient in the calculation was 0.035, which was recommended by Young et al. (1997).

9.5.3 SOIL DATA FROM THE INDIAN RIVER INLET SITE

Due to a budget deficit, it is not possible to obtain soil samples from the bridge site. As an alternative, only maximum contraction scour depth will be calculated by the SRICOS-EFA method. The maximum contraction scour depth equations require the critical shear stress of the soils. There were no EFA tests performed for this case study, however, the critical shear stresses will be assumed from 0.5 N/m² to 3 N/m² in the calculation. Using the Moody Chart (Moody, 1944), we found that the critical velocities corresponding to 0.1 N/m² and 32 N/m² are 0.16 m/s and 4.35 m/s respectively. According to the EFA results, which were previously done at Texas A&M University, the range of assumptions is reasonable.

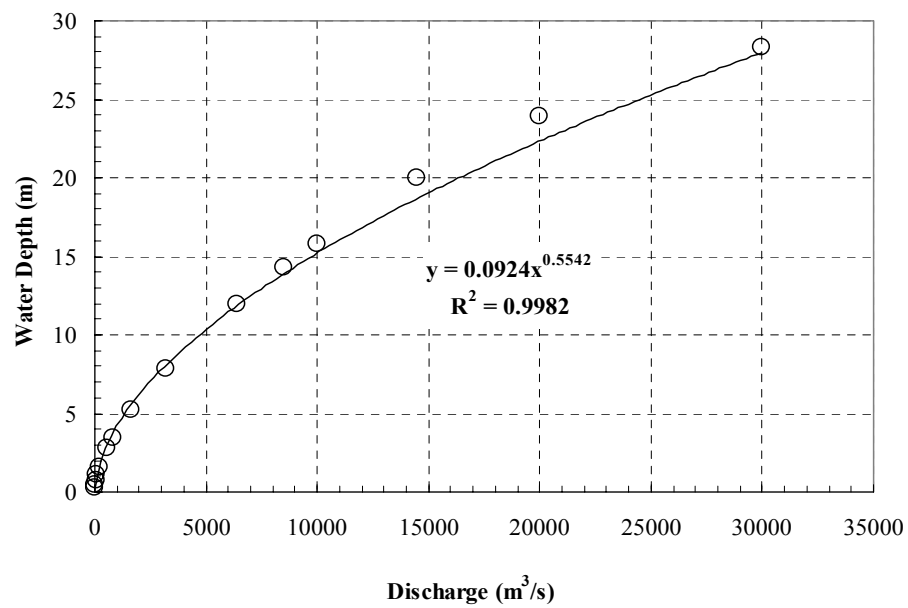
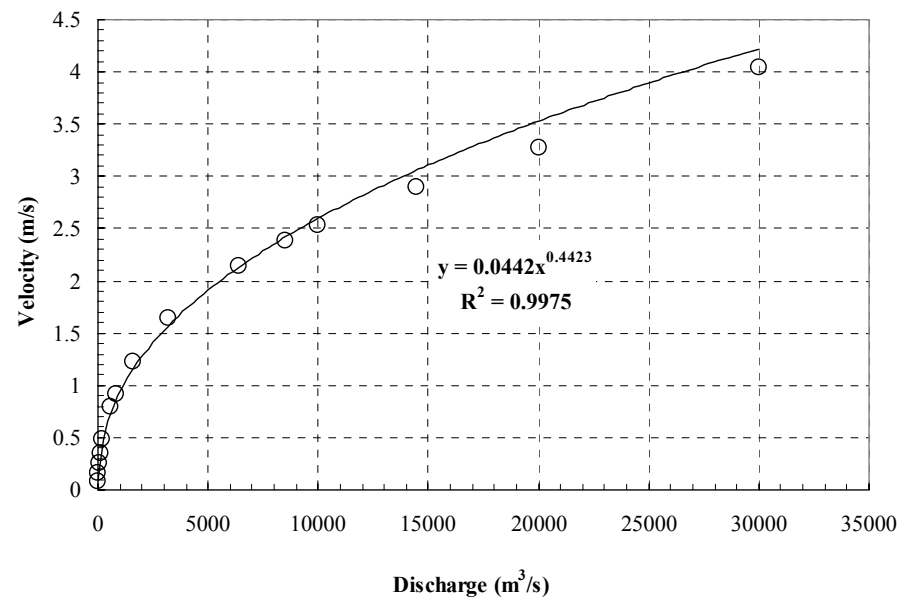


Figure 9.43: Relationships between the Discharge vs. Upstream Velocity and Discharge vs. Upstream Water Depth of Indian River Inlet

9.5.4 CONTRACTION SCOUR PREDICTIONS

The maximum contraction scour depths will be calculated for the Indian River Inlet by using the SRICOS-EFA method. The hydrograph events will be the 100-year flood and the 500-year flood. The maximum contraction scour and the uniform contraction scour will be calculated by using the Equation 9.3 and 9.4.

$$Z_{\max}(Cont) = K_{\theta}K_L \times 1.90 \left(\frac{1.38 \left(V_1 \frac{B_1}{B_2} \right)}{\sqrt{gH_1}} - \frac{\left(\frac{\tau_c}{\rho} \right)^{0.5}}{gnH_1^{1/3}} \right) H_1 \geq 0 \quad (9.3)$$

$$Z_{unif}(Cont) = K_{\theta}K_L \times 1.41 \left(\frac{1.31 \left(V_1 \frac{B_1}{B_2} \right)}{\sqrt{gH_1}} - \frac{\left(\frac{\tau_c}{\rho} \right)^{0.5}}{gnH_1^{1/3}} \right) H_1 \geq 0 \quad (9.4)$$

Table 9.26 shows the results of maximum contraction depths from SRICOS-EFA method for different critical shear stress τ_c .

Table 9.26: Maximum and Uniform Contraction Scour Depths for 100 Year and 500 Year Floods in the Indian Inlet Case

Flood Type	V_1 (m/s)	H_1 (m)	n ($s/m^{1/3}$)	τ_c (N/m^2)	Z_{max} (Cont) (m)	Z_{max} (Unif) (m)
100 year flood	2.89	20	0.035	0.1	18.72	13.19
				0.5	18.70	13.17
				1	18.69	13.17
				2	18.67	13.15
				4	18.65	13.14
				8	18.62	13.11
				16	18.57	13.07
				32	18.50	13.02
500 year flood	3.23	23.54	0.035	0.1	22.70	15.99
				0.5	22.68	15.98
				1	22.67	15.97
				2	22.65	15.95
				4	22.62	15.93
				8	22.58	15.91
				16	22.53	15.87
				32	22.46	15.81

Note

V_1 : Mean depth velocity in Upstream Channel

H_1 : Water Depth in Upstream Channel

n : Manning's Coefficient

τ_c : Critical shear stress of soil

Z_{max} (Cont): Maximum contraction scour depth

Z_{max} (Unif): Maximum uniform scour depth

9.5.5 RESULTS ANALYSIS AND COMPARISON

It is not possible to calculate the contraction scour depth development vs. time by the SRICOS-EFA method because there is no information on soil erosion properties. However, the maximum contraction scour depth results were calculated to find out the influence of the critical shear stress τ_c on the contraction scour depth in the SRICOS-EFA method. The critical shear stresses were from 0.1 N/m² to 32 N/m². The result of the analysis based on the different τ_c is presented in the following Figure 9.44.

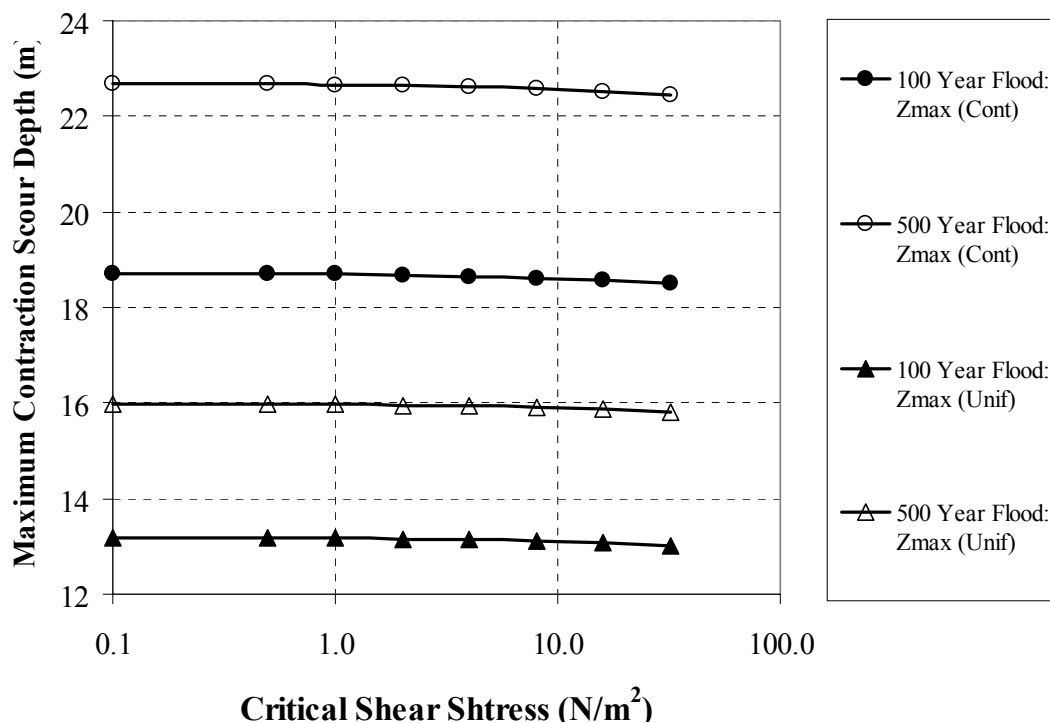


Figure 9.44: Maximum Contraction Scour Depths for Different Critical Shear Stresses

Figure 9.44 shows that the maximum contraction scour depths change only slightly with the changing of critical shear stresses τ_c , even though the τ_c was changed

from 0.1 N/m^2 to 32 N/m^2 . This result leads to the conclusion that critical shear stress has little influence on the final contraction scour depths for both maximum contraction scour and uniform contraction scour in big flood events.

9.6 VERIFICATION CASE STUDY 5: REEVALUATION OF PIER SCOUR FOR 6 SELECTED BRIDGES IN TEXAS

9.6.1 INTRODUCTION

Kwak (2000) evaluated 6 bridges in Texas for the verification of pier scour in deep water cases. Since then the methodology of scour research at Texas A&M University has advanced, therefore it is necessary to reevaluate the bridge cases by applying new equations for the complex pier case. The 6 selected bridges all satisfy the following requirements for verification purposes: the predominant soil type was fine-grained soils according to existing borings; the river bottom profiles were measured on two dates, separated by at least several years; these river bottom profiles indicated anywhere from 0.05m to 4.57m of scour; a USGS gaging station existed near the bridge; and drilling access was relatively easy. The locations of these 6 bridges are shown in the following Figure 9.45.

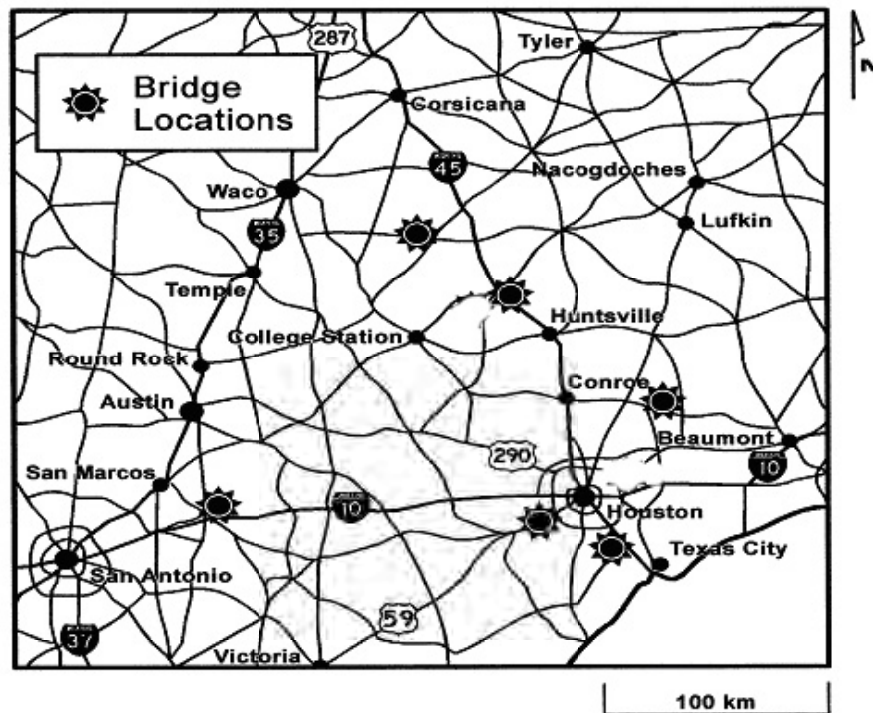


Figure 9.45: Location of Case History Bridges

These 6 selected bridges are briefly introduced as follows:

- **The Navasota River Bridge at SH7** was built in 1956. The main channel bridge has an overall length of 82.8m and consists of 3 continuous steel girder main spans with 4 concrete pan girder approach spans. The foundation type is steel piling down to 5.5m below the channel surface, which consists of silty and sandy clay down to the bottom of the piling, according to data from existing borings. Between 1956 and 1996 the peak flood took place in 1992 and generated a measured flow of $1600 \text{ m}^3/\text{s}$, which corresponds to a HEC-RAS calculated mean approach flow velocity of 3.9 m/s at bent 5 and 2.6 m/s at bent 3. The pier at bent 3 was square with a side of 0.36m, while the pier at bent 5 was 0.36m wide, 8.53m long and had a square nose. The angle between the

flow direction and the pier main axis was 5° for bent 5. River bottom profiles exist for 1956 and 1996 and show 0.76m of pier scour at bent 3 and 1.8m of total scour at bent 5. At bent 5 the total scour consisted of 1.41m of pier scour and 0.39m of contraction scour as explained later.

- **The Brazos River Bridge at US 90A** was built in 1965. The bridge has an overall length of 287m and consists of 3 continuous steel girder main spans with 8 prestressed concrete approach spans. The foundation type is concrete piling penetrating 9.1m below the channel bed surface, which consists of sandy clay, clayey sand, and sand down to the bottom of the piling, according to data from existing borings. Between 1965 and 1998 the peak flood occurred in 1966 and generated a measured flow of $2600 m^3/s$, which corresponds to a HEC-RAS calculated mean approach velocity of 4.2 m/s at bent 3. The pier at bent 3 was 0.91m wide, 8.53m long and had a round nose. The pier was in line with the flow. River bottom profiles exist for 1965 and 1997 and show 4.43m of total scour at bent 3 made up of 2.87m of pier scour and 1.56m of combined contraction and general scour as explained later.

- **The Trinity River Bridge at FM 787** was built in 1976. The bridge has three main spans and three approach spans with an overall length of 165.2m. The foundation type is timber piling and the soil is sandy clay to clayey sand. Between 1976 and 1993 the peak flood took place in 1990 and generated a measured flow of $2950 m^3/s$, which corresponds to a HEC-RAS calculated mean approach flow velocity of 2.0 m/s at bent 3 and 4.05 m/s at bent 4. The piers at bent 3 and 4 were 0.91m wide, 7.3m long, and had a round nose. The angle between the flow direction and the pier main axis was 25°. River

bottom profiles exist for 1976 and for 1992 and show 4.57m of total scour at both bent 3 and 4 made up of 2.17m of pier scour and 2.40m of contraction and general scour as explained later.

- **The San Marcos River Bridge at SH80** was built in 1939. This 176.2m long bridge has 11 prestressed concrete spans. The soil tested from the site is low plasticity clay. Between 1939 and 1998 the peak flood occurred in 1992 and generated a measured flow of $1000 \text{ m}^3/\text{s}$, which corresponds to a HEC-RAS calculated mean approach flow velocity of 1.9 m/s at bent 9. The pier at bent 9 is 0.91m wide, 14.2m long and has a round nose. The pier is in line with the flow. River bottom profiles exist for 1939 and 1998 and show 2.66m of total scour at bent 9 made up of 1.27m of pier scour and 1.39m of contraction and general scour as explained later.

- **The Sims Bayou Bridge at SH35** was built in 1993. This 85.3m long bridge has 5 spans. Each bent rests on 4 drilled concrete shafts. Soil borings indicate mostly clay layers with a significant sand layer about 10m thick starting at a depth of approximately 4m. Between 1993 and 1996 the peak flood occurred in 1994 and generated a measured flow of $200 \text{ m}^3/\text{s}$, which corresponds to a HEC-RAS calculated mean approach flow velocity of 0.93m/s at bent 3. The pier at bent 3 is circular with a 0.76m diameter. The angle between the flow direction and the pier main axis was 5° . River bottom profiles exist for 1993 and 1995 and indicate 0.05m of pier scour at bent 3.

- **The Bedias Creek Bridge at US75** was built in 1947. This 271.9m long bridge has 29 spans and bent 26 is founded on a spread footing. The soil tested from the site varied from low plasticity clay to fine silty sand. Between 1947 and 1996 the peak flood

occurred in 1991 and generated a measured flow of $650 m^3/s$, which corresponds to a HEC-RAS calculated mean approach flow velocity of 2.15 m/s at bent 26. The pier at bent 26 is square with a side of 0.86m. The pier is in line with the flow. River bottom profiles exist for 1947 and 1996 and show 2.13m of total scour at bent 26 made up of 1.35m of pier scour and 0.78m of contraction and general scour as explained later.

9.6.2 HYDROGRAPH DATA FOR BRIDGE CASES

For each bridge, the USGS gage data was obtained from the USGS Internet site. Table 9.27 shows the number of the nearest USGS gaging station to each bridge site. The downloaded data consisted of a record of discharge Q versus time t over a time period from the building of the bridge to the time of measuring the pier scour depths. This discharge hydrograph was converted to a velocity hydrograph by using the program HEC-RAS (1997) and the following procedures. The input to HEC-RAS is the bottom profile of the river cross section (obtained from the Texas DOT records), the mean longitudinal slope of the river at the bridge site (obtained from topographic maps, Table 4.2), and Manning's roughness coefficient (estimated at 0.035 for all cases after Young et al., 1997). For a given discharge Q , HEC-RAS gives the velocity distribution in the river cross section including the mean approach velocity v at the selected pier location. One pier was selected for each bridge except for the Navasota River Bridge at SH7 and the Trinity River Bridge at FM787. For these, two piers were selected. Therefore a total of 8 predictions were made for these 6 bridges. For each bridge the SRICOS-EFA method was used to predict local scour at the chosen bridge pier location. The velocities used in the pier scour prediction, using SRICOS-EFA, were the velocities in the

locations of the piers without the presence of the piers. After many runs of HEC-RAS for different values of Q developing the relationships between Q vs. V and Q vs. H, the relationships are then used to convert the Q-t hydrograph into a v-t hydrograph at the selected pier locations. Q vs. V (Figure 9.46 to Figure 9.53) shows the discharge and velocity relationship at selected piers. For the Q vs. H relationship for the bridge cases, please refer to Figures 5.17, 5.19, 5.21, 5.23, 5.25 and 5.27.

Table 9.27: The USGS Gaging Station Numbers of Bridge Cases

Bridge Name	Gaging Station Number
Navasota River Bridge at SH 7	08110500
Brazos River Bridge at US 90A	08114000
Trinity River Bridge at FM 787	08066500
San Marcos River Bridge at SH 80	08172000
Sims Bayou River Bridge at SH 35	08075500
Bedias Creek Bridge at US 75	08065800

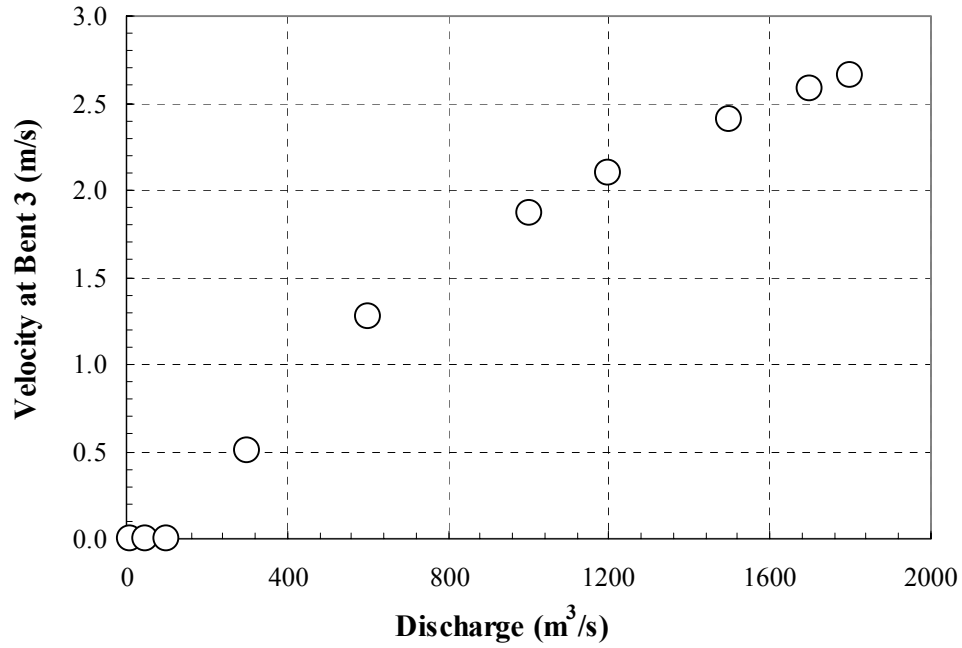


Figure 9.46: Relationship between Discharge and Velocity at Bent 3 at the Navasota River Bridge

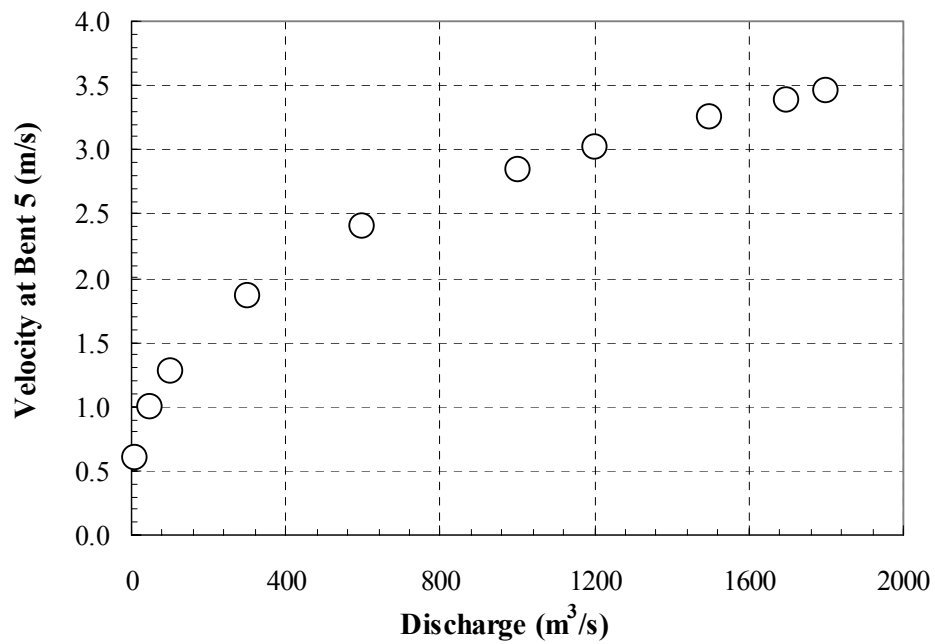


Figure 9.47: Relationship between Discharge and Velocity at Bent 5 at the Navasota River Bridge

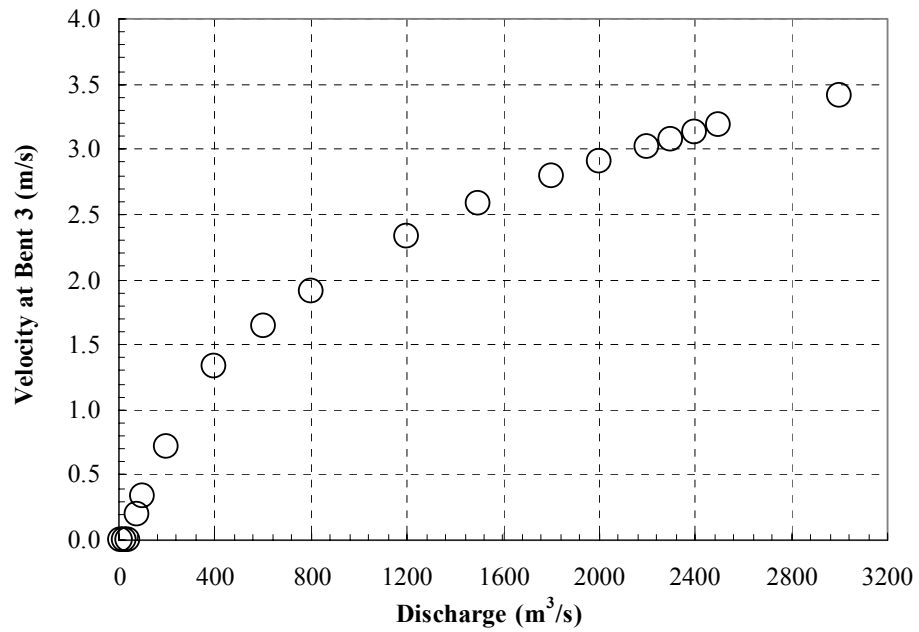


Figure 9.48: Relationship between Discharge and Velocity at Bent 3 at the Brazos River Bridge

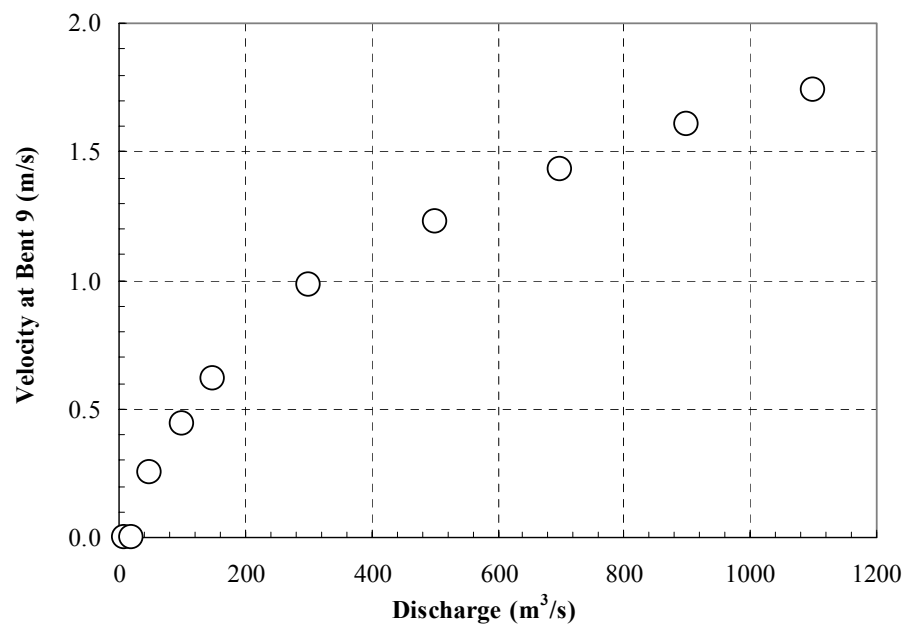


Figure 9.49: Relationship between Discharge and Velocity at Bent 9 at the San Marcos River Bridge

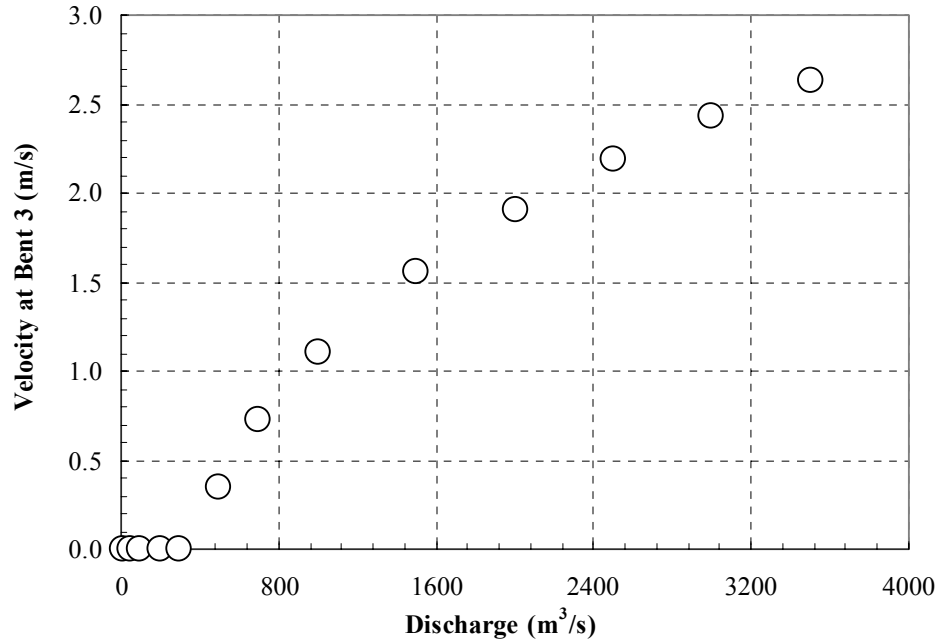


Figure 9.50: Relationship between Discharge and Velocity at Bent 3 at the Trinity River Bridge

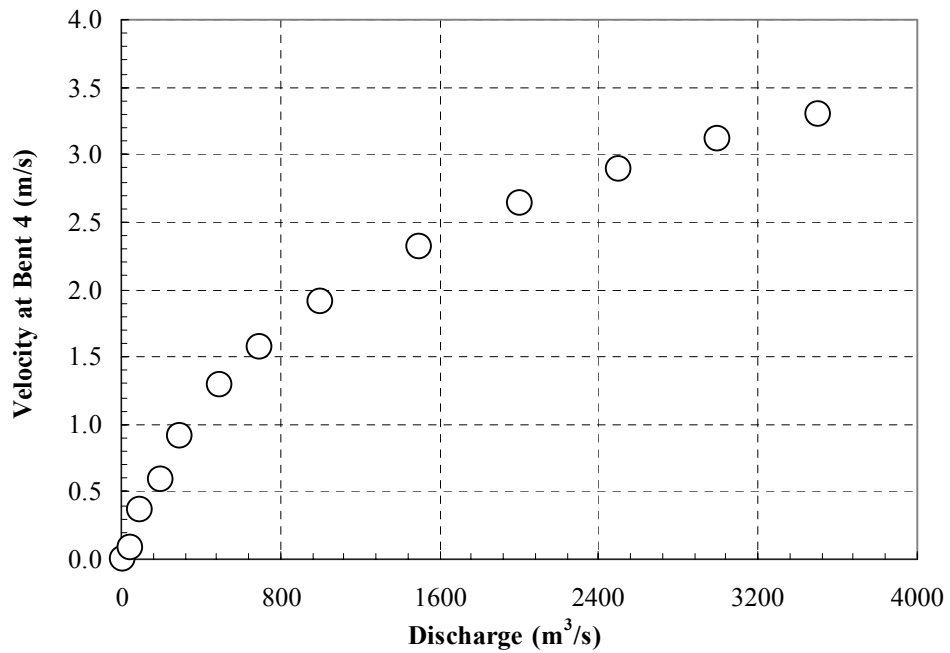


Figure 9.51: Relationship between Discharge and Velocity at Bent 4 at the Trinity River Bridge

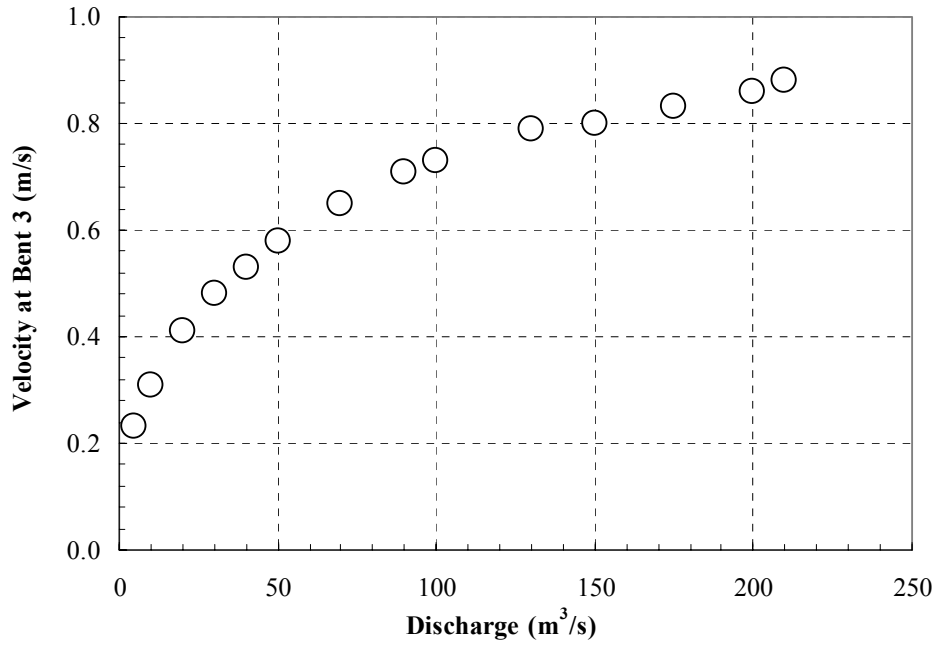


Figure 9.52: Relationship between Discharge and Velocity at Bent 3 at the Sims Bayou Bridge

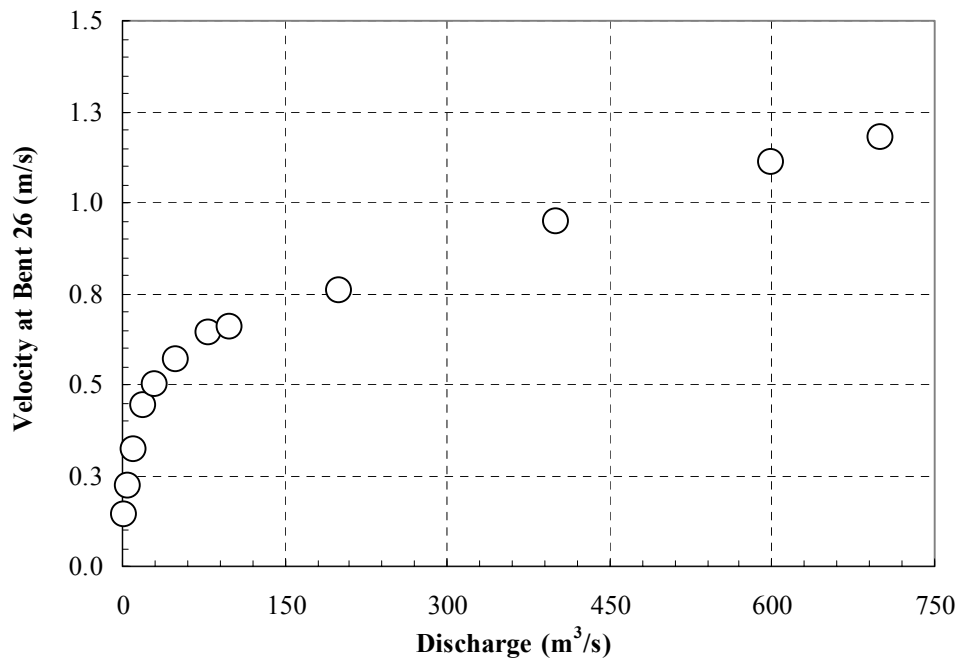


Figure 9.53: Relationship between Discharge and Velocity at Bent 26 at the Bedia Creek Bridge

9.6.3 GEOTECHNICAL AND EROSION PROPERTIES OF SOIL IN SELECTED BRIDGE CASES

Soil samples were taken and site explorations were made to determine the stratification and engineering properties of soils at the bridge sites. Some conventional geotechnical engineering tests were performed by Kwak (2000). The method of soil sampling will be the drilling technique, which is commonly used in geotechnical engineering. All the soil property tests were conducted by following the American Society for Testing and Materials (ASTM) standards. For the results of soil properties tests, please refer to Section 5.3.5 Table 5.4.

For each bridge, Shelby tube samples were taken near the bridge pier within a depth at least equal to two pier widths below the pier base. The chosen boring location was as close as practically possible to the bridge pier under consideration. The distance between the pier and the boring varied from 2.9m to 146.3m. In all instances, available boring data was studied in order to infer the relationship between the soil layers at the pier and at the sampling locations. Shelby tube samples to be tested were selected as the most probable representative samples at the bridge pier. These samples were tested at EFA and yielded erosion functions \dot{z} vs τ . The EFA results showed the shear stress vs. scour rate curve for the 6 selected bridge cases. For the EFA results, please refer to Section 5.3.5 from Figure 5.28 to Figure 5.37.

9.6.4 MEASURED PIER SCOUR DEPTH AND PIER SCOUR PREDICTIONS FOR TEXAS BRIDGE CASES

For each bridge, the SRICOS-EFA method was used to predict the local scour at the chosen bridge pier location. One pier was selected for each bridge except for the Navasota River Bridge at SH7 and the Trinity River Bridge at FM787. For these, two piers were selected. Therefore a total of 8 predictions were made for these 6 bridges. The measured pier scour depth was obtained for each case history by analyzing the two bottom profiles of the river cross-section. This analysis was necessary to separate the scour components which added to the total scour at the selected pier. The two components were pier scour and contraction/general scour. This separation was required because, at this time, SRICOS-EFA only predicts the pier scour. The contraction/general scour over the period of time separating the two river bottom profiles was calculated as the average scour over the width of the channel. This width was taken as the width corresponding to the mean flow level (width AB in Figures 9.54 and 9.55). Within this width the net area between the two profiles was calculated with scour being positive and aggradation being negative. The net area was then divided by the width AB to obtain an estimate of the mean contraction/general scour. Once this contraction/general scour was obtained, it was subtracted from the total scour at the bridge pier to obtain the pier scour at the bridge pier. Note that in some instances there was no need to evaluate the contraction/general scour. This is the case for bent 3 at the Navasota Bridge (Figure 9.54). Indeed in this case the bent was in the dry at the time of the field visit (flood plain) and the pier scour could be measured directly.

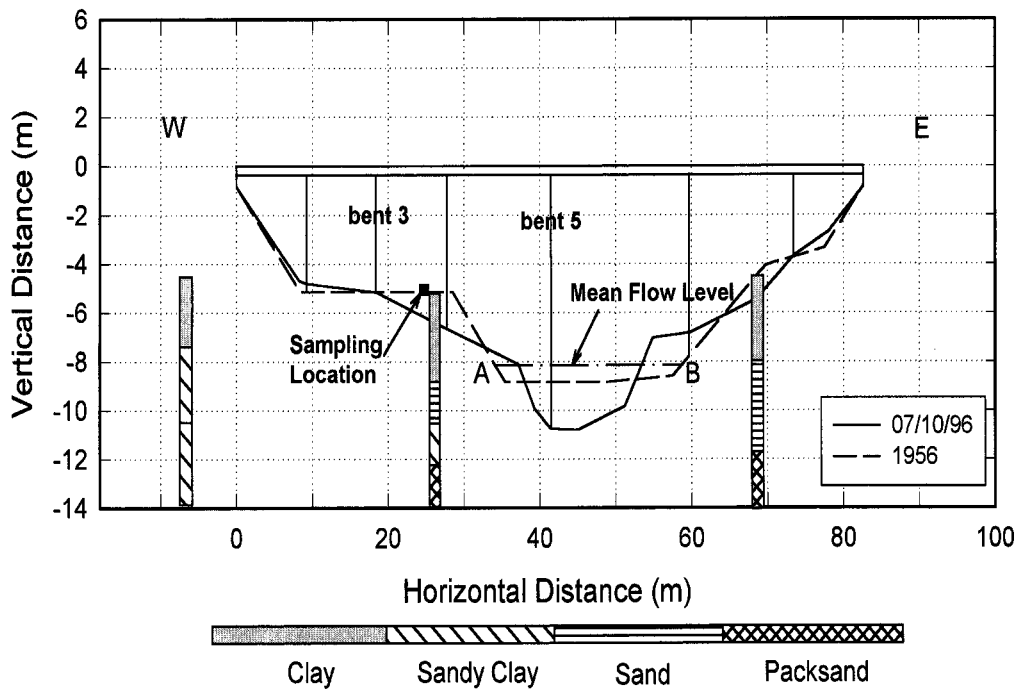


Figure 9.54: Profile of the Navasota River Bridge at SH-7

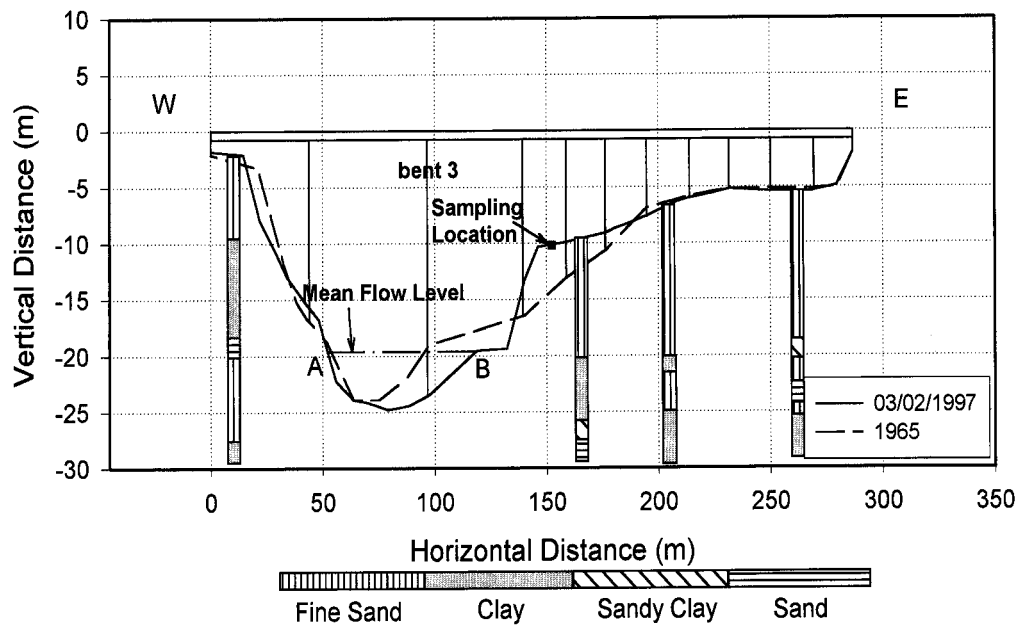


Figure 9.55: Profile of the Brazos River Bridge at US 90A

The following Table 9.28 presents the needed information for the predictions and results from the SRICOS-EFA method.

Table 9.28: Full Scale Bridges as Case Histories

Bridge	Pier Bent No.	Built Year	Pier Width (m)	Pier Length (m)	Pier Shape	Skew Angle (°)
Navasota River Bridge at SH 7	3	1956	0.36	0.36	Square	5
Navasota River Bridge at SH 7	5	1956	0.36	8.53	Square	5
Brazos River Bridge at US 90A	3	1965	0.91	8.53	Round	0
Trinity River Bridge at FM 787	3	1976	0.91	7.3	Round	25
Trinity River Bridge at FM 787	4	1976	0.91	7.3	Round	25
San Marcos River Bridge at SH 80	9	1939	0.91	14.2	Round	0
Sims Bayou River Bridge at SH 35	3	1993	0.76	0.76	circular	5
Bedias Creek Bridge at US 75	26	1947	0.86	0.86	Square	0
Bridge	Pier Bent No.	Manning's Coefficient ($s/m^{1/3}$)	Duration of Hydrograph (year)	Distance between Pier and Boring	Measured scour depth (m)	Predicted Scour depth (m)
Navasota River Bridge at SH 7	3	0.035	44	6.5	0.76	0.73
Navasota River Bridge at SH 7	5	0.035	44	16.1	1.41	1.61
Brazos River Bridge at US 90A	3	0.035	35	55.4	2.87	3.02
Trinity River Bridge at FM 787	3	0.035	24	37.8	2.17	4.52
Trinity River Bridge at FM 787	4	0.035	24	78.4	2.17	5.42
San Marcos River Bridge at SH 80	9	0.035	61	57.3	1.27	1.71
Sims Bayou River Bridge at SH 35	3	0.035	3	20	0.05	0.46
Bedias Creek Bridge at US 75	26	0.035	32	33	1.35	1.48

Figure 9.56 shows the comparison between SRICOS-EFA predicted and measured values of pier scour at the bridge piers. The precision and accuracy of the method appear reasonably good except in the Trinity Bridge case.

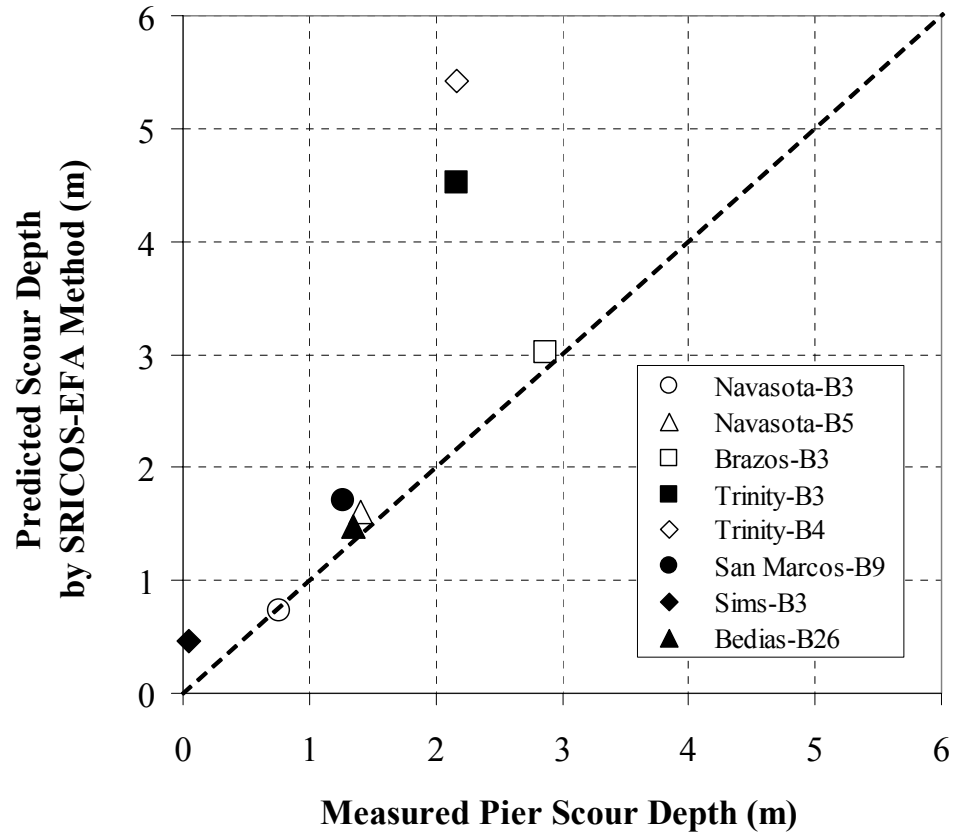


Figure 9.56: Predicted and Measured Pier Scour for the SRICOS-EFA Method

9.7 VERIFICATION CASE STUDY 6: MUELLER (1996) DATABASE, FROEHLICH (1988) DATABASE AND GILL (1981) DATABASE

9.7.1 MUELLER DATABASE (1996) FOR PIER SCOUR

The Mueller Database was collected from the FHWA-RD-95-184 report, which was titled as “Channel Scour at Bridges in the United States”. More than 380 local scour measurements presented in the report were collected at 56 bridge sites in Alaska, Arkansas, Colorado, Delaware, Georgia, Illinois, Indiana, Louisiana, Maryland, Mississippi, Montana, New York, Ohio, and Virginia.

Figure 9.57 shows a comparison between complex pier scour depth calculated by the SRICOS-EFA method and the measurements in the database. In the calculation, the equation for the maximum pier scour depth of the SRICOS-EFA method was used. Figure 9.58 shows the predictions by using the HEC-18 equation compared to the pier scour depth measurements in the Mueller (1996) database.

The results show that the HEC-18 equation does not underestimate the scour depths for most measurements; however, it often overestimates the scour by large amounts, which would result in over-design of bridge foundations. The results from the SRICOS-EFA method show they are closely to the observed scour depth, and the results fit the center of the line-of-equality fairly well. Although the SRICOS-EFA method does underestimate the scour depth for some measurement points, this method has less scatter than the HEC-18 equation. Both the SRICOS-EFA method and HEC-18 appear to be conservative, with less scatter in the SRICOS-EFA predictions. In order to investigate

the influence of D_{50} on the match between SRICOS-EFA predictions and measurements, the database was divided into three categories classified by different D_{50} values.

In SRICOS-EFA predictions for bed materials with a D_{50} larger than 75 mm, the predicted scour depths fit the line-of-equality well. The most underestimated results are the materials with a D_{50} from 0.075mm to 4.75mm. Exclusively there are no obvious tendencies to be observed.

The same approach was taken from the HEC-18 predictions, and Figure 9.60 shows the results. Again it appears that there is no major tendency to be observed.

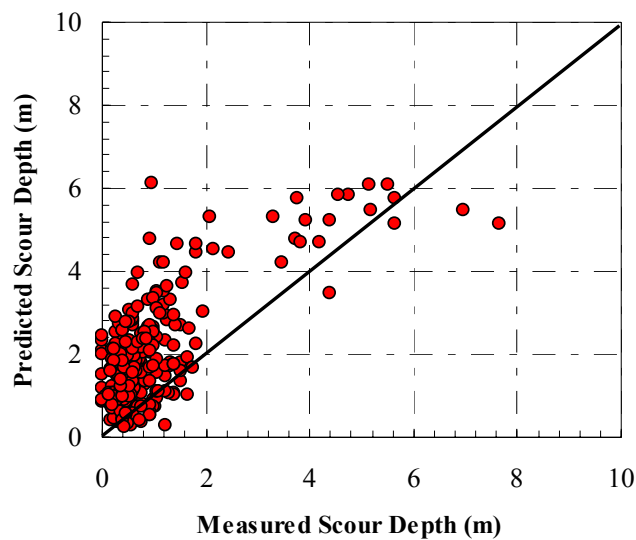


Figure 9.57: SRICOS-EFA Predictions against the Mueller (1996) Database

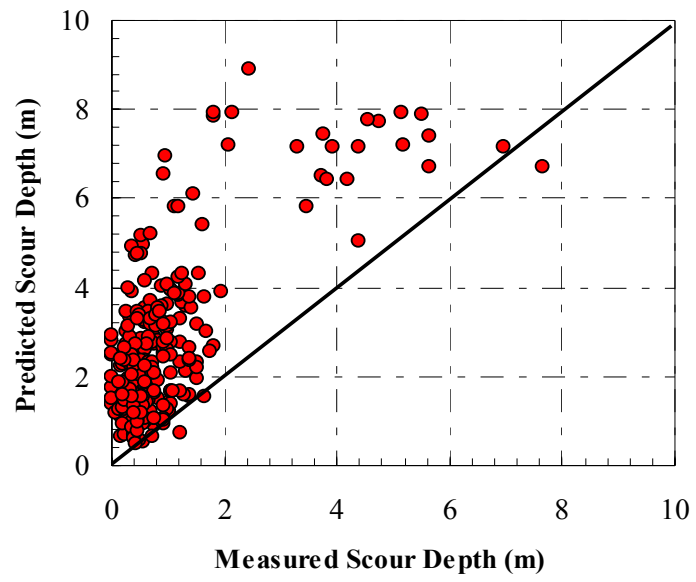


Figure 9.58: HEC-18 Method against the Mueller (1996) Database

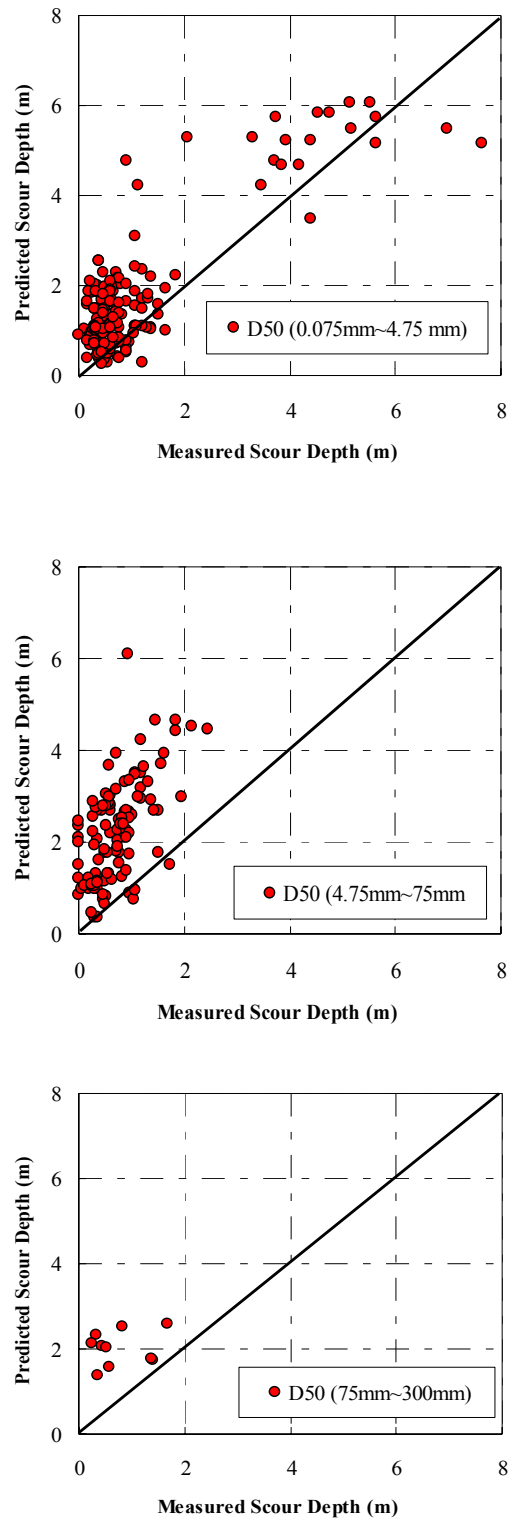


Figure 9.59: SRICOS-EFA Predictions vs. the Mueller Database for Various Ranges of D_{50}

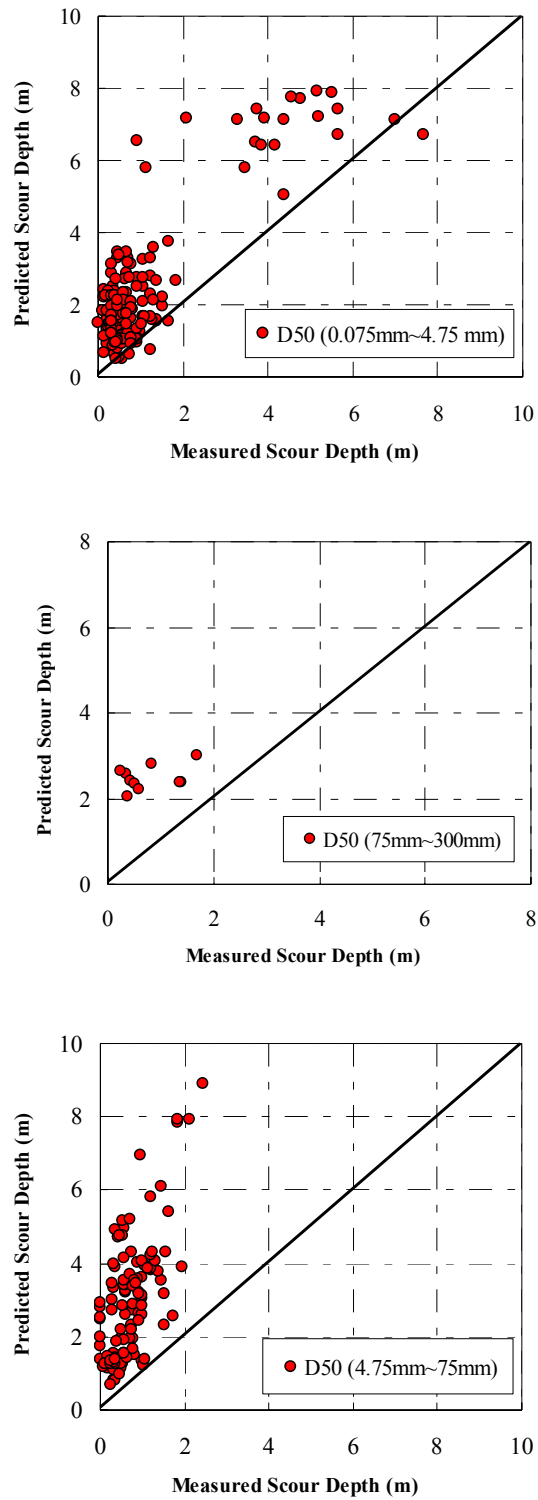


Figure 9.60: HEC-18 Predictions vs. the Mueller Database for Various Ranges of D_{50}

9.7.2 THE FROEHLICH DATABASE (1988) FOR PIER SCOUR

The Froehlich (1988) database was obtained from an ASCE (American Society of Civil Engineers) report titled “Analysis of Onsite Measurements of Scour at Piers”. In the Froehlich pier scour database, there are 79 pier scour measurement points, 50 cases for round-nosed pier, 9 cases for square-nosed pier and 20 cases for sharp-nosed pier.

Figure 9.61 shows the comparison between the complex pier scour depths calculated by the SRICOS-EFA method and the measurements in the database. The equation used was the SRICOS-EFA equation for maximum pier scour depth. Figure 9.62 shows the HEC-18 equation compared to the measurements in the same database.

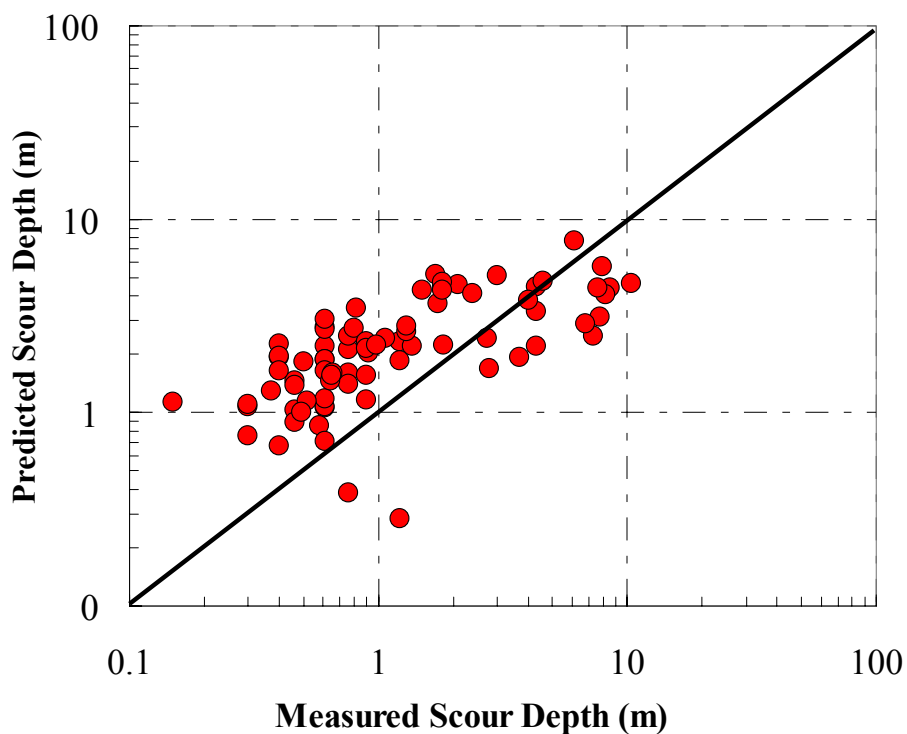


Figure 9.61: SRICOS-EFA Predictions against the Froehlich (1988) Database

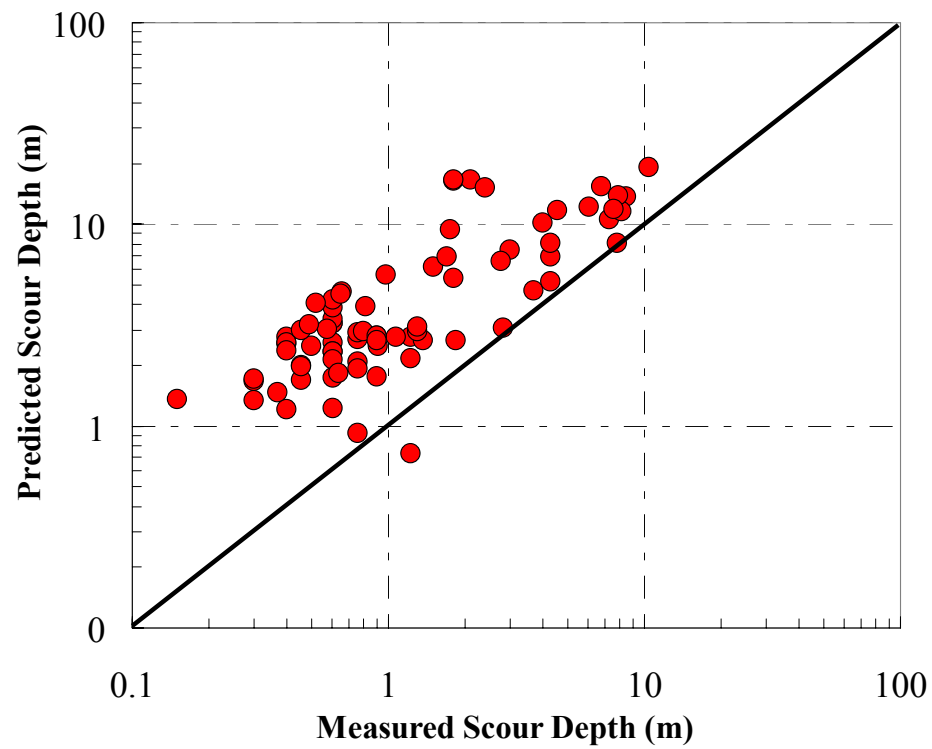


Figure 9.62: HEC-18 Predictions against the Froehlich (1988) Database

The computed values from both SRICOS-EFA and HEC-18 provide reasonable estimates of pier scour depth for most cases. With this database, HEC-18 appears to be more conservative than the SRICOS-EFA method.

9.7.3 THE GILL DATABASE (1981) FOR CONTRACTION SCOUR

The Gill (1981) database was obtained from an article titled “Bed Erosion in Rectangular Long Contraction” in the Journal of the Hydraulic Division of ASCE (American Society of Civil Engineers). Gill (1981) ran some contraction scour tests on sand in the laboratory. The experiments were conducted in a rectangular steel channel, which was 11.4 m in length, 0.76 m in width and 0.46 m in depth. There were two sizes of contracted sections in the channel. In the first series of experiments, the effective length of the contraction was 1.83 m, excluding the upstream (inlet) and downstream (outlet) transitions, each 0.46 m long. In the second series of experiments, the effective length of contraction was 2.44 m, with transitions each 0.46 m long. The width of the contracted section was 0.5 m. Two sizes of nearly uniform sand were used in the experiments. The average size of the coarse sand, D_{50} , was 1.53 mm, while D_{50} of the fine sand was 0.92 mm. The angle of transition at contraction was approximately 15° . The scour depth was obtained by averaging several depth readings taken along the longitudinal centerline of the channel. According to the locations of the measurements, the scour depths measured by Gill (1981) should be the uniform scour depth in this study. The Gill (1981) database therefore will be used to verify the uniform contraction scour equation Z_{unif} .

The SRICOS-EFA method calls for a value of the critical velocity V_c in the Z_{unif} calculation. The critical velocity can be measured in the EFA, but in this case the soil sample is not available, so the following Equation recommended in HEC-18 was used

$$V_c = 6.19y^{1/6}D_{50}^{1/3} \quad (9.5)$$

where V_c is the critical velocity above which bed material of size D and smaller will be transported, m/s; y is the water depth in the upstream flow, m; D_{50} is the particle size in a maximum of which 50% are smaller, m.

Figure 9.63 shows a comparison between the uniform contraction scour depth calculated by the SRICOS-EFA method and the measurements in the database. Figure 9.64 shows the HEC-18 equation compared with the same database. As can be seen, the SRICOS-EFA method is reasonably good while the HEC-18 method severely under-predicts the contraction scour depths.

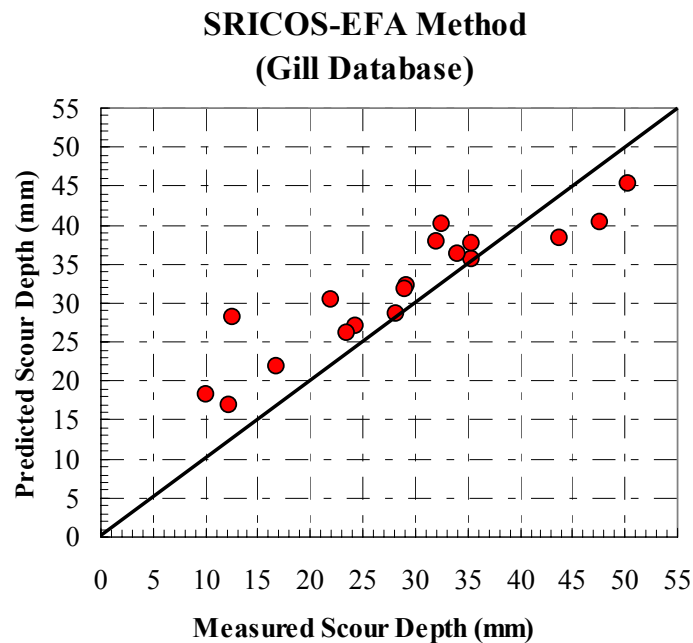


Figure 9.63: SRICOS-EFA Predictions against the Gill (1981) Database

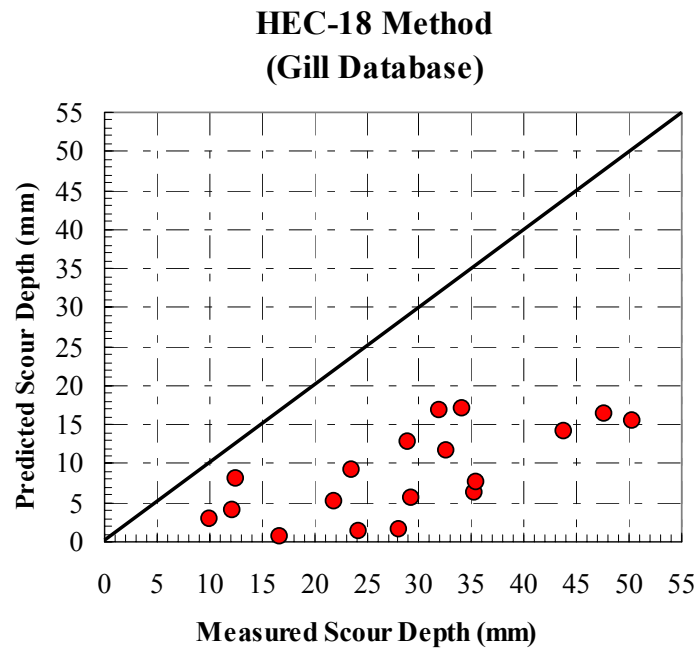


Figure 9.64: HEC-18 Predictions against the Gill (1981) Database

CHAPTER X

CONCLUSIONS AND RECOMMENDATIONS

10.1 CONCLUSIONS

Scour is the interaction between soil and flowing water. It is the result of the erosive action of flowing water, which excavates and carries away material from stream beds and banks. The leading cause of bridge failure is bridge scour in United States. Scour in cohesive soils is different from scour in non-cohesive soils, which includes the scour rate, the shape of scour hole, and the final scour depth and so on. Hence, the solutions for bridge scour based on the non-cohesive soils are not applicable for cohesive soils.

In this research, a method called SRICOS-EFA was developed at Texas A&M University. SRICOS-EFA method can predict the scour depth development as a function of time. The complex pier scour or the contraction scour problem can be solved by SRICOS-EFA method. The integrated SRICOS-EFA method based on the superposition principle was developed to handle the combined case of complex pier and contraction scour. Algorithms are used to incorporate the effect of varying velocities and multilayered soil systems in the SRICOS-EFA method. The fundamental basis of the accumulation algorithms is that the velocity histogram is a step function with a constant velocity value for each time step. The principle of accumulation algorithm is based on the equivalent time calculation, which is the time required for a flood in the hydrograph to create the same scour depth as the created by all previous flood in the hydrograph. SRICOS-EFA computer program was developed based on the procedures of SRICOS-

EFA method. The SRICOS-EFA computer program is a user friendly, interactive code that let the users operate the program very easily and directly. A simplified SRICOS-EFA method was developed based on the case histories for contraction scour. The simplified SRICOS-EFA method will predict the contraction scour in the situation that the whole hydrograph does not exist and only hand calculation will be needed. A lot of efforts were performed in the EFA testing to find out the potential relationships between the soil erodibility and soil properties. A new technique was presented on generating future hydrographs for the SRICOS-EFA method to predict the scour depth over the design life of the bridge. Case studies were used to verify the SRICOS-EFA method and compared to HEC-18 results in some cases to check whether the method is good enough to provide sound results in real cases.

The following is the main conclusions obtained from this study.

1. A methodology called SRICOS-EFA was developed to predict the complex pier and contraction scour, which can handle the multiflood hydrograph and multi-layer soil system. For complex pier scour, the effect of shallow water depth, the effect of rectangular shapes, the effect of the angle of attack on rectangular shapes, and the effect of spacing between piers positioned in a row perpendicularly to the flow were considered. For contraction scour, the effects of the ratio of the contracted channel width over the approach channel width, the contracted channel length, and the transition angle were considered.
2. The step by step procedure was established in SRICOS-EFA method for predicting the scour depths for a complex pier or contraction scour.

- 1) Collect the input data: velocity and water depth hydrograph, geometry of the pier or of the contracted channel, erosion functions of the soil layers.
 - 2) Calculate the maximum pier scour depth or contraction scour depth for the i^{th} velocity in the hydrograph.
 - 3) Calculate the initial maximum shear stress for pier scour or contraction scour using the i^{th} velocity in the hydrograph.
 - 4) Read the initial scour rate corresponding to the initial maximum shear stress of step 3 on the erosion function of the soil layer corresponding to the current scour depth.
 - 5) Use the results of steps 2 and 4 to construct the hyperbola describing the scour depth vs. time for the pier scour or contraction scour.
 - 6) Calculate the equivalent time for the given curve of step 5. The equivalent time is the time required for the i^{th} velocity on the hydrograph to scour the soil to a depth equal to the depth scoured by all the velocities occurring prior to the i^{th} velocity.
 - 7) Read the additional scour generated by the i^{th} velocity starting at the equivalent time and ending at the equivalent time plus the time increment.
 - 8) Repeat steps 2 to 9 for the $(i+1)$ th velocity and so on until the entire hydrograph is consumed.
3. The integrated SRICOS-EFA method for the pier and contraction scour was developed to calculate the total scour. This method is based on the concept of the critical shear stress and the relationship between pier scour and contraction scour. Care was taken not to simply add complex pier scour and contraction scour to get

total pier scour. Instead, advantage was taken of the factor that at the end of the maximum contraction scour, the velocity is the critical velocity of the soil and not the initial velocity in the contracted channel.

4. The simple SRICOS-EFA method for contraction scour is proposed to calculate the contraction scour depth in cohesive soils. This method can be applicable even the whole hydrograph does not exist. This method requires only the followings parameters to calculate the equivalent time: the duration of hydrograph t_{hyd} ; maximum flow velocity V_{max} and the mean initial scour rate Z_i . The simple SRICOS-EFA method for contraction scour was verified with 28 cases of scour depths results.
5. The proposed technique to predict future hydrograph consists of using a past hydrograph (from a gauge station for example), preparing the frequency distribution plot for the floods within that hydrograph, sampling the distribution randomly and preparing a future hydrograph, for the required period, which has the same mean and standard deviation as the measured hydrograph.
6. The risk analysis of bridge scour was developed based on the predicted hydrographs: for each predicted hydrograph, a final scour depth (the depth reached at the end of the design life of the bridge) is generated. This process is repeated 10,000 times. These 10,000 final depths of scour are organized in a frequency distribution plot with a mean and a standard deviation. That plot can be used to quote a scour depth with a corresponding probability of occurrence, or better, to choose a risk level and quote the corresponding final depth of scour.

7. In the EFA pH tests: the pH value of the eroding water affects the erosion process. The erosion rate was largest and the critical shear stress lowest when the water was neutral (pH=7). The erosion rate decreased and the critical shear stress increased when water became acidic and when water became alkaline. It is suggested that the total dissolved salts content is the factor which influences the erodibility of the soil through the pH values. If tap water is used as the eroding water (ph \approx 7), it will be more conservative compared to using water with a low pH or a high pH values.
8. In the EFA salinity tests: the salinity of the eroding water affects the erosion process. The erosion rate decreases and the critical shear stress increases when the salt content increases. The cations in the eroding water tend to neutralize the surface electronegativity of clay particles thereby making the clay more erosion resistant. If tap water is used as eroding water, it will be more conservative compared to using water with a higher salt concentration.
9. Potential correlations between soil erodibility and soil properties: there are more than 100 EFA tests performed. For each soil tested, the following soil properties were measured: water content, undrained shear strength, plasticity index, and percentage passing #200 sieve. All attempted correlations lead to very poor R^2 values; therefore the conclusion is that there is no simple correlation between erodibility parameters and the chosen soil properties. On the other hand it is well accepted that different soils erode at different rates. The apparent contradiction between the last two statements suggests that a relationship exists but it is complex and involves many soil parameters. If this is the case then, rather than measuring all those soil

properties, it is much easier to measure the soil erodibility function directly with the EFA.

10. A clear tendency can be observed from the comparison in the bridge cases that, with the increasing of the pier widths, the differences between the results from SRICOS-EFA and HEC-18 increase as well.
11. For comparison purpose, HEC-18 was used to apply to the most bridge cases and scour database. HEC-18 seems to provide larger predictions than SRICOS-EFA method. HEC-18 overestimates the scour depths in most cases except contraction scour.
12. Six bridges in Texas were selected to verify the SRICOS-EFA method for full scale scour measurements. In most cases, the values of pier scour depth predicted by SRICOS-EFA method were very close to the scour measurements.
13. The maximum scour depths from SRICOS-EFA method for pier and contraction scour were compared to three scour databases. These databases were mostly in sand. The comparisons between the predicted and measured scour depths are very satisfactory.
14. The HEC-18 method underestimates the contraction scour depth significantly, but SRICOS-EFA method gives reasonable results.
15. In some cases, SRICOS-EFA probably will underestimate the scour depths. Hence under such circumstances, a safety factor should be applied to the predicted scour depths to minimize the risk of having an actual scour depth larger than the predicted values. The recommended value of a safety factor is 1.5.

16. In most methods, the way to predict the combined scour of pier and the contraction scour will be: first compute the magnitude of contraction scour, the local scour at piers individually, second add them together for the combined scour. It should be noted, as often stated by engineers, that the results would be conservative. The results in the Sloop Channel Bridge scour analysis shows the integrated SRICOS-EFA method reduce the combined scour depth significantly compared to the simple superposition method.

10.2 RECOMMENDATIONS

Most of the current research is based on the results from the flume tests and the numerical simulation method. The limitations of the laboratory conditions, the method assumptions, the simplified test conditions, and few verification full scale case histories might constrain the application of the method and the conclusions. The followings are recommended for the future research:

1. More full scale bridge case histories are needed for verification purpose.
2. In SRICOS-EFA method, the channel with a rectangular cross section was assumed, but in the reality, the cross section of a channel is consists of the overbank on the two sides and the main channel. How to calculate the contraction scour in this condition needs more research.
3. Research is required for the last major unsolved bridge scour problem in cohesive soils: abutment scour. The integrated SRICOS-EFA method for pier scour, contraction scour and abutment scour needs to be developed.
4. SRICOS-EFA can not deal with the complex pier case described in HEC-18.

5. The measurement of erosion in EFA test is based on the operator's subjective judgment. Some research is needed to develop a laser device to measure the scour automatically and a warning system to remind the examiner to keep 1 mm constant protrusion during test.
6. SRICOS-EFA method cannot predict the scour in the tidal inlets, tidal estuaries, bridge crossings to islands and streams affected by tides (tidal waterways). A 2-dimensional hydraulic flow model needs to be studied in order to solve the tidal scour by using SRICOS-EFA method.

REFERENCES

- Annandale, G. W. (1995). "Erodibility." *Journal of Hydraulic Research*, 33(4), 471-494.
- Arulanandan, K. (1975). "Fundamental Aspects of Erosion in Cohesive Soils." *Journal of the Hydraulics Division*, 101(5), 635-639.
- Arulanandan, K., Loganathan, P., and Krone, R. B. (1975). "Pore and Eroding Fluid Influences on Surface Erosion of Soil." *Journal of Geotechnical Engineering*, 101(GT1), 51-66.
- ASTM (1999). *ASTM Standards for Geotechnical Engineering*, American Society for Testing and Materials, Philadelphia.
- Ayres Associates (2000). *Report on the South Shore Hydraulic and Scour Analysis*, Fort Collins, Colorado.
- Basak, V. (1975). "Scour at Square Piers." Devlet Su Isteri Genel Mudulugu, *Report No. 583*, Ankara, Turkey.
- Benjamin, J.R., and Cornell, C. A. (1970). *Probability, Statistics, and Decisions for Civil Engineers*, McGraw-Hill, New York.
- Bonasoundas, M. (1973). "Non-stationary Hydro-morphological Phenomena and Modeling of Scour Processes." *Proceedings of 16th Congress I.A.H.R.*, Sao Paulo, Brazil, Vol. 2, 9-16.
- Brady, N.C. (1990). *The Nature and Properties of Soil*, Macmillan Publishing Company, New York.
- Bras, R. L., and Rodriguez-Iturbe, I. (1986). *Random Functions and Hydrology*, Dover, New York.
- Breusers, H.N.C., and Raudkivi, A.J. (1991). *Scouring*, Balkema, Rotterdam, The Netherlands.
- Briaud J.-L., Ting F., Chen H.-C., Gudavalli R., Kwak K., Philogene B., Han S.-W., Perugu S., Wei G.S., Nurtjahyo P., Cao Y.W., and Li Y. (1999). "SRICOS: Prediction of Scour Rate at Bridge Piers." *TTI Report No. 2937-1* to the Texas DOT, Texas A&M University, College Station.
- Briaud, J.-L., Ting, F., Chen, H.C., Gudavalli, S.R., Perugu, S., and Wei, G. (1999). "SRICOS: Prediction of Scour Rate in Cohesive Soils at Bridge Piers." *Journal of Geotechnical and Geoenvironmental Engineering*, 125(4), 237-246.

- Briaud J.-L., Ting F., Chen H.C., Cao Y., Han S.-W., and Kwak K. (2001a). "Erosion Function Apparatus for Scour Rate Predictions." *Journal of Geotechnical and Geoenvironmental Engineering*, 127(2), 105-113.
- Briaud, J. L., Chen, H. C. Kwak K., Han S.-W., and Ting F. (2001b). "Multiflood and Multilayer Method for Scour Rate Prediction at Bridge Piers." *Journal of Geotechnical and Geoenvironmental Engineering*, 127(2), 105-113.
- Briaud, J. L., Chen, H. C. Li Y., Nurtjahyo, P., and Wang, J. (2002). "NCHRP Report 24-15: Complex Pier Scour and Contraction Scour in Cohesive Soils." *Report No. NCHRP 24-15* to Transportation Research Board, Texas A&M University, College Station.
- Cao, Y.W. (2001). "The Influence of Certain Factors on the Erosion Functions of Cohesive Soil." M.S. Thesis, Texas A&M University, College Station.
- Chabert, J., and Engeldinger, P. (1956). "Etude des affouillements autour des piles de ponts." Lab. Nat.d'Hydr., Chatou, France.
- Chang, F., and Davis, S. (1995). "Maryland SHA Procedure for Estimating Scour at Bridge Abutments: Part 2-Clear Water Scour." *ASCE Compendium of Conference Scour Papers*, Reston, Virginia.
- Chee, R. K. (1982). "Live-bed Scour at Bridge Piers." *Report No. 290*, University of Auckland, Auckland, New Zealand.
- Chen, H. C. (1995a). "Submarine Flows Studied by Second-Moment Closure." *Journal of Engineering Mechanics*, 121, 1136-1146.
- Chen, H. C. (1995b). "Assessment of a Reynolds Stress Closure Model for Appendage Hull Junction Flows." *Journal of Fluids Engineering*, 117, 557-563.
- Chen, H. C., Chen, M., and Davis, D. A. (1997). "Numerical Simulation of Transient Flows Induced by a Berthing Ship." *International Journal of Offshore and Polar Engineering*, 7, 277-284.
- Chen, H. C., and Korpus, R. A. (1993). "A Multi-Block Finite-Analytic Reynolds-Average Navier-Stokes Method for 3D Incompressible Flow." *Journal of Fluids Engineering*, 115, 113-121.
- Chen, H. C., and Patel, V. C. (1988). "Near-Wall Turbulence Models for Complex Flows Including Separation." *AIAA Journal*, 26(6), 641-648.

- Chen, H. C., and Patel, V. C. (1989). "The Flow around Wing-Body Junctions." *Proceedings of 4th Symposium on Numerical and Physical Aspects of Aerodynamic Flows*, Long Beach, California, 1-15.
- Chen, H. C., Patel, V. C., and Ju, S. (1990). "Solutions of Reynolds-Averaged Navier-Stokes Equations for Three-Dimensional Incompressible Flows." *Journal of Computational Physics*, 88(2), 305-336.
- Chiew, Y.M. (1984). "Local Scour at Bridge Piers." *Report No. 355*, University of Auckland, Auckland, New Zealand.
- Chow V.T., Maidment, D.R., and Mays, L.W. (1988). *Applied Hydrology*, McGraw-Hill, New York.
- Colorado State University (1966). *Mechanics of Local Scour*, Prepared for U.S. Department of Commerce, Under Contract CPR 11-8022, Fort Collins, Colorado.
- Dargahi, B. (1987). "Flow Field and Local Scouring around a Cylinder." *Bulletin TITRA-VBI-137*, Department of Hydraulics Engineering, Royal Institute of Technology, Stockholm, Sweden.
- Das, B. M. (1998). *Principle of Geotechnical Engineering*, 4th edition, PWS Publishing Company, Boston, Massachusetts.
- Dietz, J. W. (1972). *Ausbildung von Langen Pfeilern bei Schraganströmung am Beispiel der BAB-Mainbrücke Eddersheim*, Mitteilungsblatt de BAW, Karlsruhe, Germany.
- Dou, G.R. (1980). "The Stochastic Theory and the General Law of All Flow Regions for Turbulent Open Channel Flows." *Proceedings of First International Symposium on River Sedimentation*, Beijing, China.
- Dou, X. (1997). "Numerical Simulation of Three-Dimensional Flow Field and Local Scour at Bridge Crossings." PhD Dissertation, the University of Mississippi, Oxford, Mississippi.
- Elliott, K. R., and Baker, C. J. (1985). "Effect of Pier Spacing on Scour around Bridge Piers." *Journal of Hydraulic Engineering*, 111(7), 1105-1109.
- Ettema, R. (1980). "Scour at Bridge Piers." *Report No. 216*, University of Auckland, Auckland, New Zealand.
- Flaxman, E. M. (1963). "Channel Stability in Undisturbed Cohesive Soils." *Proceedings of ASCE*, 89(HY2), 87-96.

- Froehlich, D. C. (1988). "Analysis of Onsite Measurements of Scour at Piers." *Proceedings of the ASCE National Hydraulic Engineering Conference*, Colorado Springs, Colorado, 887-892.
- Gao, D.G. (1994). "Pier Scour Equation Used in China." *ASCE Compendium of Conference Scour Papers*, Reston, Virginia, 217-222.
- Gill, M. A. (1981). "Bed Erosion in Rectangular Long Contraction." *Journal of the Hydraulics Division*, 107(3), 273-284.
- Graf, W.H. (1998). *Fluvial Hydraulics: Flow and Transport Process in Channels of Simple Geometry*, John Wiley & Sons, London, England.
- Gudavalli, S. R. (1997). "Prediction Model for Scour Rate around Bridge Piers in Cohesive Soils on the Basis of Flume Tests." PhD Dissertation, Texas A&M University, College Station.
- Hancu, S. (1971). "Sur le calcul des Affouillements Locaux dans la Zone des Piles due Pont." *Proceedings of the 14th Congress, IAHR*, Vol.3, 299-306.
- HEC-RAS River Analysis System (1997). *User's Manual, Version 2.0*, Hydrologic Engineering Center, U.S. Army Corps of Engineers, Davis, California.
- Herbich, J.B. (1984). *Scour around Pipelines, Piles and Sea Walls: Handbook of Coastal and Ocean Engineering*, Gulf Publishing Company, Houston, Texas.
- Hoffmans, G. J. C. M., and Booij, R. (1993). "Two-Dimensional Mathematical Modeling of Local Scour Holes." *Journal of Hydraulic Research*, 31(5), 615-634.
- Hoffmans G.J.C.M., and Verheij H.J. (1997). *Scour Manual*, A.A.Balkema, Rotterdam, The Netherlands.
- Hosny, H.M. (1995). "Experimental Study of Local Scour around Circular Bridge Piers in Cohesive Soils." PhD Dissertation, Colorado State University, Fort Collins, Colorado.
- Hjorth, P. (1975). "Studies on the Nature of Local Scour." *Bulletin Series A. No. 46*, Department of Water Resources Engineering, Lund Institute of Technology/University of Lund, Sweden.
- Iverson, W. R. (1998). "Scour and Erosion in Clay Soils." *ASCE Compendium of Conference Scour Papers*, Reston, Virginia, 104-119.

- Jain, S.C., and Fischer, E.E. (1979). "Scour around Circular Bridge Piers at High Froude Number." *Report No. FHWA-RD-79-104*, Washington D.C.
- Johnson, P. A. (1994). "Scour at Wide Piers Relative to Flow Depth." *ASCE Compendium of Conference Scour Papers*, Reston, Virginia, 280-287.
- Johnson, P. A. and Jones, J. S. (1992). "Shear Stress at Base of Bridge Pier." *Transportation Research Board Report No.1350*, Washington D.C., 14-18.
- Kirsten, H.A.D. (1982). "A Classification System for Excavation of Natural Materials." *Journal of Civil Engineering in South Africa*, 24(7), 293-308.
- Komura, S. (1996). "Equilibrium Depth of Scour in Long Contractions." *Journal of the Hydraulics Division*, 92(5), 17-37.
- Kwak, K. (2000). "Prediction of Scour Depth versus Time for Bridge Piers in Cohesive Soils in the Case of Multi-flood and Soil System." PhD Dissertation, Texas A&M University, College Station.
- Kwak K., Briaud J.-L., and Chen H.-C. (2001). "SRICOS: Computer Program for Bridge Pier Scour." *Proceedings of the 15th International Conference on Soil Mechanics and Geotechnical Engineering*, Rotterdam, The Netherlands, 3, 2235-2238.
- Kwak, K., Briaud, J.-L., Cao, Y., Chung M.-K., Hunt, B., and Davis, S. (2002). "Pier Scour at Woodrow Wilson Bridge and SRICOS Method." *Proceedings of First International Conference on Scour of Foundations*, Texas A&M University, College Station, Texas.
- Laursen, E. M. (1960). "Scour at Bridge Crossings." *Journal of the Hydraulics Division*, 86(HY2), 39-53.
- Laursen, E. M. (1963). "An Analysis of Relief Bridge Scour." *Journal of the Hydraulics Division*, 89(HY3), 93-118.
- Laursen, E. M., and Toch, A. (1956). "Scour Around Bridge and Abutment." *Bulletin No.4*, Iowa Highway Research Board, Ames, Iowa.
- Li, Y. (2002). "Bridge Pier Scour and Contraction Scour in Cohesive Soils on the Basis of Flume Test." PhD Dissertation, Texas A&M University, College Station.
- Lim, S.-Y., and Cheng, N.-S. (1998). "Scouring in Long Contractions." *Journal of Irrigation and Drainage Engineering*, 124(5), 258-261.

- Melville, B. W. (1997). "Pier and Abutment Scour: Integrated Approach." *Journal the Hydraulics Division*, 123(2), 125-136.
- Melville, B. W., and Coleman, S.E. (1999). *Bridge Scour*, Water Resources Publications, LLC, Bloomington, Indiana.
- Melville, B. W., and Sutherland, A. J. (1988). "Design Method for Local Scour at Bridge Piers." *Journal of Hydraulic Engineering*, 114(10), 1210-1226.
- Mohammad, S., and Jones, S. (1998). "Scour around Exposed Pile Foundations." *Compendium of Papers ASCE Water Resources Engineering Conference*, Reston, Virginia, 335-346.
- Molinas, A., Jones, S., and Hosny, M. (1999). "Effect of Cohesive Material Properties on Local Scour around Piers." *Transportation Research Board, 78th annual Meeting*, Washington, D. C.
- Montanari, A., Rosso, R., and Taqqu, M.S. (1997). "Fractionally Differenced ARIMA Models Applied to Hydrologic Time Series: Identification, Estimation and Simulation." *Water Resources Res.*, 33(4), 1035-1044.
- Montanari, A., Rosso, R., and Taqqu, M.S. (2000). "A Seasonal Fractional ARIMA Model Applied to the Nile River Monthly Flows at Aswan." *Water Resources, Res.*, 36(5), 1249-1259.
- Moody, L.F., (1944). "Friction Factors for Pipe Flow." *Transactions of the American Society of Civil Engineers*, 66, 671-684.
- Mostafa, E.A. (1994). "Scour around Skewed Bridge Piers." PhD Dissertation, Alexandria University, Alexandria, Egypt.
- Mueller, D.S. (1996). "Channel Scour at Bridges in the United States." *Report No. FHWA-RD-95-184*, Federal Highway Administration, Richmond, Virginia.
- Munson, B. R., Young, D. F., and Okiishi, T. H. (1990). *Fundamentals of Fluid Mechanics*, Wiley, New York.
- Neill, C. R. (1973). *Guide to Bridge Hydraulics*, University of Toronto Press, Toronto, Canada.
- Nurtjahyo, P. Y. (2002). "Numerical Simulation of Pier Scour and Contraction Scour." PhD Dissertation, Texas A&M University, College Station.

- Olsen, N. R. B., and Melaaen, M. C. (1993). "Three-Dimensional Calculation of Scour around Cylinder Pier." *Journal of Hydraulic Engineering*, 119(9), 1048-1054.
- Raudkivi, A.J. (1991). *Scour at Bridge Piers: Hydraulic Structures Design Manual No.2*, A.A Balkema, Rotterdam, The Netherlands.
- Richardson, E. V. and Davis S. R. (1996). *Evaluating Scour at Bridges*, Hydraulic Engineering Circular No.18, US Department of Transportation, Washington, D. C.
- Richardson, E. V. and Davis S. R. (2001). *Evaluating Scour at Bridges*, Hydraulic Engineering Circular No.18, US Department of Transportation, Washington, D. C.
- Roulund, A., Sumer, B. M., Fredsoe, J., and Michelsen, J. (1998). "3D Mathematical Modeling of Scour around a Circular Pile." *Proceedings of ISRS 98*, Hong Kong, China, 131-137.
- Salim, M., and Jones J. S. (1998). "Scour around Exposed Pile Foundations." *ASCE Compendium of Conference Scour Papers*, Reston, Virginia, 104-119.
- Sargunan, A., Riley, P., Arulanandan, K., and Krone, R.B. (1973). "Physico-Chemical Factors in Erosion of Cohesive Soils." *Journal of the Hydraulics Division*, 99(HY3), 555-558.
- Shaikh, A., Ruff, J. F. and Abt, S. R. (1988). "Erosion Rate of Compacted Na-Montmorillonite Soils." *Journal of Geotechnical and Geoenvironmental Engineering*, 114(3), 296-305.
- Shen, H. W., Schneider, V. R., and Karaki, S. S. (1969). "Local Scour around Bridge Piers." *Proceedings of ASCE*, 95(6), 1919-1940.
- Sherard, J.L., Decker, R.S., and Ryka, N.L. (1972). "Piping in Earth Dams of Dispersive Clay." Presented at *ASCE Soil Mechanics and Foundation Conference*, Purdue University, Lafayette, Indiana.
- Shields, A. (1936). "Application of Similarity Principles and Turbulence Research to Bed-load Movement." California Institute of Technology, Pasadena, California.
- Shirole, A.M., and Holt, R.C. (1991). "Planning for Comprehensive Bridge Safety Assurance Program." *Transportation Research Report No.1290*, Transportation Research Board, Washington, D.C., 137-142.
- Smith, C. D. (1967). "Simplified Design for Flume Inlets." *Journal of the Hydraulics Division*, 93(6), 25-34.

- Smith, P. (1976). *Bridge Hydraulics*, E&FN Spon Publishing Company, London, England.
- Straub, L. G. (1934). "Effect of Channel Contraction Works upon Regime of Movable Bed Streams." *Transportation Report Part II*, American Geophysical Union, 454-463.
- US Geological Survey (1996). *General Information from Internet*, USGS National Center, Reston, Virginia.
- Vanoni, V.A. (1975). "Sedimentation Engineering." *ASCE-Manuals and Reports on Engineering Practice No. 54*, Prepared by the ASCE Task Committee, Washington, D.C.
- Van Rijn, L. C., and Meijer, K. (1986). "Three-Dimensional Modeling of Suspended Sediment Transport for Currents and Waves." *Report No. Q250/Q432/H461*, Delft Hydraulic, Delft, The Netherlands.
- Wei, G., Chen, H. C., Ting, F., Briaud, J.-L., Gudavalli, S. R., and Perugu, S. (1997). "Numerical Simulation to Study Scour Rate in Cohesive Soils." *Research Report No. 2937-F* to the Texas Department of Transportation, Texas A&M University, College Station.
- Yanmaz, M., and Altinbilek, D. (1991). "Study of Time-Dependent Local Scour around Bridge Pier." *Journal of Hydraulic Engineering*, 117(10), 1247-1268.
- Young, D.F., Munson, B.R., and Okiishi T.H. (1997). *A Brief Introduction to Fluid Mechanics*, John Wiley & Sons, New York.

APPENDIX
DATABASES OF CASE HISTORIES

Table 1 – MUELLER (1996) Database

Test No.	Pier Data				Flow Data			SRICOS-EFA K Factors Approach					HEC-18 Method					Measured Pier Scour (m)
	Pier Type	Pier Width (m)	Pier Length (m)	B (m)	Attack Angle (degree)	H (m)	R _e	H/B	K _w Depth	K _{sp}	K _{sh}	Z _{max} (m)	K ₁	K ₂	K ₃	F _r	HEC-18 (m)	
1	SS	1.52	6.10	1.52	0	5.79	3020895	3.8	1.00	1	0.9	2.11	0.9	1.00	1.10	0.26	2.71	0.76
2	SS	1.52	6.10	1.52	0	5.33	4647531	3.5	1.00	1	0.9	2.77	0.9	1.00	1.10	0.42	3.23	0.61
3	SS	1.52	6.10	1.52	0	4.11	3950402	2.7	1.00	1	0.9	2.50	0.9	1.00	1.10	0.41	2.90	0.76
4	SS	1.52	6.10	1.52	0	6.55	4415155	4.3	1.00	1	0.9	2.69	0.9	1.00	1.10	0.36	3.24	0.61
5	SS	1.52	6.10	1.52	0	3.35	3253272	2.2	1.00	1	0.9	2.21	0.9	1.00	1.10	0.37	2.60	0.61
6	SS	1.52	6.10	1.52	0	5.18	5344661	3.4	1.00	1	0.9	3.03	0.9	1.00	1.10	0.49	3.41	0.61
7	SS	1.52	6.10	1.52	0	4.11	2323766	2.7	1.00	1	0.9	1.79	0.9	1.00	1.10	0.24	2.31	1.52
8	SS	1.52	6.10	1.52	0	5.33	4415155	3.5	1.00	1	0.9	2.69	0.9	1.00	1.10	0.40	3.16	1.52
9	SS	1.83	8.84	1.83	0	5.49	6692445	3.0	1.00	1	0.9	3.50	0.9	1.00	1.10	0.50	3.94	1.07
10	RS	1.52	11.25	1.52	0	2.13	2323766	1.4	0.95	1	1.0	1.89	1	1.00	1.10	0.33	2.35	0.61
11	RS	1.52	11.25	1.52	0	0.91	1440735	0.6	0.71	1	1.0	1.05	1	1.00	1.10	0.32	1.71	0.46
12	RS	1.52	11.25	1.52	0	1.98	2370241	1.3	0.93	1	1.0	1.87	1	1.00	1.10	0.35	2.35	0.61
13	RS	1.52	11.25	1.52	0	0.91	1487210	0.6	0.71	1	1.0	1.07	1	1.00	1.10	0.33	1.73	0.61
14	RS	1.52	11.25	1.52	0	1.22	743605	0.8	0.79	1	1.0	0.76	1	1.00	1.10	0.14	1.34	0.30
15	RS	1.52	11.25	1.52	0	3.05	2416716	2.0	1.00	1	1.0	2.03	1	1.00	1.10	0.29	2.51	0.91
16	RS	1.52	11.25	1.52	0	1.83	1673111	1.2	0.90	1	1.0	1.46	1	1.00	1.10	0.26	2.00	0.46
17	RS	1.52	11.25	1.52	0	1.52	1161883	1.0	0.85	1	1.0	1.09	1	1.00	1.10	0.20	1.67	0.30
18	RS	1.52	11.25	1.52	0	3.20	3020895	2.1	1.00	1	1.0	2.34	1	1.00	1.10	0.35	2.78	1.22
19	RS	1.52	11.25	1.52	0	2.44	1766062	1.6	1.00	1	1.0	1.66	1	1.00	1.10	0.24	2.13	0.61
20	RS	1.52	11.25	1.52	0	1.22	1347784	0.8	0.79	1	1.0	1.11	1	1.00	1.10	0.26	1.72	0.30
21	RS	1.52	11.25	1.52	0	3.05	2742043	2.0	1.00	1	1.0	2.20	1	1.00	1.10	0.33	2.65	1.37
22	RS	1.52	11.25	1.52	0	2.29	1719587	1.5	0.98	1	1.0	1.60	1	1.00	1.10	0.24	2.09	0.76
23	RS	1.52	11.25	1.52	0	0.46	418278	0.3	0.56	1	1.0	0.38	1	1.00	1.10	0.13	0.91	0.76
24	RS	1.52	11.25	1.52	0	2.59	3160321	1.7	1.00	1	1.0	2.41	1	1.00	1.10	0.41	2.75	1.07
25	RS	1.52	11.25	1.52	0	1.52	1719587	1.0	0.85	1	1.0	1.39	1	1.00	1.10	0.29	1.97	0.46

Test No.	Pier Data				Flow Data			SRICOS-EFA K Factors Approach					HEC-18 Method					Measured Pier Scour (m)
	Pier Type	Pier Width (m)	Pier Length (m)	B (m)	Attack Angle (degree)	H (m)	R _e	H/B	K _w Depth	K _{sp}	K _{sh}	Z _{max} (m)	K ₁	K ₂	K ₃	F _r	HEC-18 (m)	
26	RS	1.52	11.25	1.52	0	0.61	232377	0.4	0.62	1	1.0	0.29	1	1.00	1.10	0.06	0.74	1.22
27	RS	1.52	11.25	1.52	0	3.05	2788519	2.0	1.00	1	1.0	2.23	1	1.00	1.10	0.33	2.67	1.83
28	RS	1.52	11.25	1.52	0	1.98	1487210	1.3	0.93	1	1.0	1.39	1	1.00	1.10	0.22	1.92	0.76
29	RS	1.22	6.40	1.22	0	2.29	2007733	1.9	1.00	1	1.0	1.81	1	1.00	1.10	0.35	2.12	1.31
30	RS	1.22	6.40	1.22	0	2.29	2007733	1.9	1.00	1	1.0	1.81	1	1.00	1.10	0.35	2.12	0.46
31	RS	1.22	6.40	1.22	0	0.64	817965	0.5	0.68	1	1.0	0.70	1	1.00	1.10	0.27	1.21	0.30
32	RS	1.22	6.40	1.22	0	0.64	817965	0.5	0.68	1	1.0	0.70	1	1.00	1.10	0.27	1.21	0.30
33	RS	1.22	6.40	1.22	0	1.04	1226948	0.9	0.80	1	1.0	1.06	1	1.00	1.10	0.32	1.54	0.30
34	RS	1.22	6.40	1.22	0	1.04	1226948	0.9	0.80	1	1.0	1.06	1	1.00	1.10	0.32	1.54	0.34
35	RS	0.91	10.21	0.91	0	5.12	281640	5.6	1.00	1	1.0	0.52	1	1.00	1.10	0.04	0.95	0.43
36	RS	0.91	10.21	0.91	0	5.94	697130	6.5	1.00	1	1.0	0.92	1	1.00	1.10	0.10	1.44	1.04
37	RS	0.91	13.11	0.91	0	5.09	1171178	5.6	1.00	1	1.0	1.28	1	1.00	1.10	0.18	1.76	0.67
38	SS	4.27	16.46	4.27	0	11.58	10930993	2.7	1.00	1	0.9	4.77	0.9	1.00	1.10	0.24	6.49	3.72
39	SS	4.27	16.46	4.27	0	12.25	10930993	2.9	1.00	1	0.9	4.77	0.9	1.00	1.10	0.23	6.54	0.91
40	SS	4.27	16.46	4.27	0	9.42	8979030	2.2	1.00	1	0.9	4.21	0.9	1.00	1.10	0.22	5.80	3.47
41	SS	4.27	16.46	4.27	0	9.39	8979030	2.2	1.00	1	0.9	4.21	0.9	1.00	1.10	0.22	5.80	1.13
42	SS	4.27	16.46	4.27	0	11.95	13533611	2.8	1.00	1	0.9	5.47	0.9	1.00	1.10	0.29	7.14	6.98
43	SS	4.27	16.46	4.27	0	12.62	13533611	3.0	1.00	1	0.9	5.47	0.9	1.00	1.10	0.28	7.20	5.18
44	SS	4.27	16.46	4.27	0	9.78	12362433	2.3	1.00	1	0.9	5.16	0.9	1.00	1.10	0.30	6.69	7.65
45	SS	4.27	16.46	4.27	0	9.78	12362433	2.3	1.00	1	0.9	5.16	0.9	1.00	1.10	0.30	6.69	5.64
46	RS	4.27	12.19	4.27	0	11.67	10670732	2.7	1.00	1	1.0	5.22	1	1.00	1.10	0.23	7.14	4.39
47	RS	4.27	12.19	4.27	0	11.73	10670732	2.8	1.00	1	1.0	5.22	1	1.00	1.10	0.23	7.15	3.93
48	RS	4.27	12.19	4.27	0	10.82	10930993	2.5	1.00	1	1.0	5.31	1	1.00	1.10	0.25	7.15	3.29
49	RS	4.27	12.19	4.27	0	11.28	10930993	2.6	1.00	1	1.0	5.31	1	1.00	1.10	0.24	7.19	2.07
50	RS	4.27	12.19	4.27	0	9.33	8979030	2.2	1.00	1	1.0	4.68	1	1.00	1.10	0.22	6.44	3.84
51	RS	4.27	12.19	4.27	0	9.27	8979030	2.2	1.00	1	1.0	4.68	1	1.00	1.10	0.22	6.43	4.18
52	RS	4.27	12.19	4.27	0	11.73	12752826	2.8	1.00	1	1.0	5.85	1	1.00	1.10	0.28	7.72	4.75

Test No.	Pier Data				Flow Data			SRICOS-EFA K Factors Approach					HEC-18 Method					Measured Pier Scour (m)
	Pier Type	Pier Width (m)	Pier Length (m)	B (m)	Attack Angle (degree)	H (m)	R _e	H/B	K _w Depth	K _{sp}	K _{sh}	Z _{max} (m)	K ₁	K ₂	K ₃	F _r	HEC-18 (m)	
53	RS	4.27	12.19	4.27	0	12.04	12752826	2.8	1.00	1	1.0	5.85	1	1.00	1.10	0.27	7.75	4.54
54	RS	4.27	12.19	4.27	0	11.19	13533611	2.6	1.00	1	1.0	6.08	1	1.00	1.10	0.30	7.87	5.52
55	RS	4.27	12.19	4.27	0	11.67	13533611	2.7	1.00	1	1.0	6.08	1	1.00	1.10	0.30	7.91	5.15
56	RS	4.27	12.19	4.27	0	9.69	12362433	2.3	1.00	1	1.0	5.74	1	1.00	1.10	0.30	7.42	3.75
57	RS	4.27	12.19	4.27	0	9.63	12362433	2.3	1.00	1	1.0	5.74	1	1.00	1.10	0.30	7.42	5.64
58	SS	1.52	12.71	1.52	0	2.41	3560009	1.6	0.99	1	0.9	2.33	0.9	1.00	1.10	0.48	2.58	0.34
59	SS	1.52	12.71	1.52	0	2.07	3183559	1.4	0.94	1	0.9	2.06	0.9	1.00	1.10	0.46	2.41	0.43
60	SS	1.52	12.71	1.52	0	3.02	4006172	2.0	1.00	1	0.9	2.52	0.9	1.00	1.10	0.48	2.80	0.82
61	SS	1.52	12.71	1.52	0	2.44	2881469	1.6	1.00	1	0.9	2.04	0.9	1.00	1.10	0.39	2.36	0.52
62	RS	4.57	9.75	4.57	0	3.54	3680845	0.8	0.78	1	1.0	2.07	1	1.00	1.10	0.14	3.91	0.37
63	RS	4.57	9.75	4.57	0	3.11	5967430	0.7	0.75	1	1.0	2.69	1	1.00	1.10	0.24	4.73	0.43
64	RS	4.57	9.75	4.57	0	2.44	5186645	0.5	0.69	1	1.0	2.27	1	1.00	1.10	0.23	4.31	0.73
65	RS	4.57	9.75	4.57	0	2.44	7250149	0.5	0.69	1	1.0	2.81	1	1.00	1.10	0.32	4.97	0.55
66	RS	4.57	9.75	4.57	0	1.92	4628941	0.4	0.63	1	1.0	1.95	1	1.00	1.10	0.23	3.97	0.30
67	RS	4.57	9.75	4.57	0	2.01	7515058	0.4	0.64	1	1.0	2.69	1	1.00	1.10	0.37	4.92	0.37
68	RS	4.57	9.75	4.57	0	3.08	7333804	0.7	0.74	1	1.0	3.06	1	1.00	1.10	0.29	5.16	0.52
69	US	4.57	10.67	4.57	0	1.89	3039485	0.4	0.63	1	1.0	1.48	1	1.00	1.10	0.15	3.31	1.22
70	US	4.57	10.67	4.57	0	3.08	3527476	0.7	0.74	1	1.0	1.92	1	1.00	1.10	0.14	3.76	1.65
71	US	4.57	10.67	4.57	0	2.23	3513534	0.5	0.67	1	1.0	1.72	1	1.00	1.10	0.16	3.60	1.31
72	US	4.57	10.67	4.57	0	2.16	1896193	0.5	0.66	1	1.0	1.15	1	1.00	1.10	0.09	2.75	0.73
73	US	4.57	10.67	4.57	0	1.49	989924	0.3	0.58	1	1.0	0.67	1	1.00	1.10	0.06	1.98	0.61
74	US	4.57	10.67	4.57	0	1.13	1254833	0.2	0.53	1	1.0	0.71	1	1.00	1.10	0.08	2.11	0.49
75	US	4.57	10.67	4.57	0	2.13	2635150	0.5	0.66	1	1.0	1.41	1	1.00	1.10	0.13	3.16	0.70
76	US	4.57	10.67	4.57	0	1.46	1450030	0.3	0.58	1	1.0	0.85	1	1.00	1.10	0.08	2.32	0.67
77	CS	2.44	2.44	2.44	0	3.05	4610351	1.3	0.92	1	1.0	2.81	1	1.00	1.10	0.35	3.67	1.25
78	CS	2.44	2.44	2.44	0	2.59	4640095	1.1	0.87	1	1.0	2.67	1	1.00	1.10	0.38	3.60	0.98

Test No.	Pier Data				Flow Data			SRICOS-EFA K Factors Approach					HEC-18 Method					Measured Pier Scour (m)
	Pier Type	Pier Width (m)	Pier Length (m)	B (m)	Attack Angle (degree)	H (m)	R _e	H/B	K _w Depth	K _{sp}	K _{sh}	Z _{max} (m)	K ₁	K ₂	K ₃	F _r	HEC-18 (m)	
79	CS	2.44	2.44	2.44	0	3.93	5205235	1.6	1.00	1	1.0	3.31	1	1.00	1.10	0.34	4.01	0.88
80	CS	2.44	2.44	2.44	0	2.65	4535990	1.1	0.87	1	1.0	2.65	1	1.00	1.10	0.36	3.58	0.88
81	CS	2.44	2.44	2.44	0	2.90	5160619	1.2	0.90	1	1.0	2.97	1	1.00	1.10	0.40	3.83	1.19
82	CS	2.44	2.44	2.44	0	2.65	5502677	1.1	0.87	1	1.0	3.00	1	1.00	1.10	0.44	3.89	1.95
83	CS	2.44	2.44	2.44	0	3.05	4268293	1.3	0.92	1	1.0	2.68	1	1.00	1.10	0.32	3.55	1.43
84	CS	2.44	2.44	2.44	0	3.11	4870613	1.3	0.92	1	1.0	2.93	1	1.00	1.10	0.36	3.77	1.37
85	SS	0.94	10.36	0.94	0	2.65	2305175	2.8	1.00	1	0.9	1.78	0.9	1.00	1.10	0.48	1.95	0.76
86	SS	0.94	10.36	0.94	0	2.53	2362805	2.7	1.00	1	0.9	1.81	0.9	1.00	1.10	0.50	1.96	0.70
87	SS	0.94	10.36	0.94	0	2.01	1411920	2.1	1.00	1	0.9	1.30	0.9	1.00	1.10	0.34	1.53	0.58
88	SS	0.98	10.36	0.98	0	2.50	2260559	2.6	1.00	1	0.9	1.76	0.9	1.00	1.10	0.47	1.94	0.49
89	SS	0.94	10.36	0.94	0	2.38	2305175	2.5	1.00	1	0.9	1.78	0.9	1.00	1.10	0.50	1.93	0.55
90	SS	0.98	10.36	0.98	0	1.89	1427722	1.9	1.00	1	0.9	1.31	0.9	1.00	1.10	0.34	1.53	0.34
91	SS	0.94	10.36	0.94	0	2.26	950885	2.4	1.00	1	0.9	1.01	0.9	1.00	1.10	0.21	1.31	0.09
92	SS	0.94	10.36	0.94	0	2.07	1037329	2.2	1.00	1	0.9	1.07	0.9	1.00	1.10	0.24	1.34	0.12
93	SS	0.94	10.36	0.94	0	1.83	1008514	1.9	1.00	1	0.9	1.05	0.9	1.00	1.10	0.25	1.30	0.12
94	SS	1.04	10.97	1.04	0	0.52	1706573	0.5	0.67	1	0.9	0.99	0.9	1.00	1.10	0.73	1.41	0.37
95	SS	1.04	10.97	1.04	0	0.46	1390541	0.4	0.64	1	0.9	0.83	0.9	1.00	1.10	0.63	1.27	0.52
96	SS	1.04	10.97	1.04	0	0.40	1327335	0.4	0.61	1	0.9	0.77	0.9	1.00	1.10	0.65	1.22	0.46
97	SS	1.04	10.97	1.04	0	0.40	1706573	0.4	0.61	1	0.9	0.90	0.9	1.00	1.10	0.83	1.36	0.98
98	SS	1.04	10.97	1.04	0	0.30	1485351	0.3	0.56	1	0.9	0.75	0.9	1.00	1.10	0.83	1.23	1.04
99	SS	1.04	10.97	1.04	0	0.46	1706573	0.4	0.64	1	0.9	0.94	0.9	1.00	1.10	0.78	1.38	1.07
100	SS	1.04	10.97	1.04	0	0.27	1295732	0.3	0.54	1	0.9	0.67	0.9	1.00	1.10	0.76	1.15	0.49
101	SS	1.04	10.97	1.04	0	0.12	790080	0.1	0.41	1	0.9	0.37	0.9	1.00	1.10	0.70	0.83	0.30
102	SS	1.04	10.97	1.04	0	0.15	663667	0.1	0.44	1	0.9	0.36	0.9	1.00	1.10	0.52	0.79	0.37
103	RS	1.52	14.63	1.52	0	1.74	743605	1.1	0.89	1	1.0	0.86	1	1.00	1.10	0.12	1.40	0.00
104	RS	1.52	14.63	1.52	0	5.79	4043352	3.8	1.00	1	1.0	2.82	1	1.00	1.10	0.35	3.41	0.61
105	RS	1.52	14.63	1.52	0	3.78	3439173	2.5	1.00	1	1.0	2.55	1	1.00	1.10	0.37	3.01	0.27

Test No.	Pier Data				Flow Data			SRICOS-EFA K Factors Approach					HEC-18 Method					Measured Pier Scour (m)
	Pier Type	Pier Width (m)	Pier Length (m)	B (m)	Attack Angle (degree)	H (m)	R _e	H/B	K _w Depth	K _{sp}	K _{sh}	Z _{max} (m)	K ₁	K ₂	K ₃	F _r	HEC-18 (m)	
106	RS	1.52	14.63	1.52	0	2.59	2509667	1.7	1.00	1	1.0	2.08	1	1.00	1.10	0.33	2.49	0.00
107	RS	1.52	14.63	1.52	0	2.04	1161883	1.3	0.94	1	1.0	1.20	1	1.00	1.10	0.17	1.73	0.00
108	RS	1.52	14.63	1.52	0	8.08	4879908	5.3	1.00	1	1.0	3.18	1	1.00	1.10	0.36	3.87	1.19
109	RS	1.52	14.63	1.52	0	5.43	4136303	3.6	1.00	1	1.0	2.86	1	1.00	1.10	0.37	3.42	0.58
110	RS	1.52	14.63	1.52	0	3.60	3020895	2.4	1.00	1	1.0	2.34	1	1.00	1.10	0.33	2.82	0.00
111	RS	1.52	14.63	1.52	0	2.38	1533685	1.6	0.99	1	1.0	1.51	1	1.00	1.10	0.21	2.00	0.00
112	RS	1.52	14.63	1.52	0	9.72	5205235	6.4	1.00	1	1.0	3.31	1	1.00	1.10	0.35	4.08	1.31
113	RS	1.52	14.63	1.52	0	5.70	4415155	3.7	1.00	1	1.0	2.98	1	1.00	1.10	0.39	3.54	0.58
114	RS	1.52	14.63	1.52	0	3.75	3253272	2.5	1.00	1	1.0	2.46	1	1.00	1.10	0.35	2.93	0.00
115	RS	1.52	14.63	1.52	0	3.41	2323766	2.2	1.00	1	1.0	1.98	1	1.00	1.10	0.26	2.51	0.00
116	RS	1.52	14.63	1.52	0	9.57	5716463	6.3	1.00	1	1.0	3.52	1	1.00	1.10	0.39	4.24	1.19
117	RS	1.52	14.63	1.52	0	5.79	4833432	3.8	1.00	1	1.0	3.16	1	1.00	1.10	0.42	3.69	0.70
118	RS	1.52	14.63	1.52	0	3.84	3532124	2.5	1.00	1	1.0	2.59	1	1.00	1.10	0.38	3.05	1.01
119	RS	1.52	14.63	1.52	0	3.66	2788519	2.4	1.00	1	1.0	2.23	1	1.00	1.10	0.31	2.73	0.27
120	RS	1.52	14.63	1.52	0	9.48	5995315	6.2	1.00	1	1.0	3.62	1	1.00	1.10	0.41	4.32	1.25
121	RS	1.52	14.63	1.52	0	4.94	3718025	3.2	1.00	1	1.0	2.67	1	1.00	1.10	0.35	3.22	0.91
122	RS	1.52	14.63	1.52	0	3.81	3020895	2.5	1.00	1	1.0	2.34	1	1.00	1.10	0.32	2.85	0.52
123	RS	1.52	14.63	1.52	0	8.32	6227692	5.5	1.00	1	1.0	3.71	1	1.00	1.10	0.45	4.32	1.55
124	RS	1.68	13.11	1.68	0	5.09	5623513	3.0	1.00	1	1.0	3.48	1	1.00	1.10	0.47	3.95	1.07
125	RS	1.68	13.11	1.68	0	5.46	6134741	3.3	1.00	1	1.0	3.68	1	1.00	1.10	0.50	4.14	0.58
126	RS	1.52	12.19	1.52	0	5.52	3857451	3.6	1.00	1	1.0	2.74	1	1.00	1.10	0.34	3.32	0.34
127	RS	1.52	12.19	1.52	0	5.58	4182778	3.7	1.00	1	1.0	2.88	1	1.00	1.10	0.37	3.45	0.27
128	RS	1.52	12.19	1.52	0	5.12	3392698	3.4	1.00	1	1.0	2.52	1	1.00	1.10	0.31	3.11	0.98
129	RS	1.83	6.71	1.83	0	6.40	5298186	3.5	1.00	1	1.0	3.35	1	1.00	1.10	0.37	4.05	0.98
130	RS	3.05	17.68	3.05	0	7.65	13663742	2.5	1.00	1	1.0	6.11	1	1.00	1.10	0.52	6.97	0.94
131	RS	1.07	24.93	1.07	0	3.87	1463972	3.6	1.00	1	1.0	1.48	1	1.00	1.10	0.22	1.93	0.49
132	RS	1.07	24.93	1.07	0	4.08	1463972	3.8	1.00	1	1.0	1.48	1	1.00	1.10	0.22	1.95	0.30

Test No.	Pier Data				Flow Data			SRICOS-EFA K Factors Approach					HEC-18 Method					Measured Pier Scour (m)
	Pier Type	Pier Width (m)	Pier Length (m)	B (m)	Attack Angle (degree)	H (m)	R _e	H/B	K _w Depth	K _{sp}	K _{sh}	Z _{max} (m)	K ₁	K ₂	K ₃	F _r	HEC-18 (m)	
133	RS	0.98	10.85	0.98	0	1.95	1160024	2.0	1.00	1	1.0	1.28	1	1.00	1.10	0.27	1.56	0.55
134	RS	0.76	7.41	0.76	0	2.56	1068932	3.4	1.00	1	1.0	1.21	1	1.00	1.10	0.28	1.48	0.18
135	RS	0.76	7.41	0.76	0	2.32	1115407	3.0	1.00	1	1.0	1.25	1	1.00	1.10	0.31	1.49	0.82
136	RS	0.76	7.41	0.76	0	1.71	859793	2.2	1.00	1	1.0	1.06	1	1.00	1.10	0.28	1.28	0.21
137	RS	0.76	11.37	0.76	0	1.65	580941	2.2	1.00	1	1.0	0.82	1	1.00	1.10	0.19	1.07	0.76
138	RS	0.76	11.37	0.76	0	3.17	975982	4.2	1.00	1	1.0	1.14	1	1.00	1.10	0.23	1.47	0.67
139	RS	0.76	11.37	0.76	0	1.49	185901	2.0	1.00	1	1.0	0.40	1	1.00	1.10	0.06	0.65	0.15
140	RS	0.76	11.37	0.76	0	3.11	511228	4.1	1.00	1	1.0	0.76	1	1.00	1.10	0.12	1.11	0.15
141	RS	1.13	11.89	1.13	0	1.55	1788370	1.4	0.95	1	1.0	1.59	1	1.00	1.10	0.41	1.88	0.40
142	RS	1.13	11.89	1.13	0	2.87	2407421	2.5	1.00	1	1.0	2.03	1	1.00	1.10	0.40	2.32	0.73
143	RS	1.13	11.89	1.13	0	3.08	2029112	2.7	1.00	1	1.0	1.82	1	1.00	1.10	0.33	2.18	0.49
144	RS	1.31	11.89	1.31	0	2.04	2198282	1.6	0.99	1	1.0	1.89	1	1.00	1.10	0.37	2.21	0.73
145	RS	1.34	11.89	1.34	0	3.20	2862879	2.4	1.00	1	1.0	2.27	1	1.00	1.10	0.38	2.64	0.91
146	RS	1.37	11.89	1.37	0	3.38	2718806	2.5	1.00	1	1.0	2.19	1	1.00	1.10	0.34	2.62	0.98
147	RS	0.76	9.60	0.76	0	2.23	557704	2.9	1.00	1	1.0	0.80	1	1.00	1.10	0.16	1.10	0.40
148	RS	0.76	9.60	0.76	0	2.77	697130	3.6	1.00	1	1.0	0.92	1	1.00	1.10	0.18	1.25	0.43
149	RS	0.91	10.67	0.91	0	6.46	482414	7.1	1.00	1	1.0	0.73	1	1.00	1.10	0.07	1.24	0.98
150	RS	0.91	10.67	0.91	0	5.00	281640	5.5	1.00	1	1.0	0.52	1	1.00	1.10	0.04	0.95	0.91
151	RS	0.91	10.67	0.91	0	5.03	337411	5.5	1.00	1	1.0	0.58	1	1.00	1.10	0.05	1.03	0.49
152	RS	0.91	10.67	0.91	0	5.33	362507	5.8	1.00	1	1.0	0.61	1	1.00	1.10	0.05	1.07	0.91
153	RS	0.91	10.67	0.91	0	5.15	284429	5.6	1.00	1	1.0	0.52	1	1.00	1.10	0.04	0.96	0.61
154	RS	0.91	10.67	0.91	0	4.75	264909	5.2	1.00	1	1.0	0.50	1	1.00	1.10	0.04	0.92	0.55
155	RS	0.91	10.67	0.91	0	5.52	435009	6.0	1.00	1	1.0	0.68	1	1.00	1.10	0.06	1.16	0.49
156	RS	0.91	10.67	0.91	0	5.61	376450	6.1	1.00	1	1.0	0.62	1	1.00	1.10	0.06	1.09	0.61
157	RS	0.91	10.67	0.91	0	5.76	474048	6.3	1.00	1	1.0	0.72	1	1.00	1.10	0.07	1.21	0.70
158	RS	0.91	10.67	0.91	0	8.75	1271565	9.6	1.00	1	1.0	1.35	1	1.00	1.10	0.15	1.96	1.52
159	RS	0.91	10.67	0.91	0	7.32	881172	8.0	1.00	1	1.0	1.07	1	1.00	1.10	0.11	1.64	0.76

Test No.	Pier Data				Flow Data			SRICOS-EFA K Factors Approach					HEC-18 Method					Measured Pier Scour (m)
	Pier Type	Pier Width (m)	Pier Length (m)	B (m)	Attack Angle (degree)	H (m)	R _e	H/B	K _w Depth	K _{sp}	K _{sh}	Z _{max} (m)	K ₁	K ₂	K ₃	F _r	HEC-18 (m)	
160	RS	0.91	10.67	0.91	0	4.94	886749	5.4	1.00	1	1.0	1.08	1	1.00	1.10	0.14	1.56	1.37
161	RS	0.91	10.67	0.91	0	6.95	923000	7.6	1.00	1	1.0	1.10	1	1.00	1.10	0.12	1.66	1.07
162	RS	0.91	10.67	0.91	0	6.71	839344	7.3	1.00	1	1.0	1.04	1	1.00	1.10	0.11	1.58	1.37
163	RS	0.91	10.67	0.91	0	6.49	791939	7.1	1.00	1	1.0	1.00	1	1.00	1.10	0.11	1.54	1.65
164	RS	0.91	10.67	0.91	0	6.61	858864	7.2	1.00	1	1.0	1.05	1	1.00	1.10	0.12	1.60	1.28
165	RS	0.91	10.67	0.91	0	7.50	931365	8.2	1.00	1	1.0	1.11	1	1.00	1.10	0.12	1.68	1.22
166	RS	0.91	10.67	0.91	0	7.44	897903	8.1	1.00	1	1.0	1.09	1	1.00	1.10	0.11	1.65	1.07
167	RS	0.91	10.67	0.91	0	7.56	909057	8.3	1.00	1	1.0	1.09	1	1.00	1.10	0.12	1.66	1.10
168	RS	0.91	10.67	0.91	0	8.02	521453	8.8	1.00	1	1.0	0.77	1	1.00	1.10	0.06	1.32	0.91
169	RS	0.91	10.67	0.91	0	5.94	348565	6.5	1.00	1	1.0	0.59	1	1.00	1.10	0.05	1.07	0.46
170	RS	0.91	10.67	0.91	0	6.10	334622	6.7	1.00	1	1.0	0.58	1	1.00	1.10	0.05	1.05	0.61
171	RS	0.91	10.67	0.91	0	5.73	228659	6.3	1.00	1	1.0	0.46	1	1.00	1.10	0.03	0.89	0.37
172	RS	0.91	10.67	0.91	0	5.64	298372	6.2	1.00	1	1.0	0.54	1	1.00	1.10	0.04	0.99	0.46
173	RS	0.91	10.67	0.91	0	5.88	264909	6.4	1.00	1	1.0	0.50	1	1.00	1.10	0.04	0.95	0.40
174	RS	0.91	10.67	0.91	0	6.34	323468	6.9	1.00	1	1.0	0.57	1	1.00	1.10	0.04	1.04	0.46
175	RS	0.91	10.67	0.91	0	6.40	301160	7.0	1.00	1	1.0	0.54	1	1.00	1.10	0.04	1.01	0.46
176	RS	0.91	10.67	0.91	0	7.13	301160	7.8	1.00	1	1.0	0.54	1	1.00	1.10	0.04	1.03	0.91
177	RS	0.88	9.75	0.88	0	4.27	754759	4.8	1.00	1	1.0	0.97	1	1.00	1.10	0.13	1.41	0.27
178	RS	0.88	9.75	0.88	0	4.39	690065	5.0	1.00	1	1.0	0.92	1	1.00	1.10	0.12	1.36	0.24
179	RS	0.88	9.75	0.88	0	4.51	816757	5.1	1.00	1	1.0	1.02	1	1.00	1.10	0.14	1.47	0.27
180	RS	0.88	9.75	0.88	0	4.27	757455	4.8	1.00	1	1.0	0.97	1	1.00	1.10	0.13	1.41	0.34
181	RS	0.88	9.75	0.88	0	4.39	760150	5.0	1.00	1	1.0	0.98	1	1.00	1.10	0.13	1.42	0.49
182	RS	0.88	9.75	0.88	0	4.63	894929	5.2	1.00	1	1.0	1.08	1	1.00	1.10	0.15	1.54	0.43
183	RS	0.88	9.75	0.88	0	4.36	846408	4.9	1.00	1	1.0	1.05	1	1.00	1.10	0.15	1.49	0.43
184	RS	0.88	9.75	0.88	0	4.63	903015	5.2	1.00	1	1.0	1.09	1	1.00	1.10	0.15	1.54	0.55
185	RS	0.88	9.75	0.88	0	4.63	843713	5.2	1.00	1	1.0	1.04	1	1.00	1.10	0.14	1.50	0.46
186	RS	0.88	9.75	0.88	0	4.69	873364	5.3	1.00	1	1.0	1.07	1	1.00	1.10	0.15	1.52	0.40

Test No.	Pier Data				Flow Data			SRICOS-EFA K Factors Approach					HEC-18 Method					Measured Pier Scour (m)
	Pier Type	Pier Width (m)	Pier Length (m)	B (m)	Attack Angle (degree)	H (m)	R _e	H/B	K _w Depth	K _{sp}	K _{sh}	Z _{max} (m)	K ₁	K ₂	K ₃	F _r	HEC-18 (m)	
187	RS	0.88	9.75	0.88	0	4.72	800584	5.3	1.00	1	1.0	1.01	1	1.00	1.10	0.13	1.47	0.34
188	RS	0.88	9.75	0.88	0	4.88	706239	5.5	1.00	1	1.0	0.93	1	1.00	1.10	0.12	1.40	0.46
189	RS	0.88	9.75	0.88	0	5.03	878755	5.7	1.00	1	1.0	1.07	1	1.00	1.10	0.14	1.54	0.37
190	RS	0.88	9.75	0.88	0	4.79	921884	5.4	1.00	1	1.0	1.10	1	1.00	1.10	0.15	1.56	0.37
191	RS	0.88	9.75	0.88	0	4.48	816757	5.1	1.00	1	1.0	1.02	1	1.00	1.10	0.14	1.47	0.37
192	RS	0.88	9.75	0.88	0	5.03	994665	5.7	1.00	1	1.0	1.16	1	1.00	1.10	0.16	1.63	0.40
193	RS	0.88	9.75	0.88	0	5.09	884146	5.8	1.00	1	1.0	1.07	1	1.00	1.10	0.14	1.55	0.55
194	RS	0.88	9.75	0.88	0	4.85	986578	5.5	1.00	1	1.0	1.15	1	1.00	1.10	0.16	1.61	0.61
195	RS	0.88	9.75	0.88	0	5.15	929971	5.8	1.00	1	1.0	1.11	1	1.00	1.10	0.15	1.58	0.61
196	RS	0.88	9.75	0.88	0	4.69	959622	5.3	1.00	1	1.0	1.13	1	1.00	1.10	0.16	1.59	0.61
197	RS	0.76	13.11	0.76	0	2.71	487991	3.6	1.00	1	1.0	0.74	1	1.00	1.10	0.12	1.07	0.76
198	RS	0.98	25.30	0.98	0	6.25	1558596	6.4	1.00	1	1.0	1.54	1	1.00	1.10	0.20	2.08	1.07
199	RS	0.98	25.30	0.98	0	7.92	1832243	8.1	1.00	1	1.0	1.71	1	1.00	1.10	0.21	2.30	1.22
200	RS	0.98	25.30	0.98	0	5.82	1284949	6.0	1.00	1	1.0	1.36	1	1.00	1.10	0.17	1.89	0.82
201	RS	0.98	25.30	0.98	0	9.30	2114813	9.5	1.00	1	1.0	1.87	1	1.00	1.10	0.23	2.50	1.07
202	RS	0.98	25.30	0.98	0	8.38	1624033	8.6	1.00	1	1.0	1.58	1	1.00	1.10	0.18	2.20	1.52
203	RS	0.61	12.50	0.61	0	0.46	342058	0.8	0.77	1	1.0	0.45	1	1.00	1.10	0.26	0.68	0.24
204	RS	0.61	12.50	0.61	0	0.67	948096	1.1	0.88	1	1.0	0.99	1	1.00	1.10	0.61	1.12	0.18
205	RS	0.61	12.50	0.61	0	1.68	970405	2.8	1.00	1	1.0	1.14	1	1.00	1.10	0.39	1.28	0.49
206	RS	0.61	12.50	0.61	0	1.22	752900	2.0	1.00	1	1.0	0.97	1	1.00	1.10	0.36	1.10	0.30
207	RS	0.61	12.50	0.61	0	1.52	987136	2.5	1.00	1	1.0	1.15	1	1.00	1.10	0.42	1.27	0.37
208	RS	0.61	12.50	0.61	0	2.62	1580161	4.3	1.00	1	1.0	1.55	1	1.00	1.10	0.51	1.67	0.76
209	RS	0.69	8.53	0.69	0	1.71	449649	2.5	1.00	1	1.0	0.70	1	1.00	1.10	0.16	0.94	0.40
210	RS	0.69	8.53	0.69	0	1.80	470563	2.6	1.00	1	1.0	0.72	1	1.00	1.10	0.16	0.97	0.37
211	RS	0.69	8.53	0.69	0	1.55	439192	2.3	1.00	1	1.0	0.69	1	1.00	1.10	0.16	0.92	0.21
212	RS	0.69	8.53	0.69	0	0.88	263515	1.3	0.93	1	1.0	0.46	1	1.00	1.10	0.13	0.69	0.40
213	RS	0.69	8.53	0.69	0	1.40	355536	2.0	1.00	1	1.0	0.60	1	1.00	1.10	0.14	0.83	0.43

Test No.	Pier Data				Flow Data			SRICOS-EFA K Factors Approach					HEC-18 Method					Measured Pier Scour (m)
	Pier Type	Pier Width (m)	Pier Length (m)	B (m)	Attack Angle (degree)	H (m)	R _e	H/B	K _w Depth	K _{sp}	K _{sh}	Z _{max} (m)	K ₁	K ₂	K ₃	F _r	HEC-18 (m)	
214	RS	0.69	8.53	0.69	0	1.62	359719	2.4	1.00	1	1.0	0.61	1	1.00	1.10	0.13	0.85	0.37
215	RS	0.69	8.53	0.69	0	0.98	129666	1.4	0.96	1	1.0	0.30	1	1.00	1.10	0.06	0.51	0.55
216	RS	0.69	8.53	0.69	0	0.88	221687	1.3	0.93	1	1.0	0.41	1	1.00	1.10	0.11	0.64	0.73
217	RS	0.69	8.53	0.69	0	0.88	165220	1.3	0.93	1	1.0	0.34	1	1.00	1.10	0.08	0.56	0.49
218	RS	0.69	8.53	0.69	0	0.79	221687	1.2	0.89	1	1.0	0.40	1	1.00	1.10	0.12	0.63	0.40
219	RS	0.69	8.53	0.69	0	0.61	129666	0.9	0.82	1	1.0	0.26	1	1.00	1.10	0.08	0.48	0.43
220	RS	0.69	8.53	0.69	0	1.07	340896	1.6	0.99	1	1.0	0.58	1	1.00	1.10	0.15	0.79	0.46
221	RS	0.61	9.14	0.61	0	0.76	687835	1.3	0.92	1	1.0	0.84	1	1.00	1.10	0.41	0.99	0.46
222	RS	0.61	9.14	0.61	0	3.20	1024316	5.3	1.00	1	1.0	1.18	1	1.00	1.10	0.30	1.43	0.64
223	RS	0.61	9.14	0.61	0	3.20	1199063	5.3	1.00	1	1.0	1.30	1	1.00	1.10	0.35	1.53	0.55
224	RS	0.61	8.99	0.61	0	2.16	758477	3.6	1.00	1	1.0	0.97	1	1.00	1.10	0.27	1.19	0.06
225	RS	0.61	8.99	0.61	0	2.41	855146	4.0	1.00	1	1.0	1.05	1	1.00	1.10	0.29	1.27	0.12
226	RS	0.61	8.99	0.61	0	2.59	830979	4.3	1.00	1	1.0	1.03	1	1.00	1.10	0.27	1.27	0.24
227	RS	0.61	8.99	0.61	0	2.96	855146	4.9	1.00	1	1.0	1.05	1	1.00	1.10	0.26	1.31	0.30
228	RS	0.61	8.99	0.61	0	3.02	890467	5.0	1.00	1	1.0	1.08	1	1.00	1.10	0.27	1.33	0.24
229	RS	0.61	8.99	0.61	0	3.26	948096	5.4	1.00	1	1.0	1.12	1	1.00	1.10	0.27	1.38	0.37
233	SU	2.99	11.58	2.99	0	11.73	5647680	3.9	1.00	1	1.0	3.49	1	1.00	1.10	0.18	5.03	4.39
234	SS	1.68	8.08	1.68	0	8.05	1789300	4.8	1.00	1	1.0	1.68	1	1.00	1.10	0.12	2.57	1.74
235	RS	1.52	9.45	6.90	37	3.66	14942788	0.5	0.68	1	1.0	4.43	1	2.67	1.10	0.36	7.85	1.83
236	RS	1.52	9.45	6.90	37	3.66	15363711	0.5	0.68	1	1.0	4.51	1	2.67	1.10	0.37	7.94	2.13
237	RS	1.52	9.45	6.90	37	4.57	14311402	0.7	0.74	1	1.0	4.65	1	2.67	1.10	0.31	7.94	1.83
238	RS	1.52	13.53	9.36	37	4.27	16267093	0.5	0.65	1	1.0	4.44	1	3.25	1.10	0.27	8.89	2.44
239	SS	0.53	7.09	2.92	20	1.83	4101565	0.6	0.72	1	0.9	1.86	0.9	2.86	1.10	0.33	2.89	0.34
240	SS	0.53	7.09	2.92	20	1.83	4101565	0.6	0.72	1	0.9	1.86	0.9	2.86	1.10	0.33	2.89	0.67
241	SS	0.53	7.09	2.92	20	1.55	5171539	0.5	0.69	1	0.9	2.04	0.9	2.86	1.10	0.45	3.13	0.30
242	SS	0.53	7.09	2.92	20	1.55	5171539	0.5	0.69	1	0.9	2.04	0.9	2.86	1.10	0.45	3.13	0.79
243	SS	0.53	7.09	5.22	43	1.40	5095275	0.3	0.54	1	0.9	1.60	0.9	4.15	1.10	0.26	3.46	0.46

Test No.	Pier Data				Flow Data			SRICOS-EFA K Factors Approach					HEC-18 Method					Measured Pier Scour (m)
	Pier Type	Pier Width (m)	Pier Length (m)	B (m)	Attack Angle (degree)	H (m)	R _e	H/B	K _w Depth	K _{sp}	K _{sh}	Z _{max} (m)	K ₁	K ₂	K ₃	F _r	HEC-18 (m)	
244	SS	0.53	7.09	5.22	43	1.40	5095275	0.3	0.54	1	0.9	1.60	0.9	4.15	1.10	0.26	3.46	0.67
245	SS	0.53	7.09	2.92	20	1.31	4101565	0.4	0.65	1	0.9	1.66	0.9	2.86	1.10	0.39	2.77	0.91
246	SS	0.53	7.09	5.22	43	1.01	5413730	0.2	0.49	1	0.9	1.48	0.9	4.15	1.10	0.33	3.39	0.49
247	QS	0.29	7.32	3.47	26	1.01	2747781	0.3	0.56	1	1.1	1.36	1.1	3.26	1.10	0.25	1.95	0.61
248	QS	0.29	7.32	3.47	26	1.01	2747781	0.3	0.56	1	1.1	1.36	1.1	3.26	1.10	0.25	1.95	0.58
249	QS	0.29	7.32	2.17	15	0.58	1523494	0.3	0.54	1	1.1	0.91	1.1	2.49	1.10	0.29	1.31	0.21
250	QS	0.29	7.32	2.17	15	0.58	1523494	0.3	0.54	1	1.1	0.91	1.1	2.49	1.10	0.29	1.31	0.43
251	QS	0.29	7.32	3.47	26	1.01	3698936	0.3	0.56	1	1.1	1.64	1.1	3.26	1.10	0.34	2.22	0.15
252	QS	0.29	7.32	3.47	26	1.01	3698936	0.3	0.56	1	1.1	1.64	1.1	3.26	1.10	0.34	2.22	0.46
253	QS	0.29	7.32	2.05	14	1.01	2375371	0.5	0.67	1	1.1	1.48	1.1	2.41	1.10	0.37	1.70	0.30
254	QS	0.29	7.32	2.05	14	1.01	2375371	0.5	0.67	1	1.1	1.48	1.1	2.41	1.10	0.37	1.70	0.34
255	QS	0.29	7.32	2.77	20	0.34	2283109	0.1	0.41	1	1.1	0.89	1.1	2.86	1.10	0.45	1.50	0.30
256	QS	0.29	7.32	2.77	20	0.34	2283109	0.1	0.41	1	1.1	0.89	1.1	2.86	1.10	0.45	1.50	0.00
257	QS	0.29	7.32	3.12	23	1.31	3714833	0.4	0.63	1	1.1	1.86	1.1	3.07	1.10	0.33	2.27	0.18
258	QS	0.29	7.32	3.12	23	1.31	3714833	0.4	0.63	1	1.1	1.86	1.1	3.07	1.10	0.33	2.27	0.34
259	QS	0.29	7.32	2.29	16	0.34	2308278	0.1	0.44	1	1.1	0.96	1.1	2.57	1.10	0.55	1.47	0.37
260	QS	0.29	7.32	2.29	16	0.34	2308278	0.1	0.44	1	1.1	0.96	1.1	2.57	1.10	0.55	1.47	0.24
261	QS	0.29	7.32	2.29	16	1.86	2867861	0.8	0.79	1	1.1	1.97	1.1	2.57	1.10	0.29	2.03	0.64
262	QS	0.29	7.32	2.29	16	1.86	2867861	0.8	0.79	1	1.1	1.97	1.1	2.57	1.10	0.29	2.03	0.49
263	QS	0.29	7.32	1.68	11	0.43	1894877	0.3	0.53	1	1.1	1.02	1.1	2.16	1.10	0.55	1.34	0.55
264	QS	0.29	7.32	1.68	11	0.43	1894877	0.3	0.53	1	1.1	1.02	1.1	2.16	1.10	0.55	1.34	0.40
265	QS	0.29	7.32	2.29	16	2.65	2727965	1.2	0.89	1	1.1	2.16	1.1	2.57	1.10	0.23	2.09	0.73
266	QS	0.29	7.32	2.29	16	2.65	2727965	1.2	0.89	1	1.1	2.16	1.1	2.57	1.10	0.23	2.09	0.76
267	QS	0.29	7.32	1.30	8	0.52	1431928	0.4	0.62	1	1.1	1.00	1.1	1.89	1.10	0.49	1.19	0.52
268	QS	0.29	7.32	1.30	8	0.52	1431928	0.4	0.62	1	1.1	1.00	1.1	1.89	1.10	0.49	1.19	0.40
269	QS	0.29	7.32	2.05	14	2.80	3250508	1.4	0.95	1	1.1	2.55	1.1	2.41	1.10	0.30	2.24	0.40
270	QS	0.29	7.32	2.05	14	2.80	3250508	1.4	0.95	1	1.1	2.55	1.1	2.41	1.10	0.30	2.24	0.40

Test No.	Pier Data				Flow Data			SRICOS-EFA K Factors Approach					HEC-18 Method					Measured Pier Scour (m)
	Pier Type	Pier Width (m)	Pier Length (m)	B (m)	Attack Angle (degree)	H (m)	R _e	H/B	K _w Depth	K _{sp}	K _{sh}	Z _{max} (m)	K ₁	K ₂	K ₃	F _r	HEC-18 (m)	
271	QS	0.29	7.32	1.93	13	0.67	2174180	0.3	0.59	1	1.1	1.24	1.1	2.33	1.10	0.44	1.54	0.52
272	QS	0.29	7.32	1.93	13	0.67	2174180	0.3	0.59	1	1.1	1.24	1.1	2.33	1.10	0.44	1.54	0.37
273	QS	0.29	7.32	1.68	11	2.87	2202154	1.7	1.00	1	1.1	2.11	1.1	2.16	1.10	0.25	1.85	0.21
274	QS	0.29	7.32	1.68	11	2.87	2202154	1.7	1.00	1	1.1	2.11	1.1	2.16	1.10	0.25	1.85	0.61
275	RS	1.22	6.40	2.52	12	2.10	2538753	0.8	0.80	1	1.0	1.68	1	1.60	1.10	0.22	2.72	0.64
276	RS	1.22	6.40	2.52	12	2.10	2538753	0.8	0.80	1	1.0	1.68	1	1.60	1.10	0.22	2.72	0.43
277	SS	0.91	27.43	12.84	26	1.22	21147195	0.1	0.38	1	0.9	2.77	0.9	3.26	1.10	0.48	4.74	0.52
278	SS	0.91	27.43	12.84	26	1.22	21147195	0.1	0.38	1	0.9	2.77	0.9	3.26	1.10	0.48	4.74	0.46
279	RS	0.91	10.52	1.83	5	9.42	2897134	5.2	1.00	1	1.0	2.28	1	1.57	1.10	0.16	3.29	0.70
280	RS	0.91	10.52	1.83	5	9.42	2897134	5.2	1.00	1	1.0	2.28	1	1.57	1.10	0.16	3.29	0.46
281	RS	0.91	14.48	2.17	5	3.44	2384652	1.6	0.99	1	1.0	2.01	1	1.59	1.10	0.19	2.49	0.37
282	RS	0.91	14.48	2.17	5	3.17	2185931	1.5	0.97	1	1.0	1.85	1	1.59	1.10	0.18	2.37	0.40
283	RS	0.91	14.48	2.17	5	3.17	2185931	1.5	0.97	1	1.0	1.85	1	1.59	1.10	0.18	2.37	0.24
284	RS	0.61	12.80	2.82	10	6.55	4647506	2.3	1.00	1	1.0	3.08	1	2.07	1.10	0.21	3.23	1.07
285	QS	1.65	8.17	3.57	14	6.80	7625698	1.9	1.00	1	1.1	4.64	1.1	1.66	1.10	0.26	6.08	1.46
286	QS	1.65	8.17	2.77	8	7.50	5904989	2.7	1.00	1	1.1	3.95	1.1	1.40	1.10	0.25	5.22	0.70
287	QS	1.86	8.17	2.98	8	8.56	5902017	2.9	1.00	1	1.1	3.95	1.1	1.36	1.10	0.22	5.40	1.62
288	QS	1.83	8.17	3.35	11	8.81	6544316	2.6	1.00	1	1.1	4.21	1.1	1.48	1.10	0.21	5.82	1.19
289	SS	1.31	15.24	2.63	5	2.62	6705238	1.0	0.85	1	0.9	2.97	0.9	1.57	1.10	0.50	3.87	1.13
290	SS	1.31	15.24	2.63	5	1.95	5653278	0.7	0.77	1	0.9	2.41	0.9	1.57	1.10	0.49	3.46	0.82
291	SS	1.31	15.24	2.63	5	2.29	5605097	0.9	0.81	1	0.9	2.53	0.9	1.57	1.10	0.45	3.52	0.82
292	SS	1.31	15.24	2.63	5	1.40	4015113	0.5	0.69	1	0.9	1.73	0.9	1.57	1.10	0.41	2.85	0.98
293	SS	1.31	15.24	2.63	5	2.16	5243737	0.8	0.80	1	0.9	2.38	0.9	1.57	1.10	0.43	3.39	0.79
294	SS	1.31	15.24	2.63	5	1.71	4826165	0.6	0.73	1	0.9	2.08	0.9	1.57	1.10	0.45	3.17	0.91
295	SS	1.31	15.24	2.63	5	1.92	5605097	0.7	0.76	1	0.9	2.39	0.9	1.57	1.10	0.49	3.44	0.85
296	SS	1.31	15.24	2.63	5	1.25	2914972	0.5	0.66	1	0.9	1.36	0.9	1.57	1.10	0.32	2.45	0.91
297	SS	1.04	11.98	1.66	3	1.46	4256144	0.9	0.81	1	0.9	2.14	0.9	1.36	1.10	0.68	2.66	0.24

Test No.	Pier Data				Flow Data			SRICOS-EFA K Factors Approach					HEC-18 Method					Measured Pier Scour (m)
	Pier Type	Pier Width (m)	Pier Length (m)	B (m)	Attack Angle (degree)	H (m)	R _e	H/B	K _w Depth	K _{sp}	K _{sh}	Z _{max} (m)	K ₁	K ₂	K ₃	F _r	HEC-18 (m)	
298	SS	1.04	11.98	1.66	3	1.01	2584087	0.6	0.72	1	0.9	1.37	0.9	1.36	1.10	0.49	2.04	0.37
299	SS	1.04	11.98	1.66	3	1.04	3141439	0.6	0.72	1	0.9	1.57	0.9	1.36	1.10	0.59	2.23	0.58
300	SS	1.04	12.04	1.66	3	1.68	5381156	1.0	0.85	1	0.9	2.59	0.9	1.36	1.10	0.80	3.00	1.68
301	SS	1.04	12.04	1.66	3	1.13	3553593	0.7	0.74	1	0.9	1.74	0.9	1.36	1.10	0.64	2.38	1.40
302	SS	1.04	12.04	1.66	3	1.16	3553593	0.7	0.75	1	0.9	1.76	0.9	1.36	1.10	0.63	2.39	1.37
303	SS	1.14	10.18	2.55	8	1.83	932434	0.7	0.76	1	0.9	0.76	0.9	1.68	1.10	0.09	1.57	0.21
304	SS	1.14	10.18	2.55	8	2.53	1243245	1.0	0.85	1	0.9	1.02	0.9	1.68	1.10	0.10	1.85	0.12
305	SS	1.14	10.18	2.55	8	4.24	1942571	1.7	1.00	1	0.9	1.59	0.9	1.68	1.10	0.12	2.41	0.15

Reference:

D.S. Mueller, 1996, "Channel Scour at Bridges in the United States", FHWA-RD-95-184, Federal Highway Administration, VA, USA

Note

- | | | |
|--|---|---|
| B: pier projected width; | K₂: correction factor for angle of attack of flow from HEC-18 | QS: Square single |
| CS: Cylinder single | K₃: correction factor for bed condition from HEC-18 | R_e: Reynolds number |
| F_r: froude number | K_{sh}: pier shape effect on Zmax for SRICOS-EFA method | RS: Round single |
| H: Approching flow depth | K_{sp}: pier spacing effect on Zmax for SRICOS-EFA method | SS: Sharp single |
| K₁: correction factor for pier shape from HEC-18 | K_w: water depth effect on Zmax for SRICOS-EFA method | Z_{max}: the predicted maximum scour depth |

Table 2 – FROEHLICH (1988) Database

Test No.	Pier Data			Approach Flow Data			Bed Material	SRICOS-EFA Method							HEC-18 Method					Measured Scour Depth (m)
	Type code	Width (m)	Length (m)	Depth (m)	Velocity (m/s)	Attack Angle	D50 (mm)	H (m)	H/B	K _w	K _{sp}	K _{sh}	R _e	Z _{max} (m)	F _r	K ₁	K ₂	K ₃	HEC-18 (m)	
1	2	4.50	14.00	18.80	1.84	0	0.250	4.50	4.18	1.0	1.0	1.0	8280000	4.45	0.135	1.0	1.0	1.1	6.91	4.30
2	2	4.50	14.00	17.40	2.28	0	0.250	4.50	3.87	1.0	1.0	1.0	10260000	5.10	0.175	1.0	1.0	1.1	7.50	3.00
3	2	1.92	17.37	5.39	1.80	5	0.500	3.43	1.57	1.0	1.0	1.0	6167860.3	3.66	0.248	1.0	2.8	1.1	9.47	1.74
4	2	8.50	8.50	9.00	0.65	12	0.670	10.08	0.89	0.8	1.0	1.0	6552977.6	3.14	0.069	1.0	1.3	1.1	8.10	7.80
5	1	2.40	8.85	3.45	0.96	10	0.780	3.90	0.88	0.8	1.0	1.1	3744312	2.41	0.165	1.1	2.2	1.1	6.58	2.75
6	3	1.52	6.10	5.80	1.98	0	70.000	1.52	3.82	1.0	1.0	0.9	3009600	2.11	0.262	0.9	1.0	1.1	2.71	0.76
7	3	1.52	6.10	4.10	2.59	0	70.000	1.52	2.70	1.0	1.0	0.9	3936800	2.50	0.408	0.9	1.0	1.1	2.90	0.76
8	3	1.52	6.10	3.40	2.13	0	70.000	1.52	2.24	1.0	1.0	0.9	3237600	2.21	0.369	0.9	1.0	1.1	2.60	0.61
9	3	1.52	6.10	5.30	3.05	0	70.000	1.52	3.49	1.0	1.0	0.9	4636000	2.77	0.423	0.9	1.0	1.1	3.22	0.61
10	3	1.52	6.10	6.60	2.90	0	70.000	1.52	4.34	1.0	1.0	0.9	4408000	2.68	0.360	0.9	1.0	1.1	3.24	0.61
11	3	1.52	6.10	5.20	3.51	0	70.000	1.52	3.42	1.0	1.0	0.9	5335200	3.03	0.491	0.9	1.0	1.1	3.41	0.61
12	3	1.80	9.60	5.50	3.67	0	1.500	1.80	3.06	1.0	1.0	0.9	6606000	3.47	0.500	0.9	1.0	1.1	3.91	0.82
13	2	1.52	11.58	1.20	0.49	0	0.500	1.52	0.79	0.8	1.0	1.0	744800	0.76	0.143	1.0	1.0	1.1	1.33	0.30
14	2	1.52	11.58	1.50	0.76	0	0.500	1.52	0.99	0.8	1.0	1.0	1155200	1.08	0.198	1.0	1.0	1.1	1.66	0.30
15	2	1.52	11.58	1.20	0.88	0	0.500	1.52	0.79	0.8	1.0	1.0	1337600	1.10	0.256	1.0	1.0	1.1	1.71	0.30
16	2	1.52	11.58	0.50	0.27	0	0.500	1.52	0.33	0.6	1.0	1.0	410400	0.38	0.122	1.0	1.0	1.1	0.92	0.76
17	2	1.52	11.58	0.60	0.15	0	0.500	1.52	0.39	0.6	1.0	1.0	228000	0.28	0.062	1.0	1.0	1.1	0.73	1.22
18	2	1.52	11.58	2.10	1.52	0	1.600	1.52	1.38	0.9	1.0	1.0	2310400	1.88	0.335	1.0	1.0	1.1	2.34	0.61
19	2	1.52	11.58	2.00	1.55	0	1.600	1.52	1.32	0.9	1.0	1.0	2356000	1.87	0.350	1.0	1.0	1.1	2.34	0.61
20	2	1.52	11.58	3.00	1.58	0	1.600	1.52	1.97	1.0	1.0	1.0	2401600	2.03	0.291	1.0	1.0	1.1	2.50	0.91
21	2	1.52	11.58	3.20	1.98	0	1.600	1.52	2.11	1.0	1.0	1.0	3009600	2.34	0.353	1.0	1.0	1.1	2.77	1.22
22	2	1.52	11.58	3.00	1.80	0	1.600	1.52	1.97	1.0	1.0	1.0	2736000	2.20	0.332	1.0	1.0	1.1	2.64	1.37
23	2	1.52	11.58	2.60	2.07	0	1.600	1.52	1.71	1.0	1.0	1.0	3146400	2.41	0.410	1.0	1.0	1.1	2.75	1.07
24	2	1.52	11.58	3.00	1.83	0	1.600	1.52	1.97	1.0	1.0	1.0	2781600	2.23	0.337	1.0	1.0	1.1	2.66	1.83

Test No.	Pier Data			Approach Flow Data			Bed Material	SRICOS-EFA Method							HEC-18 Method					Measured Scour Depth (m)
	Type code	Width (m)	Length (m)	Depth (m)	Velocity (m/s)	Attack Angle	D50 (mm)	H (m)	H/B	K _w	K _{sp}	K _{sh}	R _c	Z _{max} (m)	F _r	K ₁	K ₂	K ₃	HEC-18 (m)	
25	2	1.52	11.58	0.90	0.94	0	1.600	1.52	0.59	0.7	1.0	1.0	1428800	1.04	0.316	1.0	1.0	1.1	1.70	0.46
26	2	1.52	11.58	0.90	0.98	0	1.600	1.52	0.59	0.7	1.0	1.0	1489600	1.06	0.330	1.0	1.0	1.1	1.73	0.61
27	2	1.52	11.58	1.80	1.10	0	1.600	1.52	1.18	0.9	1.0	1.0	1672000	1.45	0.262	1.0	1.0	1.1	1.99	0.46
28	2	1.52	11.58	2.40	1.16	0	1.600	1.52	1.58	1.0	1.0	1.0	1763200	1.65	0.239	1.0	1.0	1.1	2.12	0.61
29	2	1.52	11.58	2.30	1.13	0	1.600	1.52	1.51	1.0	1.0	1.0	1717600	1.60	0.238	1.0	1.0	1.1	2.08	0.76
30	2	1.52	11.58	1.50	1.13	0	1.600	1.52	0.99	0.8	1.0	1.0	1717600	1.39	0.295	1.0	1.0	1.1	1.97	0.46
31	2	1.52	11.58	2.00	0.98	0	1.600	1.52	1.32	0.9	1.0	1.0	1489600	1.40	0.221	1.0	1.0	1.1	1.92	0.76
33	3	4.60	4.60	3.70	2.90	0	90.000	4.60	0.80	0.8	1.0	0.9	13340000	4.28	0.481	0.9	1.0	1.1	6.16	1.50
34	3	4.60	4.60	4.60	3.51	0	90.000	4.60	1.00	0.9	1.0	0.9	16146000	5.20	0.523	0.9	1.0	1.1	6.89	1.70
35	3	4.60	4.60	1.50	0.61	0	90.000	4.60	0.33	0.6	1.0	0.9	2806000	1.17	0.159	0.9	1.0	1.1	2.79	0.90
36	2	1.52	10.36	3.70	2.16	35	14.000	7.19	0.51	0.7	1.0	1.0	15524704	4.50	0.359	1.0	5.6	1.1	16.35	1.80
37	2	1.52	10.36	3.70	2.22	35	14.000	7.19	0.51	0.7	1.0	1.0	15955946	4.58	0.368	1.0	5.6	1.1	16.55	2.10
38	2	1.52	10.36	4.60	2.07	35	14.000	7.19	0.64	0.7	1.0	1.0	14877841	4.71	0.308	1.0	5.6	1.1	16.54	1.80
39	2	1.52	10.36	4.30	1.74	35	14.000	7.19	0.60	0.7	1.0	1.0	12506012	4.13	0.268	1.0	5.6	1.1	15.21	2.40
40	2	3.05	17.60	6.70	2.59	0	15.000	3.05	2.20	1.0	1.0	1.0	7899500	4.32	0.319	1.0	1.0	1.1	5.41	1.80
41	2	0.98	0.98	1.70	1.61	0	8.000	0.98	1.73	1.0	1.0	1.0	1577800	1.55	0.394	1.0	1.0	1.1	1.75	0.90
44	2	8.20	8.20	4.90	0.46	0	0.060	8.20	0.60	0.7	1.0	1.0	3772000	1.93	0.066	1.0	1.0	1.1	4.69	3.70
45	2	8.20	8.20	4.30	0.61	0	0.060	8.20	0.52	0.7	1.0	1.0	5002000	2.20	0.094	1.0	1.0	1.1	5.20	4.30
46	2	13.00	38.00	4.10	0.55	5	0.027	16.26	0.25	0.5	1.0	1.0	8944347.1	2.49	0.087	1.0	1.6	1.1	10.64	7.30
47	2	13.00	38.00	3.40	0.66	15	0.027	22.39	0.15	0.4	1.0	1.0	14778825	2.88	0.114	1.0	2.2	1.1	15.34	6.80
48	2	13.00	13.00	5.40	1.16	20	0.027	16.66	0.32	0.6	1.0	1.0	19328228	4.42	0.159	1.0	1.4	1.1	13.72	8.50
49	3	9.80	12.50	11.00	0.73	5	0.008	10.85	1.01	0.9	1.0	0.9	7922073	3.32	0.070	0.9	1.3	1.1	8.11	4.30
50	3	9.80	12.50	12.80	0.81	30	0.008	14.74	0.87	0.8	1.0	0.9	11937010	4.09	0.072	0.9	1.7	1.1	11.56	8.20
51	3	9.80	12.50	13.60	1.08	15	0.008	12.70	1.07	0.9	1.0	0.9	13717416	4.80	0.094	0.9	1.5	1.1	11.75	4.60
52	3	9.80	12.50	16.30	1.22	25	0.008	14.16	1.15	0.9	1.0	0.9	17280744	5.70	0.096	0.9	1.6	1.1	13.87	7.90
53	3	9.80	12.50	11.60	0.82	15	0.008	12.70	0.91	0.8	1.0	0.9	10415075	3.82	0.077	0.9	1.5	1.1	10.22	4.00
54	3	9.80	12.50	13.40	0.91	25	0.008	14.16	0.95	0.8	1.0	0.9	12889736	4.42	0.079	0.9	1.6	1.1	11.91	7.60

Test No.	Pier Data			Approach Flow Data			Bed Material	SRICOS-EFA Method							HEC-18 Method					Measured Scour Depth (m)
	Type code	Width (m)	Length (m)	Depth (m)	Velocity (m/s)	Attack Angle	D50 (mm)	H (m)	H/B	K _w	K _{sp}	K _{sh}	R _c	Z _{max} (m)	F _r	K ₁	K ₂	K ₃	HEC-18 (m)	
55	1	9.40	19.50	19.50	1.80	0	0.036	9.40	2.07	1.0	1.0	1.1	16920000	7.70	0.130	1.1	1.0	1.1	12.22	6.10
56	2	19.50	38.00	11.30	0.66	15	0.036	28.67	0.39	0.6	1.0	1.0	18922647	4.66	0.063	1.0	1.8	1.1	19.12	10.40
57	2	3.66	17.30	3.60	0.64	0	0.100	3.66	0.98	0.8	1.0	1.0	2342400	1.69	0.108	1.0	1.0	1.1	3.07	2.80
58	2	1.50	1.50	3.10	2.38	0	20.000	1.50	2.07	1.0	1.0	1.0	3570000	2.61	0.432	1.0	1.0	1.1	2.96	1.30
59	2	1.50	1.50	3.00	2.69	0	20.000	1.50	2.00	1.0	1.0	1.0	4035000	2.82	0.496	1.0	1.0	1.1	3.11	1.30
60	2	1.50	1.50	2.50	2.54	0	20.000	1.50	1.67	1.0	1.0	1.0	3810000	2.72	0.513	1.0	1.0	1.1	2.96	0.80
61	2	1.50	1.50	1.40	2.65	0	20.000	1.50	0.93	0.8	1.0	1.0	3975000	2.32	0.715	1.0	1.0	1.1	2.79	0.90
62	2	1.50	1.50	1.30	2.43	0	20.000	1.50	0.87	0.8	1.0	1.0	3645000	2.14	0.680	1.0	1.0	1.1	2.66	0.90
63	2	1.50	1.50	1.30	2.68	0	20.000	1.50	0.87	0.8	1.0	1.0	4020000	2.28	0.750	1.0	1.0	1.1	2.77	0.40
64	2	1.50	1.50	1.00	2.39	0	20.000	1.50	0.67	0.7	1.0	1.0	3585000	1.94	0.763	1.0	1.0	1.1	2.55	0.40
65	2	1.50	1.50	0.90	2.33	0	20.000	1.50	0.60	0.7	1.0	1.0	3495000	1.84	0.784	1.0	1.0	1.1	2.49	0.50
66	2	1.50	1.50	0.90	2.56	0	20.000	1.50	0.60	0.7	1.0	1.0	3840000	1.95	0.862	1.0	1.0	1.1	2.59	0.40
67	2	1.50	1.50	0.70	2.24	0	20.000	1.50	0.47	0.7	1.0	1.0	3360000	1.65	0.855	1.0	1.0	1.1	2.36	0.40
69	1	0.29	3.66	0.76	1.04	15	1.500	1.23	0.62	0.7	1.0	1.1	1276492	1.08	0.381	1.1	6.0	1.1	3.86	0.61
70	1	0.29	3.66	0.61	1.36	15	1.500	1.23	0.50	0.7	1.0	1.1	1669258.8	1.19	0.556	1.1	6.0	1.1	4.21	0.61
71	1	0.29	3.66	0.73	1.17	15	1.500	1.23	0.59	0.7	1.0	1.1	1436053.5	1.15	0.437	1.1	6.0	1.1	4.04	0.52
72	1	0.29	3.66	0.43	1.13	10	2.300	0.92	0.47	0.7	1.0	1.1	1040895.6	0.86	0.550	1.1	4.8	1.1	3.01	0.58
73	1	0.29	3.66	0.58	1.02	10	2.300	0.92	0.63	0.7	1.0	1.1	939569.51	0.89	0.428	1.1	4.8	1.1	3.00	0.46
74	1	0.29	3.66	0.70	1.12	10	2.300	0.92	0.76	0.8	1.0	1.1	1031684.2	1.01	0.427	1.1	4.8	1.1	3.20	0.49
75	1	0.29	3.66	1.81	1.22	15	2.300	1.23	1.47	1.0	1.0	1.1	1497423.4	1.60	0.290	1.1	6.0	1.1	4.65	0.66
76	2	1.22	6.40	2.13	1.17	0	0.600	1.22	1.75	1.0	1.0	1.0	1427400	1.46	0.256	1.0	1.0	1.1	1.82	0.64
77	2	1.22	6.40	0.55	0.69	0	0.600	1.22	0.45	0.6	1.0	1.0	841800	0.68	0.297	1.0	1.0	1.1	1.21	0.40
78	2	1.22	6.40	2.32	1.70	0	0.600	1.22	1.90	1.0	1.0	1.0	2074000	1.85	0.356	1.0	1.0	1.1	2.16	1.22
79	2	1.22	6.40	0.70	0.66	0	0.600	1.22	0.57	0.7	1.0	1.0	805200	0.71	0.252	1.0	1.0	1.1	1.22	0.61
80	3	0.94	27.43	1.40	1.54	0	7.900	0.94	1.49	1.0	1.0	0.9	1447600	1.29	0.416	0.9	1.0	1.1	1.47	0.37
81	3	0.94	27.43	1.22	1.35	0	4.300	0.94	1.30	0.9	1.0	0.9	1269000	1.13	0.390	0.9	1.0	1.1	1.36	0.15
82	3	0.52	8.29	3.21	1.68	10	1.200	1.95	1.64	1.0	1.0	0.9	3278761	2.22	0.299	0.9	4.8	1.1	5.60	0.98

Test No.	Pier Data			Approach Flow Data			Bed Material	SRICOS-EFA Method							HEC-18 Method					Measured Scour Depth (m)
	Type code	Width (m)	Length (m)	Depth (m)	Velocity (m/s)	Attack Angle	D50 (mm)	H (m)	H/B	K _w	K _{sp}	K _{sh}	R _e	Z _{max} (m)	F _r	K ₁	K ₂	K ₃	HEC-18 (m)	
83	3	0.52	8.29	2.14	1.17	10	1.800	1.95	1.10	0.9	1.0	0.9	2283422.8	1.55	0.255	0.9	4.8	1.1	4.54	0.65

Reference

Froehlich D.C. (1988), "Analysis of Onsite Measurement of Scour at Piers", Proceedings of ASCE National Hydraulic Engineering Conference, Colorado Springs, Colorado

Note:

- | | | |
|-------------------------------------|---|--|
| 1: Square-nosed; | H: Approching flow depth | |
| 2: Round-nosed; | K₁: correction factor for pier shape from HEC-18 | K_{sp}: pier spacing effect on Zmax for SRICOS-EFA method |
| 3: Sharp-nosed; | K₂: correction factor for angle of attack of flow from HEC-18 | K_w: water depth effect on Zmax for SRICOS-EFA method |
| B: pier projected width; | K₃: correction factor for bed condition from HEC-18 | R_e: Reynolds number |
| F_r: froude number | K_{sh}: pier shape effect on Zmax for SRICOS-EFA method | Z_{max}: the predicted maximum scour depth |

Table 3 – Gill (1981) Contraction Scour Database

Test No.	D ₁ (mm)	Q (m ³ /s)	D ₂ (mm)	B ₁ (m)	B ₂ (m)	Sand D ₅₀ (mm)	τ_c/τ_1	B ₁ /B ₂	n	V _c (m/s)	V ₁ (m/s)	Measured (mm)	SRICOS- EFA (mm)	HEC-18 (mm)
1	67.10	0.01504	91.40	0.76	0.50	1.53	1.51	1.52	0.01444	0.36	0.29	24.30	26.50	1.36
2	72.50	0.01646	100.60	0.76	0.50	1.53	1.40	1.52	0.01444	0.35	0.30	28.10	29.68	1.47
3	80.50	0.0199	115.80	0.76	0.50	1.53	1.26	1.52	0.01444	0.36	0.32	35.30	36.58	6.39
4	80.80	0.0224	131.10	0.76	0.50	1.53	1.26	1.52	0.01444	0.41	0.36	50.30	40.52	15.56
5	36.30	0.0091	48.80	0.76	0.50	1.53	1.26	1.52	0.01444	0.37	0.33	12.50	24.48	8.12
6	47.60	0.0133	91.40	0.76	0.50	1.53	1.00	1.52	0.01444	0.37	0.37	43.80	35.78	14.18
7	63.40	0.0150	85.30	0.76	0.50	1.53	1.60	1.52	0.01444	0.39	0.31	21.90	26.24	5.06
8	68.30	0.0165	97.50	0.76	0.50	1.53	1.49	1.52	0.01444	0.39	0.32	29.20	28.40	5.67
9	74.10	0.0196	106.70	0.76	0.50	1.53	1.37	1.52	0.01444	0.41	0.35	32.60	34.59	11.73
10	83.50	0.0210	118.90	0.76	0.50	1.53	1.22	1.52	0.01444	0.37	0.33	35.40	37.58	7.64
11	40.80	0.0122	88.40	0.76	0.50	1.53	1.03	1.52	0.01444	0.40	0.39	47.60	34.87	16.42
12	65.50	0.0122	82.30	0.76	0.50	0.92	1.51	1.52	0.01327	0.30	0.25	16.80	21.66	0.67
13	68.60	0.0165	100.60	0.76	0.50	0.92	1.44	1.52	0.01327	0.38	0.32	32.00	29.32	16.94
14	38.70	0.0071	48.80	0.76	0.50	0.92	2.55	1.52	0.01327	0.38	0.24	10.10	8.86	2.86
15	43.60	0.0094	67.10	0.76	0.50	0.92	1.34	1.52	0.01327	0.33	0.28	23.50	21.85	9.13
16	53.30	0.0122	82.30	0.76	0.50	0.92	1.08	1.52	0.01327	0.31	0.30	29.00	30.11	12.87
17	54.30	0.0133	88.40	0.76	0.50	0.92	1.00	1.52	0.01327	0.32	0.32	34.10	33.95	17.14
18	27.40	0.0051	39.60	0.76	0.50	0.92	1.52	1.52	0.01327	0.30	0.25	12.20	14.06	3.99

Reference:

Gill M.A. (1981), "Bed Erosion in Rectangular Long Contraction", *ASCE Journal of Hydraulic Division*, Vol. 107, n. HY3, 273-284.

Note:

B₁:	width of normal channel	D₅₀:	diameter which 50% of the bed material size are smaller	V_c:	critical velocity for D50 bed material size
B₂:	width of contracted channel	n:	manning coefficient	τ₁:	bed shear stress in the normal channel
D₁:	flow depth in normal channel	Q:	discharge	τ_c:	critical shear stress of bed material
D₂:	flow depth in contracted channel	V₁:	flow velocity in normal channel		

VITA**JUN WANG**

Jun Wang was born on July 5, 1975 in Shengzhou, China. He was admitted to the Department of Geotechnical Engineering at Tongji University in 1993. He was awarded with a People's Scholarship for four consecutive years and he graduated with honors from Tongji University as a recipient of the Excellent Student Leadership Award in August 1997. In February 1998, he went to the University of New South Wales in Sydney, Australia for his M.S.Eng. Degree and obtained it in October 1999. He started his PhD study in August 2000 at Texas A&M University, where he worked with Dr. Briaud on the scour research team. During studies at Texas A&M University, he was the president of the Chinese Student and Scholar Association and a member of Phi Kappa Phi Academic Honor Society. He also received the Shibata International Memorial Scholarship and was a finalist for the Eppright Outstanding International Student Award.

His permanent address is: Yuexiou Li, No. 14, Apt. #302
Shengzhou, Post Code: 312400
Zhejiang Province, China